Regional and seasonal differences in aerosol radiative forcing over India and adjoining oceanic regions

A THESIS

submitted for the Award of Ph. D. degree of

MOHANLAL SUKHADIA UNIVERSITY

in the

Faculty of Science

by

Sumita Kedia

Under the Supervision of

Dr. S. Ramachandran

Associate Professor
Space and Atmospheric Sciences Division
Physical Research Laboratory, Ahmedabad, India.

DEPARTMENT OF PHYSICS

MOHANLAL SUKHADIA UNIVERSITY

UDAIPUR

2010

CERTIFICATE

I feel great pleasure in certifying the thesis entitled "**Regional and seasonal differences in aerosol radiative forcing over India and adjoining oceanic regions**" by Sumita Kedia under my guidance. She has completed the following requirements as per Ph.D. regulations of the University

(a) Course work as per the university rules.

(b) Residential requirements of the university.

(c) Presented her work in the departmental committee.

(d) Published/accepted minimum of one research paper in a referred research journal,

I am satisfied with the analysis of data, interpretation of results and conclusions drawn.

I recommend the submission of thesis.

Date: 2010

Dr. S. Ramachandran
(Supervisor)
Physical Research Laboratory
Ahmedabad, India.

Countersigned by
Head of the Department

DECLARATION

*I Ms Sumita Kedia, D/o Mr. Bishwanath Kedia, resident of A-4, PRL residences, Navrangpura, Ahmedabad - 380009, hereby declare that the research work incorporated in the present thesis entitled "***Regional and seasonal differences in aerosol radiative forcing over India and adjoining oceanic regions***" is my own work and is original. This work (in part or in full) has not been submitted to any University for the award of a Degree or a Diploma. I have properly acknowledged the material collected from secondary sources wherever required. I solely own the responsibility for the originality of the entire content.*

Date:

Sumita Kedia

(Author)

Dedicated To my

Parents

Acknowledgements

Considerable efforts have been taken to bring the thesis to the current form. It is a great pleasure to thank all who gave their support with dedicated spirit and have been part of my life as teachers, friends, colleagues and family members.

First and foremost, I express my honest gratitude to Dr. S. Ramachandran under whose guidance the work has been carried out. I thank him for his continuous support, inspiration, encouragement and motivation during this entire work period. His guidance helped me throughout my research and writing of this thesis. The sublime blend of freedom and supervision provided by him made the thesis work thoroughly enjoyable. I could not have imagined having a better advisor and mentor for me for my Ph.D study.

I am also thankful to Prof A. Jayaraman for his concern towards me and about the progress of my work. I express my sincere thanks to T. A. Rajesh for his help and support throughout the period. I thank him for maintaining various instruments in the laboratory.

I thank Prof. J. N. Goswami, Director, Physical Research Laboratory, for providing me all the necessary facilities to carry out my thesis work.

I would like to thank Prof. Rajesh Pandey, Physics Department and the Ph. D. section of Mohanlal Sukhadia University for their kind co-operation throughout my thesis.

I am very much indebted to Profs. A. K. Singhvi, Shyam Lal, R. Sekar, S. A. Haider, U. Sarkar, R. Ramesh, M. M. Sarin, P. K. Panigrahi, J. Banerji and Drs. B. Bapat, K. P. Subramanian, Pallamraju, Varun Sheel, H. Mishra, S. Mohanty, D. Angom, and R. P. Singh for encouragement at various stages of my research.

I would like to thank Acharya sir and Modh sir for solving the problems related to sun photometer. Thanks to Sunil bhai, Venkataramani sir, Dipu da, Som Sharma, Sudheer, Rengarajan, Ravi bhushan and Navin Juyal for their support on various occasions.

I thank Dr. P. Sharma and for his help and care during course work at PRL. I also thank Dr. Bhushit for advice and help during reviews at PRL and Ph.D. registration at Udaipur.

I am grateful to Prof. Swapna Mohapatra (Utkal University), who is a great inspiration for me. She has contributed a lot through her care, personal guidance and encouragement.

I wish to express my sincere thanks to Drs. C. B. S. Dutt (ISRO HQS., Bengaluru), R. Sridharan, K. Krishna Moorthy and Suresh Babu (SPL, VSSC, Trivandrum) for giving me the opportunity to participate in the ICARB 2006 and WICARB 2009 cruises, and for their support and encouragement. I am also thankful to ISRO-GBP for funding support during campaigns. I thank my friends Spandana (Andhra University), Shailesh (NRSC), Sumit (IITM), Shilpa and Reachal (Goa University), and Liji (SPL) for making the cruises memorable.

I acknowledge NOAA Air Resources Laboratory, USA for the HYSPLIT model and NOAACIRES Climate Diagnostic Center, USA for providing NCEP reanalysis data. MODIS and MISR AODs, and TOMS ozone used in the study are downloaded from the GES-DISC, NASA. Rainfall data are obtained from NOAA, NESDIS National Climatic Data Center, USA. I am grateful to the National Centre for Antarctic and Ocean Research (NCAOR) and the Department of Ocean Development (Ministry of Earth Sciences) for giving me an opportunity to sail and conduct measurements on board Sagar Kanya. I thank Drs. B. N. Holben and S.N. Tripathi for their efforts in establishing and maintaining the AERONET sun/sky radiometer at Gandhi College and Kanpur the data of which are used in the present study.

I cannot forget to thank my friends Ribu (IITB) and Madhav (Andhra University) who were always ready to help me everytime I needed. Thanks are due to both of them for helping me in improving my computational skills. I also thank to Rajesh (ARIES) for making my participation in the SOLAS 2007 fruitful and enjoyable.

I am thankful to Dr. Ramya with whom I have spent a good time at PRL. My special thanks to my junior Rohit for his help, support and cooperation during the course of this thesis.

I wish to thank my seniors Drs. H. Gadhavi, D. Ganguly, N. Rastogi, L. Sahu, S. K. Rai, Y. C. Nagar, A. S. Maurya for their concern and help. Thanks to Amit, Satya, Subimal, Shreyash, Rohit, Sanat, Uma, Ritesh and Rajesh who helped me

in various ways and gave me valuable suggestions during this period.

I would like to thank all the members of the Computer center, especially Jigar bhai, Tejas, Alok, Mishra Ji for the help in computer related problems. The help from Uma madam, Nishtha madam, Pragya, Alam, and all the supporting staff of PRL library are thankfully acknowledged. Thanks to Parul madam, Priti madam, Pauline, Nandini madam, Jayashree, Ranganathan, R. S. Gupta, Ghanshyam Bhai, Senthil Babu and Sivadasan for their help in various stages.

I was lucky to enjoy the cheerful friendship of many people at PRL. Arvind, Anil, Gyana, Alok, Kirpa, Vishal, Bhavik, Rahman, Sanjeev, Ramji, Manan, Harinder, Lokesh, Shuchita, Sumanta and Timmy for making me feel at home. I feel great that I have a friend like Ashwini. I have spent a memorable time in his company onboard cruises, at Mount Abu and obviously in PRL. I would also like to thank my friends Pradeep, Sumit, Surya, Rashmi, Annu, Bharat and Ananta for their care and support.

I wish to thank my juniors Iman, Chinmay, Arvind Saxena, Kabitri, Amzad, Fazlul, Srinivas, Prashant, Neeraj, Vimal, Patra, Bhaswar, Jayati, Suratna, Yogita, Moumita and many others have helped me in several ways in the course of my Ph.D.

I cannot finish without saying how grateful I am to my parents, for their care, concern, blessing and love. I thank them for allowing me to get everything I wanted in my life. I am grateful to my didi and jiju for their continued support. My brother Sunil and my sister Monika are a source of happiness and refreshment for me. I am extremely indebted to my in laws for their love and support.

I was lucky enough to get my soul-mate Naveen (my husband) during the course of Ph.D. in PRL. I owe my loving thanks to him for his care, affection, love and support. He has contributed in enormous amount during the entire period in making my life happy. I have found him standing with me always when I required. Without his support, it would have been impossible for me to finish this work.

Sumita Kedia

Abstract

The concept of aerosol radiative forcing (ARF) is used to quantify the strength of aerosols from both natural and anthropogenic sources in causing climate change. The work is motivated from the rising concern for global climate change and the existing uncertainty in the current understanding due to the incomplete knowledge of aerosol optical and radiative properties, and their regional variations. The goal of present work is to study the optical, physical and radiative properties of aerosols including ARF, and their spatial and temporal variabilities over different environments in the Indian subcontinent and adjoining oceanic regions. The study locations in India include, Ahmedabad (urban, industrialized location), Gurushikhar (high altitude, remote site), Kanpur (urban, industrialized location over the Indo-Gangetic plain) and Gandhi College (rural site over the Indo-Gangetic plain). The oceanic regions include the Bay of Bengal and the Arabian Sea where the study has been carried out.

A large spatial and temporal variation in aerosol optical depth (AOD) is observed over both continental and marine environments. AODs over Ahmedabad and Gurushikhar showed winter low and summer or premonsoon high, while in Kanpur and Gandhi College winter AODs are found to be higher. AODs are found to be about 1.4 times higher over the Bay of Bengal (0.36) when compared to that over the Arabian Sea (0.25). Spectral distribution of AODs are further analyzed to obtain some crucial information on the physical and optical characteristics of aerosols by deriving the second derivative of spectral AOD ($\alpha^{'}$). The analysis revealed the dominance of wide range of fine mode fractions or mixture of modes during winter over Ahmedabad, Kanpur and Gandhi College; while coarse mode aerosols dominate over Gurushikhar. Over the marine environments, AOD spectra over the Bay of Bengal were predominantly made up of a mixture of fine modes while the Arabian Sea had more coarse mode particles during the study period.

The clear sky shortwave ARF and heating rate is estimated over all the study locations/regions and discussed. A large spatial and seasonal variability is observed in the ARF over all the study locations in India. The ARF values are found to be

highly sensitive to the single scattering albedo. Atmospheric forcing is found to be in the range of 12.3-54.0, 4.3-8.9, 20.8-36.2 and 22.2-34.2 Wm^{-2} over Ahmedabad, Gurushikhar, Kanpur and Gandhi College respectively during different seasons. Over the Bay of Bengal, the ARF is found to be higher than the forcing obtained over the Arabian Sea. The average atmospheric heating rate over Bay of Bengal is found to be $\sim$0.3 K/d, which is a factor of 2 higher than that over Arabian Sea. A sensitivity analysis revealed that (1) the curvature effect in AOD spectra has insignificant impact in modifying the ARF and heating rate, and (2) the net Earth-atmosphere energy content shows minor differences when aerosol vertical profiles are used for the estimation of forcing. The present study aims to improve the knowledge about the spatiotemporal variability and radiative effects of aerosols over the Indian landmass and the adjoining oceanic regions which will help in reducing the uncertainty in aerosol radiative forcing and its future projection on climate.

Key words: Aerosol optical depth, Spectral variabilities, Radiative forcing, Heating rates, Single scattering albedo, Vertical profile

Contents

Chapter 1

Introduction

1.1 Atmospheric Aerosols

Atmospheric aerosols are tiny particles, either solid or liquid, which are suspended in air. These are found with widely varying size, concentration and chemical composition depending on their sources and production mechanisms. Aerosols are produced both from natural processes as well as due to anthropogenic activities. The natural emission processes include volcanic eruptions, soil-dust uplift, sea-spray uplift, natural biomass burning fires and biological material release. Major anthropogenic sources include fossil fuel combustion, anthropogenic biomass burning and industrial emissions. These particles get distributed in the atmosphere through turbulent mixing and transport which result in their large spatial and temporal variations. On a global scale, the natural sources of aerosols are dominant over the anthropogenic sources (10-15%) [*Andreae*, 1995], but regionally anthropogenic sources can be three to five times larger than natural ones [*Ramanathan et al.*, 2001].

The size of aerosols extend over several order of magnitudes ranging from 0.001 μm to 100 μm. Based on their size, aerosols are generally classified into three categories *viz.,* (i) Nucleation mode (0.001-0.1 μm radius), (ii) Accumulation mode (0.1-1.0 μm radius) and (iii) Coarse mode (>1.0 μm radius) particles. Nucleation

mode aerosols are mostly formed through gas-to-particle conversion process in the atmosphere and due to the nucleation of atmospheric species. Aerosols in the accumulation mode are usually produced either by coagulation of smaller particles or by heterogeneous condensation of gas vapor onto existing smaller nucleation mode particles. Coarse mode aerosols are mainly formed by mechanical processes such as wind blown dust, breaking of bubbles on the sea surface, volcanic eruptions etc.

Aerosols get removed or destroyed from the atmosphere continuously through variety of dry and wet removal mechanisms. Dry deposition is the process by which particles are removed by the action of gravity, or impact on the surface because of its inertia or due to their Brownian motion (due to constant collisions with other particles and the surrounding gas molecules). The mobility of aerosols is less in lower altitude where the atmosphere is denser and it increases with increase in altitude. Since fall velocity is directly proportional to the particle mobility, the fall velocity is less at lower levels when compared to that at upper levels of the atmosphere. Also, larger and heavier particles have higher fall velocity compared to finer ones. Wet deposition of aerosols includes rainout, washout and sweepout. Rainout is the process by which aerosols are removed after acting as cloud condensation nuclei and subsequently start falling gravitationally to the surface as rain drops. When an aerosol is incorporated into an already existing cloud drop, and if that drop grows large enough to fall as rain, then the particle is said to have been washed out. Aerosols which are present below the base of a raining cloud are often impacted by the falling raindrops and if such an impact leads to the incorporation of the aerosol into the drop, the aerosol is deposited with the raindrop and is considered to be swept out from the atmosphere [*Seinfeld and Pandis*, 1998; *Jacobson*, 2002].

Once suspended in the atmosphere, aerosols can get transported over short or long distances before they are finally removed. During the course of transport, aerosols can grow due to coagulation or by condensation of vapors on them. The

processes of formation, coagulation, removal and transformation influence the residence times of aerosols in the atmosphere [*Jaenicke*, 1993]. The residence time of aerosol also depends on its size as well as the altitude at which they are present in the atmosphere. Nucleation mode aerosols get removed more quickly than the larger ones because of greater coagulation rate. On the other hand, larger particles (>10 μm) having higher settling velocities exhibit higher sedimentation rate and hence they too have smaller residence time in the atmosphere. For particles in the size range of 0.01 to 10 μm, the residence time in the lower troposphere is about a week, whereas in the upper troposphere they can stay up to a few months [*Ramachandran*, 1995].

1.2 The role of aerosols in the global atmosphere

The major driving force behind Earth's atmosphere is the solar radiation energy. The balance between the heating by incoming solar radiation and cooling by outgoing terrestrial radiation is the key factor that controls the Earth's climate [*Seinfeld and Pandis*, 1998]. In an equilibrium climate state of Earth's atmosphere, the total amount of solar radiation received by the Earth must be equal to the emission from the Earth's surface and atmosphere to space. Any factor that disturbs/alters this balance between the incoming and outgoing radiation or changes the redistribution of energy within the atmosphere can perturb the atmosphere and cause climate change. The imbalance in the net irradiance at any atmospheric level can be quantified in units of watts per square meter (Wm^{-2}) and is termed as '*radiative forcing*'. A positive radiative forcing tends to warm the atmospheric level while negative forcing cools it.

The radiative forcing for all the greenhouse gases is positive as all of them absorb the infrared radiation in the atmosphere. Greenhouse gases are globally well mixed due to longer lifetimes and their radiative effects are homogeneous throughout the globe and one of warming. In contrast, aerosols exhibit regional signatures and act to either warm or cool the atmosphere depending on their ability

to scatter or absorb the radiation. In the present scenario, atmospheric aerosols are gaining large importance because of their ability to affect the Earth's climate in different ways. Atmospheric aerosols play a crucial role in altering the balance of Earth-atmosphere system by scattering and absorbing the solar and terrestrial radiation which is known as the *direct effect*. Whether the particle will scatter or absorb the radiation depends on its chemical composition, refractive index and the size distribution. Presence of scattering and absorbing aerosols decreases the amount of radiation reaching the surface thereby producing cooling at the Earth's surface, however their effect in atmosphere vary with altitude [*Charlson et al.*, 1992; *Haywood and Boucher*, 2000; *IPCC*, 2007]. A completely scattering aerosol (e.g., sulfate) will cool the atmosphere, while an absorbing aerosol (e.g., black carbon) will warm the atmosphere. Since the aerosol properties show large spatial and temporal variability, the regional impact of aerosols can be different when compared to the global scale.

In addition to the direct effect, aerosols can also modify the microphysical properties and the lifetime of clouds which is known as the *indirect effect*. Aerosols play an important role in the formation of clouds. Aerosols serve as cloud condensation nuclei (CCN) around which cloud droplets are formed. An increase in the aerosol concentration can result in the formation of larger number of smaller droplets (as compared to an unperturbed cloud), but with decreased droplet radius. This results in an increased cloud albedo and thereby leads to a cooling effect known as *Twomey effect* [*Twomey*, 1977]. *Albrecht* [1989] proposed that an increase in the number of cloud droplets leads to a decrease in the mean droplet size for a given amount of available water. As the droplet becomes smaller, the precipitation will slow down resulting in an increased lifetime of cloud. Although the climatic effects of aerosols is mostly concentrated downwind of their source regions owing to their short lifetimes, but both direct and indirect effects of aerosols play significant roles on a global scale also as the radiative effects can get transported due to changes in the atmospheric dynamics. However, only direct effect of aerosols are the main

focus of the present study.

Some of the recent important results regarding direct and indirect effect of aerosols are:

Recently *Murphy et al.* [2009] examined the Earth's energy balance since 1950 through the measurements and radiative transfer models of ocean heat content, long-lived trace gases and volcanic eruptions. They found that about 20% of the total energy available to warm the Earth from greenhouse gases and solar radiation since 1950 has been diffused back into space. In contrast, 10% has gone into heating the Earth, almost all into the oceans. An additional 20% has been balanced by cooling associated with volcanic eruptions. The remaining 50% has been balanced by anthropogenic aerosols.

Christopher and Zhang [2004] used satellite data during 2000-2001 to estimate the direct clear sky shortwave ARF at the top of the atmosphere over the global oceans. The diurnal averaged clear sky ARF was found to be -5.3±1.7 Wm^{-2} at the top of the atmosphere. ARF over the northern hemisphere was reported to be about 1.5 times higher when compared to the forcing value over southern hemisphere. *Patadia et al.* [2008] followed a similar approach to estimate the direct shortwave ARF at the top of the atmosphere over the global land areas during 2000-2001. The forcing was found to vary from -3.5 Wm^{-2} to -7.8 Wm^{-2} with a global mean of -5.1±1.1 Wm^{-2}. In addition, the ARF in the northern hemisphere was found to be about 10% higher than that of the southern hemisphere.

Black carbon (BC), among the carbonaceous aerosols, is gaining considerable significance because of its ability to influence air quality and climate on local, regional and global scales. Black carbon aerosols are produced as primary particles from incomplete combustion processes such as fossil fuel and biomass burning, and hence most of the BC in the atmosphere mainly originates from human-made activities. BC emissions have varied in response to changes of fossil fuel usage and technology development, and the estimated fossil fuel BC emissions are the highest in the developing countries, especially China and India [*Novakov et al.*, 2003]. The

radiative and climate impacts of BC are increasingly recognized as it can absorb sunlight, heat the air, and contribute to global warming, unlike the other aerosol types (e.g., sulfate) which produce cooling. BC is the second strongest contributor to global warming next to carbon dioxide [*Ramanathan and Carmichael*, 2008].

Ramanathan and Carmichael [2008] have shown that BC forcing is 0.9 Wm^{-2} which is about 55% of the forcing due to CO_2 at the top of the atmosphere. In contrast, non-BC aerosols such as sulfates, nitrates and organics reflect more radiation and result in a negative top of the atmosphere forcing. This implies that, different aerosols behave differently with the radiation depending on their chemical properties. Therefore, a detailed knowledge of aerosol properties and their interaction with the radiation is essential to reduce the uncertainty in the estimation of their radiative effect.

The large amount of BC in emissions from biofuel combustion in south Asia has the potential for significant atmospheric impact. *Venkataraman et al.* [2005] examined the potential contribution of biofuel emissions by estimating spatial distributions of biofuel combustion and related BC emissions. They found that, the biofuel combustion (especially wood) is a potentially significant source of atmospheric BC and related climate effects in south Asia [*Venkataraman et al.*, 2005].

Lau et al. [2006] used General Simulation Model simulations to examine the direct effect of aerosols on the south Asian monsoon water cycle variability. According to their study, dust mixed with black carbon aerosols over the Indo-Gangetic Plain (IGP) get accumulated over the foothills of the Himalayas during premonsoon. This provides an elevated heat source through absorption of solar radiation and heats the air above the slope of Himalayas. As the air warms, it rises over the southern escarpment of the Tibetan Plateau, and subsequently more warm and moist low level air are drawn from the Indian Ocean as the monsoon season approaches. Because of the surface cooling due to aerosol absorption over central India, rainfall is suppressed. As a result, the moist air is able to penetrate farther inland into the foothills of the Himalayas, producing anomalous rainfall there.

This phenomenon was referred to as the Elevated Heat Pump (EHP) hypothesis and this process may lead to a strengthening of south Asian monsoon [*Lau et al.*, 2006].

Atmospheric brown clouds (ABC) are the layers of air pollution consisting of aerosols such as BC, organic carbon and dust which scatter and absorb the solar radiation. This absorption and scattering by ABC leads to a large reduction of UV and visible rays of solar radiation at the Earth's surface and this effect is known as solar dimming effect [*Ramanathan et al.*, 2005]. *Ramanathan et al.* [2005] showed that the solar dimming effect causes a reduction in evaporation from the ocean surface, thereby the latitudinal gradient in the sea surface temperature (which plays an important role in the monsoon dynamics and the tropical climate) decreases [*Meehl and Arblaster*, 2002]. This whole process increases the atmospheric stability, reduces the amount of moisture inflow into South Asia which in turn causes weakening of the monsoon rainfall [*Ramanathan et al.*, 2005].

Menon et al. [2002] used global climate model to investigate the possible contribution of aerosols in changing precipitation trend in recent decades over China and India. They suggested that increasing BC concentration from various industrial emissions and fossil fuel combustion could significantly enhance the intensity of storms and result in downwind rainfall. According to their study, the amount of solar radiation reaching the Earth's surface reduces due to absorption of sunlight by BC. This whole mechanism increases the atmospheric instability and can significantly contribute to the increased rainfall in the south while dust storms and drought in the north China, as well as to the climate change in India.

From this discussion, it is clear that aerosols not only affect the radiation budgets but can also the rainfall pattern in different ways. A detailed information of aerosol characteristics is important to understand variability in aerosol properties over different environments and their effects on the global climate. Therefore, there is a strong need for high quality, consistent and scientifically useful real time data of aerosol characteristics on a regional basis. The information about the aerosol

characteristics can be used in modeling, remote sensing as well as to assess the impact of these aerosols on the Earth's climate.

1.3 Motivation

In recent years, there has been a substantial increase in the interest for studying the influence of natural and anthropogenic aerosols on climate by direct and indirect effects over different environments [e.g., *Ramanathan et al.*, 2001; *Eldering et al.*, 2002; *Moorthy et al.*, 2004; *Di Girolamo et al.*, 2004; *Jayaraman et al.*, 2006; *Ganguly et al.*, 2006a; *Ramachandran and Cherian*, 2008; *Moorthy et al.*, 2008; *Dutkiewicz et al.*, 2009; *Kedia et al.*, 2010]. Despite this, aerosols are still a major source of uncertainty in the prediction of climate change due to inadequate information on the variabilities of aerosol characteristics at regional and temporal scales [*IPCC*, 2007]. The uncertainty in the estimation of climate forcing by aerosols can be reduced by studying the seasonal and interannual variations in aerosol properties over different locations in a region.

In this regard, aerosol characteristics retrieved from remote sensing technique such as, MODerate Imaging Spectroradiometer (MODIS) and Multi-angle Imaging Spectrometer (MISR) sensors on board Terra and Aqua satellites can provide a detailed knowledge over a large spatial range on long time scale. MODIS (Terra, Aqua) provides near-global daily observations of the Earth in a wide spectral range which are used to derive different aerosol properties over land and ocean [e.g., *Remer et al.*, 2008]. Similarly, MISR observes the Earth's environment globally and makes near simultaneous measurements at nine view angles to provide greater sensitivity while deriving aerosol optical depths (AODs) [*Di Girolamo et al.*, 2004; *Kahn et al.*, 2007]. However, validation of satellite derived data through collocated ground based direct measurements is very essential [*Remer et al.*, 2008] as the satellite retrieval involves *apriori* assumptions including the atmospheric composition over different regions across the globe. Furthermore, satellite retrievals are based on the radiant energy reflected and emitted by the Earth [*Remer et*

al., 2008]. In contrast, ground based instruments rely on the measurements of attenuation of solar radiation reaching the surface to determine AODs. The in situ measurements of optical, physical and chemical properties and their variability on various time scales provide essential inputs for validation of global models. Despite the fact that in situ data corresponds to point measurements, the AODs retrieved from ground based measurements are considered as the most reliable owing to lesser uncertainties as compared to satellite retrievals. In addition, ground based measurements can reliably be used to obtain continuous data on a variety of aerosol characteristics over a particular location [*Dubovik et al.*, 2002].

The Indian subcontinent and the surrounding regions are rich sources for many kinds of aerosols of both natural and anthropogenic origin such as mineral dust, soot, nitrates, sulfate and organic aerosols. The Indian subcontinent experiences tropical and subtropical climatic conditions resulting in extreme temperatures, rainfall and relative humidity. These features introduce large variabilities in aerosol characteristics on spatial and temporal scales over India. Synoptic scale wind patterns over India exhibit differing seasonal signatures during the year. During December-February winds are northeasterly which transport the pollutants which are mainly anthropogenic from the land (the polluted northern hemisphere) to the surrounding marine environments such as the Arabian Sea, the Bay of Bengal and the Indian Ocean. In contrast, during the southwest monsoon season of June-September winds are stronger, moist and are from the marine and western regions surrounding India. Measurements and analysis of aerosol properties and radiative forcing during different seasons are necessary to understand the influence of varying meteorological conditions on aerosol properties and radiative forcing.

In a few recent studies, spatiotemporal variability in aerosol properties over the Indian region have been studied using ground based and/or satellite measurements. However, either these studies are based on the results obtained from in situ measurements over a particular location [e.g., *Dey et al.*, 2004; *Singh et al.*, 2004; *Tripathi et al.*, 2005; *Ganguly et al.*, 2006a; *Niranjan et al.*, 2007; *Sreekanth et al.*,

2007; *Babu et al.*, 2008; *Dey and Tripathi*, 2008; *Gadhavi and Jayaraman*, 2010; *Menon*, 2004; *Singh et al.*, 2010] or the ground based data over a particular location are used for validation of satellite data, and further the satellite data has been employed to study a larger region [e.g., *Jethva et al.*, 2005; *Ramachandran*, 2007; *Ramachandran and Cherian*, 2008]. However, in the present study, for the first time, aerosol data are analyzed from a number of ground based stations (Ahmedabad, Gurushikhar, Kanpur and Gandhi College) situated in different regimes in south Asia. In addition, the present study is also conducted over the marine environments (the Bay of Bengal and the Arabian Sea) surrounding India. The analysis and documentation of the spatial, seasonal and interannual variabilities in aerosol characteristics, which is the objective of the present study, attain significance in the context of air quality and air pollution over this region, and regional and global climate as well.

1.4 Objective and scope of the present work

The present study has been carried out to study the aerosol characteristics over an urban/industrial environment *Ahmedabad*, a high altitude remote location *Gurushikhar*, an urban location *Kanpur* and a rural village location *Gandhi College* situated in most polluted and highly populated Indo-Gangetic plain. In addition, the study is also conducted over the marine regions surrounding India (the Bay of Bengal and the Arabian Sea).

Major part of thesis is dedicated to the seasonal and interannual as well as spatial variations of aerosol optical, physical and radiative properties over different environments during 2006-2008. The specific objectives of the thesis are as follows:

- *To characterize the spatial and temporal variabilities in aerosol optical and physical characteristics over different regions of the Indian subcontinent and the adjoining oceanic regions.*
- *To study the spectral dependence of the optical properties of aerosols over*

India and the surrounding marine environments.

- *To estimate the aerosol radiative forcing and heating rates and their seasonal variability over urban, remote and marine regions using aerosol optical, physical and chemical characteristics and their climate implications.*

The details about the measurements, methodology, data and analysis procedure used to retrieve different aerosol properties from ground based measurements and the data obtained from different satellite measurements are given in *Chapter 2*. Results obtained on the spatial and temporal variability of aerosol optical properties and the spectral dependence over different locations in India are discussed in *Chapter 3*. During favorable wind conditions, anthropogenic aerosols from the continents get transported to the otherwise pristine oceanic regions such as the Bay of Bengal, the Arabian Sea and the tropical Indian Ocean.

In order to study the transport of aerosols, their physical characteristics and to estimate the amount of anthropogenic aerosols over oceanic regions, a cruise campaign was conducted over the Bay of Bengal and the Arabian Sea during pre-monsoon season of March-May 2006. The campaign provided a unique opportunity to study the spatial and temporal variability in the aerosol properties over the two marine environments. Results obtained on aerosol optical properties and size distribution from this study are discussed in *Chapter 4*. The implication of the measured aerosol properties and the radiative forcing with their spatial and temporal variabilities are estimated. The measured aerosol parameters have been utilized for the estimation of aerosol radiative forcing for all the study locations/regions both over land and oceans. In addition, the vertical distribution of aerosol radiative forcing and the atmospheric heating rate is determined and discussed. Results obtained on the model estimates of aerosol radiative forcing and its sensitivity to different parameters are presented and discussed in *Chapter 5*. The summary of the results obtained and the scope for future research are projected in *Chapter 6*.

Chapter 2

Measurements, Methodology, Data, and Analysis

The physical and optical properties of aerosols have been examined in detail by both in situ and remote sensing measurements over different environments during the study period. The instruments used along with a brief description of their measurement techniques and working principles are presented in this chapter. As the same instruments have been used for the measurement of aerosol parameters over different study locations, discussions on methodology and working principle of these instruments are not repeated in subsequent chapters.

2.1 Aerosol optical depth

Aerosol optical depth (AOD) is a measure of the attenuation of solar radiation due to aerosols when it passes through the atmosphere from the top of the atmosphere to the surface. The AOD value depends on the concentration of aerosols in the atmosphere and aerosol size distribution. In the present study, three different sun photometers are used for the measurement of AOD (hand held sun photometer, a pair of Microtops II sun photometers) over Ahmedabad and Gurushikhar. Measurements of AOD are conducted using hand held sun photometers (October 2006 - December 2007), and a pair of Microtops-II sun photometer (January 2008 -

December 2008) over Ahmedabad and Gurushikhar. The measurements were conducted everyday at 1-hour time interval from 0900 to 1700 Local Standard Time (LST) under clear sky conditions. Every month, for about a week, AODs were measured over Gurushikhar during the entire study period.

2.1.1 Sun photometer

The sun photometer measures the solar radiation intensity at six different wavelength bands centered around 0.40, 0.50, 0.675, 0.75, 0.875 and 1.02 μm each with a bandwidth of about 0.01 μm. The field of view of the sun photometer is about 4^o [*Acharya and Jayaraman*, 1995; *Kedia et al.*, 2010]. Filters were calibrated routinely using a UV-visible spectrophotometer. The photometer was pointed towards the Sun manually with the help of a pointer attached to the instrument. It should be noted that over the oceanic regions (the Bay of Bengal and the Arabian Sea) AODs were measured at 0.65 μm (instead of 0.675 μm) [*Kedia and Ramachandran*, 2008a].

2.1.2 Microtops II sun photometer

The hand held Microtops II sun photometer (Solar Light Co., USA) can measure AODs at five wavelength bands centered around 0.38, 0.44, 0.50, 0.675 and 0.87 μm [*Morys et al.*, 2001]. AODs at 1.02 μm have been measured using another Microtops-II. Field of view for Microtops instrument is 2.5^o and the band width of each filter is about 0.01 μm. A sun target and pointing assembly is present which ensures accurate alignment of Microtops II with the optical channels.

2.1.3 Theoretical background and calibration constants: Sun photometer and Microtops II

AOD values are derived from the direct measurement of solar radiance at each wavelength and using a calibration constant corresponding to that wavelength. Derivation of AOD is based on *Beer-Lambert-Bouguer* law as follows,

$$\tau_\lambda = \frac{-1}{m}\left[ln\left(\frac{I_\lambda}{I_{0\lambda}}\right) - 2ln\left(\frac{r_o}{r}\right)\right] \tag{2.1}$$

where τ_λ is the total columnar optical depth of the atmosphere at wavelength λ, I_λ is the instantaneous solar radiation intensity measured using sun photometer (and/or Microtops II) and $I_{o\lambda}$ is the solar radiation intensity at the top of the atmosphere derived using Langley plot technique (*discussed next*), m is the relative air mass, r is the instantaneous Sun-Earth distance and r_o is the Sun-Earth distance when $I_{o\lambda}$ is evaluated. The relative air mass (m) is the ratio of actual path length traveled by light beam in the atmosphere to that it would have traveled in vertical direction. The air mass depends upon solar zenith angle and is calculated using an empirical relation given by *Young* [1994]:

$$m = \frac{1.002432\ cos^2\chi + 0.148386\ cos\chi + 0.0096467}{cos^3\chi + 0.149864\ cos^2\chi + 0.0102963\ cos\chi + 0.000303978} \tag{2.2}$$

where χ is the solar zenith angle at the time of measurement which is calculated from,

$$cos\chi = cos\delta\ cos\phi\ cosH + sin\delta\ sin\phi \tag{2.3}$$

where δ is the Sun's declination angle taken from *Astronomical ephemeris* for individual day, ϕ is longitude of the measurement location and H is the hour angle. Equation 2.2 takes care of atmospheric refraction and Earth's curvature effect to provide better accuracy at all zenith angles. However, equation 2.2 simplifies to m = secχ for smaller zenith angles ($<60^o$) .

The solar radiation intensities measured at a high altitude remote location, Gurushikhar (at ∼1.7 km above mean sea level) are periodically used for the calibration of both sun photometer and Microtops-II using Langley plot technique. The $I_{o\lambda}$ values calculated for all the wavelengths were then used for subsequent measurements. In Langley plot technique, the natural logarithm of solar intensity

measured at ground level is plotted as a function of airmass. A least square fitted straight line is drawn through these observed data points and extrapolated to meet zero airmass in the abscissa. The intercept obtained for each wavelength which provides $I_{o\lambda}$.

Table 2.1: *Calibration constants I_o (in mV) as a function of wavelength for hand held sun photometer and Microtops II obtained using Langley plot technique from the measurements made during 2006-2008 at Gurushikhar.*

Sun photometer							
		Wavelengths (μm)					
Month	Year	0.40	0.50	0.675	0.75	0.875	1.02
November	2006	2.92	8.49	10.62	8.25	11.47	6.08
March	2007	2.88	8.38	10.76	8.30	11.52	6.10
April	2007	2.97	8.61	10.47	8.19	11.42	6.05
Microtops II							
		Wavelengths (μm)					
Month	Year	0.38	0.44	0.50	0.675	0.87	1.02
January	2008	2.05	1.01	0.90	1.08	0.65	1.07
April	2008	2.08	1.03	0.91	1.09	0.65	1.05

Ideally $I_{o\lambda}$ should remain constant in time for a particular photometer. However, because of deterioration in detector or filter characteristics $I_{o\lambda}$ value can change and a periodical calibration of sun photometer is therefore necessary. Table 2.1 presents the $I_{o\lambda}$ values for sun photometer and Microtops II for different months during 2006-2008. It should be noted that each of these values represents the mean of I_o calculated from the measurements made in Gurushikhar for about a week. The sun photometer was calibrated during 18-25 Feb 2006 and $I_{o\lambda}$ values were calculated before the cruise expedition that was conducted over the Bay of Bengal and the Arabian Sea during Mar-May 2006. These $I_{o\lambda}$ values were then used in the estimation of AODs at the respective wavelengths [*Kedia and Ramachandran*, 2008; *Kedia et al.*, 2010].

The total columnar optical depths (τ_λ) are calculated for each wavelengths and for individual set of measurements. The total optical depth is given by,

$$\tau = \tau_r + \tau_a + \tau_m \tag{2.4}$$

where τ_r is the optical depth due to Rayleigh scattering (air molecules), τ_m is the optical depth due to molecular absorption such as ozone, water vapor and nitrogen dioxide and τ_a is the AOD. An air column density of 2.16×10^{25} molecules cm^{-2} appropriate for the tropical region is used for the estimation of Rayleigh scattering contribution [*Ramachandran and Jayaraman*, 2003a]. Molecular absorption has been taken into account for the air molecules, ozone, water vapor and O_2 based on their concentrations defined for the tropical atmosphere. Contribution due to nitrogen dioxide is less than 0.5% in this wavelength region and is not considered in the present study. The uncertainties in the AOD measurement arise from (i) instrumental error due to bias and precision, and (ii) ignoring the forward scattering contribution to the measured irradiance.

For the sun photometer, the solar radiation intensities are measured with an accuracy better than 1%. The forward scattered radiation within the field of view of sun photometer is found to decrease by <8% at 0.4 μm and 5% at 0.875 μm. Typically, at 0.4 μm Rayleigh scattering contributes about 40% and aerosols contribute the rest to the total optical depth; at 0.875 μm the contribution from Rayleigh scattering decreases to 5% while the contribution due to aerosols increases to >90%. The maximum uncertainty in retrieved AODs due to errors in measurements and assumptions involved is estimated to be <15% [*Kedia et al.*, 2010]. The absolute uncertainty in AODs retrieved from Microtops II measurements is found to be <0.03 for all the wavelengths.

2.1.4 AERONET

AEosol RObotic NETwork (AERONET) is a ground based sun/sky scanning radiometer established by National Aeronautics and Space Administration (NASA),

USA which measures the total ambient aerosol characteristics at different wavelengths [*Holben et al.*, 1998; *Smirnov et al.*, 2000]. The radiometer makes measurements of the direct Sun and diffuse sky radiance in the spectral range of 0.34-1.02 μm with a field of view of 1.2^o [*Holben et al.*, 1998]. The direct solar radiation measurements made at every 15 minutes and at different wavelengths are used to acquire AOD data. In addition, there are two basic sky radiance observation modes (almucantar and principle plane) which are used to retrieve the size distribution, single scattering albedo (SSA) and refractive indices of the aerosols [*Holben et al.,1998*; *Smirnov et al.*, 2000; *Dubovik et al.*, 2000; *Dubovik and King*, 2000]. In the present study, AOD data obtained in the wavelength bands of 0.38, 0.5, 0.675, 0.87 and 1.02 μm, while SSA and aerosol volume size distribution obtained at 0.44, 0.675, 0.87 and 1.02 μm for two AERONET sites Kanpur and Gandhi College during 2006-2008 are used. The uncertainty in calculation of AOD under cloud free conditions is $< \pm 0.01$ when $\lambda > 0.44$ μm and $< \pm 0.02$ for shorter wavelengths, and is $< \pm 5\%$ for the sky radiance measurements (e.g., SSA and size distribution) [*Holben et al.*, 1998; *Smirnov et al.*, 2000]. In the present study, AERONET level 2.0 data which are quality assured and cloud screened are utilized.

2.2 Ångström coefficients (α, β)

Characterization of aerosols and the spectral dependence of their optical properties are key parameters that strongly influence the Ångström parameters (α, β), and the aerosol radiative properties such as aerosol phase function, single scattering albedo [*Eck et al.*, 1999; 2001]. Such a characterization is useful for modeling the radiative effects of aerosols on the surface and the atmosphere, retrieval of aerosol parameters from satellite remote sensing, applying correction for aerosol effects in remote sensing of the Earth's surface, and further in identifying aerosol source regions and their evolution [*Eck et al.*, 1999].

The spectral variation of aerosol optical depth (τ) can be represented by Ångström power law [*Ångström*, 1961] given by,

$$\tau = \beta\lambda^{-\alpha} \tag{2.5}$$

where λ is the wavelength in μm, α and β are Ångström parameters. α is the Ångström exponent which depends on aerosol size distribution and β (AOD at 1 μm), the turbidity coefficient is directly proportional to the amount of aerosol particles along the Sun path. The value of α depends on the ratio of concentration of smaller to larger aerosols in the aerosol size distribution and β depends on columnar aerosol loading in the atmosphere. Higher α signifies an increase in the concentration of smaller size particles and a decrease in the concentration of larger particles whereas a lower α indicates an abundance of super micron aerosols.

Ångström exponent (α) can also be computed following the Volz method using any pair of wavelengths as,

$$\alpha = -\frac{dln\tau}{dln\lambda} = -\frac{ln(\frac{\tau_1}{\tau_2})}{ln(\frac{\lambda_1}{\lambda_2})} \tag{2.6}$$

where τ_1 and τ_2 are the AODs at wavelengths λ_1 and λ_2. The above expression shows that α is the negative of the slope of ln AOD versus ln λ data. Typical values of α estimated from AODs measured in the 0.44-0.87 μm wavelength regime are found to vary from 1 to 3 for fresh smoke particles which is dominated by accumulation mode aerosols to nearly zero for the atmosphere dominated by coarse mode aerosols such as dust and sea salt [*Holben et al.*, 2001; *Eck et al.*, 2001]. In the present work, α and β values are estimated by further analysing the individual data set of AODs in the wavelength range of 0.40-0.875 μm (0.4, 0.5, 0.675 and 0.875 μm) incase of sun photometer and 0.38-0.87 μm (0.38, 0.5, 0.675 and 0.87 μm) in case of data obtained from Microtops II and AERONET. To maintain uniformity and for comparison purposes AODs obtained at 0.4 μm (and at 0.38 μm in case of Microtops II and AERONET), 0.5 μm, 0.675 μm, 0.875 μm (and at 0.87 μm in case of Microtops II and AERONET), and 1.02 μm from sun photometer, Microtops II and AERONET over the study locations only are utilized. The differences, if any,

due to small changes ($\leq$0.025 μm in wavelengths) at which the AOD measurements were made, are expected to be negligible and are not considered in the present study. The α and β values are calculated by least squares fitting AODs against the respective wavelength on a log-log plot.

Ångström exponent α has been used in many studies as a tool to quantify particle size distribution from spectral distribution of AODs and for extrapolating AOD throughout the shortwave spectral region [e.g., *Smirnov et al.*, 2002]. However, the Ångström power law is rigorously valid for all the wavelengths only if the particle size distribution fits a Junge power law function [*Hess et al.*, 1998]. The Junge power law distributions are accurate only over a limited size range, and extrapolation to smaller or larger sizes may introduce significant errors of the ambient aerosol size distribution, which is generally multimodal [*Junge*, 1955]. Therefore, the Ångström relation is not appropriate for all environments and locations [*Reid et al.*, 1999; *Eck et al.*, 1999, 2001; *Kaskaoutis and Kambezidis*, 2006] as well as in extended wavelength bands. The α value strongly depends on the wavelength region used for its determination. Negative values of α can also occur for narrow wavelength bands in the visible and near-infrared spectrum when AODs increase with wavelength, indicating an inverse spectral dependence [e.g., *Cachorro et al.*, 2001; *Adeyewa and Balogun*, 2003].

2.2.1 First order derivative of Ångström exponent

In the ambient atmosphere, the size distribution of aerosol is typically bimodal and is made up of a fine mode produced by combustion processes and/or gas to particle conversion and, a mechanically produced coarse mode. Therefore, departure from linear behavior of ln τ versus ln λ is observed [e.g., *Reid et al.*, 1999; *Eck et al.*, 1999, 2001; *O'Neill et al.*, 2001; *Kaskaoutis and Kambezidis*, 2006; *Schuster et al.*, 2006], and a linear fit is found to yield significant difference when compared to the measured AODs. Owing to this discrepancy, a curvature is observed in the AOD spectra which contains useful information about the aerosol size distribution [*Reid*

et al., 1999; *Eck et al.*, 1999, 2001; *O'Neill et al.*, 2001; *Kaskaoutis and Kambezidis*, 2006; *Schuster et al.*, 2006; *Kaskaoutis et al.*, 2007].

Under such condition, a second order polynomial fit is used to correlate with the measured AOD which can be written as,

$$ln\tau = \alpha_2 \ (ln\lambda)^2 + \alpha_1 \ ln\lambda + \alpha_0 \tag{2.7}$$

where α_0, α_1, and α_2 are constants. Coefficient α_2 represents the curvature observed in the spectral distribution of AODs. The coefficients α_1 and α_2 can be used to get significant information about aerosol type and size distribution. *Schuster et al.* [2006] showed that $\alpha_2 - \alpha_1$ values can reveal the dominant type of aerosols (whether fine or coarse) in the aerosol size distributions. This can be explained as: when curvature is negligible ($\alpha_2 \sim 0$) then $\alpha = -\alpha_1$, which is consistent with $\alpha = \alpha_2 - \alpha_1$. Accordingly, the AOD spectra for which $\alpha_2 - \alpha_1 \geq 2$ will be dominated by fine mode aerosols and $\alpha_2 - \alpha_1 \leq 1$ represents coarse mode aerosols. The AOD spectra with $\alpha_2 - \alpha_1$ values in between 1 and 2 will occur owing to a wide range of fine mode fractions or mixture of modes.

To quantify the deviation from linear behavior of ln τ versus ln λ data, derivative of Ångström exponent ($\alpha^{'}$) is derived following *Eck et al.* [1999] as,

$$\alpha^{'} = \left(\frac{-2}{ln\lambda_{i+1} - ln\lambda_{i-1}}\right)\left(\frac{ln\tau_{i+1} - ln\tau_i}{ln\lambda_{i+1} - ln\lambda_i} - \frac{ln\tau_i - ln\tau_{i-1}}{ln\lambda_i - ln\lambda_{i-1}}\right) \tag{2.8}$$

From Ångström power law (equation 2.6) and the second order polynomial fit (equation 2.7), $\alpha^{'}$ can also be obtained as,

$$\alpha^{'} = \frac{d\alpha}{dln\lambda} = -2\alpha_2 \tag{2.9}$$

Near zero value of $\alpha^{'}$ indicates a constant slope of the AOD spectra (thereby proving the validity of power law) while higher $\alpha^{'}$ values suggest rapidly changing slope of the AOD spectra. Positive $\alpha^{'}$ values indicate the dominance of fine mode

aerosols while negative $\alpha^{'}$ values suggest the dominance of coarse mode aerosols in the bimodal aerosol size distribution.

Results from the earlier studies [e.g., *Eck et al.*, 1999, 2001; *Kaskaoutis et al.*, 2007] conducted over different environments showed that the curvature in the ln τ versus ln λ data was large for low turbidity conditions when the fine mode particles were dominant in the atmosphere; for large particles (desert dust aerosols) the curvature was not significant. The curvature in the ln τ versus ln λ data was found to be concave (α_2 <0, $\alpha^{'}$ >0) when fine mode particles dominated the aerosol size distribution (such as biomass burning, urban or industrial aerosols); the curvature was convex ($\alpha_2 > 0$, $\alpha^{'}$ <0) for the atmosphere with dominant coarse mode aerosols (such as dust, sea salt) or bimodal distribution with significant relative magnitude of coarse mode particles [*Eck et al.*, 1999, 2001].

2.3 Aerosol scattering and absorption coefficients

Next to AOD, the second most important parameter required for the estimation of radiative forcing due to aerosols is the single scattering albedo (SSA). Single scattering albedo is a measure of the proportion of scattering and absorption in the light extinction by aerosol. It is defined as a ratio of scattering coefficient (β_{sca}) to extinction coefficient (β_{ext}). Aerosol scattering and absorption coefficients are measured over Ahmedabad using a 3-wavelength Integrating Nephelometer (*3563, TSI Inc., USA*) and a multiwavelength Aethalometer (*AE-47 of Magee Scientific, USA*), respectively during 2006-2008.

2.3.1 Integrating Nephelometer

An integrating Nephelometer is used to measure the total aerosol scattering (β_{sca}) and the hemispheric backscattering ($\beta_{backsca}$) coefficients at 0.45, 0.55 and 0.70 μm in the present study. The instrument draws air sample through a large diameter inlet port into the measurement volume. Then the measurement volume is illuminated by a flash lamp and the scattered light intensity is measured at 0.45, 0.55

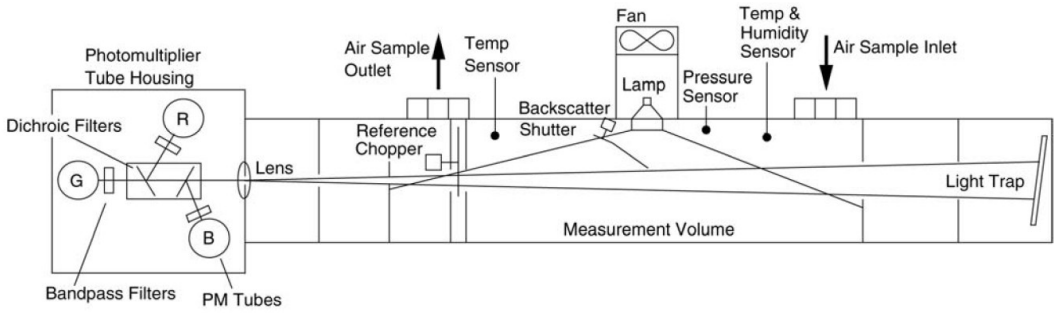

Figure 2.1: *Block diagram of the Integrating Nephelometer (model 3563, TSI Inc., USA) used in the present study for the measurement of aerosol scattering coefficient. (Source: The Integrating Nephelometer, Operation manual, TSI)*

and 0.70 μm by a photomultiplier tubes kept perpendicular to air flow. The main body of the Nephelometer consists of a thin walled aluminum tubing (Figure 2.1). The receiving optics are located at one end of the main tube and a light trap is located at the other end to provide a dark reference to view the light scattered by particles and gas as shown in Figure 2.1.

The Nephelometer uses a reference chopper to calibrate scattered signals. The chopper consists of three separate areas such as signal, dark and calibrate. The signal section allows all light to pass through unaltered. The dark section is a very black background that blocks all light providing a measurement of the photomultiplier tube background noise. The calibrate section is directly illuminated by the light source to provide a measure of lamp stability over time.

An automated ball valve built into the inlet is activated periodically and all of the aerosol sample is diverted through a high efficiency filter to obtain a measure of clean air signal pertaining to the operating environment. The span calibration is done by passing gases of high scattering coefficient such as CO_2 whose scattering coefficient is higher by a factor of 2.61 than that of particle free air. Built-in temperature and pressure sensors allow calculation of changes in Rayleigh scattering coefficients at three wavelengths. From the total signal, the clean air signal and

dark current of photomultiplier are subtracted to obtain the aerosol scatter signal [*Ramachandran and Rajesh*, 2008].

Measurements of aerosol scattering coefficient (β_{sca}) were conducted in a continuous mode during 2006-2008 with data averaging time of 5 minutes over Ahmedabad. The uncertainties in Nephelometer measurements arise due to noise in the filtered air scattering coefficient, calibration drift, calibration of the instrument for Rayleigh scattering of dry air and CO_2 and truncation of near scattered forward light [*Anderson et al.*, 1996; *Anderson and Ogren*, 1998]. The overall uncertainty in β_{sca}, taking into account all the above sources of uncertainty, is estimated to be about 15% [*Ramachandran and Rajesh*, 2008].

2.3.2 Multiwavelength Aethalometer

Black carbon (BC) mass concentration and absorption coefficient of aerosols (β_{abs}) are measured over Ahmedabad using a seven channel Aethalometer during the study period in almost continuous mode. This instrument measures the attenuation of light beam at seven different wavelengths *viz.,* 0.37, 0.47, 0.52, 0.59, 0.66, 0.88 and 0.95 μm transmitted through the sample collected on a quartz fiber filter [*Hansen et al.*, 1984]. The attenuation is directly proportional to the amount of BC loading in the filter deposit. The light transmission is detected using a set of two photo diodes, one through the sample spot and the other through a blank or an unsampled portion of the filter which is called the reference spot. Absorption coefficients of aerosols as a function of wavelength are calculated following *Bodhaine* [1995] and *Weingartner et al.* [2003] as,

$$\beta_{abs} = \frac{-1}{C\ R}\left[\frac{A\ ln(i_2/i_1)}{Q\ (t_2 - t_1)}\right] \tag{2.10}$$

where i_1 and i_2 are the ratios of the intensities of sample beam to the reference beam at time t_1 and t_2 (in seconds) respectively. Q is the volume of air sampled during the time interval Δt $(t_2 - t_1)$, and A is the area of the exposed spot on the filter where aerosols are collected. C is the correction factor applied to account

for any change in the absorption occurring due to multiple light scattering effects within the filter. R is an empirical correction factor and describes the change in the Aethalometer response with increased particle loading on the filter [*Ramachandran and Kedia*, 2010]. Black carbon mass concentrations are determined from the absorption coefficients [*Gundel et al.*, 1984; *Bodhaine*, 1995; *Weingartner et al.*, 2003] as,

$$Mass_{BC}(\lambda) = \frac{\beta_{abs}(\lambda)}{\sigma_{abs}(\lambda)} = \frac{\beta_{abs}(\lambda)C}{\sigma_{atn}(\lambda)} \tag{2.11}$$

where $\sigma_{abs}(\lambda)$ and $\sigma_{atn}(\lambda)$ ($= \sigma_{abs}(\lambda)$ C) are the mass specific absorption and attenuation cross-sections, respectively. The value of $\sigma_{atn}(\lambda)$ is taken as $14.625/\lambda$ μm m$^2 g^{-1}$ which results in an absorption efficiency of 16.6 m$^2 g^{-1}$ at 0.88 μm. BC mass concentration measured at 0.88 μm wavelength is considered to represent a true measure of BC in the atmosphere as at this wavelength BC is the principal absorber of light while the other aerosol components have negligible absorption [*Bodhaine*, 1995]. Data obtained from other channels can be considered as equivalent BC mass that will produce the same absorption. If the absorbing component of the aerosols being sampled consists only of black carbon, then the BC mass obtained from all the channels of Aethalometer would be identical.

The uncertainties in BC mass concentration estimates arise because of the changes in filter scattering due to aerosol loading, underestimation of the measured Aethalometer signals (or BC mass concentrations) with increasing filter loads, and empirical conversion from optical absorption to BC mass [*Weingartner et al.*, 2003; *Bond and Bergstrom*, 2006]. In the present study, wavelength dependent values for C following *Bodhaine* [1995] and *Bond and Bergstrom* [2006] are used. The monthly mean BC mass concentrations obtained in the present study are at least two orders of magnitude higher than the noise level BC mass concentration [*Ramachandran and Kedia*, 2010]. Another source of uncertainty in the measurement of BC could be the presence of Hematite (Fe_2O_3) in dust which is the other strong absorber

in the atmosphere at 0.88 μm. However, the absorption cross-section of dust is smaller than BC by more than 100 times. Instrumental artifacts such as flow rate, filter spot area and detector response are estimated to contribute an error of ∼1% in the measured BC mass concentrations. The overall uncertainty in the BC mass concentrations and the absorption coefficient reported in this study is estimated to be 10% [*Ramachandran and Kedia*, 2010].

Single scattering albedo (SSA) can be calculated using the aerosol scattering coefficient (β_{sca}) and the absorption coefficient (β_{abs}) as,

$$SSA = \frac{\beta_{sca}}{\beta_{sca} + \beta_{abs}} \tag{2.12}$$

Absorption coefficient at 0.55 μm over Ahmedabad is calculated using the mean of β_{sca} measured at 0.52 and 0.59 μm. The SSA at 0.55 μm is then calculated using β_{sca} and β_{abs} in equation 2.12. The error in SSA due to the uncertainty in β_{sca} is estimated to be 6%, while the error in SSA due to uncertainty in β_{abs} is about 4%. β_{sca} values are always higher than β_{abs} (at least by 50% or more, as will be seen later). The maximum error in SSA estimation taking into account the uncertainties in β_{sca} and β_{abs} is found to be 5%. Nevertheless, an underestimation of β_{sca} due to truncation loss in Nephelometer and a possible overestimation of β_{abs} from Aethalometer will exert opposite effects in the estimation of SSA. Therefore, the errors propagating from these two instruments will partially cancel the error in the estimation of SSA [*Ganguly et al.*, 2005a].

2.4 Aerosol properties obtained from remote sensing

In the present work data retrieved from two satellite sensors, namely, MODIS and MISR have also been used for the analysis of aerosol characteristics and their spatial and temporal variability over the study locations. The details of the satellite data sets used and the methodology adopted are stated below.

2.4.1 MODIS TERRA/AQUA satellites

The MODerate resolution Imaging Spectroradiometer (MODIS) is a remote sensor with two Earth Observing System (EOS) Terra and Aqua satellites the data of which can be used to study aerosols from space with high accuracy and on a nearly global scale [*Kaufman et al.*, 1997; *Yu et al.*, 2004; *Remer et al.*, 2008]. MODIS satellites operate in sun-synchronous, near polar orbits at an altitude of 705 km above the Earth. The Terra spacecraft crosses the equator at about 10.30 LST (ascending northward) while Aqua spacecraft crosses the equator at around 13.30 LST (descending southward). MODIS derived aerosol products over land and oceans have been tested, validated, compared and are being extensively used to investigate spatiotemporal variations in aerosol optical characteristics [*Levy et al.*, 2007; *Remer et al.*, 2008]. The predicted retrieval uncertainty of MODIS AODs is $\pm$ (0.05 + 0.15AOD) over land while it is $\pm$ (0.03 + 0.05AOD) over oceanic regions [*Remer et al.*, 2008]. In this work, Level 3 MODIS Collection V005 atmosphere daily global products (e.g., AOD, Ångström exponent (α) and fine mode fraction (FMF)) at $1^o \times 1^o$ grid are utilized both over land and ocean. Daily AOD and FMF, the ratio of accumulation mode optical depth to total optical depth at 0.55 μm, are obtained during the study period both over land and oceans from MODIS Terra and Aqua satellites, and daily mean (Terra+Aqua) values are calculated. The daily mean AODs are further used to calculate the seasonal mean AODs for all the study locations and utilized.

2.4.2 MISR

Multi-angle Imaging Spectroradiometer (MISR) aboard the Terra spacecraft images the Earth at nine discrete view angles ranging from 70^o aftward to 70^o forward and at four different wavelengths (0.446, 0.558, 0.672 and 0.866 μm) [*Diner et al.*, 2001; *Abdou et al.*, 2005; *Kahn et al.*, 2005, 2007]. AODs are obtained using MISR standard aerosol retrieval algorithm at a resolution of 17.6 km, by analyz-

ing MISR top-of-atmosphere radiance. Daily MISR Level-2 0.555 μm AOD data over Ahmedabad, Gurushikhar, Kanpur, and Gandhi College are obtained for the period of 2006-2008 and the seasonal mean are calculated and utilized. The uncertainty in the MISR retrieved AODs are reported to be $< \pm 0.05$ or 20% [*Patadia et al.*, 2008].

Chapter 3

Aerosol optical and physical characteristics over different locations in India

South Asia comprises India, Pakistan, Nepal, Bhutan, Bangladesh and Sri Lanka. It is densely populated as more than one-fifth of the world population lives in this region. Its landscape varies from mighty peaks of Himalayas in north, through vast plain and arid desert, to tropical forest and coastal regions in the south. The south Asian region experiences tropical and subtropical climatic conditions resulting in wide range of temperatures, rainfall and relative humidity which corroborate large spatial and temporal variability in aerosol characteristics over this region [e.g., *Ramachandran and Cherian*, 2008]. The region is a potential source for different types of both natural and anthropogenic aerosols such as mineral dust, black carbon, sulfate, nitrates and other organic water soluble substances. This region in general and India in particular, due to rapidly growing industrialization and expanding urbanization in recent years has become a major regional aerosol hot spot.

This chapter presents results on various optical and physical properties of aerosols using the measurements made over four different locations in India dur-

ing 2006-2008. In addition to the spatial variability, the seasonal and interannual variabilities in aerosol properties over the study locations are discussed which has implications for aerosol radiative forcing over the study region.

3.1 Topography

The present study focuses on studying the variabilities, in aerosol characteristics over four different locations (Ahmedabad, Gurushikhar, Kanpur and Gandhi College) situated in different regimes in India. Each of these study location is characterized by different environments (Figure 3.1, Table 3.1).

Table 3.1: *Topography and environment of study locations: (a) Ahmedabad, (b) Gurushikhar, (c) Kanpur and (d) Gandhi College.*

Location	**Latitude** (^{o}N)	**Longitude** (^{o}E)	**Altitude** (m AMSL)	**Environment**
Ahmedabad	23.03	72.55	55	*Urban, industrialized*
Gurushikhar	24.65	72.78	1680	*High altitude, remote*
Kanpur	26.51	80.23	123	*Urban, industrialized*
Gandhi College	25.87	84.13	60	*Rural, downwind of major urban centers*

Ahmedabad is an industrialized urban location in western India with several small and large scale industries including two power plants [*Ramachandran and Rajesh*, 2007]. The city has a population of ∼5.8 million and is located in the southeast direction of the Thar desert (Figure 3.1). Gurushikhar, Mount Abu is a relatively pristine site and is ∼300 km northeast of the Thar desert. The site is situated at the highest peak of Aravalli range of mountains in western India with a cleaner and stable atmosphere where the effect of local pollution is minimum. During winter Gurushikhar exhibits free tropospheric characteristics as the boundary layer height is lower than the altitude of Gurushikhar; while during summer Gurushikhar lies within the boundary layer. Kanpur and Gandhi College

are situated in the Indo-Gangetic basin which is one of the largest river basins in the world, and is one of the densely populated and highly polluted regions in India.

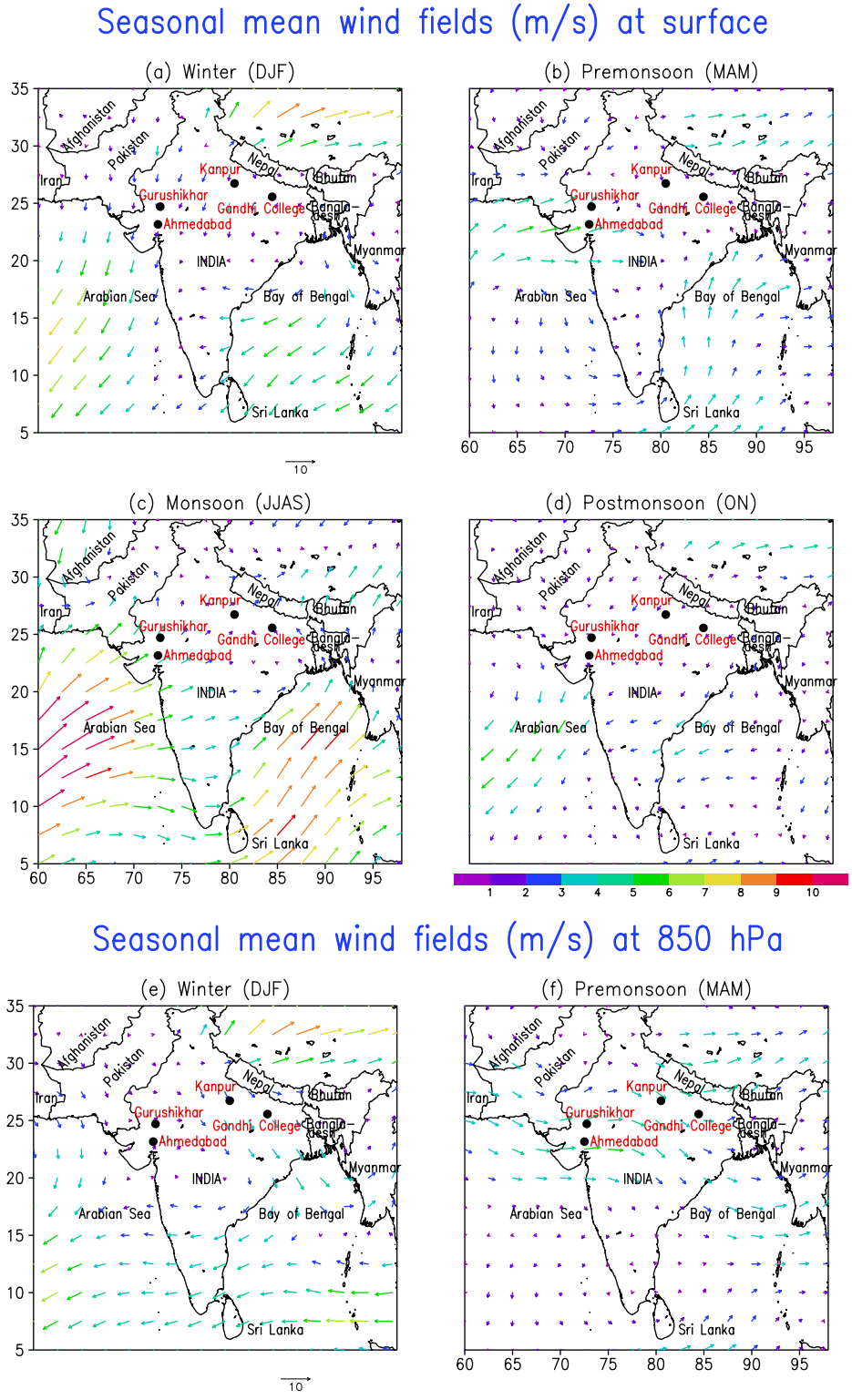

Continued

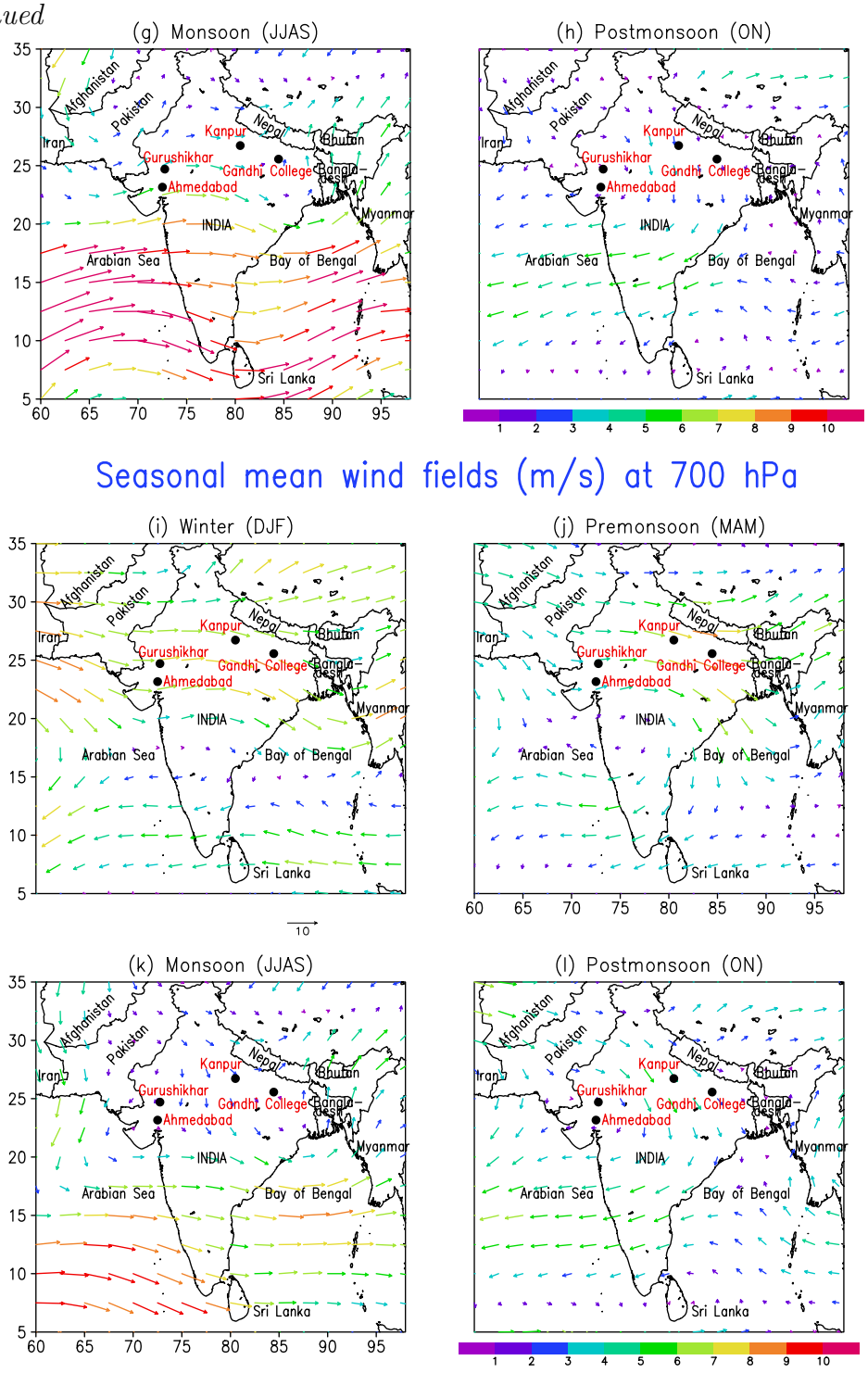

Figure 3.1: *Synoptic wind pattern at surface, 850 hPa and 700 hPa over south Asia for winter (a, e, i), premonsoon (b, f, j), monsoon (c, g, k) and postmonsoon (d, h, l) during 2008. Study locations - Ahmedabad, Gurushikhar, Kanpur and Gandhi College are shown in red color and the closed circle represents latitude-longitude of the study location.*

This region is bordered by the Himalayas to the north and Vindhyan Satpura ranges to the south. Kanpur is an urban, industrial city with a population of more than 4 million [*Singh et al.*, 2004]; while Gandhi College is a rural village site located in Ballia district of Uttar Pradesh state in India and located in Ganga basin, southeast of Kanpur. The atmosphere over Gandhi College is influenced by the mixture of rural and urban aerosol emissions as it is situated downwind of major urban centers, such as Delhi, Lucknow and Kanpur.

3.2 Meteorological conditions

Surface level daily mean temperature, relative humidity (RH), wind speed and wind direction data are obtained from National Center for Environmental Prediction (NCEP) reanalysis for all the five study locations during 2006-2008. The daily mean temperature, RH and wind speed are further used to calculate the monthly mean value and standard deviation. Daily rainfall is obtained from Tropical Rainfall Measuring Mission (TRMM) satellite $1^o \times 1^o$ latitude-longitude data centered at each study location and monthly accumulated rainfall is calculated.

Surface level synoptic winds over the study region during winter (December-January-February, DJF) are calm, north/northeasterly and are from the polluted northern hemisphere (Figure 3.1a); temperatures are colder and the atmosphere is dry (low RH) (Figures 3.2-3.5). In premonsoon (March-April-May, MAM) winds originate and travel from/through a less polluted west (arid/marine) (Figure 3.1b); temperatures increase slightly and RH is lower than winter. During monsoon (June-July-August- September, JJAS) winds are stronger, moist and are from the marine and western regions (Figure 3.1c); both temperature and RH are high during this season. During postmonsoon (October-November, ON) wind patterns start shifting in direction from southwest to northeast (Figure 3.1d); temperature and RH reduce. On the basis of meteorology, the aerosol data are grouped into four major seasons of winter, premonsoon, monsoon and postmonsoon, and discussed.

Figures 3.1e-l show the wind pattern at higher altitudes during different seasons

(Figures 3.2-3.5).

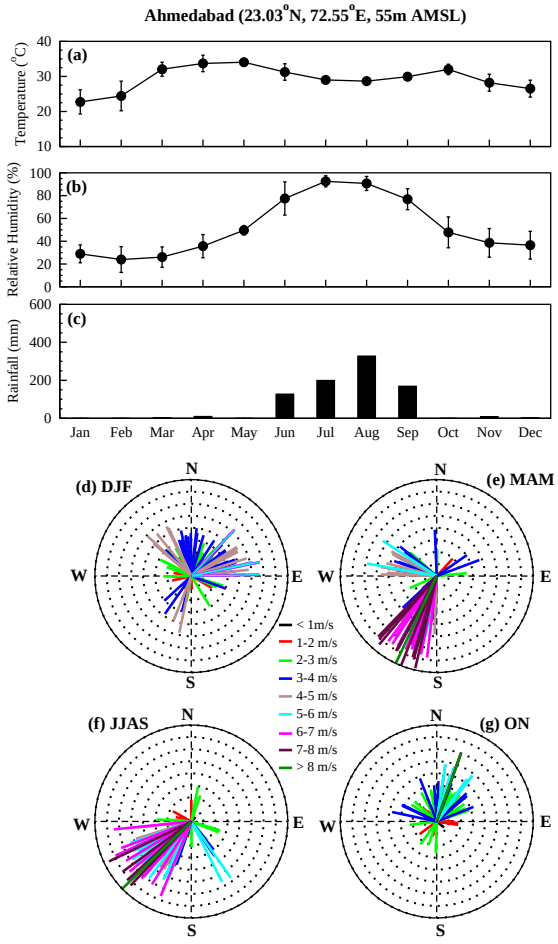

Figure 3.2: *Monthly mean (a) temperature (°C), (b) relative humidity (%), (c) rainfall (mm), and daily average wind speed and wind direction corresponding to (d) winter, (e) premonsoon, (f) monsoon and (g) postmonsoon over Ahmedabad in 2008. Vertical bars represent $\pm 1\sigma$ variation from the mean.*

Wind patterns at higher altitudes (850 hPa and 700 hPa) are different when compared to the surface level. In addition, winds at higher altitudes are found to be stronger. During monsoon the winds are more stronger and towards east, while during winter the winds are towards the oceans (Figures 3.1e-l). This type of atmospheric circulation leads to the transport of large amount of aerosols over different regions and can influence the aerosol loading and hence AODs [*Nair et al.*,

2005]. The inter annual variability in meteorological parameters are not found to be very significant over this region. Therefore, the seasonal variation in meteorological parameters for each study location are shown for 2008.

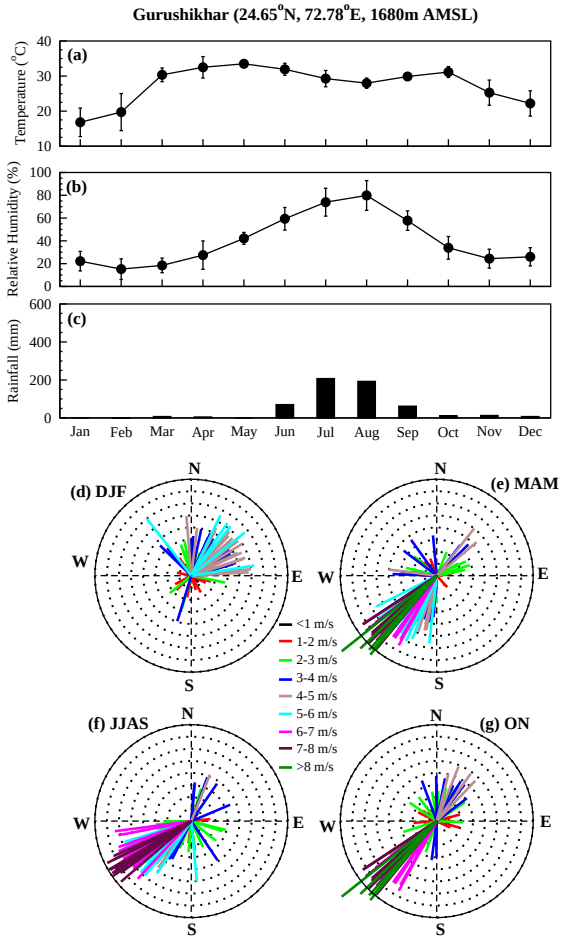

Figure 3.3: *Monthly mean (a) temperature (°C), (b) relative humidity (%), (c) rainfall (mm), and daily average wind speed and wind direction corresponding to (d) winter, (e) premonsoon, (f) monsoon and (g) postmonsoon over Gurushikhar in 2008. Vertical bars represent ±1σ variation from the mean.*

Monthly mean air temperature is found to vary from 22-34°C over Ahmedabad during Jan-Dec 2008 with a mean value of 29.4±3.5°C (Figure 3.2). As Ahmedabad is in the semiarid region, the atmosphere is mostly dry with an annual mean RH of about 50%. During winter RH decreases to ∼20%, while in monsoon RH is >90%. More than 95% of the total rainfall occurs during monsoon when winds are

southwesterly over Ahmedabad.

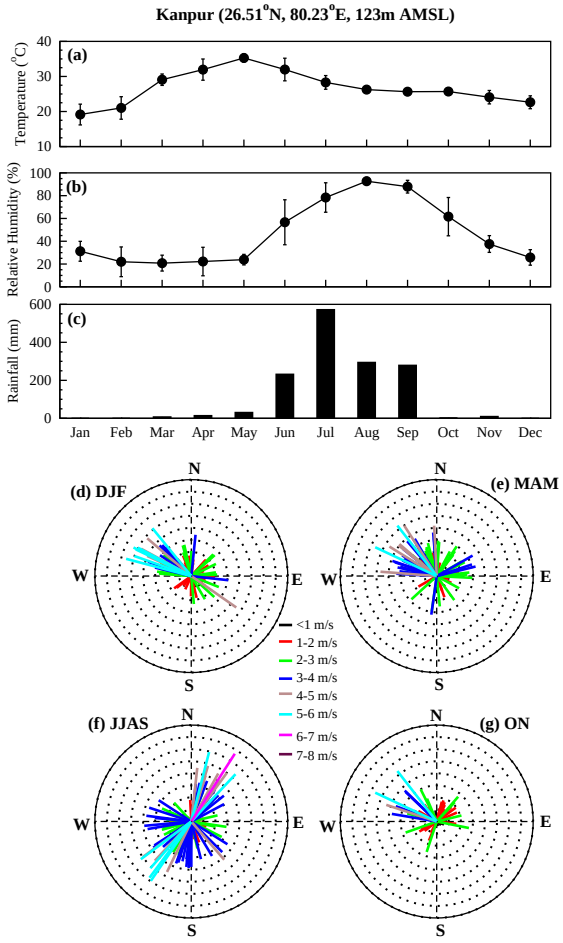

Figure 3.4: *Monthly mean (a) temperature (°C), (b) relative humidity (%), (c) rainfall (mm), and daily average wind speed and wind direction corresponding to (d) winter, (e) premonsoon, (f) monsoon and (g) postmonsoon over Kanpur in 2008. Vertical bars represent $\pm 1\sigma$ variation from the mean.*

Surface winds over Ahmedabad are found to be generally northeast/northwest and calm during postmonsoon and winter season indicating the continental origin of air masses. During premonsoon and monsoon, winds are stronger and mostly southwesterly arriving from the surrounding arid/marine regions (Figure 3.2d-g). Over Gurushikhar, the minimum temperature is found to be about 16°C during January which gradually increases and reaches the maximum value of 34°C during May (Figure 3.3). The annual mean temperature and RH are about 28°C and 40%,

respectively, during 2008 over Gurushikhar. More than 90% of the total rainfall occurs during monsoon over this location. Over Gurushikhar most of the days during winter winds are northeasterly. During other seasons, winds are stronger and are mainly from southwest direction (Figure 3.3g).

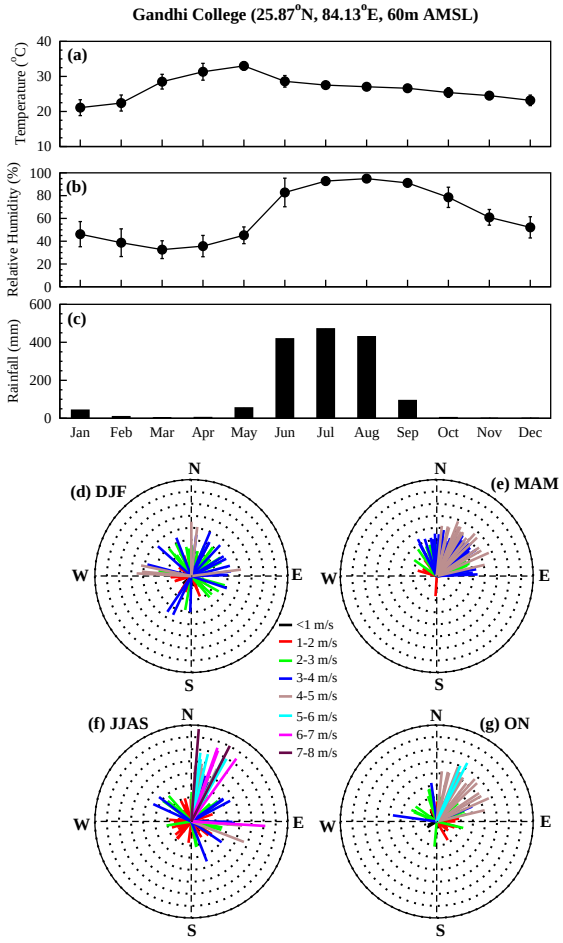

Figure 3.5: *Monthly mean (a) temperature (°C), (b) relative humidity (%), (c) rainfall (mm), and daily average wind speed and wind direction corresponding to (d) winter, (e) premonsoon, (f) monsoon and (g) postmonsoon over Gandhi College in 2008. Vertical bars represent $\pm 1\sigma$ variation from the mean.*

Over Kanpur monthly mean temperature is about 20°C during winter which increases to 35°C during May; after May the temperature steadily decreases till December (Figure 3.4a). RH during winter and premonsoon is about 20% over Kanpur, which increases to 80% during July-August (Figure 3.4b). More than

95% of total rainfall occurs during monsoon, out of which 40% occurs during July. Winds over this location are generally calm when compared to the other locations. The seasonal dependence of the wind direction is not so strongly evident over Kanpur as winds are of mixed origin during the entire year (Figure 3.4). Gandhi college is also situated in the Ganga basin region and exhibits similar meteorological conditions as that of Kanpur (Figures 3.4, 3.5). During the entire year winds are <5 ms^{-1} except for some days during monsoon (Figure 3.5f). Winds show mixed origin during winter and monsoon seasons; while the winds are mainly from northeast and/or northwest during premonsoon and postmonsoon. The meteorological features are similar in the west for Ahmedabad and Gurushikhar and in the north for Kanpur and Gandhi College; however, there exist differences in winds and rainfall.

In addition to the meteorological condition, the source region of air mass can significantly influence the aerosol properties. The back trajectory analysis provides a three dimensional (latitude, longitude and height) description of the pathways followed by air parcels as a function of time. While analyzing the columnar properties of atmospheric constituents, air mass back trajectories at different heights are important to identify the source regions and the transport pathways of the pollutants before they reach the measurement location. Figure 3.6 shows the seven days air back trajectories arriving at measurement locations during different seasons at an altitude of 500m. Seven day air back trajectory analysis has been performed considering the residence time of different types of aerosols, which is about a week in the lower atmosphere. Air back trajectories are calculated for each day corresponding to 1200 h Indian Standard Time (+0530 GMT) and for each of the study locations in India.

Daily back trajectories are further utilized to calculate the seasonal mean air trajectories at each location. Figure 3.6 shows that the air masses are strongly dependent on the seasons, and travel short or long distances before reaching the measurement locations.

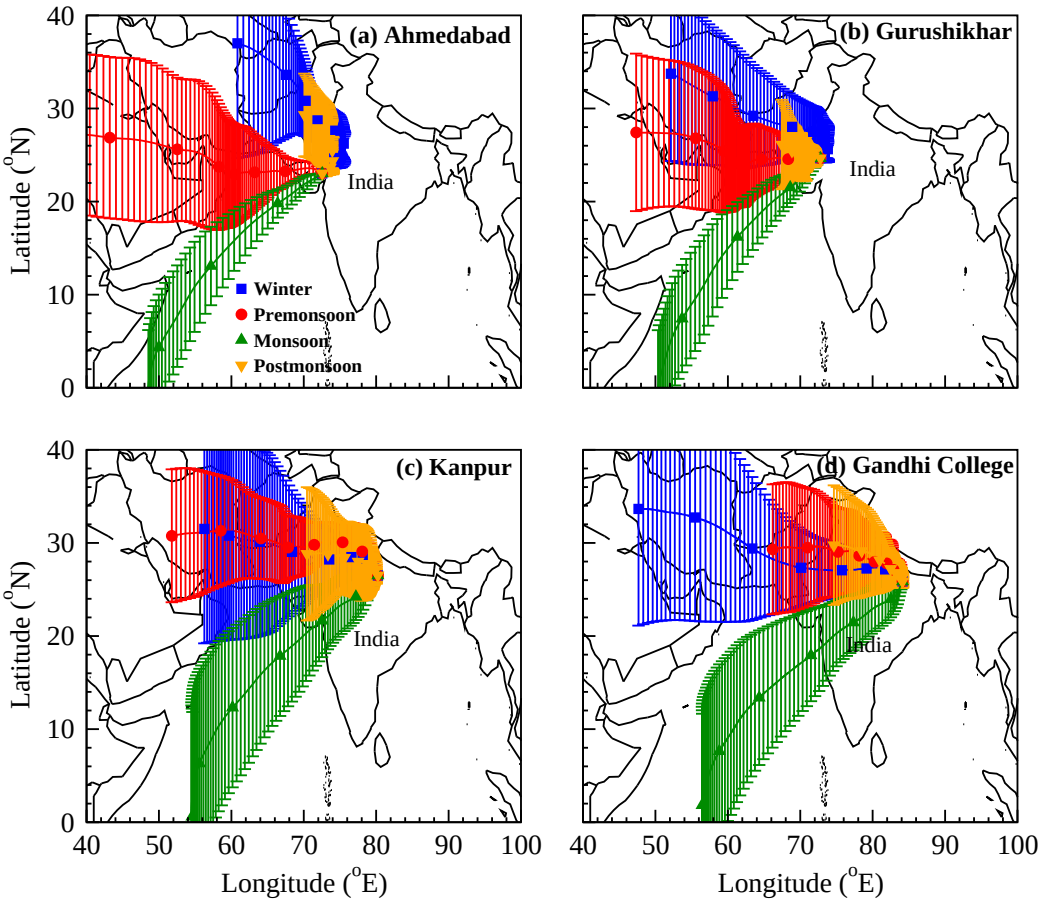

Figure 3.6: *Seven days air back trajectories over the study locations (a) Ahmedabad, (b) Gurushikhar, (c) Kanpur and (d) Gandhi College during winter, premonsoon, monsoon and postmonsoon. Vertical bars represent $\pm 1\sigma$ variation from the mean during each season.*

Air masses are found to originate mainly from the marine region during monsoon, while during postmonsoon the trajectories are mostly local. During premonsoon, the trajectories are northwesterly and cover a longer distance. During winter air masses are mostly westerly over all the locations (Figure 3.6).

3.3 Results and Discussion

3.3.1 Seasonal variation in aerosol optical depths

Seasonal mean AODs measured using hand held sun photometer, Microtops II sun photometers and AERONET sun/sky radiometers during 2006-2008 are shown

over the four study locations (Figure 3.7). AODs at 0.4, 0.875 and 1.02 μm are used in case of sun photometer; while from Microtops-II and AERONET AODs measured at the wavelengths of 0.38, 0.87 and 1.02 μm are utilized. AODs at these wavelengths are chosen as they represent the short (0.4/0.38 and 0.5 μm) and long (0.875/0.87 and 1.02 μm) wavelength regions.

It should be noted that over Ahmedabad and Gurushikhar AODs were measured using hand held sun photometer at 0.4, 0.65 and 0.875 μm between October 2006 and December 2007, while during January-December 2008 AODs were measured using Microtops-II at 0.38, 0.675 and 0.87 μm. In addition, AODs over AERONET sites Kanpur and Gandhi College are available at 0.38, 0.675 and 0.87 μm. In the present study the differences, if any, due to the small changes ($\leq$0.02 μm) in wavelengths at which the AOD measurements were made, are expected to be negligible and are not considered. At the outset, AODs exhibit strong seasonal as well as wavelength dependence. Over Ahmedabad, 0.4 μm AODs are higher than that of 0.875 and 1.02 μm AODs during the study period (Figure 3.7a). Higher AODs at lower wavelengths indicate the abundance of smaller size particles over Ahmedabad throughout the year. AODs are found to decrease from winter to premonsoon at 0.4 μm; while at 1.02 μm AOD increases. The increase of AODs in longer wavelengths can be attributed to the increase in the input of dust particles in the atmosphere as the winds are higher and are from the arid regions (Figures 3.1, 3.6).

Wet removal is one of the main mechanisms for removal of aerosols from the atmosphere. Though the rainfall is most effective in reducing the surface level aerosol concentrations, prevailing strong convection, a deeper boundary layer and hygroscopic growth of water soluble aerosols give rise to higher AODs during monsoon [*Ramachandran*, 2007]. During winter and postmonsoon AODs are lower as they are influenced mostly by fine mode aerosols produced from fossil fuel and biomass burning emissions [*Ramachandran and Rajesh*, 2007]. In contrast to Ahmedabad, the difference in AODs at smaller and longer wavelengths are not very significant

over the high altitude remote site Gurushikhar, which indicates lower concentration of fine mode aerosols (Figure 3.7b). AODs could not be measured over Gurushikhar during monsoon due to cloudy, overcast conditions. AODs in the visible wavelength region are more influenced by fine mode aerosols, on the other hand when coarse mode aerosols are dominant AODs in the longer wavelength are affected.

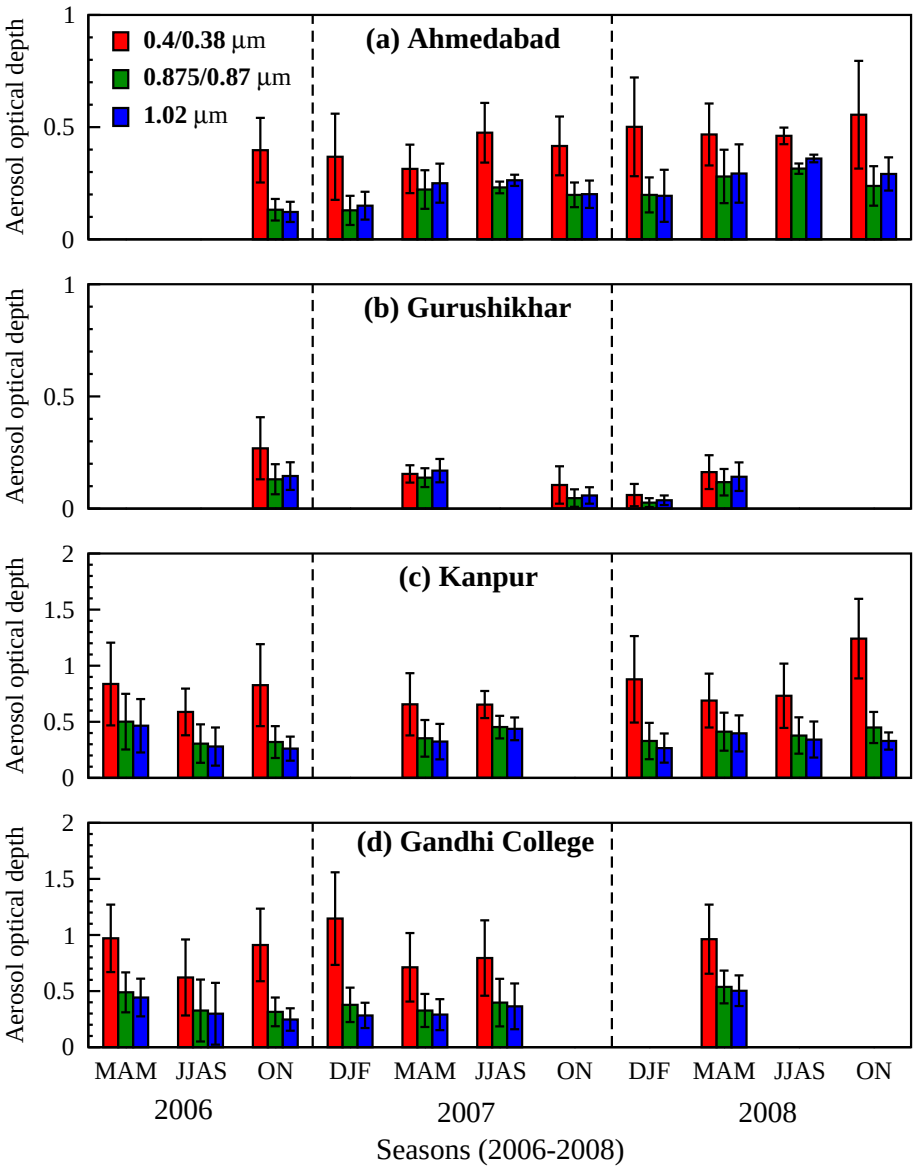

Figure 3.7: *Seasonal variation in AOD during 2006-2008 over (a) Ahmedabad, (b) Gurushikhar, (c) Kanpur and (d) Gandhi College. Gaps in the figure denote the absence or non availability of sun photometer, Microtops II and AERONET sun/sky radiometer AOD data. Vertical bars indicate* $\pm 1\sigma$ *deviation from the seasonal mean.*

AODs over Gurushikhar are lowest during winter season as the measurement site remains above the boundary layer; while the higher AODs in longer wavelengths observed during premonsoon can be attributed to the long range transport of dust particles (Figures 3.1, 3.6).

On an average 0.4 μm AODs over Kanpur and Gandhi College are about a factor of two higher than 1.02 μm AODs (Figures 3.7c, 3.7d) throughout the study period. Higher AODs over Kanpur during premonsoon and monsoon occur due to the transport of dry dust particles from the western Thar desert to Kanpur, while during postmonsoon and winter fine mode aerosols dominate this location (Figures 3.1, 3.6) [e.g., *Singh et al.*, 2004; *Ramachandran*, 2007]. Winter, premonsoon and postmonsoon AODs during 2006-2008 are comparable over Gandhi College, while monsoon AODs are lower. 0.4 μm AODs over Gandhi College are about 20% higher than Kanpur; while AODs at 1.02 μm are nearly the same for all the seasons over both the locations. This suggests that though both Kanpur and Gandhi College are located in the Indo-Gangetic basin different aerosol sources can give rise to higher AODs. AODs are higher over Gandhi College in shorter wavelengths despite the fact that it is a rural location, as Gandhi College is situated downwind of major urban centers (Figure 3.1) and due to higher biomass emissions when compared to Kanpur. Higher AODs during postmonsoon and winter is a characteristic feature of the locations in Indo-Gangetic basin.

During postmonsoon and winter the boundary layer is shallow and holds the pollutants in a smaller volume, when compared to summer, which results in confinement of aerosols. The colder temperatures along with the trapping of pollutants give rise to hazy and foggy conditions over Indo-Gangetic basin [e.g., *Di Girolamo et al.*, 2004; *Ramachandran*, 2007]. In addition, the dense population in this region contributes to large aerosol sources (due to fossil fuel consumption and biofuel used for domestic purposes) which produce higher AODs.

On an interannual basis AODs at all wavelengths are found to increase from 2006 to 2008 over Ahmedabad during all the seasons (Figure 3.7a-d). In contrast,

AODs are found to decrease from 2006 to 2008 over Gurushikhar both during premonsoon and postmonsoon but the difference is not found to be very significant. Interannual variability in AODs are found to show similar pattern over both the study locations in Indo-Gangetic basin. Monsoon AODs are found to increase by 1.2 times over both the locations, but premonsoon AODs are not found to show any significant change during 2006-2008. The maximum increase in the AODs are observed during postmonsoon over Kanpur, while over Gandhi College any inference could not be drawn due to unavailability of data. However, in general, the seasonal and spatial variabilities in AODs are found to be more dominant than the interannual variability during 2006-2008 over the study locations. Therefore, further discussion is restricted to the seasonal and spatial variations in aerosol optical characteristics in the study area.

3.3.2 Comparison of ground based and satellite derived AODs: Seasonal variability

Daily mean AODs obtained from MODIS (0.55 μm) and MISR (0.555 μm) are used to calculate the seasonal mean AODs to compare and contrast with the ground based measurements. As the ground based measurements of AODs were available at 0.5 μm, the Ångström exponent (α) derived using equation 2.5 is used to calculate the AOD corresponding to 0.55 μm and seasonal means are obtained. In Figure 3.8 seasonal mean AODs from sun photometer, Microtops II sun photometers and AERONET sun/sky radiometer at 0.55 μm are compared with MODIS and MISR retrieved AODs at 0.55 μm and 0.555 μm, respectively over all the locations.

The seasonal variation in AODs obtained from ground based measurements shows a similar trend as that of 0.4 μm AODs over all the study locations. During the entire study period and for all the study locations AODs from ground based measurements and satellites (MODIS and MISR) are found to agree within $\pm 1\sigma$ (Figure 3.8).

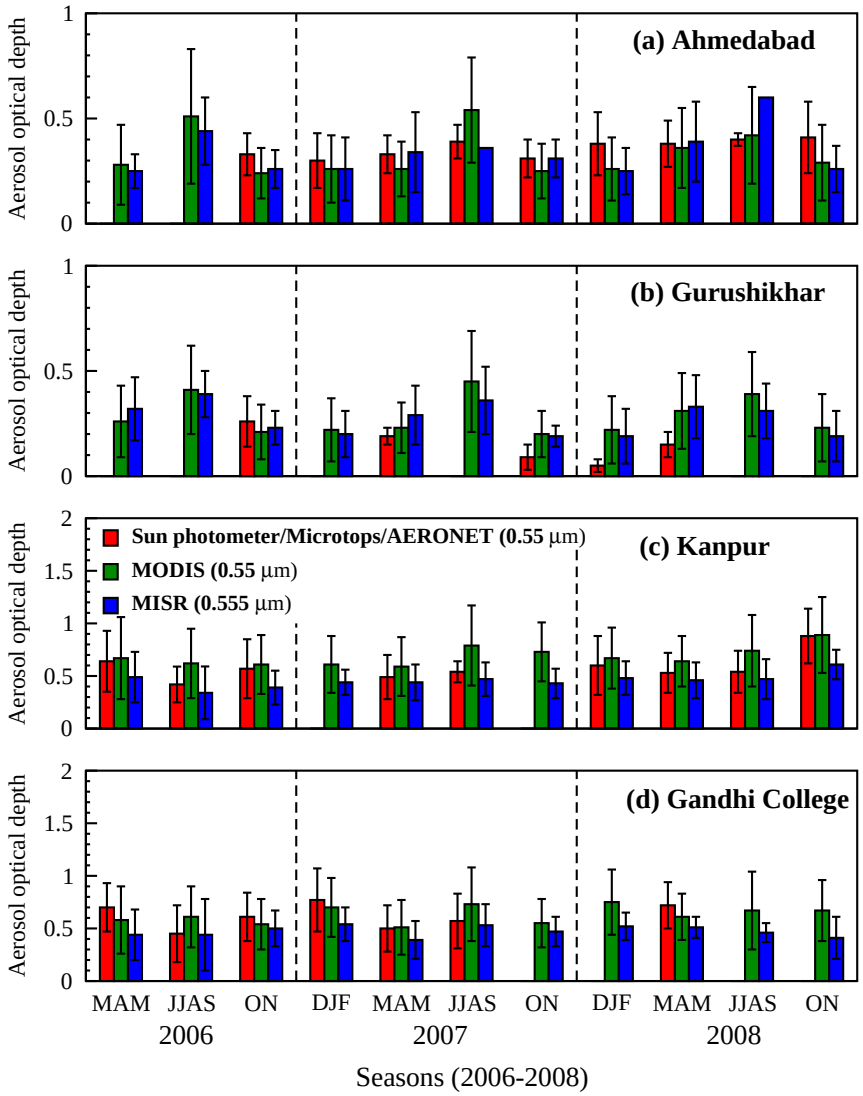

Figure 3.8: *Comparison of seasonal mean AODs obtained from ground based (sun photometer, Microtops II and AERONET sun/sky radiometers), and satellites (MODIS and MISR) during 2006-2008 over (a) Ahmedabad, (b) Gurushikhar, (c) Kanpur and (d) Gandhi College. Ground based AODs correspond to 0.55 μm (calculated using AOD at 0.5 μm and α), while MODIS and MISR retrieved AODs are at 0.55 and 0.555 μm respectively. Vertical bars denote ±1σ deviation from the seasonal mean.*

A one-to-one comparison between AODs obtained from ground based and satellite measurements is not the goal of the present study and is beyond the scope of

this thesis work. However, it is pertinent to state the possible causes for the differences between the ground based and satellite measurements. The differences between AODs retrieved from MODIS, MISR and ground based hand held and Microtops II sun photometers, and AERONET sun/sky radiometers could arise due to:

- temporal difference between the measurements (ground based AODs represent the mean of AODs measured during the whole day), while satellite derived AODs correspond to particular times in a day; Terra at 1030 LST (MODIS and MISR) and Aqua at 1330 LST (MODIS).
- spatial difference between two measurements (point *vs.,* grid); ground based measurements correspond to a particular location, while satellite derived AODs are either over a grid (MODIS, $1^o \times 1^o$) or applicable to a larger spatial regime (MISR, 17.6 km).
- uncertainties associated in deriving AODs from both ground based and satellite retrievals.
- the sampling differences that can arise due to the differences in the methods of measurements, namely, ground based (sun photometer, Microtops II and AERONET) and space borne (MODIS and MISR) [*Kedia and Ramachandran*, 2008a].

3.3.3 Ångström coefficients (α, β) and AOD ratio

Ångström parameters (α and β) estimated from AODs in the wavelength range of 0.4-0.875 μm from ground based measurement (sun photometer, Microtops II and AERONET) over all the locations during 2006-2008 on a seasonal mean scale are plotted (Figure 3.9). As discussed in Chapter 2, a higher α value indicates higher concentration of fine mode aerosols in the size distribution while a lower value represents the dominance of coarse mode particles. The value of α in the

above wavelength range can vary from 1 to 3 for an aerosol distribution dominated by accumulation mode aerosols to nearly zero for the atmosphere dominated by coarse mode aerosols such as dust and sea salt [e.g., *Holben et al.*, 2001; *Eck et al.*, 2001].

The AOD ratio (= 0.4 μm AOD/0.875 μm AOD) are calculated for all the locations to get further inference about the particle size distribution. A lower value of AOD ratio represents coarse mode dominance while a higher value indicates dominating fine mode particles in the atmosphere. All the three parameters, α, β and AOD ratio are found to show strong seasonal as well as spatial variability similar to AODs (Figure 3.9). AOD ratio (Figure 3.9) is found to show a positive correlation with α and negative correlation with β for all the stations. Over Ahmedabad higher α (>1) and AOD ratio (>2.5) while lower β (<0.3) are observed during postmonsoon and winter indicating higher concentration of fine mode aerosols. During premonsoon and monsoon α and AOD ratio are found to decrease by a factor of more than 1.5 due to the increase in coarse mode particle concentration (dust and sea salt), and therefore β and AOD increase (Figures 3.7, 3.9). Over Gurushikhar α and AOD ratio are found to be lower than that of Ahmedabad throughout the study period indicating a higher concentration of coarse mode aerosols (Figure 3.9b). In addition, β, a measure of the columnar loading of aerosols, is low confirming the presence of a cleaner atmosphere.

The seasonal variation in α is quite significant over Gurushikhar; premonsoon α is at least a factor of $\sim$3 lower when compared to postmonsoon and winter. The lower α during premonsoon is attributed to the dominance of dust particles transported from the neighboring arid regions (Figures 3.1, 3.6). The values of α, AOD ratio and β are found to be higher over the Indo-Gangetic basin (Kanpur and Gandhi College) than the other two locations in the west. Higher α and AOD ratio during postmonsoon and winter over the Indo-Gangetic basin arise due to the increase in the abundance of fine mode urban aerosols transported by northerly/northwesterly winds.

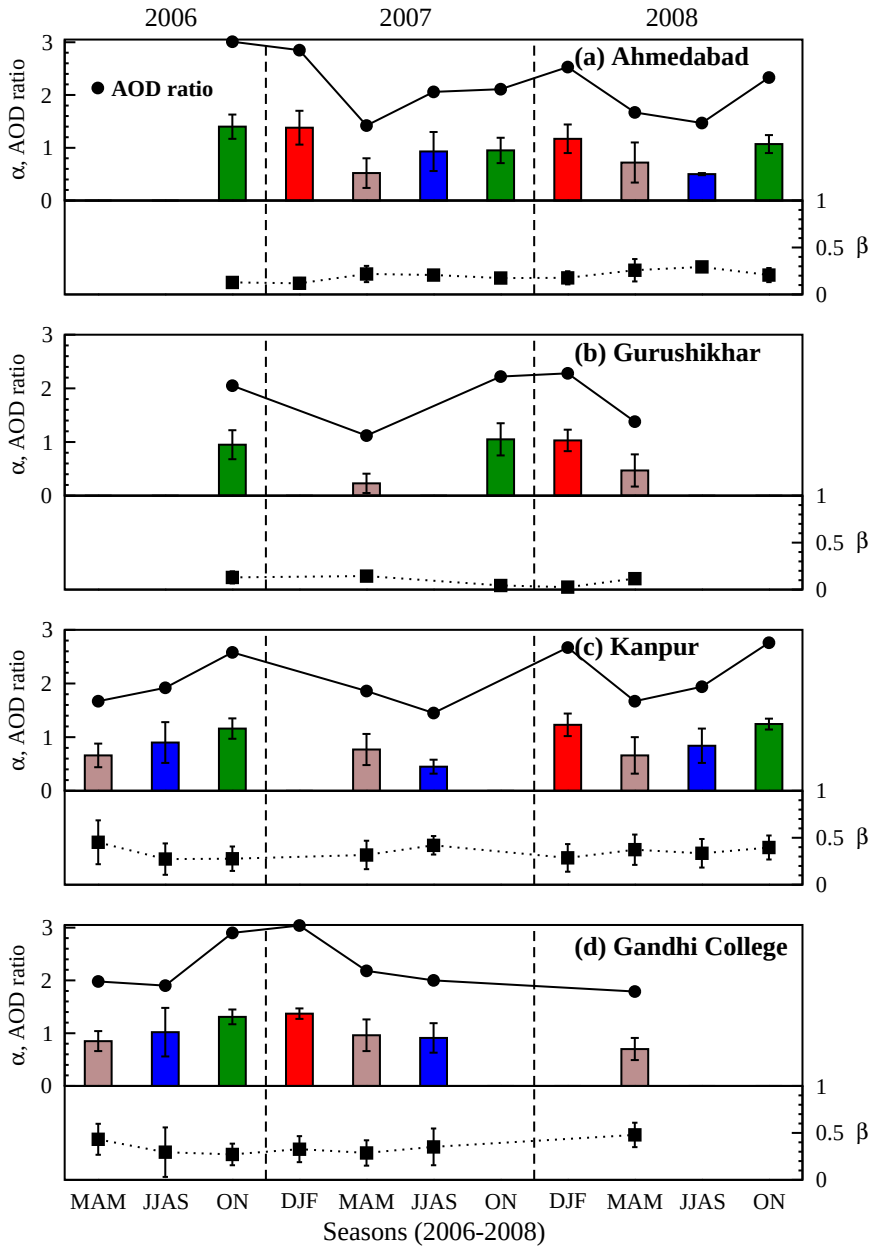

Figure 3.9: *Seasonal mean Ångström parameters (α and β) obtained from the linear fit of spectral AODs in the wavelength range of 0.4-0.875 μm during 2006-2008, and the AOD ratio (=0.4 μm AOD/0.875 μm AOD) over (a) Ahmedabad, (b) Gurushikhar, (c) Kanpur and (d) Gandhi College. The four different seasons are represented by different colors during the study period.*

In addition, the atmospheric dynamics (shallow boundary layer and colder tem-

peratures) play a crucial role in trapping the fine mode aerosols. During premonsoon and monsoon, α and AOD ratio decrease, while β increases due to dust brought to the study area by southwesterly winds (Figures 3.1, 3.6).

3.3.4 Aerosol volume size distribution and single scattering albedo

The interaction of aerosol particles with the solar radiation strongly depends on aerosol size distribution and scattering/absorption properties of aerosols [*Eck et al.*, 2005]. It should be noted that in an aerosol size distribution fine mode particles mostly are of anthropogenic origin and coarse mode particles originate from natural sources. In order to get further insight into the optical properties of aerosols and their spatial and temporal variability, aerosol volume size distribution and single scattering albedo data are also analyzed for both the AERONET locations namely Kanpur and Gandhi College. Aerosol volume size distribution is retrieved using inversion technique following *Dubovik and King* [2000].

Aerosol volume size distributions over Kanpur and Gandhi College corresponding to winter, premonsoon, monsoon and postmonsoon are shown in Figure 3.10. The volume size distributions for different seasons correspond to different years as they were not available for different seasons in a particular year. Two distinct modes, fine (particle size <0.6 μm) and coarse (particle size >0.6 μm) are observed over both the locations and for all the seasons during the study period indicating the presence of bimodal aerosol size distribution. This suggests the presence of aerosols originating dominantly from two sources, namely, anthropogenic and natural. Although at both the locations during all the seasons the volume size distribution of aerosols is bimodal, the volume and the geometric mean radius exhibit differences (Table 3.2). The volume concentration is ≤ 0.1 μm^3 μm^{-1} in the fine mode over Kanpur during all the seasons. The coarse mode volume concentration is a factor of two higher during premonsoon and monsoon over Kanpur when compared to winter and postmonsoon (Table 3.2). The higher coarse mode

volume concentration during premonsoon and monsoon arises due to the increase in dust loading [e.g., *Singh et al.*, 2004].

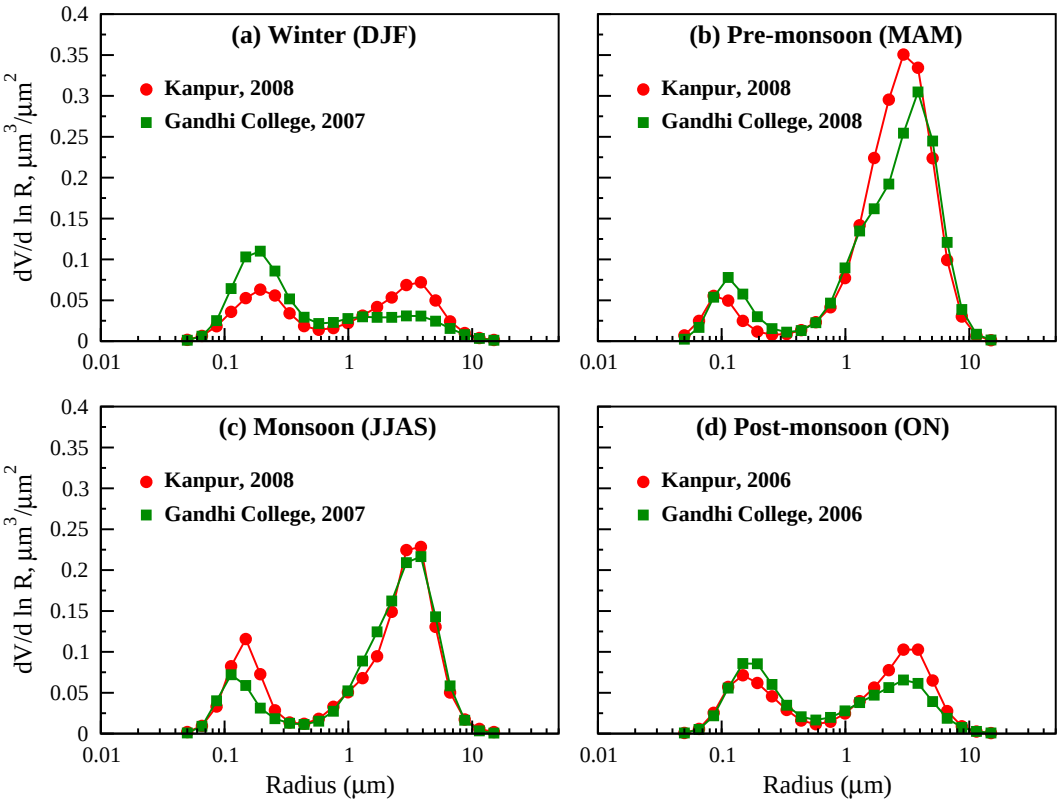

Figure 3.10: *Seasonal mean aerosol volume size distribution over Kanpur, and Gandhi College during (a) winter, (b) premonsoon, (c) monsoon and (d) postmonsoon. Years are different due to unavailability of volume size distribution data for all the seasons during a particular year.*

The contribution to the increase in coarse mode volume concentration and radius due to the hygroscopic growth of water soluble aerosols during monsoon when the ambient relative humidity exceeds 70% cannot be ruled out. That the coarse mode dust particles dominate Kanpur during premonsoon and monsoon is further evident from the decrease in fine mode radius (Table 3.2). The fine mode radius is lower over Kanpur during premonsoon and monsoon. The coarse mode radius over Kanpur is around 2.2 μm throughout the year.

The results on features of fine and coarse mode volume distributions from the present study spanning 2006-2008 over Kanpur are in agreement with earlier studies conducted during 2001-2003 [e.g., *Dey et al.*, 2004; *Singh et al.*, 2004]. During dust event, aerosol volume concentration at coarse mode was found to increase by a factor of 3 without any significant change in volume concentration of fine mode aerosols [*Dey et al.*, 2004]. The coarse mode volume concentration was found to be doubled during the premonsoon and monsoon seasons compared to that during the postmonsoon and winter during 2001-2003 [*Singh et al.*, 2004].

Table 3.2: *Parameters of aerosol volume size distribution (V is the volume concentration ($\mu m^3 \mu m^{-2}$), R_v (μm) is the volume geometric mean radius and σ is the geometric standard deviation) in Kanpur and Gandhi College during different seasons.*

		Fine mode			**Coarse mode**		
Seasons	Year	V	R_v	σ	V	R_v	σ
			Kanpur				
DJF	2008	0.08	0.17	0.48	0.11	2.26	0.64
MAM	2008	0.05	0.11	0.50	0.50	2.23	0.59
JJAS	2008	0.10	0.14	0.40	0.29	2.23	0.60
ON	2006	0.09	0.16	0.43	0.14	2.32	0.58
			Gandhi College				
DJF	2007	0.13	0.18	0.47	0.07	1.90	0.70
MAM	2008	0.07	0.12	0.45	0.44	2.23	0.64
JJAS	2007	0.07	0.14	0.41	0.30	2.14	0.59
ON	2006	0.10	0.17	0.44	0.11	1.92	0.66

In Gandhi College, the fine mode volume concentration is higher during winter when compared to that over Kanpur indicating larger abundance of fine mode aerosols. The reason for this could be higher biomass burning during winter as the location is a rural village. The fine (coarse) mode volume concentration and geometric mean mode radius are lower (higher) during premonsoon and monsoon. The volume concentration in coarse mode is a factor of three higher during premonsoon

and monsoon (Table 3.2).

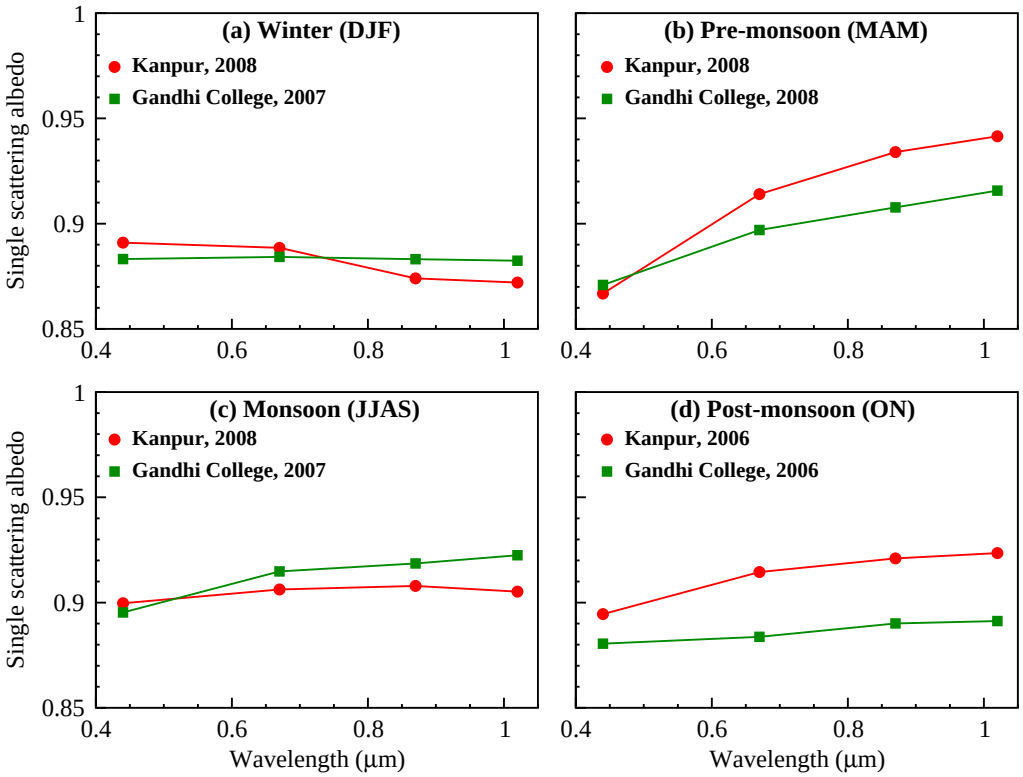

Figure 3.11: *Seasonal mean spectral variation in single scattering albedo (SSA) over Kanpur and Gandhi College during (a) winter, (b) premonsoon, (c) monsoon and (d) postmonsoon. Years are different due to unavailability of SSA data*

Spectral single scattering albedo (SSA) gives information about the abundance of scattering and absorbing aerosols in different size ranges. The spectral variation in SSA over Kanpur and Gandhi College obtained from AERONET [*Dubovik and King*, 2000] are shown in the wavelength range of 0.44-1.02 μm for different seasons in Figure 3.11. The results on SSA for different seasons correspond to different years as SSA corresponding to different seasons were not available for the same year. A strong seasonally varying spectral dependence is explicit in SSA over both the locations. During winter SSA decreases as wavelength increases due to the dominance of fine mode particles. A decrease in SSA with increasing wavelength is generally caused due to the dominance of fine mode absorbing aerosols. During

premonsoon and monsoon SSA increases with wavelength (in accordance with lower α and higher β (Figure 3.9)) which is attributed to the increase in the concentration of coarse mode particles in the atmosphere.

As dust and sea salt more efficiently scatter the radiation, their dominance in the aerosol size distribution during premonsoon and monsoon result in higher SSA at the longer wavelengths. The spectral dependence in SSA is weak during postmonsoon due to the wet removal of both fine and coarse mode particles. SSA is found to be >0.85 over both the locations throughout the study period. SSA over Kanpur is found to be higher than Gandhi College in all the seasons except during monsoon, indicating the presence of more absorbing aerosols over Gandhi College due to the admixture of both urban and rural emissions.

3.3.5 Spectral distribution of AODs: Spatial and temporal variability

In the ambient atmosphere, the size distribution of aerosol is typically bimodal and is made up of a fine mode produced by combustion processes and/or gas to particle conversion and, a mechanically produced coarse mode. Therefore, departure from linear behavior of ln τ versus ln λ is observed which indicates that the size distribution does not follow Ångström power law. Under such condition, a linear fit is found to yield significant difference when compared to the measured AODs, and a curvature is observed in the AOD spectra which contains useful information about the aerosol size distribution [e.g., *Reid et al.*, 1999; *Eck et al.*, 1999, 2001; *O'Neill et al.*, 2001; *Kaskaoutis and Kambezidis*, 2006; *Schuster et al.*, 2006]. In the presence of curvature in the AOD spectra, α is not single valued and depends on the wavelength band used for its determination.

Estimation of α in short and long wavelength spectral regions helps in determining whether fine or coarse mode aerosols are dominant in an aerosol size distribution [*Schuster et al.*, 2006]. Higher α values in the 0.4-0.5 μm wavelength region indicate the dominance of fine mode aerosols, while lower values indicate

the presence of larger aerosol particles. To examine the size distribution of aerosols over different environments, values of α in short (0.4-0.5 μm) and long (0.65-0.90 μm) spectral ranges have been calculated for eight different aerosol models (e.g., continental clean, continental average, continental polluted, urban, desert, maritime tropical, maritime clean and maritime polluted) given by *Hess et al.* [1998]. These aerosol models consist of water soluble, water insoluble, black carbon, mineral dust and sea salt with varying concentrations (Table 3.3). The water soluble aerosol originates from gas to particle conversion and consists of various kinds of sulfates, nitrates and water soluble organic substances. The water insoluble aerosol consists mostly soil particles with a certain amount of water insoluble organic material. The black carbon aerosols are produced as primary particles from incomplete combustion processes such as fossil fuel and biomass burning. Mineral aerosols in nucleation, accumulation and coarse modes are produced in arid regions. It mainly consists of a mixture of quartz and clay minerals. Sea salt particles in different size range consist of different kinds of salt contained in seawater. Water soluble and black carbon exist in submicron size range. The sea salt aerosols are represented in accumulation and coarse modes allowing for different wind speed dependent increase of number concentration for particles of different size range. Mineral dust particles are found in accumulation and coarse modes and insoluble are present in submicron range. Water soluble and sea salt aerosols are hygroscopic while rest three aerosol types are hydrophobic in nature [*Hess et al.*, 1998].

Continental clean aerosol model represents remote continental locations without or with very low anthropogenic influence. Continental average aerosol type refers to continental areas influenced by anthropogenic activities, which contains black carbon and an increased amount of insoluble and water soluble components than continental clean aerosol model (Table 3.3). Continental polluted aerosol model is applicable to the areas which are highly polluted by manmade activities. The number concentration of water soluble aerosol is more than double that in continental average aerosol model. Urban aerosol model represents strong pollu-

tion in urban areas. Desert aerosol model describes the aerosols present over all the deserts of the world, and which are long range transported [*Hess et al.*, 1998].

Table 3.3: *Composition of different aerosol models along with the concentration of aerosol species given in Hess et al. [1998].*

Aerosol Model	**Aerosol component**	**Number concentration (cm^{-3})**
Continental clean	Water soluble	2600
	Water insoluble	0.15
Continental average	Water soluble	7000
	Water insoluble	0.40
	Black carbon	8300
Continental polluted	Water soluble	15700
	Water insoluble	0.60
	Black carbon	34300
Urban	Water soluble	28000
	Water insoluble	1.5
	Black carbon	130000
Desert	Water soluble	2000
	Mineral (nucleation)	269.5
	Mineral (accumulation)	30.5
	Mineral (coarse)	0.142
Maritime tropical	Water soluble	590
	Sea salt (accumulation)	10
	Sea salt (coarse)	0.0013
Maritime clean	Water soluble	1500
	Sea salt (accumulation)	20
	Sea salt (coarse)	0.0032
Maritime polluted	Water soluble	3800
	Black carbon	5180
	Sea salt (accumulation)	20
	Sea salt (coarse)	0.0032

In maritime tropical aerosol model, the density of water soluble aerosols is low. In addition, the wind speed is assumed to be very low which corresponds to a lower number density of sea salt. Maritime clean represents undisturbed remote maritime conditions with no black carbon. Maritime clean and tropical

aerosol models contain water soluble and sea salt particles in accumulation and coarse modes. Maritime polluted represents a maritime environment under the influence of anthropogenic aerosols with highly variable amount of black carbon and water soluble particles [*Hess et al.*, 1998]. Maritime polluted aerosol model has more number of water soluble and black carbon aerosols than maritime clean aerosol model. However, all these aerosol types defined here may have additional components with varying number densities according to the actual location for which they are assumed to be valid (discussed later in Chapter 5).

The variation in the spectral aerosol properties such as AOD, α_{short} ($\alpha_{0.4-0.5}$), α_{long} ($\alpha_{0.65-0.875}$), $\alpha^{'}$ and α_2 (equations 2.6, 2.7, 2.8 in Chapter 2) as a function of relative humidity for all the eight aerosol models are given in Table 3.4. At the outset, different values of α are observed in short and long wavelength interval which confirms the deviation of AOD spectra from Junge power law for all the aerosol models. The α in the full (0.4-0.90 μm) spectral range are found to be the average of $\alpha_{0.4-0.5}$ and $\alpha_{0.65-0.90}$ (not shown). $\alpha_{0.4-0.5}$ value is found to decrease with increasing RH for all the aerosol models except for desert model. In contrast, except for maritime aerosol models the $\alpha_{0.65-0.9}$ is found to increase with RH for all the aerosol models. As RH increases, size of hygroscopic aerosols starts increasing with RH. As α can be regarded as the ratio of fine to coarse mode AOD, $\alpha_{0.4-0.5}$ value decreases and $\alpha_{0.65-0.9}$ increases with increasing RH. For desert aerosols, α values are <0.3 in short and long wavelengths owing to the strong dominance of coarse mode particles. The $\alpha_{0.4-0.5}$ and $\alpha_{0.65-0.9}$ values for desert aerosols increase as RH increases because of the increase in the fine mode radius of water soluble aerosols.

The value of $\alpha_{0.4-0.5}$ for the urban model is highest due to presence of highest concentration of submicron black carbon particles followed by continental polluted model (Table 3.3). Variation in the α value in both short and long wavelength range is found to increase with increase in RH for all the atmospheric models. This can be explained as, when RH increases the size of water soluble aerosols

increases and the size distribution changes as the number concentration of water soluble aerosols are larger (Table 3.3). AOD at 0.5 μm is highest for urban aerosol model (Table 3.3), while the lowest AOD (a factor of 10 lower than urban AOD) is observed over continental clean model. This is because of very high concentration of black carbon and water soluble aerosols in fine mode which affect AODs mostly in the visible wavelength range.

The α value in short and long spectral ranges are found to decrease when RH increases for all the three maritime aerosol models. This occurs because for maritime aerosols, sea salt aerosols in accumulation and coarse modes hydrate with RH. Since the coarse mode is larger than the fine mode, the volume of the coarse mode increases more rapidly with RH than the fine mode; hence, the coarse mode fraction increases and α decreases. Value of α for the maritime polluted aerosol model is higher than that of maritime clean and maritime tropical model α value (Table 3.4) because of the presence of additional submicron soot aerosols [*Kedia and Ramachandran*, 2009].

Significant differences in the $\alpha^{'}$ value is observed for different aerosol models, which vary with RH. The value of $\alpha^{'}$ is found to be <0 for desert aerosols and decreases with increase in RH (Table 3.4). A negative value of $\alpha^{'}$ for desert aerosols occurs owing to the strong dominance of coarse mode particles in the aerosol size distribution. In addition, water soluble aerosols can swell with increasing RH and contribute to bigger particles. $\alpha^{'}$ is positive in maritime clean, tropical and polluted aerosol models when the atmosphere is dry (0% RH) (Table 3.4) and become negative as RH increases. This can be explained as, all maritime models consist of sea salt aerosols which grow in size as RH increases. This leads to an increase in the percentage of bigger particles and give rise to negative $\alpha^{'}$. A comparison of $\alpha^{'}$ values for different aerosol models as a function of RH reveals that (a) $\alpha^{'}$ is positive for an aerosol size distribution dominated by fine mode aerosols, (b) $\alpha^{'}$ is low, but positive for an aerosol size distribution consisting of fine and coarse mode aerosols when RH is 0% and (c) $\alpha^{'}$ is negative when coarse

mode aerosols are dominant (Table 3.4). However, it should be mentioned that the measured spectral distribution of AODs can have fine/coarse and/or a mixture of modes depending on the environment in which AOD measurements are made, the dominant aerosol sources and long range transport.

Table 3.4: *Ångström wavelength exponent (α) in short (0.4-0.5 μm) and long (0.65-0.9 μm) wavelength range, aerosol optical depth (AOD) (0.5 μm), second derivative of Ångström wavelength exponent ($\alpha^{'}$) and curvature (α_2 in equation 2.9) for different aerosol models given in Hess et al. [1998] for a range of relative humidity values.*

Models	**Spectral parameter**	**Relative Humidity (%)**				
		0	50	70	80	90
Continental clean	α_{short}	1.17	1.17	1.16	1.14	1.10
	α_{long}	1.54	1.57	1.57	1.57	1.54
	AOD	0.04	0.06	0.06	0.07	0.09
	$\alpha^{'}$	0.68	0.72	0.74	0.78	0.80
	α_2	-0.33	-0.35	-0.37	-0.38	-0.40
Continental average	α_{short}	1.20	1.19	1.18	1.16	1.11
	α_{long}	1.49	1.54	1.55	1.54	1.52
	AOD	0.09	0.13	0.15	0.17	0.23
	$\alpha^{'}$	0.56	0.65	0.69	0.72	0.77
	α_2	-0.26	-0.31	-0.33	-0.35	-0.37
Continental polluted	α_{short}	1.24	1.23	1.21	1.18	1.12
	α_{long}	1.54	1.57	1.58	1.57	1.54
	AOD	0.19	0.27	0.32	0.37	0.50
	$\alpha^{'}$	0.56	0.65	0.68	0.73	0.77
	α_2	-0.26	-0.31	-0.33	-0.35	-0.38
Urban	α_{short}	1.25	1.23	1.21	1.19	1.13
	α_{long}	1.45	1.50	1.51	1.52	1.50
	AOD	0.41	0.55	0.64	0.73	0.96
	$\alpha^{'}$	0.41	0.53	0.57	0.63	0.70
	α_2	-0.17	-0.24	-0.26	-0.29	-0.33
Desert	α_{short}	0.15	0.20	0.22	0.24	0.29
	α_{long}	0.11	0.14	0.16	0.18	0.23
	AOD	0.27	0.28	0.29	0.29	0.31
	$\alpha^{'}$	-0.09	-0.11	-0.11	-0.11	-0.10
	α_2	0.05	0.06	0.06	0.06	0.06

Continued

Maritime tropical	α_{short}	0.83	0.58	0.52	0.48	0.40
	α_{long}	1.00	0.59	0.49	0.41	0.30
	AOD	0.03	0.05	0.05	0.06	0.07
	$\alpha^{'}$	0.31	0.02	-0.05	-0.11	-0.19
	α_2	-0.16	-0.01	0.03	0.06	0.09
Maritime clean	α_{short}	0.71	0.43	0.38	0.35	0.29
	α_{long}	0.80	0.43	0.34	0.28	0.20
	AOD	0.04	0.07	0.09	0.10	0.13
	$\alpha^{'}$	0.20	-0.02	-0.08	-0.13	-0.18
	α_2	-0.11	0.00	0.04	0.06	0.09
Maritime polluted	α_{short}	0.83	0.61	0.56	0.53	0.48
	α_{long}	0.95	0.59	0.51	0.46	0.38
	AOD	0.06	0.09	0.11	0.12	0.16
	$\alpha^{'}$	0.21	-0.04	-0.08	-0.12	-0.17
	α_2	-0.11	0.02	0.05	0.07	0.09

α_2 values are found to be negative for continental (clean, average and polluted) and urban aerosol models in which fine mode aerosols dominate the aerosol size distribution (Table 3.4). α_2 values are positive but close to zero for desert aerosols. α_2 values for maritime aerosol models change sign from negative to positive as RH increases (Table 3.4). This can be attributed to the increase in the coarse mode aerosol concentration as RH increases because sea salt and water soluble aerosol species are hygroscopic. These model results show that α derived in different wavelength regions can exhibit variability depending on the dominant aerosol type in the size distribution.

The aerosol optical depth spectra measured over Ahmedabad, Gurushikhar, Kanpur and Gandhi College are analyzed for the presence of any curvature and deviation from linearity during different seasons. The value of α is calculated in two narrow spectral intervals for both short (0.4-0.5 μm) and long (0.675-0.875 μm) wavelength range and the seasonal variability are shown as a function of AOD at 0.5 μm (Figure 3.12).

The spread in the difference between α values in the short (0.4-0.5 μm) and

long (0.675-0.875 μm) wavelength regions is quite large over the study locations indicating multimodal aerosol size distribution. The difference in the α values are also found to exhibit strong seasonal dependence (Figure 3.12).

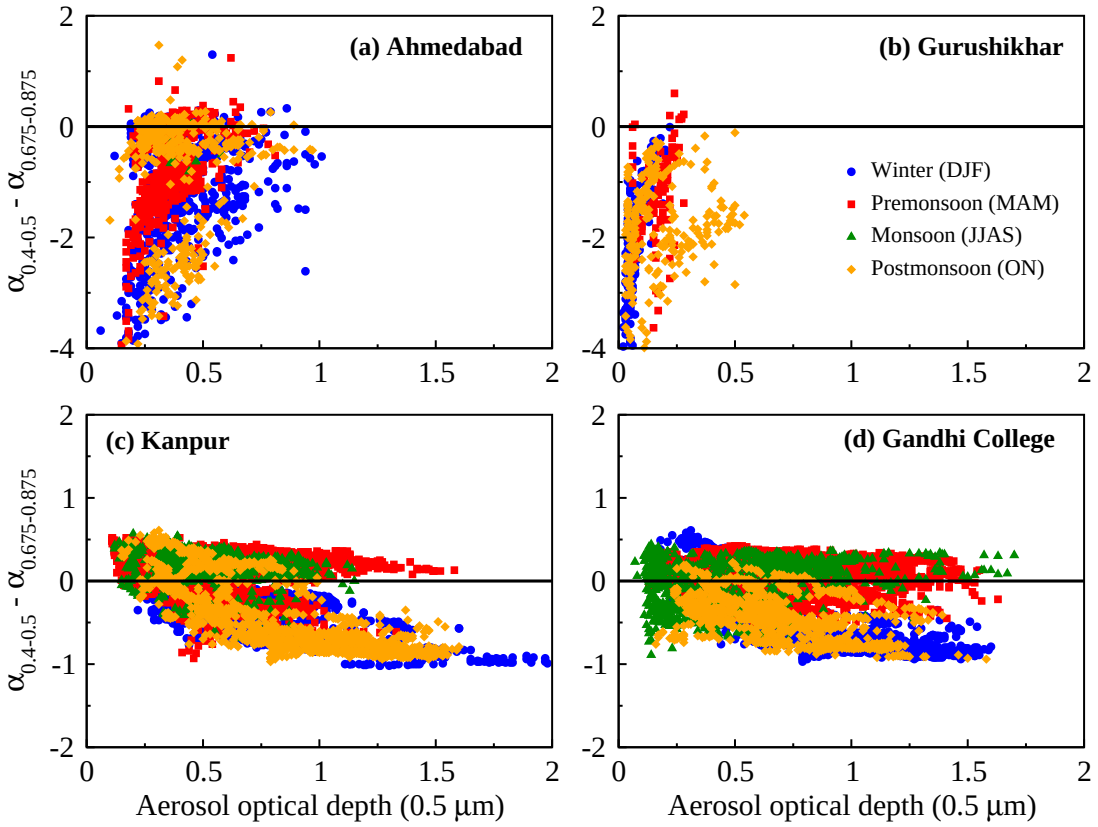

Figure 3.12: *Differences in α values obtained between short (0.4-0.5 μm) and long (0.675-0.875 μm) ranges correlated with 0.5 μm aerosol optical depths over the (a) Ahmedabad, (b) Gurushikhar, (c) Kanpur and (d) Gandhi College corresponding different seasons.*

Over all the study locations, the value of α is not unique as evidenced by the values lying above and below 0. Values located above 0 indicates a negative curvature and the presence of fine mode aerosols, while $\alpha_{0.40-0.5} - \alpha_{0.675-0.875}$ values below 0 indicate positive curvature and presence of coarse mode aerosols. The differences in α values in the spectral ranges are larger when 0.5 μm AODs are <0.5 (e.g., Ahmedabad and Gurushikhar, Figure 3.12). Near zero values of $\alpha_{0.40-0.5} -$

$\alpha_{0.675-0.875}$ represent absence of curvature in the ln τ versus ln λ data. Most of the differences in α values in the spectral ranges lie between -2 and +2 over the study locations. 58% of $\alpha_{0.40-0.5} - \alpha_{0.675-0.875}$ lie between -1 and +1 over Ahmedabad as compared to 22% over Gurushikhar. About 99% and 100% of $\alpha_{0.40-0.5} - \alpha_{0.675-0.875}$ lie between -1 and +1 over Kanpur and Gandhi College. Over Ahmedabad and Gurushikhar 41% and 78% of $\alpha_{0.40-0.5} - \alpha_{0.675-0.875}$ values are lower than -1 (Figure 3.12), respectively. This suggests the presence of coarse mode particles over Ahmedabad and Gurushikhar throughout the year and that their abundance is about a factor of two higher over Gurushikhar.

3.3.6 Curvatures in the spectral distribution of aerosol optical depth

The curvature effects in spectral distribution of AODs can be better quantified by deriving the second derivative of Ångström exponent, namely, $\alpha^{'}$ (equation 2.8) and by fitting a second order polynomial to the measured spectral distribution of AODs (equation 2.7). Variation of $\alpha^{'}$ as a function of 0.5 μm AODs over all the four study locations are shown in Figure 3.13.

Over Ahmedabad and Gurushikhar for all the four seasons $\alpha^{'}$ is mostly positive, thus, suggesting the dominance of a concave curvature and the presence of a bimodal distribution. In contrast to other study locations $\alpha^{'}$ values are higher over Ahmedabad and Gurushikhar (Figure 3.13).

Over Kanpur and Gandhi College $\alpha^{'}$ values are both negative and positive, and exhibit strong seasonal variation, indicating contribution from varied aerosol sources and types (fossil fuel/biomass burning, dust and sea salt) to the aerosol size distribution. A higher $\alpha^{'}$ value over Gurushikhar and Ahmedabad are attributed to low turbidity condition when compared to the locations in Indo-Gangetic plain. Over Kanpur and Gandhi College, most of the $\alpha^{'}$ values are found to be positive during winter and postmonsoon, while during premonsoon and monsoon negative values are also observed.

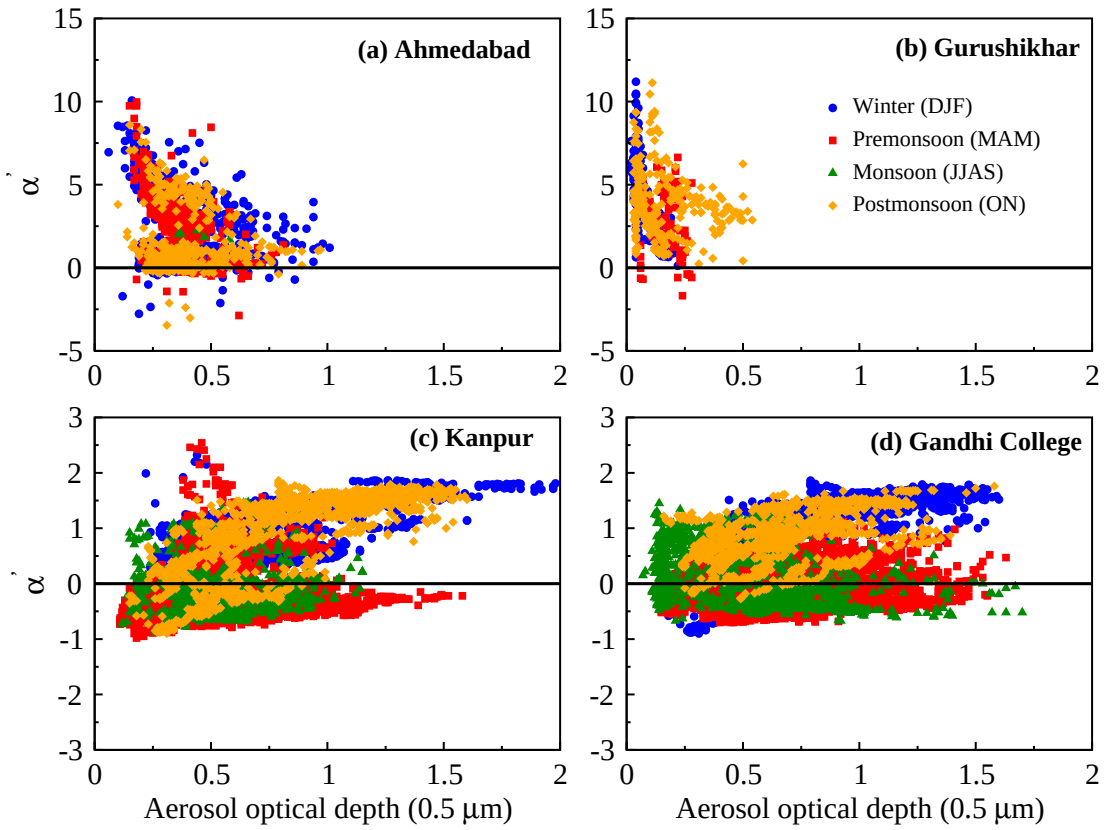

Figure 3.13: *Seasonal variation in the second order Ångström exponent (α') plotted against 0.5 μm aerosol optical depth over (a) Ahmedabad, (b) Gurushikhar, (c) Kanpur and (d) Gandhi College during different seasons.*

To further identify the dominant mode of aerosols over the study locations correlation between $\alpha_{0.4-0.5}$ and $\alpha_{0.675-0.875}$ values categorized on the basis of α_2 is plotted (Figure 3.14). Fine mode particles dominate the size distribution when the correlation between $\alpha_{0.4-0.5}$ and $\alpha_{0.675-0.875}$ is in the α_2 <0 bin, while coarse mode aerosols are dominant when the correlation falls in the α_2 >0 range [e.g., *Schuster et al.*, 2006]. The correlation between $\alpha_{0.4-0.5}$ and $\alpha_{0.675-0.875}$ exhibit seasonal and spatial variabilities (Figure 3.14).

Seasonal variation in the coefficients of polynomial fit α_1 and α_2 (equation 2.7) for all the study locations are plotted in Figure 3.15. The α_1 and α_2 are found to show strong seasonal as well as spatial variability. Higher α_2 implies a significant

curvature in the AOD spectra and the change in the sign represents the change in the dominant aerosol species, while higher α_1 value indicates a higher concentration of fine mode aerosols and vice versa.

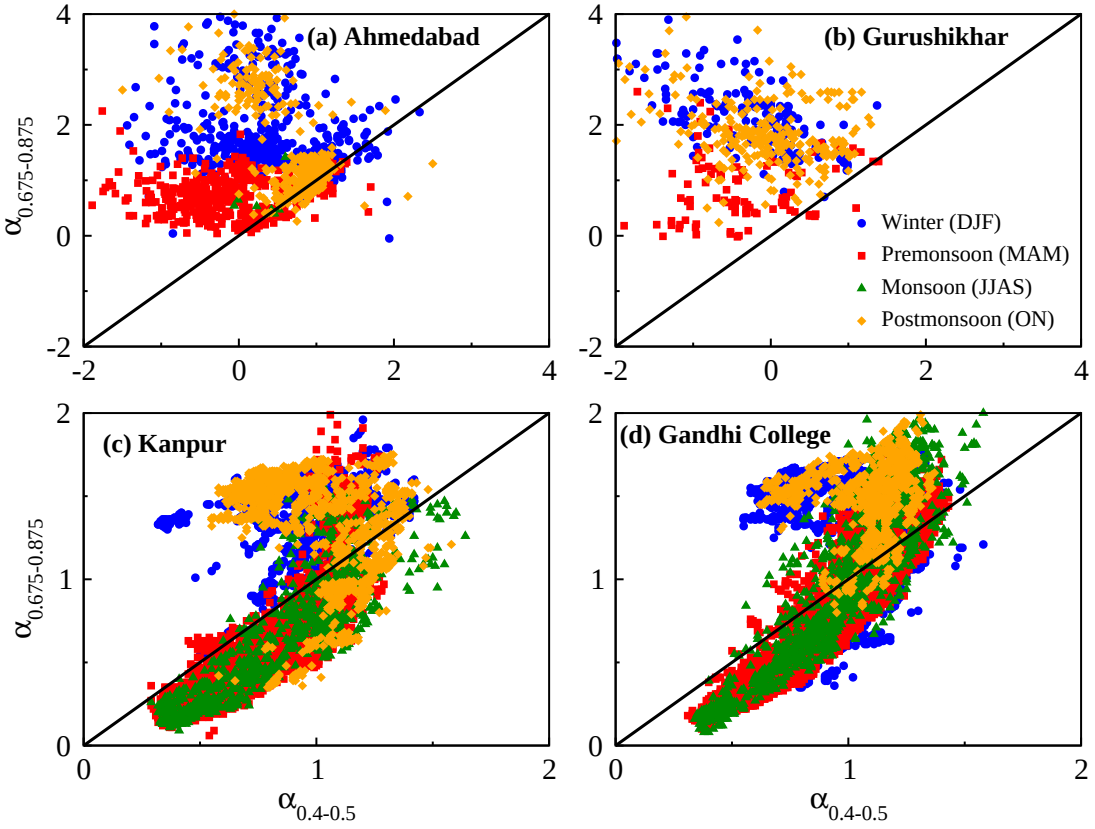

Figure 3.14: *Correlation between $\alpha_{0.675-0.875}$ and $\alpha_{0.4-0.5}$ over (a) Ahmedabad, (b) Gurushikhar, (c) Kanpur and (d) Gandhi College. The correlations are divided on the basis of curvature (α_2) of the aerosol optical depth spectra.*

α_1 values are <0 for all the seasons and for all the locations. Higher negative α_1 over Ahmedabad and Gurushikhar can be attributed to a higher concentration of fine mode aerosols in the atmosphere. Decrease in α_1 during premonsoon and monsoon is attributed to increase in coarse mode aerosols (dust, sea salt and hygroscopic growth of water soluble aerosols). Negative α_2 values in Gurushikhar and Ahmedabad during postmonsoon and winter suggest a relatively higher concentration of fine mode aerosols [e.g., *Ramachandran and Rajesh*, 2007]. During

premonsoon and monsoon, when coarse mode aerosols become dominant, both α_1 and α_2 become less negative over Ahmedabad and Gurushikhar (Figures 3.14, 3.15).

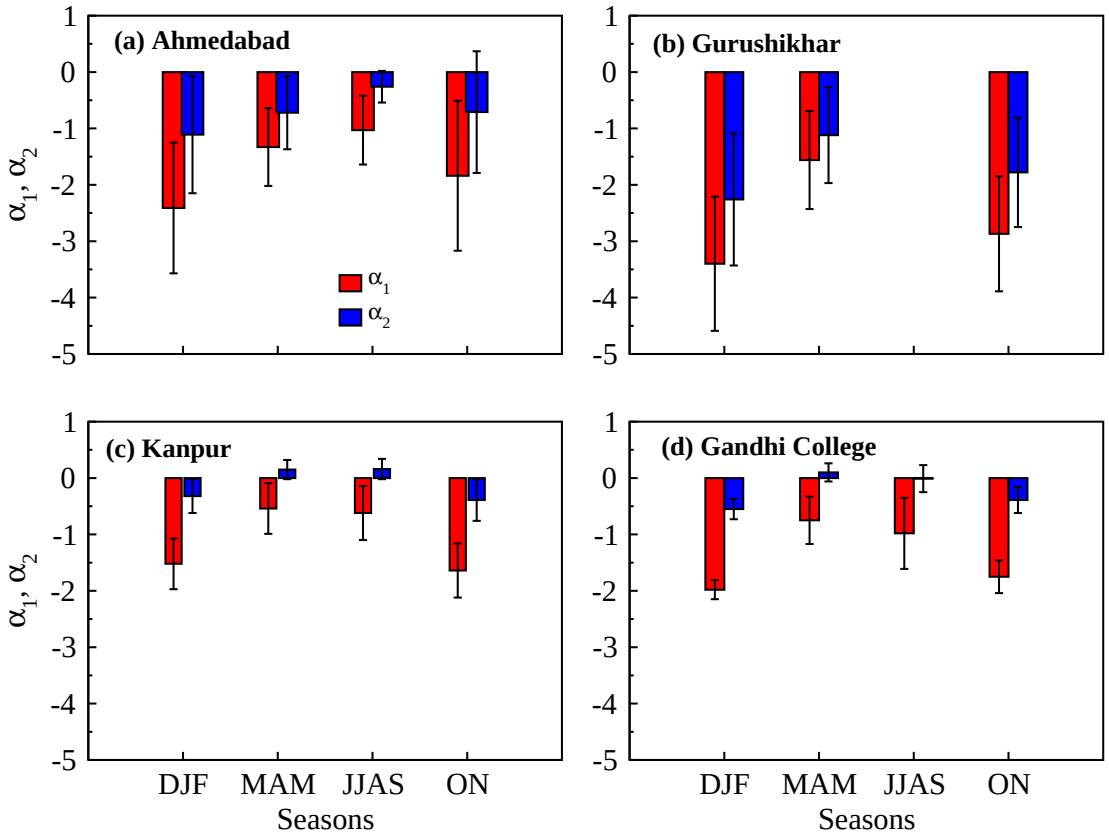

Figure 3.15: *Seasonal variation in the coefficients of polynomial fit α_1 and α_2 over (a) Ahmedabad, (b) Gurushikhar, (c) Kanpur and (d) Gandhi College computed from the polynomial fit of AODs in the spectral interval of 0.4-0.875 μm. Vertical bars correspond to $\pm 1\sigma$ variation from the mean.*

Over the locations in the Indo-Gangetic plain, the correlation between $\alpha_{0.4-0.5}$ and $\alpha_{0.675-0.875}$ lies in both α_2 <0 and α_2 >0 bins suggesting the presence of both fine and coarse mode aerosols (Figure 3.14). However, α_1 is more negative over Gandhi College when compared to Kanpur during all the seasons. This indicates the presence of a higher fine mode aerosol concentration over Gandhi College than Kanpur. A higher fine mode concentration over Gandhi College may arise due to

the fact that it is situated downwind of major urban centers and a higher amount of biomass burning as it is a rural location. Over both the locations, α_1 value is found to decrease (Figure 3.15) during premonsoon and monsoon due to the change in wind pattern as dust and sea salt can get transported over the study locations during these seasons (Figures 3.1, 3.6).

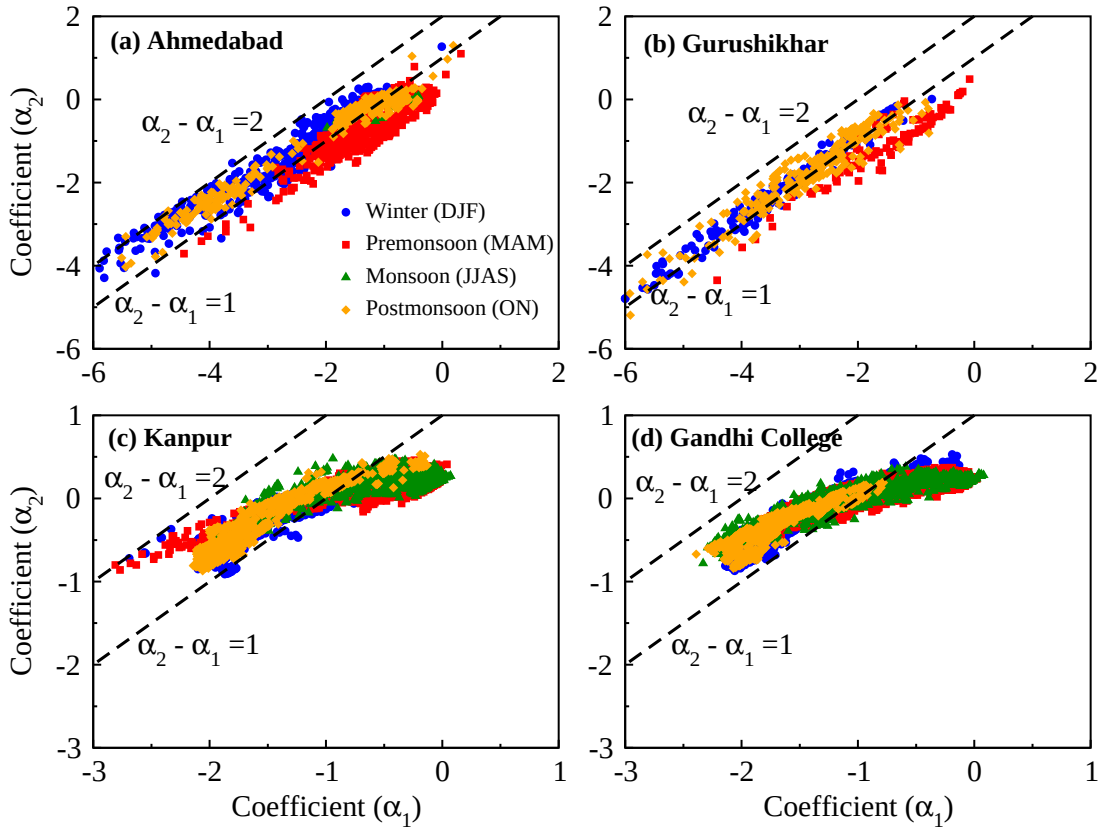

Figure 3.16: *Seasonal variation in the correlation between the coefficients α_1 and α_2 computed in the spectral range of 0.4-0.875 µm over (a) Ahmedabad, (b) Gurushikhar, (c) Kanpur and (d) Gandhi College. Straight lines correspond to α_2 - α_1 =1 and α_2 - α_1 =2.*

In Figure 3.16 α_2 and α_1 obtained for all the AOD spectra measured during 2006-2008 over Ahmedabad, Gurushikhar, Kanpur and Gandhi College are plotted. The differences in values between α_2 and α_1 can provide confirmation of the dominant mode of aerosols contributing to the aerosol size distribution. The per-

centage of AOD spectra having α_2 - α_1 $\leq$1 and α_2 - α_1 >1 and <2 are found to exhibit strong spatial as well as temporal variation (Figure 3.16; Table 3.5).

Table 3.5: *Percentage of aerosol optical depth spectra classified on the basis of whether $\alpha_2 - \alpha_1$ $\leq$1 or >1 and <2 over (a) Ahmedabad, (b) Gurushikhar, (c) Kanpur and (d) Gandhi College corresponding to different seasons.*

	Ahmedabad	**Gurushikhar**	**Kanpur**	**Gandhi College**
$\alpha_2 - \alpha_1$		**Winter**		
≤ 1 *	12	78	20	0
> 1 and < 2 **	87	22	80	100
		Premonsoon		
≤ 1 *	85	92	84	69
> 1 and < 2 **	15	8	16	31
		Monsoon		
≤ 1 *	70	-	73	51
> 1 and < 2 **	30	-	27	49
		Postmonsoon		
≤ 1 *	36	38	7	1
> 1 and < 2 **	64	62	93	99

* *Coarse mode dominance.*
** *Presence of wide range of fine mode fractions or mixture of modes.*

Ahmedabad, Kanpur and Gandhi College (Table 3.5) are marked by the dominance of wide range of fine mode fractions or mixture of modes during winter; $\geq$80% of the AOD spectra lie in the α_2 - α_1 >1 and <2 range. During winter over Gurushikhar more than 75% of the AOD spectra are in the α_2 - α_1 <1 range owing to the dominance of coarse mode (e.g., dust and sea salt) aerosols. It is notable that 20% of AOD spectra over Kanpur had α_2 - α_1 value <1 indicating the presence of coarse mode aerosols, whereas over Gandhi College not a single AOD spectra indicated the presence of coarse mode aerosols (Table 3.5).

During premonsoon and monsoon, coarse mode aerosols (dust and sea salt)

become dominant in the atmosphere over all the study locations as more than 50% of AOD spectra have α_2 - α_1 $\leq$1 (Table 3.5). Over Ahmedabad, in quite contrast to the other study locations on some days during winter and postmonsoon α_2 - α_1 >2 (Figure 3.16), indicating that only fine mode aerosols contributed to the aerosol size distribution. However, the percentage of AOD spectra in this case was low (1%). Over Ahmedabad and Gurushikhar for more than 35% of AOD spectra, α_2 - α_1 $\leq$1 indicating the presence of coarse mode aerosols during postmonsoon.

The presence of coarse mode (mainly dust and remnants of sea salt) aerosols during postmonsoon can be attributed to the long range transport as on certain days winds are from the south west over both the locations (Figures 3,1, 3.6) [e.g., *Ramachandran and Rajesh*, 2007]. The largest change in the size distribution occurs from winter to premonsoon over Ahmedabad, Kanpur and Gandhi College while over Gurushikhar the largest change is observed from postmonsoon to winter (Table 3.5).

These results are further corroborated in Figure 3.17 where the differences between α_2 and α_1 are plotted with respect to 0.5 μm AODs for different seasons corresponding to each study location. Over all the study locations, winter and postmonsoon AODs lie in the α_2 - α_1 >1 and <2 range indicating the presence of mixture of fine modes.

The findings from the current study agree well with the results obtained from other studies e.g., *Reid et al.* [1999], *Cachorro et al.* [2001], *Holben et al.* [2001] and with those obtained over four AERONET sites which encounter varied aerosol types [*Kaskaoutis et al.*, 2007]. For more than 90% of the AOD spectra over Nauru and Solar Village α_2 - α_1 were <1 which indicated a significant coarse mode fraction in the size distribution, comprising sea salt and desert dust particles. Nauru is a remote island in the tropical Pacific Ocean and has a small aerosol loading, while Solar village in Saudi Arabia is a continental remote site with significant contribution of desert aerosols. α_2 - α_1 values were between 1 and 2 or >2 for most of the time during the year over Alta Floresta and Ispra [*Kaskaoutis et al.*, 2007].

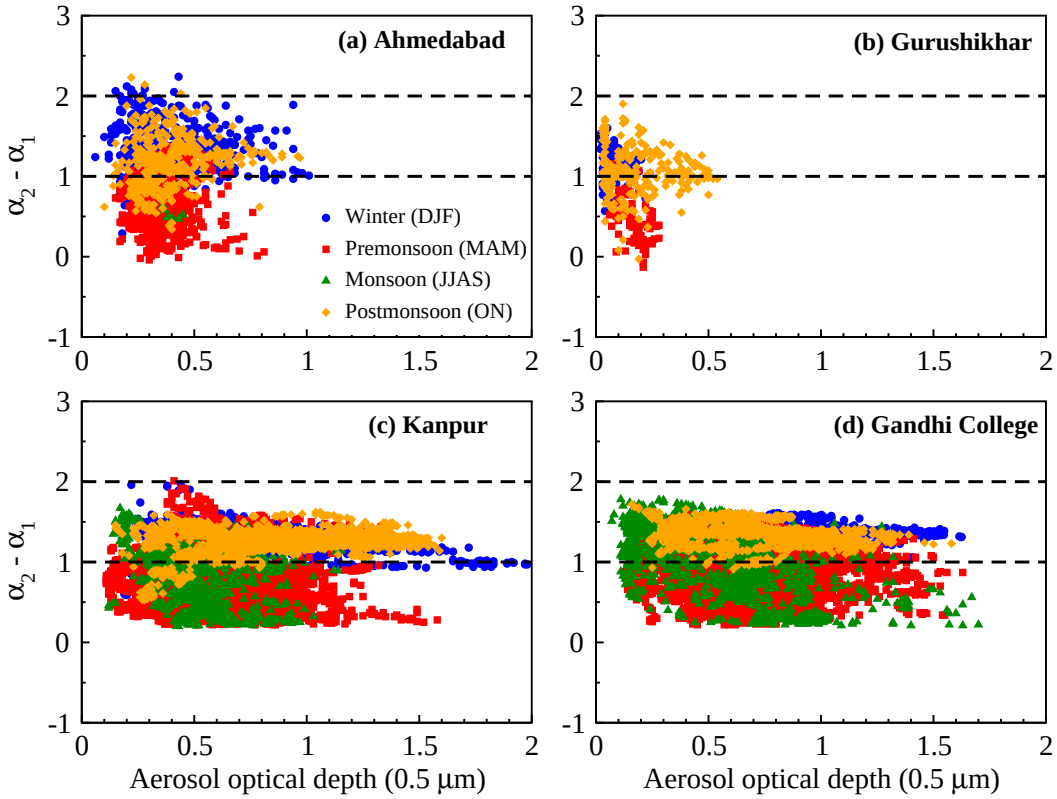

Figure 3.17: *Seasonal variation in the differences between the coefficients* α_2 *and* α_1 *as a function of 0.5 μm aerosol optical depths over (a) Ahmedabad, (b) Gurushikhar, (c) Kanpur and (d) Gandhi College. Straight lines represent* α_2 - α_1 *=1 and* α_2 - α_1 *=2.*

Alta Floresta in Brazil is a rural site which gets influenced by biomass burning smoke during the fire season (August-September) while Ispra in Italy is an urban/industrial location with significant anthropogenic and industrial activities.

3.4 Conclusions

A detailed analysis of ground based measurements of aerosol characteristics has been performed over four different locations (Ahmedabad, Gurushikhar, Kanpur and Gandhi College) in the Indian subcontinent during 2006-2008. Seasonal and interannual variabilities in AOD and aerosol size distribution are investigated over these locations. AODs over Ahmedabad and Gurushikhar obtained at wavelengths

$\geq$0.875 μm show winter low and summer or premonsoon high, while AODs at visible wavelengths do not exhibit significant seasonal variation. Over Kanpur and Gandhi College winter AODs are higher at lower wavelength (0.4 μm). α values during postmonsoon and winter are higher than premonsoon and monsoon over all the locations. α values are lower over Gurushikhar ($\leq$1.0) indicating the dominance of coarse mode aerosols (dust and/or sea salt). AOD ratio, ratio of AODs obtained at 0.4 and 0.875 μm, during postmonsoon and winter are higher than those obtained during premonsoon and monsoon. Aerosol volume size distributions obtained over Kanpur and Gandhi College showed a bimodal distribution during all seasons. SSA values over Kanpur and Gandhi College exhibit strong spectral and seasonal dependence. SSA is lower in winter due to abundant fine mode particles, while premonsoon and monsoon season SSA increases with wavelength due to dominance of coarse mode particles. Postmonsoon SSA spectra is linear due to wet removal of submicron and supermicron aerosols.

Spectral distribution of AODs are examined by deriving the α value in the 0.4-0.875 μm spectral range, in narrow spectral ranges (0.4-0.5 μm and 0.675-0.875 μm), second derivative of Ångström exponents ($\alpha^{'}$) and by second order polynomial fits to determine the curvature. The analysis has been performed to determine the dominant mode of aerosols that governs the aerosol size distribution on seasonal and spatial scales over the Indian subcontinent. The second order polynomial fits to the spectral distribution of AODs revealed the presence of both concave and convex curvatures during different seasons indicative of the presence of bimodal aerosol distribution over the study locations. The α values determined in narrow wavelength bands are not single valued thereby confirming that the aerosol size distribution is of mixed type with contribution from fine and coarse mode aerosols over the study locations. The second derivative of Ångström exponents ($\alpha^{'}$) over Ahmedabad and Gurushikhar for all the four seasons is mostly positive, and higher than the other locations. Over Kanpur and Gandhi College $\alpha^{'}$ values are negative and positive, and exhibit strong seasonal variation, suggesting the contribution

from varied aerosol sources. The differences between α_2 and α_1 revealed the dominance of wide range of fine mode fractions or mixture of modes during winter over Ahmedabad, Kanpur and Gandhi College. During premonsoon and monsoon, coarse mode aerosols (dust and sea salt) are dominant over all the study locations. More than 90% of AOD spectra are dominated by fine mode or a mixture of modes aerosols during postmonsoon over the locations in the Indo-Gangetic region.

Thus, the current analysis and results over a regional aerosol hot spot, for the first time, have given new and important insights on the spatial and temporal variabilities in the dominant aerosol types that contribute to the spectral distribution of AODs in different seasons. These results will be helpful in remote sensing for refinement, evaluation and validation of the retrieval algorithms, and in estimating the impact of seasonal and spatial variations due to aerosols on regional and global climate.

Chapter 4

Aerosol optical and physical characteristics over oceanic regions

The Indian subcontinent is densely populated and has industrialized areas on the east and western sides. The prevailing meteorological conditions during winter transport the pollutants from these areas, which are mainly anthropogenic to the surrounding marine environments such as the Arabian Sea, the Bay of Bengal and the Indian Ocean. During southwest monsoon winds are stronger, moist and are from the marine and western regions surrounding India which brings large amount of sea salt to the continent. The Bay of Bengal and the Arabian Sea provides an ideal condition to study the formation and transport of wide variety of different aerosol species, their physical and chemical characteristics, and the effect of these diverse aerosols on the regional climate forcing.

Several cruise expeditions have been conducted during the last two decades over the oceanic regions adjoining India, such as, Indian Ocean Experiment (INDOEX), ARMEX (Arabian Sea Monsoon Experiment), and Bay of Bengal Monsoon Experiment (BOBMEX) etc. for studying the aerosol characteristics over the marine environment surrounding India [*Jayaraman et al.*, 1998; *Bates et al.*, 1998; *Devara et al.*, 2001; *Rajeev et al.*, 2000; *Quinn et al.*, 2000; *Ramanathan et al.*, 2001; *Bhat et al.*, 2001; *Tahnk and Coakley*, 2002; *Dani et al.*, 2003; *Ramachandran*, 2004;

Moorthy et al., 2005; *Babu et al.*, 2008].

INDOEX was conducted during the winter monsoon seasons of 1996-1999 over the Indian Ocean and the Arabian Sea [*Tahnk and Coakley*, 2002; *Quinn et al.*, 2000]. During INDOEX, the top of the atmosphere aerosol radiative forcing was found to vary from -30 to -33 Wm^{-2}, the surface forcing ranged from -64 to -71 Wm^{-2} and the atmospheric forcing varied from +32 to +38 Wm^{-2} per unit 0.55 μm optical depth in the Northern Hemisphere [*Tahnk and Coakley*, 2002]. ARMEX was conducted over northern and central Arabian Sea during the Indian summer monsoon season. The fraction of anthropogenic components to the total aerosol was found to decrease from 60% in March to 18% in June, while that of the sea salt aerosol increased from 38% in March to 65% in June during ARMEX [*Babu et al.*, 2008]. BOBMEX was conducted in the central and north Bay of Bengal during July-August, 1999. During BOBMEX, a bimodal aerosol size distribution was observed near the coast while a power law size distribution was observed away from the coastal region indicating large variability in the size distribution of aerosols [*Dani et al.*, 2003].

Recently, an Integrated Campaign for Aerosols, gases and Radiation Budget (ICARB) was conducted over the Indian subcontinent and adjoining oceanic regions during the premonsoon season of March-May 2006. The aim of this observational campaign was to characterize the spatiotemporal distribution of aerosols, trace gases and radiative forcing over these regions. The important objectives of ICARB were to

(a) study the effect of different aerosol species present in the atmosphere over India and surrounding oceanic regions, identify the main natural and anthropogenic sources of aerosols.

(b) study the effect of long range transport of aerosols from different sources over the oceanic regions, their effect on the regional climate, and the sinks of these aerosol particles in the atmosphere.

(c) capture the regional and temporal variability in natural and anthropogenic hot

spots, and their radiative impact over the Bay of Bengal and the Arabian Sea.

This chapter discusses the features of aerosol optical properties measured during ICARB on board a ship cruise over the Bay of Bengal and the Arabian Sea.

4.1 Cruise track

The ICARB cruise expedition was conducted on the Oceanographic Research Vessel *Sagar Kanya* during 18 March to 10 May 2006 (Figure 4.1). The first phase of ICARB was conducted over the Bay of Bengal during the months of March-April which started on 18 March 2006. The ship originated from the Chennai port (13.1^{o}N, 80.2^{o}E), a metro city on the coast of India. Initially, the ship went toward the north of the Bay of Bengal and moved around the coastal regions of southeast India. It reached near Bangladesh on 21 March which was the maximum latitude covered over the Bay of Bengal during the cruise. After this the cruise moved westward along the direction of wind flow and then it changed its direction opposite to the wind direction, to address the potential impact of long range transport from different regions. This type of alternate motion toward and away from the wind direction was followed for the next few days during which it cruised to the maximum longitude of 92.6^{o}E in the mid ocean on 26 March (Figure 4.1). On its return the cruise passed Sri Lanka on 10 April and reached Kochi (9.97^{o}N, 76.2^{o}E) on 12 April thereby completing the first phase of ICARB.

The second phase of ICARB started on 18 April from Kochi toward the Arabian Sea. The ship moved toward the west of the Arabian Sea in the initial days following a near straight path and reached the interior oceanic region. The ship reached 9.59^{o}N, 58.02^{o}E near the horn of Africa in the west on 22 April, which was the farthest position the ship went from the Indian coast during the cruise. On 22 April it changed its direction from west to east and came near the continent. For the next few days it continued its path around the continent of southwest part of India. The maximum latitude up to which the ship went was 21.37^{o}N on 9 May

near the Gujarat coast.

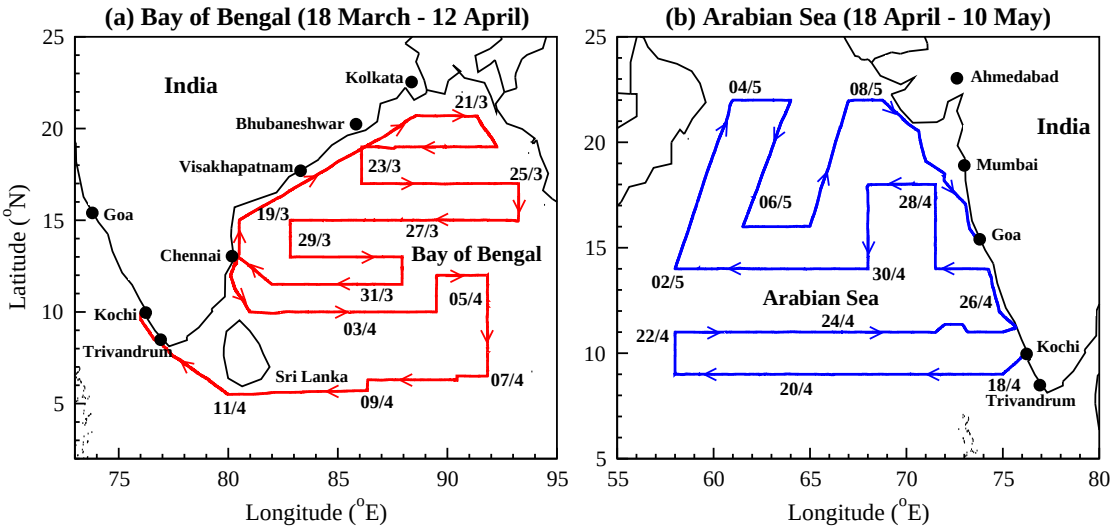

Figure 4.1: *Cruise track of oceanographic research vessel Sagar Kanya over the (a) Bay of Bengal and (b) Arabian Sea during ICARB.*

The ship reached Goa port (15.4^{o}N, 73.8^{o}E) on 10 May after 23 days of sailing and completed the second phase. The total duration of the cruise including both phases was 55 days.

4.2 Wind pattern and meteorological conditions

Surface level mean wind patterns are plotted in Figure 4.2 for the first (18 March-12 April) and second (18 April-10 May) phases of the ICARB cruise. Over the Bay of Bengal (Figure 4.2a) the winds were calm which arised mainly from the Bay of Bengal with signatures of transport from the Indian subcontinent. The wind patterns were found to be more stronger in the southern part during the second phase (Figure 4.2b). The wind fields during April-May 2006 showed an anticyclonic circulation over the Arabian Sea and transport from the west Africa which was also found to affect the coastal India. Meteorological parameters (temperature, wind speed, relative humidity and precipitation) were measured on board the ship at 1-hour interval during the ICARB period.

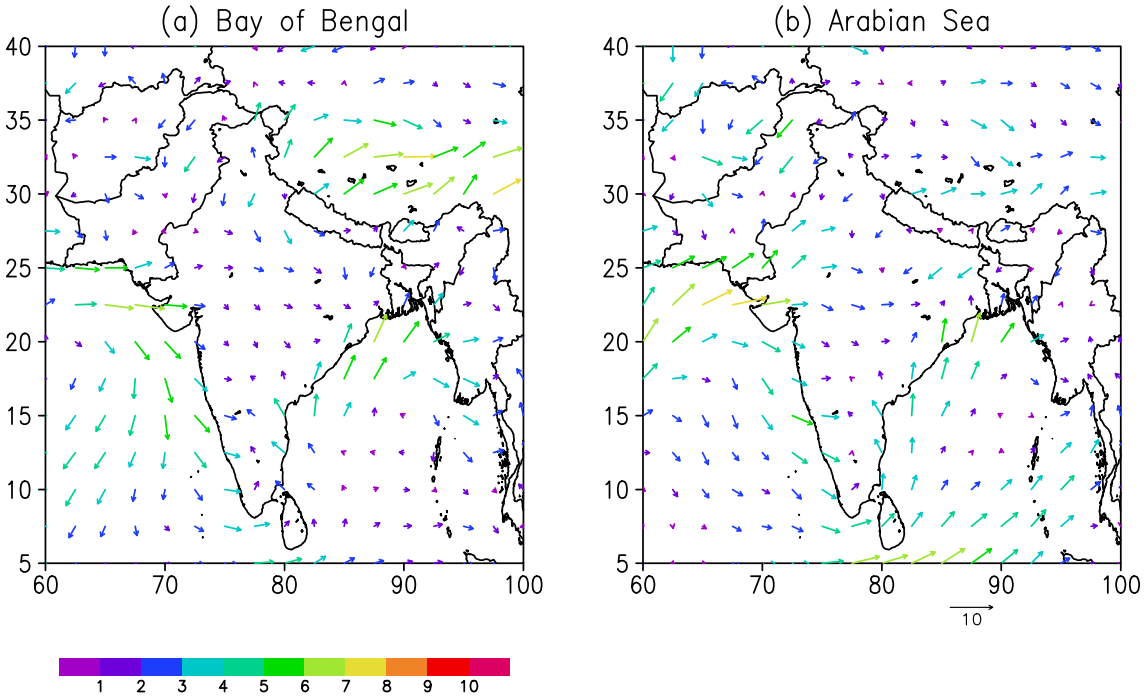

Figure 4.2: *Surface level mean winds (ms^{-1}) from NCEP reanalysis data over the (a) Bay of Bengal and (b) Arabian Sea during ICARB.*

The daily mean and $\pm 1\sigma$ in temperature, wind speed and relative humidity over the Bay of Bengal and the Arabian Sea are shown in Figure 4.3. The daily mean air temperature over the Bay of Bengal and the Arabian Sea was found to be in the range of 26-30^{o}C. In general, the daily mean temperature over the Arabian Sea was higher than the Bay of Bengal. The average surface level wind speed was 4.5 ms^{-1} over the Bay of Bengal while over the Arabian Sea it was about 5.4 ms^{-1}. The daily mean wind speeds varied from a low of about 2 ms^{-1} on 20 March to a high of about 8 ms^{-1} on 11 April over the Bay of Bengal.

Over the Arabian Sea, the wind speeds were higher than 5 ms^{-1} during 26-30 April, with maximum wind speed of 9.7 ms^{-1} occurring on 28 April (Figure 4.3). The mean relative humidity (RH) was found to be around 73% and 72% over the Bay of Bengal and the Arabian Sea respectively, and RH varied by about 5-10% from the mean. Note that RH from 1 to 10 May were not available.

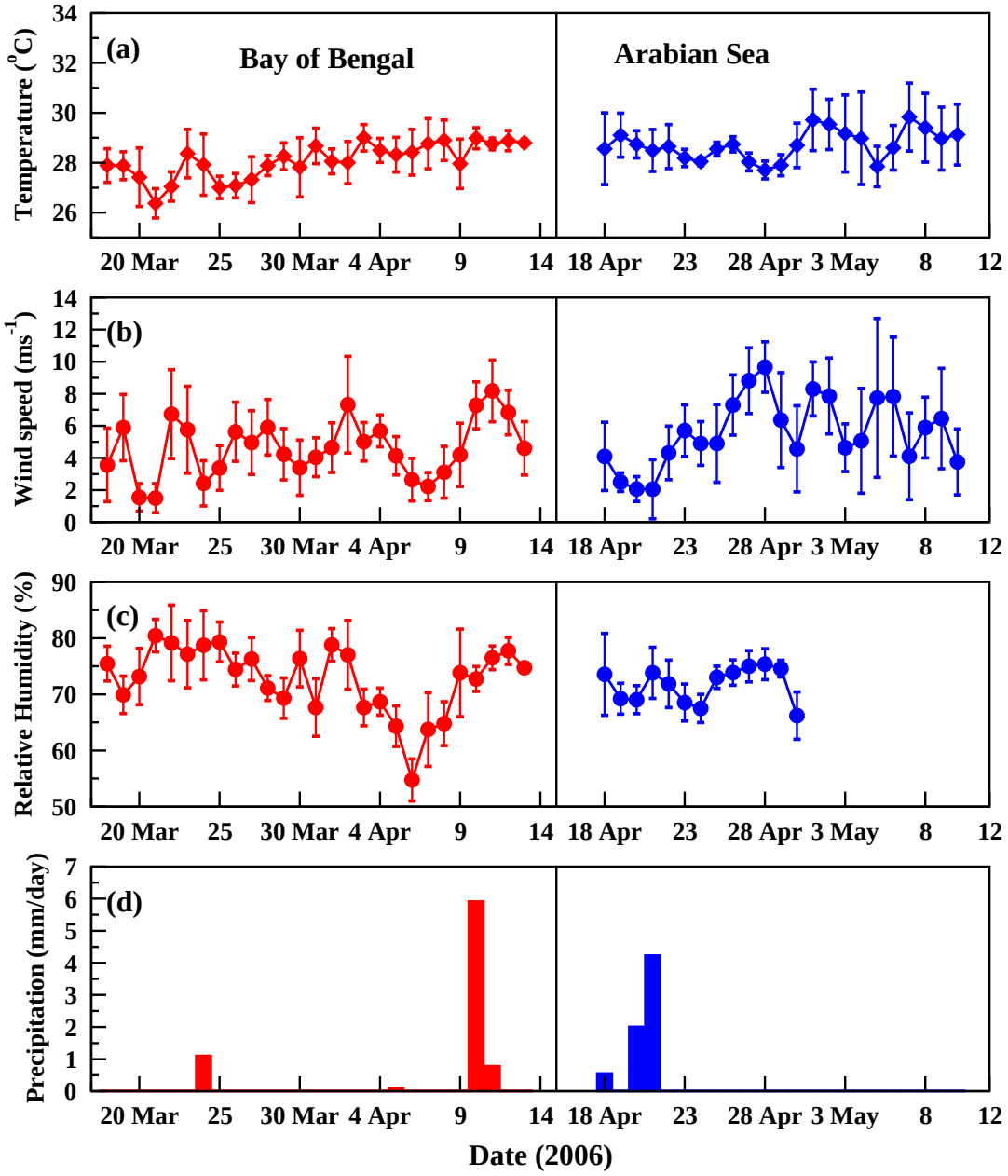

Figure 4.3: *Daily mean meteorological conditions (a) Temperature (°C), (b) wind speed (ms^{-1}), (c) relative humidity (%) and (d) precipitation (mm/day) over the Bay of Bengal and the Arabian Sea during the cruise period. Vertical bars represent $\pm 1\sigma$ from the mean.*

The sky conditions were generally clear, while on some days cloud patches were seen. In this work, measurements made during clear sky conditions only are analyzed and discussed [*Kedia and Ramachandran*, 2008a].

4.3 Back trajectory analysis

Seven day air back trajectory analysis has been performed considering the residence time of different types of aerosols, which is about a week in the lower atmosphere.

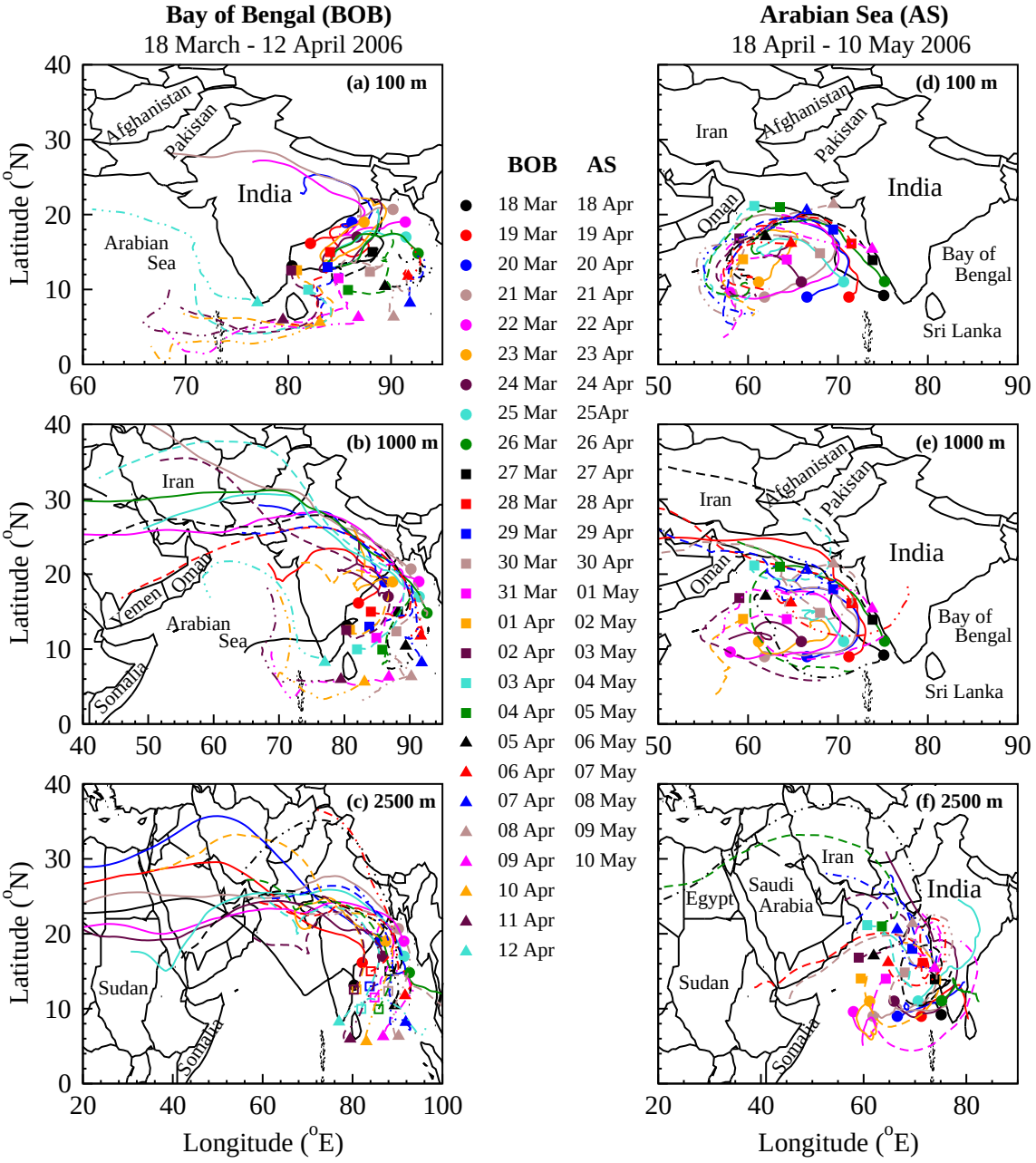

Figure 4.4: *Seven day air back trajectory corresponding to 100 m, 1000 m, and 2500 m over (a, b, c) the Bay of Bengal and (d, e, f) Arabian Sea, calculated using vertical velocity fields at an hourly interval. Symbols denote the mean latitude-longitude position of the ship corresponding to each day of the cruise.*

Air back trajectories are calculated for each day corresponding to 1200 Indian Standard Time (+0530 GMT) and for the mean latitude-longitude position of the ship (Figures 4.4a-f) at different heights using the HYSPLIT meteorological model's vertical velocity fields [*Draxler and Hess*, 1998]. The 10 m air back trajectories are quite close to the surface and aerosols at this height will settle faster; in addition, the 10 m air back trajectories are more or less similar to the air back trajectories corresponding to 100 m. Thus, due to the above reasons, and for the purposes of clarity and illustration, air back trajectory analysis is restricted to those obtained at 100, 1000 and 2500 m heights.

Air back trajectories over the Bay of Bengal and the Arabian Sea originate from different arid/semiarid, continental and marine locations suggesting different source regions and aerosol types (Figure 4.4). The air back trajectories originate from arid/semiarid regions (Pakistan, Iran and Saudi Arabia) and pass through continental India and Indo-Gangetic plain before reaching the Bay of Bengal.

In contrast, over the Arabian Sea most of the air back trajectories are of marine origin (Bay of Bengal, Arabian Sea, Figures 4.4), though on a few days air masses are found to originate and pass through continental India before reaching the Arabian Sea.

4.4 Results and Discussion

Daily mean as well as latitudinal and longitudinal variation in aerosol optical properties have been studied during March-May 2006 over the Bay of Bengal and the Arabian Sea. In this chapter, a brief description of the important features observed in the aerosol properties over both the oceanic regions are presented.

4.4.1 Aerosol optical depth

Aerosol optical depths were measured using a hand held sun photometer for five wavelength bands (0.4, 0.5, 0.65, 0.75, 0.875 μm) and their daily mean values were obtained. The variation in daily mean AOD at two representative wavelengths of

0.5 and 0.875 μm for the entire cruise period are shown in Figure 4.5. For purposes of clarity, further discussion on AODs is restricted to 0.5 μm AODs; the features discussed are similar at other wavelengths as can be seen in 0.875 μm (Figure 4.5b).

At the outset, it is clear that the AODs exhibit large day to day variations over both oceanic regimes. AOD value on 18 March, when the ship started sailing away from Chennai coast is about 0.4. In the initial days of sailing the ship covered the oceanic regions closer to the eastern coastline which has highly populated cities (e.g., Kolkata, Visakhapatnam). After 20 March, AODs start increasing and reach the highest value of about 0.9 over the Bay of Bengal on 24 March, when the ship was in the interior region of the Bay of Bengal. The higher AODs could have resulted due to the change in the wind pattern and due to transport of pollutants from the continent. A sharp decrease in AOD is seen around 26 March which is attributed to wet deposition of aerosols from the precipitation that occurred on 24-25 March (Figure 4.3d). No significant variation in the AOD value is observed for the next 5 days because of a relatively cleaner atmosphere due to rain.

The minimum value of AOD over the Bay of Bengal during this period is around 0.1 on 4 April. After 4 April, AODs again start increasing slowly and constantly as the ship changed its direction and moved in the direction of wind flow. The value of AOD is found to be higher (0.38) when the ship passed near Sri Lanka and AOD is found to be 0.55 when the ship reached Kochi after completing the first phase of the ICARB cruise. 7-day back trajectory analysis shows that during 10-11 April winds above 1000 m originated from central, west India and traveled through India before reaching the measurement location (Figure 4.4).

During the second phase of ICARB over the Arabian Sea the measured AODs are found to be relatively lower. After about 5 days of sailing in the Arabian Sea, AODs increase sharply and reach the highest value of about 0.8 on 26 April after which AODs start decreasing sharply. The minimum value of AOD over the Arabian Sea is about 0.1 (30 April-3 May). The high AODs occur when the ship was cruising near the coast and when the winds were found to originate and pass

through arid and urban regions before reaching the measurement locations.

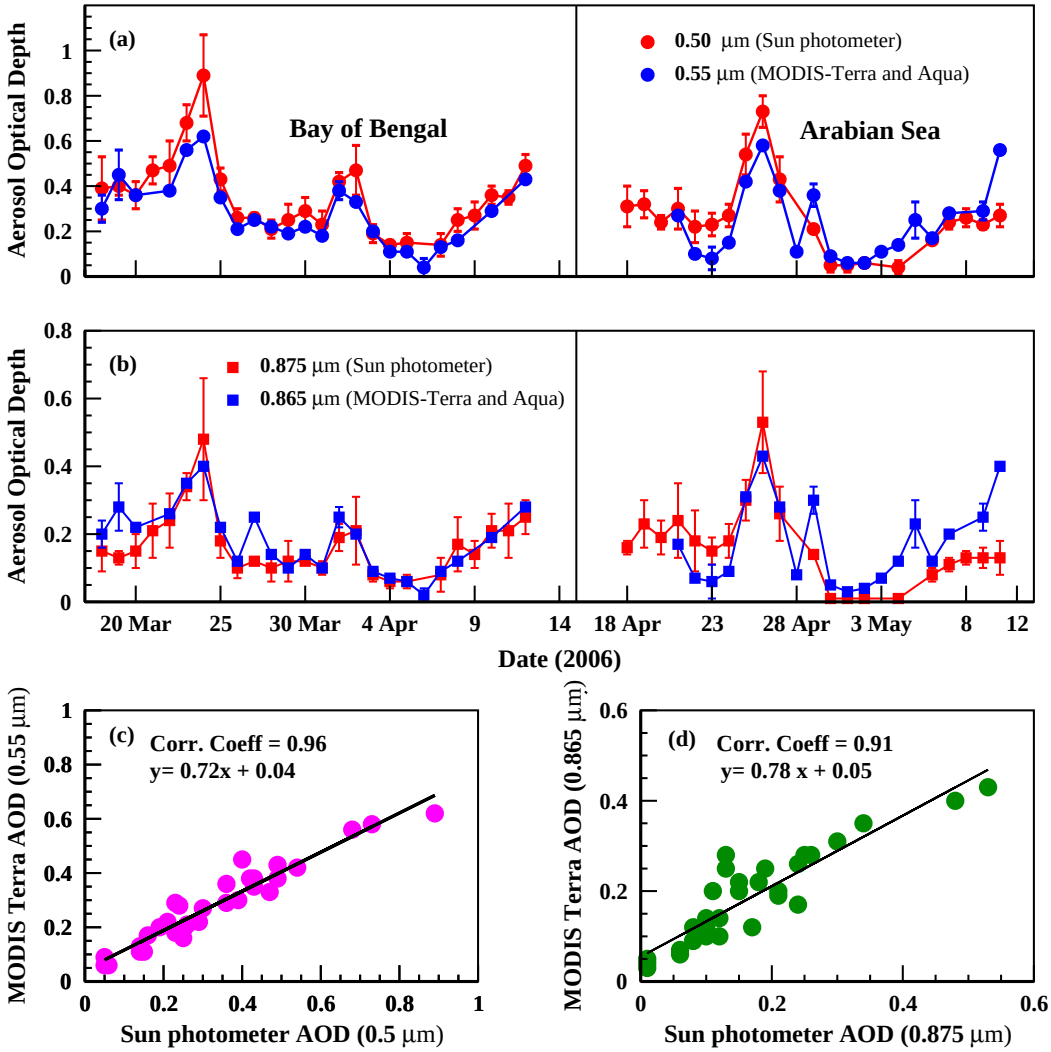

Figure 4.5: *(a) Comparison of daily mean 0.5 µm AODs derived using sun photometer with that of MODIS Terra and Aqua satellites derived AODs at 0.55 µm. (b) Daily mean 0.875 µm AODs measured using Sun photometer in comparison with MODIS Terra and Aqua AODs at 0.865 µm. The vertical lines in the graphs mark the end of first leg of the ICARB cruise. (c) Scatter plot between 0.5 µm AODs measured using sun photometer and 0.55 µm AODs derived from MODIS Terra and Aqua satellites. (d) Scatter plot of sun photometer measured 0.875 µm AODs and MODIS Terra and Aqua derived 0.865 µm AODs.*

AODs are low when the ship was in the middle of the Arabian Sea (28 April-1 May) and when the winds that transport pollutants were of marine origin. AODs

start increasing after 3 May when the ship was near the coast and moved eastward along the direction of wind flow. AOD was about 0.3 when the ship reached Goa port on 11 May after completing ICARB cruise. The mean value of 0.5 μm aerosol optical depth over the Bay of Bengal (first phase average) is found to be 0.36 whereas that over the Arabian Sea (second phase average) is 0.25. These results suggest that day to day and spatial differences in aerosol optical characteristics across the Bay of Bengal and the Arabian Sea arise due to variations in aerosols produced locally and long range transport. 7-day back trajectory analysis shows that during 10-11 April winds above 1000 m originated from central, west India and traveled through India before reaching the measurement location (Figure 4.4) [*Kedia et al.*, 2010].

A comparison between the daily mean 0.55 and 0.865 μm AODs from ground based measurements and MODIS Terra and Aqua satellites are also shown in Figure 4.5. It is found that variations in AOD obtained from MODIS track well the variation in AODs measured using sun photometer. The increasing and decreasing trends are similar for ground based and satellite derived AODs. The mean value of MODIS AODs at 0.55 μm over the Bay of Bengal and the Arabian Sea are calculated to be 0.28 and 0.23, respectively. The difference in the AODs calculated by ground based and satellite measurements could arise due to the (1) difference in the wavelengths used between the two measurements (0.5 and 0.875 μm for sun photometer, and 0.55 and 0.865 μm for MODIS); (2) temporal difference between the two systems (sun photometer AOD is the mean AOD derived from 0800 LST to 1700 LST, while MODIS AOD is the mean of 1030 and 1330 LST AODs); (3) spatial difference (sampling error associated with the satellite derived AOD, because while obtaining the satellite derived values, the mean latitude and longitude are only taken); and finally the (4) uncertainties associated in deriving AODs from both ground based and satellite retrievals.

The scatter plots between daily mean AODs at 0.5 and 0.875 μm from ground based measurements, and 0.55 and 0.865 μm from satellite measurements are shown

in Figures 4.4c and 4.4d. In spite of all the differences mentioned above, the correlation is greater than 0.90 (0.96 for 0.5 μm AODs and 0.91 for 0.875 μm AODs) indicating a good agreement between the ground based and satellite derived AODs [*Kedia and Ramachandran*, 2008a].

4.4.2 Aerosol fine mode fraction

Fine mode fraction (FMF) is defined as the ratio of the accumulation mode optical depth to the total optical depth at 0.55 μm [*Anderson et al.*, 2005; *Remer et al.*, 2005]. The FMF value (ranges from 0 to 1) provides quantitative information on the nature of the size distribution of aerosol particles in the atmosphere. When FMF = 1, it represents a pure accumulation mode particles (below 1 μm which produces mainly from anthropogenic activities); where as FMF = 0 represents a single coarse mode particles (originating from natural sources such as wind blown mineral dust and sea salt). For any intermediate value it represents a bimodal type particle distribution, where both accumulation and coarse modes can contribute to the total AOD in proportion [*Remer at al.*, 2005; *Anderson et al.*, 2005; *Gassò and O'Neill*, 2006].

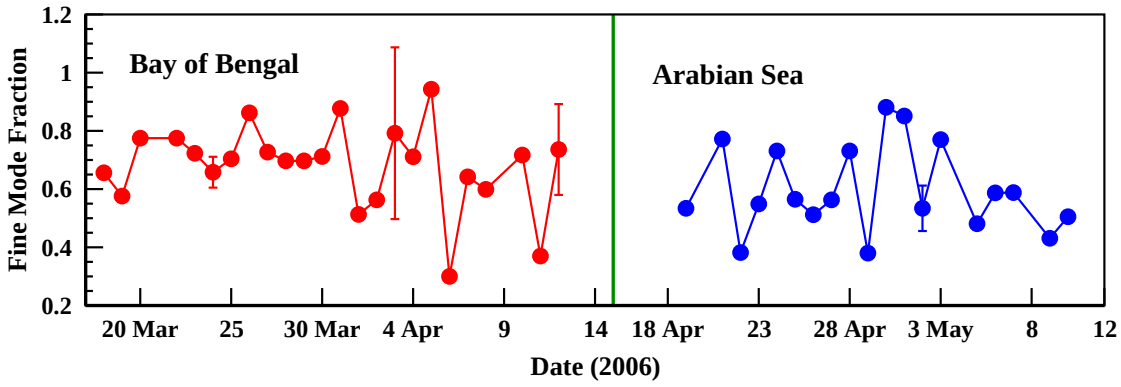

Figure 4.6: *Daily mean MODIS fine mode fraction along with* $\pm 1\sigma$ *variation from the mean during ICARB.*

It should be noted that lower FMF values can also result because of hygroscopic growth of water soluble aerosols [*Ramachandran*, 2007]. It has been seen that

MODIS slightly overestimates fine mode fraction for dust-dominated aerosols and underestimates in smoke- and pollution-dominated aerosol conditions on the order of about 0.1-0.2 [*Kleidman et al.*, 2005; *Anderson et al.*, 2005; *Gassò and O'Neill*, 2006].

Daily mean FMF derived using MODIS (Terra and Aqua) over the Bay of Bengal and the Arabian Sea are shown in Figure 4.6. The average FMF value over the Bay of Bengal is found to be 0.71±0.10 while that over the Arabian Sea is 0.60±0.09 (Figure 4.6). A higher FMF over Bay of Bengal represents an abundance of accumulation mode particles, which resulted in higher AODs at shorter wavelengths as seen earlier, when compared to the Arabian Sea.

4.4.3 Ångström coefficients (α, β)

The daily mean Ångström coefficients (equation 2.5) obtained from the in situ AODs in the wavelength range of 0.4-0.875 μm during the ICARB period are shown in Figure 4.7. Large variation in the value of both α and β are seen both over the Bay of Bengal and the Arabian Sea. On 18 March, when the ship started from Chennai α is about 1.45 and increases to 1.65 the next day after which the values decrease when the ship moved away from the continent (Figure 4.7a). The decrease in α could be due to the increase in sea salt concentration while traversing from coastal region toward interior oceanic regions. Minimum value of α ($\sim$0.25), on 7 April, indicates a still higher concentration of larger particles in the atmosphere on this day or a lower concentration of smaller particles. Thereafter, α increases when the ship traveled toward the coast. The average value of α over the Bay of Bengal region is 1.12 which is lower than the value 1.80± 0.12 measured earlier in February 2001 [*Ramachandran and Jayaraman*, 2003a]. Lower value of α indicates a relatively larger concentration of bigger size particles over the Bay of Bengal during March-April 2006 when compared to February 2001.

In the second phase of ICARB over the Arabian Sea, α decreases during the initial days and reaches a minimum value of about 0.2 on 22 April after which α

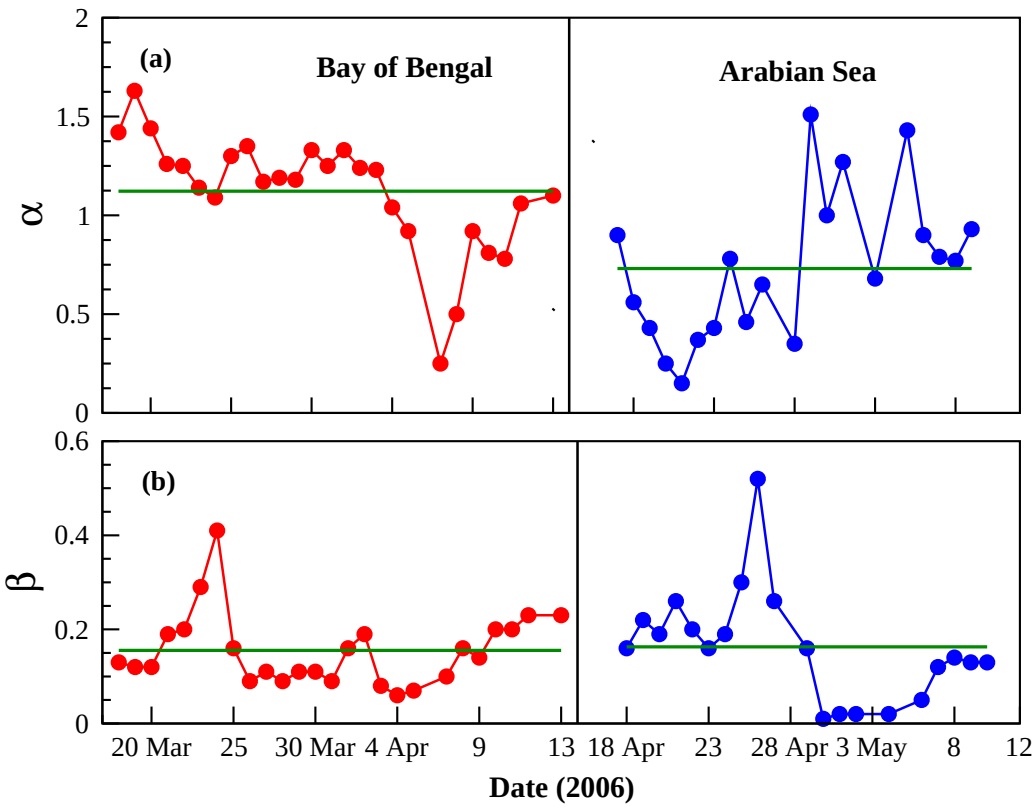

Figure 4.7: *Daily mean variation of Ångström parameters over the Bay of Bengal and the Arabian Sea during ICARB. The mean of daily averaged (a) α, (b) β values over the Bay of Bengal and the Arabian Sea during the cruise period is represented by solid horizontal line.*

increases. The maximum value of α is found to be 1.6 (29 April) which indicates a significant change in particle size. α value is found to be $\sim$ 1 on 10 May when the cruise reaches Goa port. The mean value of α over the Arabian Sea is 0.73 which is lower than that observed over the Bay of Bengal (1.12). The higher α value over the Bay of Bengal when compared to Arabian Sea indicates higher concentration of smaller particles which is reflected also in AODs and FMFs (Figures 4.5 and 4.6). Lower α over the Arabian Sea could be due to sea salt and transport of wind blown dust from the surrounding arid and semi arid regions (as also seen in back trajectory). In Figure 4.7b, the variation of aerosol columnar loading (β, AOD at 1.0 μm) over the Bay of Bengal and the Arabian Sea during the cruise period

is plotted. The aerosol loading in the atmosphere depends on the proximity of measurement location to the source regions, wind speed and direction. β shows large variability both over the Bay of Bengal and the Arabian Sea similar to α. The mean β values over the Bay of Bengal and Arabian Sea are found to be 0.15 and 0.16 respectively [*Kedia and Ramachandran*, 2008a].

4.4.4 Latitudinal and longitudinal variations in aerosol properties

Spatial variations in aerosol optical properties as function of latitude and longitude are analyzed over the Bay of Bengal and the Arabian Sea during ICARB from in situ sun photometer and MODIS (Terra, Aqua) satellite measurements [*Kedia and Ramachandran*, 2008b]. The mean AODs measured from sun photometer and that obtained from MODIS are binned in 4^o latitude and 5^o longitude bins and shown in Figure 4.8. From the mean AODs in a particular bin the latitudinal and the longitudinal means are calculated and plotted. Vertical bars indicate $\pm 1\sigma$ variation from the mean AODs in each latitude and longitude band.

At the outset, the measured and MODIS AODs agree quite well within $\pm 1\sigma$ variation. Over the Bay of Bengal, an increase in AOD as the latitude increases is seen. A higher AOD in 16-20^{o}N is expected as the ship cruised very near to the densely populated Indo-Gangetic Plain and Kolkata (Figure 4.1). The AODs are about a factor of 2 higher in the 16-20^o latitude band when compared to 4-8^{o}N over the Bay of Bengal. In the 4-8^o latitude band the cruise was located far away from the aerosol source regions, thus resulting in lower AODs. The Arabian Sea AODs show markedly different features than the Bay of Bengal AODs. No significant variability in AODs over the Arabian Sea is evident in different latitude bins. MODIS AODs are more or less similar in all the four latitude bins, while sun photometer AODs are found to decrease slightly from 8-12^{o}N to 12-16^{o}N. AODs are similar in the 16-20^{o}N and 20-24^{o}N latitude bands. Note that no measurements were made over the Arabian Sea in the 4-8^{o}N latitude band. These latitudinal

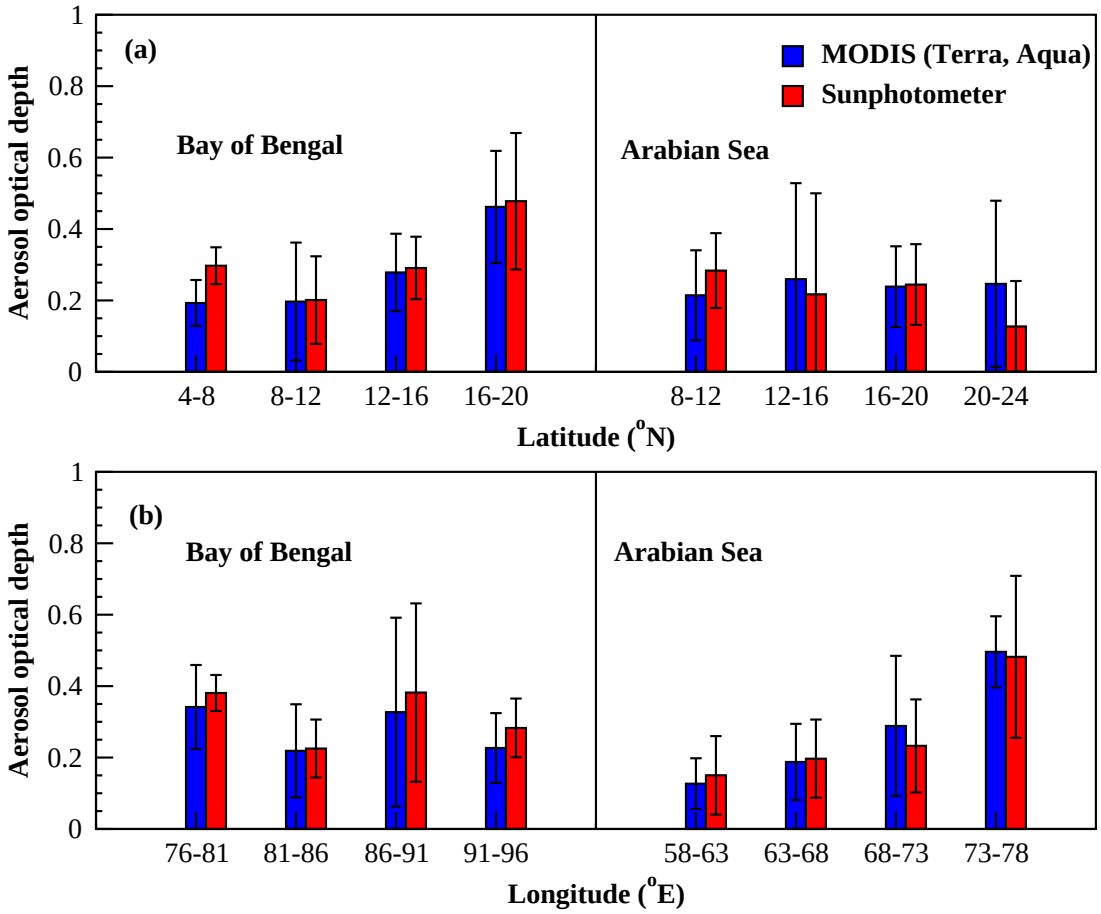

Figure 4.8: *(a) Latitudinal and (b) longitudinal variations in aerosol optical depths measured in situ and MODIS (Terra and Aqua) satellites over the Bay of Bengal and Arabian Sea during ICARB.*

variations in AODs over the Arabian Sea occur despite the fact that the surface winds over the marine boundary layer were strong and clear. The AODs are found to exhibit a larger deviation from the mean indicating not only a large temporal (day to day) but spatial variability in different latitude bins (Figure 4.8a), as opposed to a significant increase in AODs with latitude over the Bay of Bengal.

The scenario is different when the AODs are grouped as function of longitude (Figure 4.8b). Over the Bay of Bengal, AODs are found to decrease from 76-81^{o}E to 81-86^{o}E whereafter the AODs increase in the 86-91^{o}E band; AODs decrease slightly in the 91-96^{o}E longitudinal band over the Bay of Bengal. AODs in the

76-81^{o}E and 81-86^{o}E longitudinal bands were measured when the cruise was close to the eastern coast along Chennai, and Kolkata resulting in higher AOD values. AODs at 91-96^{o}E longitudinal band were obtained when the cruise was far away from the Indian coast, which resulted in lower AODs. Over the Arabian Sea, the AODs are found to increase as a function of longitude when it changes from 58^{o}E to 78^o. 58-63^{o}E longitude band is quite far away from the coastline of India while the 73-78^{o}E is very close to the western coast; urban centers such as Kochi, Goa and Mumbai are situated along the western coast and are manmade aerosol source regions. Note that in situ measured and MODIS AODs exhibit a good correlation over the Bay of Bengal and the Arabian Sea. The variations in AODs over different latitude and longitude bins could be due to the differences in the anthropogenic environs, changes in the meteorological conditions, wind patterns, production and subsequently the transport of aerosols, and the various source regions from where the aerosols originated, in addition, to the local production of sea salt aerosols.

FMF variations as a function of latitude and longitude over the Bay of Bengal and the Arabian Sea are shown in Figure 4.9. FMF is found to be about 0.6 or higher over the Bay of Bengal, while over the Arabian Sea FMF is about 0.6 or higher in the 8^{o}N to 20^{o}N bands only. FMF is about 0.3 over the Arabian Sea in the 20-24^{o}N latitude region. It is worth mentioning that the decrease in FMF over the Arabian Sea in the 20-24^{o}N latitude could be due to higher wind speeds (Figure 4.2) that can produce larger amount of sea salt aerosols and/or due to the transport of larger size mineral dust particles from the nearby desert regions (Figure 4.4).

On the longitudinal scale FMF over the Bay of Bengal and the Arabian Sea are more or less similar (Figure 4.9b). Over the Bay of Bengal FMF is found to be about 0.4 in the 76-81^{o}E band, while in the 81-86^{o}E and 86-91^{o}E bands FMF is $\geq$0.7. In the 91-96^{o}E band FMF is about 0.6. No significant longitudinal variation in FMF is seen over the Arabian Sea in the 58-78^{o}E region. FMF is in the 0.53-0.61 range in the entire longitudinal sector over the Arabian Sea.

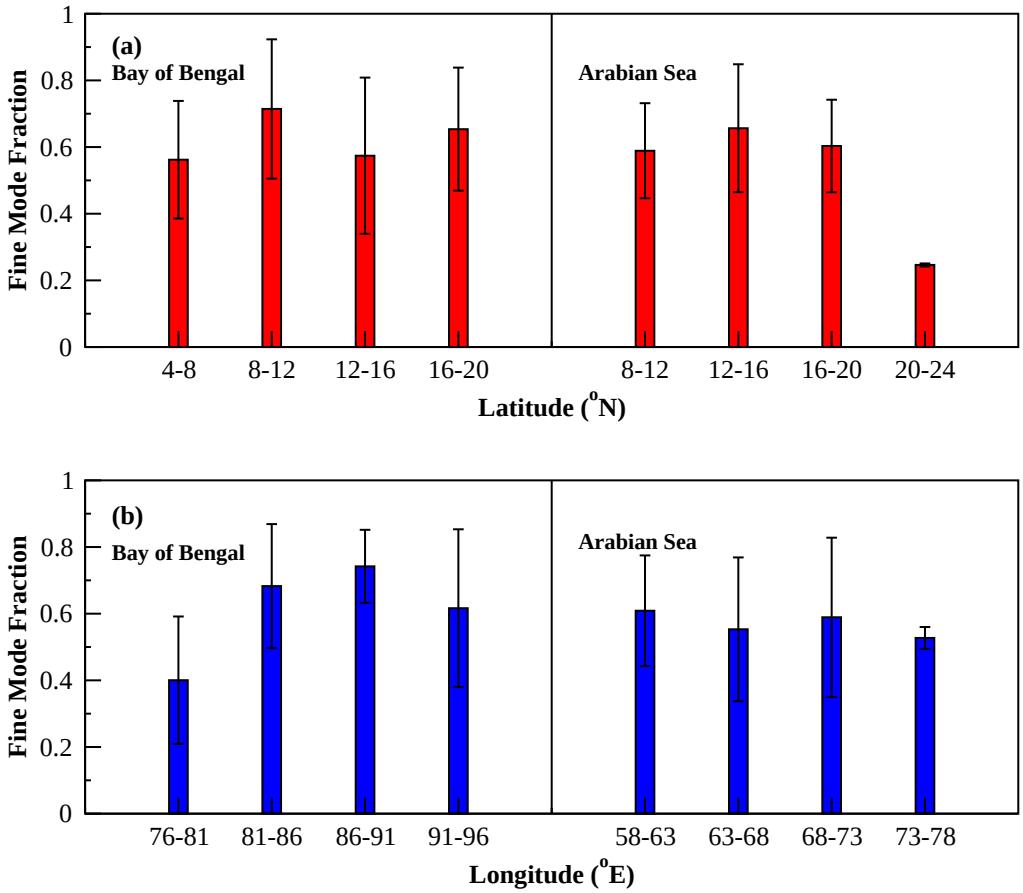

Figure 4.9: *(a) Latitudinal and (b) longitudinal variations in fine mode fraction (FMF) obtained from MODIS (Terra and Aqua) satellites over the Bay of Bengal and Arabian Sea during ICARB.*

Mean FMF values in the longitudinal belts over the Bay of Bengal and Arabian Sea are found to be 0.61 and 0.57, respectively.

4.4.5 Anthropogenic contribution in the measured AODs

The anthropogenic contribution to the measured AODs over the Bay of Bengal and the Arabian Sea are determined by using three independent approaches (method 1, method 2, method 3). The percentage contribution of the anthropogenic aerosols to the AODs measured over the Bay of Bengal (BOB) and the Arabian Sea (AS) are determined by comparing those with the background (Bkg) AODs (methods 1 and 2), such that,

$$\%_{contribution} = \frac{AOD_{BoB}\ (or)\ AOD_{AS} - AOD_{Bkg}}{AOD_{BoB}\ (or)\ AOD_{AS}} \times 100 \tag{4.1}$$

Method 1

In this method, the anthropogenic contribution to the measured AODs are determined by comparing the wind speed dependent AODs. The minimum AODs observed during the entire study period at 0.5 μm was found to be 0.049 $\pm$ 0.025 on 1 May when the ship was in the mid Arabian Sea. Using a mean value of 0.049 for τ_{ss0} [*Rajeev and Ramanathan*, 2001; *Ramachandran and Jayaraman*, 2003b] wind speed dependent AODs (τ_{ss}) were calculated following *Rajeev et al.* [2000] using the equation,

$$\tau_{ss} = \tau_{ss0}\ e^{(0.16\ U)} \tag{4.2}$$

where U is the mean wind speed in ms^{-1}. Then τ_{ss} (AOD$_{Bkg}$) corresponding to the Bay of Bengal and the Arabian Sea were used in equation (4.1) to estimate anthropogenic contribution to the 0.5 μm AODs. The mean wind speeds over the Bay of Bengal and the Arabian Sea were 4.5 ms^{-1} and 5.4 ms^{-1}, respectively. τ_{ss} values were found to be 0.10$\pm$ 0.06 and 0.12$\pm$0.07 over the Bay of Bengal and the Arabian Sea, respectively, for the respective mean wind speeds.

Method 2

In method 2, the measured AODs are compared with the AOD corresponding to the maritime clean aerosol model to estimate the anthropogenic contribution. Maritime clean aerosol model has 1500 water soluble particles, 20 sea salt aerosols in the accumulation mode, and 3.2×10^{-3} sea salt particles in the coarse mode per cm^3 [*Hess et al.*, 1998], and represents clean marine regions. The mean value of RH during the observation period was 73% over the Bay of Bengal and 72% over the Arabian Sea. AODs for maritime clean model at 70% RH and 80% RH were used to derive the AODs at 72% and 73% RH, respectively. The maritime clean model

AODs corresponding to 73% RH (the Bay of Bengal) and 72% RH (the Arabian Sea) were found to be 0.090 and 0.089, respectively, at 0.5 μm. These values are used as AOD_{Bkd} in equation (4.1) to estimate the percentage of anthropogenic contribution to the measured AODs over the Bay of Bengal and the Arabian Sea [*Kedia and Ramachandran*, 2008a].

Method 3

FMF derived from MODIS satellites can be used as a surrogate for separating anthropogenic from natural sources thereby increasing the accuracy of estimating the man made impact on aerosol forcing [*Kaufman et al.*, 2002; *Remer et al.*, 2005]. In this method (method 3), the anthropogenic contribution to the aerosol optical depths is calculated using MODIS AODs and FMF values over the Bay of Bengal and the Arabian Sea following *Kaufman et al.* [2005]. The anthropogenic fraction of the total AOD can be determined from the following equation [*Kaufman et al.*, 2005],

$$\tau_{anth} = \frac{(f_{0.55} - f_{dust})\ \tau_{0.55} - (f_{mar} - f_{dust})\ \tau_{mar}}{(f_{anth} - f_{dust})} \tag{4.3}$$

where τ_{anth} is the anthropogenic fraction of AOD, $f_{0.55}$ is the fine mode fraction at 0.55 μm, f_{dust} is FMF due to dust, $\tau_{0.55}$ is the total AOD at 0.55 μm, f_{mar} is FMF due to marine aerosols, τ_{mar} is AOD due to marine aerosols and f_{anth} is the anthropogenic fraction of FMF at 0.55 μm. The values of f_{dust}, f_{mar} and f_{anth} used in the present estimation are obtained from *Kaufman et al.* [2005]. f_{mar} is obtained for the clean marine and has the value of 0.32±0.07. f_{dust} is 0.51±0.03 determined for the West African coast. f_{anth} was obtained over the Western Atlantic and the value is 0.92±0.03. Using these values and the above equation the anthropogenic contribution (τ_{anth}) has been determined over the Bay of Bengal and the Arabian Sea from the daily mean MODIS AODs and FMF values at 0.55 μm. τ_{mar} is taken as 0.06±0.01 which was the average marine optical depth for calm conditions [*Kaufman et al.*, 2005].

The anthropogenic contribution to the AODs measured over the Bay of Bengal and the Arabian Sea using sun photometer was estimated using methods 1 and 2; while using method 3 the anthropogenic fraction of aerosol optical depths was determined from MODIS AODs and FMFs. The background aerosol models used in methods 1 and 2 did not explicitly account for the presence of dust. However, the background AODs in methods 1 and 2 are higher than the marine AOD value of 0.06 used in method 3. The mean background AODs used in methods 1 and 2 are 0.10 and 0.090, respectively, over the Bay of Bengal, and 0.12 and 0.089, respectively, over the Arabian Sea. The higher background AODs used in methods 1 and 2 when compared to 0.06 could compensate for the absence of dust. Thus the anthropogenic fraction estimated from these three methods correspond to the range in the anthropogenic contribution to the AODs and represent the uncertainty in anthropogenic influence.

It was found in some earlier studies that over the Indian Ocean during the winter monsoon season sulfate, sea salt, nitrate, potassium, organics, black carbon (BC), dust, fly ash, and ammonium [*Ramanathan et al.*, 2001] contribute to the AODs. BC and fly ash arise only from man made sources as their natural sources are negligible [*Novakov et al.*, 2003]. About 90% of the organics are found to be of anthropogenic origin. Sea salt from bubble bursting, air borne mineral dust and non sea salt sulfate produced by gas to particle conversion of dimethyl sulfide emitted from the oceans are the natural sources of aerosols over oceanic regions. Over the northern Indian Ocean the man made contribution to the aerosol was found to be about 80% [*Ramanathan et al.*, 2001].

The mean percentage contributions due to anthropogenic sources over the Bay of Bengal and the Arabian Sea from different methods are given in Table 4.1. The mean anthropogenic contribution at 0.5 μm from method 1 is 71% over the Bay of Bengal while it is 52% over the Arabian Sea. In method 2, the anthropogenic contribution is found to be 75% over the Bay of Bengal and 65% over the Arabian Sea. The wind speed dependent AOD values at 0.5 μm are higher ($\geq$0.10)

than the maritime clean aerosol model AODs (∼0.09). This could be due to the higher background AOD of 0.049 used in this study as compared to 0.01 used by *Ramachandran and Jayaraman* [2003b] and 0.02 used by *Rajeev et al.* [2000] for deriving wind speed dependent AODs.

Table 4.1: *Mean anthropogenic contribution (%, at 0.5 μm) to the AODs over the Bay of Bengal and the Arabian Sea from methods 1 and 2 in comparison with the anthropogenic fraction from MODIS AODs and FMFs (Method 3).*

	Anthropogenic contribution (%)	
Method	**Bay of Bengal**	**Arabian Sea**
1	71±7	52±6
2	75±12	65±13
3	68±9	51±8

Thus the mean contribution by the anthropogenic sources to the AODs over the Bay of Bengal and the Arabian Sea from these two methods is in the range of 71-75% and 52-65% respectively. These values are lower than those obtained earlier over the Bay of Bengal, the Arabian Sea and the tropical Indian Ocean [*Ramanathan et al.*, 2001; *Ramachandran and Jayaraman*, 2003b; *Ramachandran*, 2004] during the winter monsoon season.

The mean anthropogenic fraction in AODs over the Bay of Bengal and the Arabian Sea using method 3 are found to be 0.68±0.09 and 0.51±0.08 respectively. σ in the anthropogenic fraction is obtained using the mean, maximum and minimum values of f_{dust}, f_{mar} and f_{anth} in equation (4.3). Higher anthropogenic fractions over the Bay of Bengal and the Arabian Sea suggest a high man made influence in aerosol optical depths. Note that the mean anthropogenic fractions over the Bay of Bengal and the Arabian Sea agree quite well within $\pm 1\sigma$ (Table 4.1) of the mean anthropogenic contribution determined using wind speed dependent AODs and maritime clean aerosol model AODs. The results clearly illustrate that the

contribution of anthropogenic sources to the aerosols over the Bay of Bengal is higher than that of the Arabian Sea.

4.4.6 Variability in spectral distribution of aerosol optical depths

As already discussed in Chapter 3, aerosol size distribution in the ambient atmosphere is multimodal which imposes a curvature in the aerosol spectra. This curvature contains useful information about the size distribution of aerosols in the atmosphere.

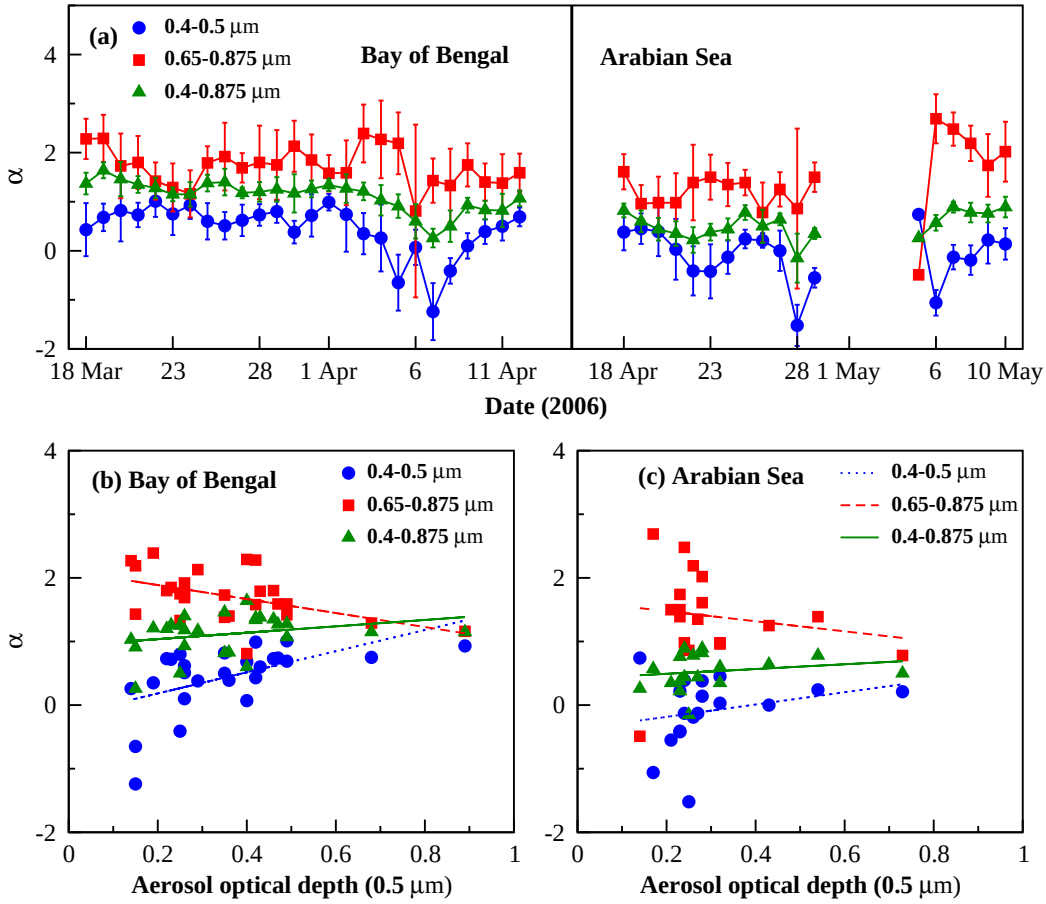

Figure 4.10: *(a) Daily mean Ångström exponent (α) obtained from AODs in different spectral ranges over the Bay of Bengal and the Arabian Sea. Vertical bars denote ±1σ variation from the mean values. Daily mean α in three spectral bands versus the daily mean AOD at 0.5 μm over the (b) Bay of Bengal and (c) Arabian Sea. Lines (dotted, dashed, and solid) correspond to least square fits drawn for a in three spectral ranges.*

Therefore, the spectral variation of aerosol extinction has been examined with a second order polynomial fit over the Bay of Bengal and the Arabian Sea during ICARB 2006. In the present study, Ångström exponents (α) have been calculated for four wavelength bands (0.40-0.50, 0.50-0.65, 0.65-0.75, and 0.75-0.875 μm) using Volz method (Equation 2.6). α values are also calculated in the 0.40-0.875 μm spectral band applying least squares method to each individual data set over both the oceanic regions. Daily mean α have been computed using α derived from individual AOD data sets for comparison.

Daily mean α value in three spectral ranges, namely, short (0.4-0.5 μm), long (0.65-0.875 μm) and full (0.4-0.875 μm) are plotted in Figure 4.10 for the Bay of Bengal and the Arabian Sea. A large variation in α is observed over both the oceanic regions which is a strong function of the wavelength interval used for its determination. The value of $\alpha_{0.4-0.5}$ is found to be lower, while $\alpha_{0.65-0.875}$ is higher than $\alpha_{0.4-0.875}$ over these oceans nearly for all the days of measurement.

Value of $\alpha_{0.4-0.875}$ is >1 over the Bay of Bengal while it is <1 over the Arabian Sea for most of the days suggesting the presence of relatively more abundant larger-size aerosols over the Arabian Sea. Over both the oceanic regions, $\alpha_{0.4-0.5}$ exhibit an increasing trend while $\alpha_{0.65-0.875}$ show a decreasing trend with increasing AODs (Figure 4.10a,b) indicating mixed type or bimodal aerosol distribution. $\alpha_{0.4-0.875}$ shows a neutral trend over both the oceans, while $\alpha_{0.65-0.875}$ showed much less spread over the Bay of Bengal when compared to the Arabian Sea indicating the presence of larger curvature over the Arabian Sea. A large spread in α values in short and long spectra is found to occur during low-turbidity conditions. The features in spectral aerosol characteristics are seen more clearly when individual AOD spectra are used. Hence, in the further discussion the individual AOD spectra measured over the Bay of Bengal (n = 462) and the Arabian Sea (n = 405) have been utilized.

Figures 4.11a and 4.11b explicitly show that the aerosol size distribution is a bimodal or a mixed one over the Bay of Bengal and the Arabian Sea where

differences in α between short and long spectral regions are plotted with respect to 0.5 μm AODs. Most of the time $\alpha_{0.4-0.5} - \alpha_{0.65-0.875}$ values are found to be negative, which confirms the presence of fine mode aerosols over both the oceanic regions.

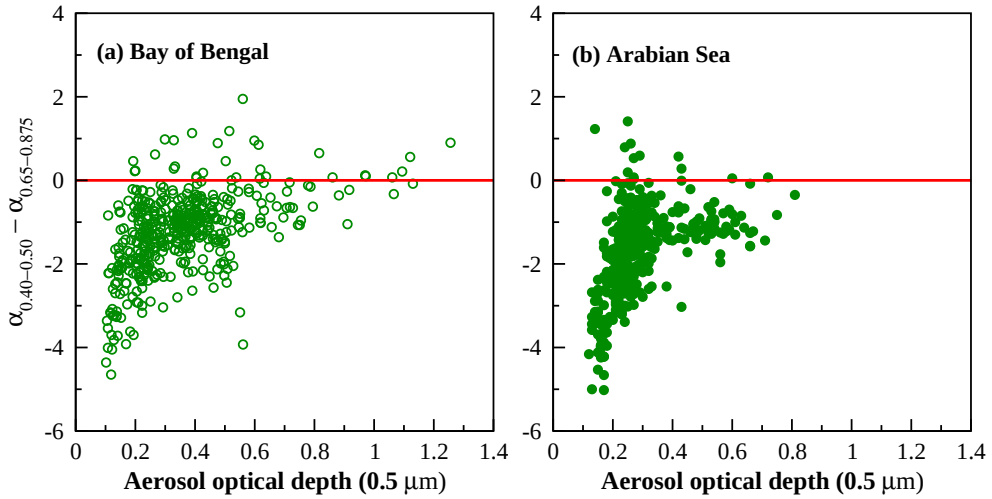

Figure 4.11: *Differences in α values obtained between short (0.4-0.5 μm) and long (0.65-0.875 μm) ranges correlated with 0.5 μm aerosol optical depths over the (a) Bay of Bengal and (b) Arabian Sea.*

Difference between the two α values is found to be large for low turbidity condition over both oceanic regions. This difference decreases as AOD increases (Figures 4.11a and 4.11b). Nearly zero value of $\alpha_{0.4-0.5} - \alpha_{0.65-0.875}$ represents absence of curvature in the ln τ versus ln λ data. About 44% of $\alpha_{0.4-0.5} - \alpha_{0.65-0.875}$ lie between -1 and 1 over the Bay of Bengal, while over the Arabian Sea it is only 23%; 80% of $\alpha_{0.4-0.5} - \alpha_{0.65-0.875}$ are between -2 and 2 over the Bay of Bengal as opposed to 64% over the Arabian Sea. This conclusion supports the higher average fine mode fraction obtained over the Bay of Bengal (0.71) when compared to the Arabian Sea (0.60) [*Kedia and Ramachandran*, 2008a].

4.4.7 Curvatures in aerosol optical depth spectra

The curvature effects in spectral distribution of AODs are quantified by deriving second-order Ångström exponent ($\alpha^{'}$, equation 2.8) and by fitting a second order

polynomial to the measured spectral distribution of AODs (equation 2.7). Variation of $\alpha^{'}$ as a function of 0.5 μm AODs over the Bay of Bengal and the Arabian Sea are plotted in Figure 4.12.

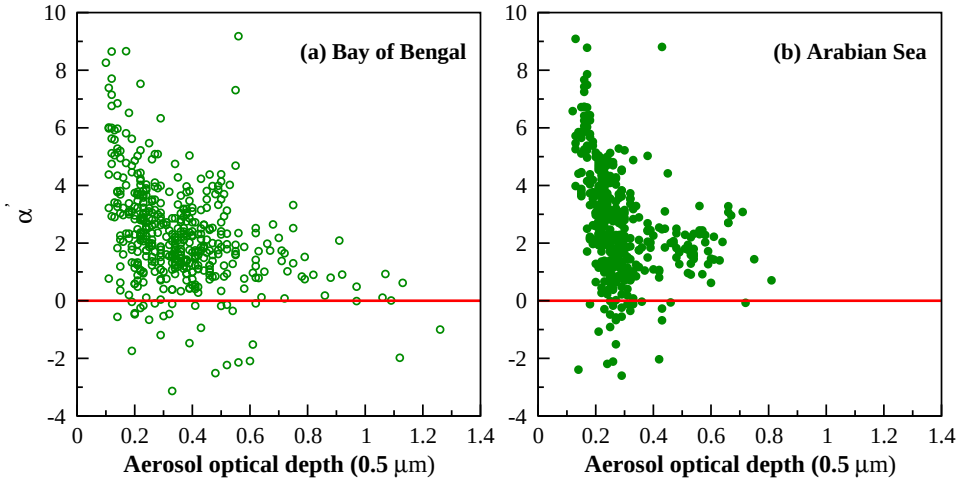

Figure 4.12: *Second order Ångström exponent ($\alpha^{'}$) plotted against 0.5 μm aerosol optical depth over the (a) Bay of Bengal and (b) Arabian Sea.*

More than 90% of the AOD spectra measured over the Bay of Bengal and the Arabian Sea are found to have positive $\alpha^{'}$ thus suggesting a concave curvature and a bimodal distribution. A decreasing trend in $\alpha^{'}$ is observed with increasing AOD over both the oceanic regions (Figure 4.12). It is observed that for lower AODs (<0.2), $\alpha^{'}$ exhibits quite a high variation ranging from near zero and going up to 10. The decreasing trend in $\alpha^{'}$ values can be explained as: for lower AODs, both fine and coarse mode particles are present in the atmosphere with higher fine mode particles, but when the AOD is high (>0.4), a single type of particle becomes dominant (either fine or coarse). Therefore, for higher AODs the curvature is less and $\alpha^{'}$ approaches zero. The $\alpha^{'}$ is negative for a few cases (Figure 4.12) which arise when the coarse mode particles are dominant [*Kedia and Ramachandran*, 2009].

The coefficient of determination (R^2) is a measure of how well the regression line approximates the real data points, and provides information about the quality of the fit. R^2 is obtained for both linear and polynomial fits of ln τ versus ln λ

data over the Bay of Bengal and the Arabian Sea and shown in Table 4.3. Over the Bay of Bengal, >80% of AOD spectra had R^2 values for linear fit in the range of 0.81-1.00 (Table 4.2).

Table 4.2: *Frequency distribution of R^2 values obtained for aerosol optical depth spectra over the Bay of Bengal (n=462) and the Arabian Sea (n=405) for linear (equation 2.5) and polynomial (equation 2.7) fits.*

	Bay of Bengal		**Arabian Sea**	
R^2	**Linear fit**	**Polynomial fit**	**Linear fit**	**Polynomial fit**
<0.5	5	1	34	3
0.51-0.60	3	0	9	0
0.61-0.70	3	1	10	3
0.71-0.80	5	1	16	3
0.81-0.90	15	5	16	11
0.91-1.00	69	92	15	80

On the contrary, over the Arabian sea for only ∼30% of AOD spectra, R^2 values are in the 0.81-1.00 range. High value of R^2 over Bay of Bengal means a good agreement of first-order linear fit with the measurements indicating that the particle distribution is unimodal. It is seen that as R^2 for linear fit increases, α' approaches zero, thus decreasing the curvature. On the other hand, a large variability in R^2 values over the Arabian Sea is observed which is attributed to the low-turbidity conditions over the Arabian Sea.

It is remarkable to note that more than 90% of the AOD spectra over the Bay of Bengal (97%) and the Arabian Sea (91%) have R^2 values between 0.81 and 1.00 when polynomial fits are applied to the AOD spectra (Table 4.2), thus revealing the existence of curvature, and confirming the polynomial behavior of ln τ versus ln λ data. In addition, the number of AOD spectra which had significant curvature was more over the Arabian Sea [*Kedia and Ramachandran*, 2009].

The α' depends on α, and the dependence between the two is a function of the wavelength interval used for the determination of α [*Eck et al.*, 2001]. Figure 4.13

shows the scatter diagram between the second derivative α' (0.4-0.875 μm) and the Ångström exponent α calculated at four different wavelength intervals (0.4-0.5 μm, 0.5-0.65 μm, 0.65-0.75 μm, and 0.75-0.875 μm) over the Bay of Bengal and the Arabian Sea, respectively.

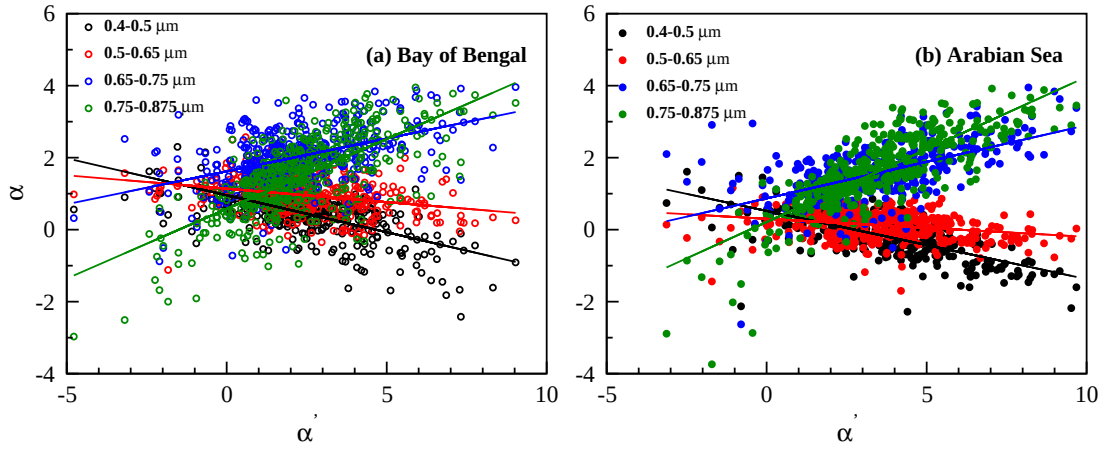

Figure 4.13: *Ångström exponent (α) obtained from AODs in four spectral ranges of 0.4-0.5 μm, 0.5-0.65 μm, 0.65-0.75 μm, and 0.75-0.875 μm drawn against second-order Ångström exponent (α') over the (a) Bay of Bengal and (b) Arabian Sea. Lines correspond to least square fits drawn for α in four spectral ranges.*

The α determined using AODs measured at different wavelength intervals are seen to vary and exhibit different relationships with α'. The α' is found to be negatively correlated with $\alpha_{0.4-0.5}$ over the Bay of Bengal and the Arabian Sea. The α' exhibits a neutral trend with α in the midvisible wavelengths, while α' shows an increasing trend with $\alpha_{0.65-0.75}$ and $\alpha_{0.75-0.875}$. In the present study, the difference in the α values at different wavelength intervals is quite large for the days on which significant curvature is observed in the spectral distribution of AODs as seen in Figure 4.10. More than a fourfold increase in α is observed when the wavelength interval varies from shorter (0.40-0.50 μm) to longer (0.75-0.875 μm) on some days, confirming the existence of nonlinear behavior in the spectral distribution of AODs.

A correlation between $\alpha_{0.4-0.5}$ and $\alpha_{0.65-0.875}$ values categorized on the basis of curvature (α_2) is shown in Figure 4.14.

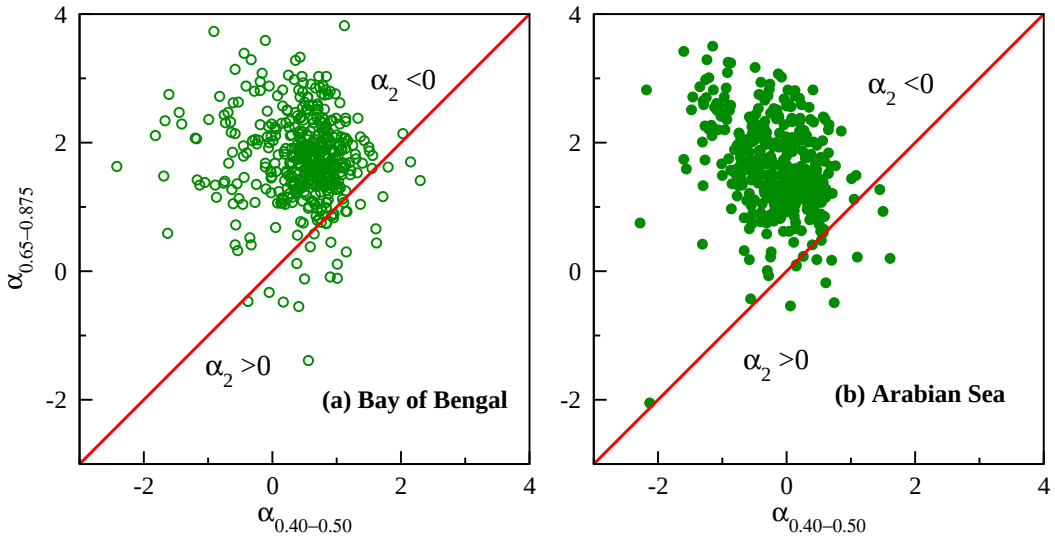

Figure 4.14: *Correlation between* $\alpha_{0.65-0.875}$ *and* $\alpha_{0.4-0.5}$ *over the (a) Bay of Bengal and (b) Arabian Sea. The correlations are divided on the basis of curvature* (α_2) *of the aerosol optical depth spectra.*

This analysis is performed to further identify the dominant mode of aerosols contributing to the aerosol size distributions over the Bay of Bengal and the Arabian Sea. As already discussed in chapter 3, the α_2 values will be less than zero for an atmosphere with higher fine mode aerosol concentration, while α_2 will be >0 for an atmosphere in which coarse mode aerosol concentration is high or due to a bimodal distribution with higher coarse mode contribution [*Eck et al.*, 1999; *Schuster et al.*, 2006; *Kaskaoutis et al.*, 2007].

Over both the oceanic regions, more than 90% of the AOD spectra lie in α_2 <0 zone indicating a relatively higher concentration of fine mode aerosols in the aerosol size distribution. It is worth noting that there are spectra which fall in the α_2 >0 bin, indicating that coarse mode aerosols are also present.

In Figure 4.15, α_2 and α_1 values for all the AOD spectra measured over the Bay of Bengal and the Arabian Sea are plotted. Over the Bay of Bengal, for 76% of AOD spectra the $\alpha_2 - \alpha_1$ value is >1 and <2, suggesting the dominance of fine mode aerosols from a wide variety of fine mode fractions or mixture of modes.

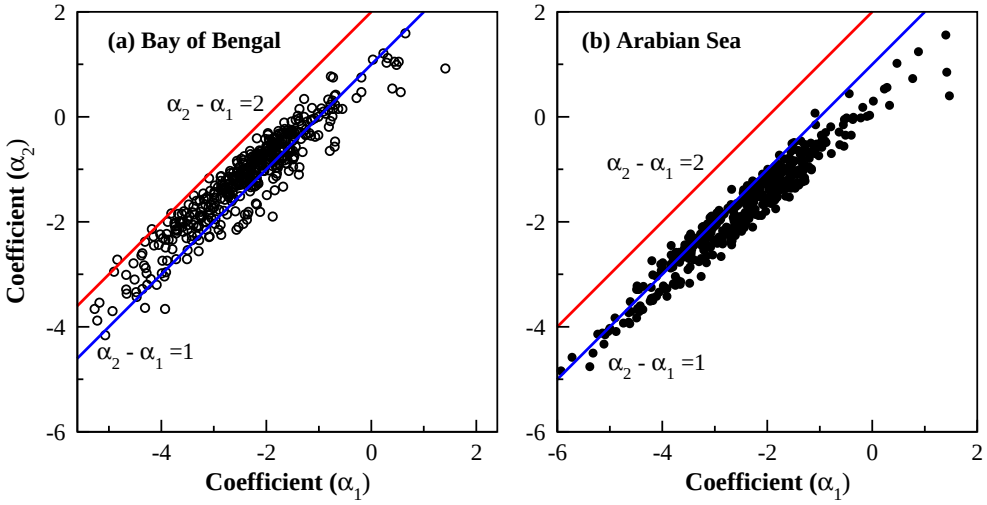

Figure 4.15: *Correlation between the coefficients α_1 and α_2 computed in the spectral range of 0.4-0.875 μm over the (a) Bay of Bengal and (b) Arabian Sea. Straight lines correspond to $\alpha_2 - \alpha_1 = 1$ and $\alpha_2 - \alpha_1 = 2$.*

In contrast, over the Arabian Sea, $\alpha_2 - \alpha_1$ is >1 and <2 for only 16% of the AOD spectra indicating the presence of coarse mode aerosols.

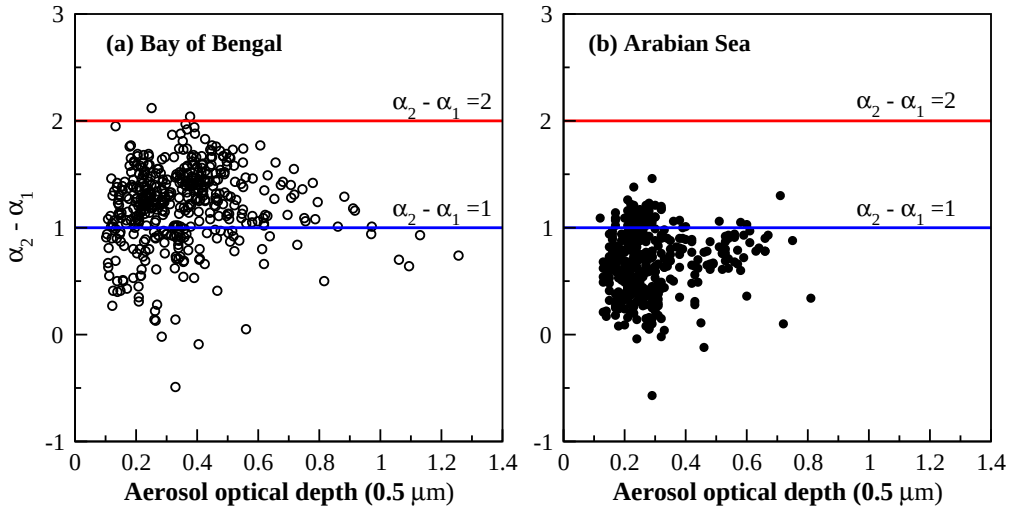

Figure 4.16: *Differences between the coefficients α_1 and α_2 plotted as a function of 0.5 μm AOD over the (a) Bay of Bengal and (b) Arabian Sea. Straight lines represent $\alpha_2 - \alpha_1 = 1$ and $\alpha_2 - \alpha_1 = 2$.*

This issue is further examined in Figure 4.16 where $\alpha_2 - \alpha_1$ are plotted with respect to the 0.5 μm AODs for the Bay of Bengal and the Arabian Sea. It is clear that the Bay of Bengal AOD spectra are predominantly made up of particles from

a mixture of modes while the Arabian Sea had more coarse particles.

4.5 Conclusions

A detailed study on aerosol optical and physical properties has been conducted using the measurements conducted during an integrated campaign, ICARB. ICARB cruise campaign was conducted over the Bay of Bengal and the Arabian Sea during premonsoon season of March-May 2006 to characterize the spatio-temporal distribution of aerosols, trace gases and radiative forcing over these regions. The air parcels at different heights were found to originate from arid/semiarid regions and pass through continental India and Indo-Gangetic plain before reaching the Bay of Bengal. In contrast, most of the air trajectories were of marine origin over the Arabian Sea. Day to day variability in AODs are found to be very large over both the oceanic regions during ICARB.

AODs at 0.5 μm are found to be higher over the Bay of Bengal (0.36) when compared to that over the Arabian Sea (0.25). Satellite measured AODs are found to track well the variations in the in situ measured AODs and a good correlation (>0.9) is observed between the two over both the regions. Aerosol fine mode fraction is found to be higher over Bay of Bengal (0.71) when compared to that over the Arabian Sea (0.60) indicating larger abundance of fine mode anthropogenic aerosols over the Bay of Bengal. This result is also supported by Ångström exponent α which is about 1.5 times higher over Bay of Bengal. The anthropogenic contribution to the measured AODs obtained from three independent methods are found to show a good agreement with a range of 71-75% over Bay of Bengal and 52-65% over the Arabian Sea. The spectral distribution of AODs are further analyzed to quantify the spectral distribution of AODs by using the second order polynomial fit of spectral AOD and deriving second-order Ångström exponent ($\alpha^{'}$). Analysis performed using the coefficients of polynomial fits and the value of $\alpha^{'}$ revealed that AOD spectra over Bay of Bengal are predominantly made up of a mixture of fine modes while the Arabian Sea had more coarse mode particles.

Chapter 5

Aerosol radiative forcing over India and surrounding oceanic regions

Atmospheric aerosols from both natural and anthropogenic sources exert a cooling effect on the Earth's climate through direct and indirect effects which partially offset the warming caused due to greenhouse gases [*IPCC*, 2007]. However, the combined impact of different aerosol species on global climate need not be additive because of the inhomogeneity in the distribution of different aerosol types over both space and time, differences in their mixing states, differences in albedo of the underlying surface and differences in the vertical distribution of aerosols in the atmosphere [*Haywood and Ramaswamy,* 1998; *Jacobson*, 2001]. The potential for aerosol forcing of climate can vary according to regional differences in aerosol columnar concentration, chemical composition and the age of the airmass [*Spencer et al.*, 2008]. Man-made pollutant emissions can change the atmospheric composition contributing to climate change, and climate change in turn through changes in temperature, dynamics, the hydrological cycle, atmospheric stability, and biosphere-atmosphere interactions can alter the atmospheric composition [*Isaksen et al.*, 2009]. The greenhouse gases are globally well mixed (e.g.,

CO_2) and their radiative effects are homogeneous and one of warming. In contrast, aerosols exhibit regional signatures and depending on their chemical composition can either warm (black carbon) or cool (sulfate) the atmosphere. Aerosols are abundant near source regions, however, they can impact global climate as their radiative influence get transported due to changes in the mean atmospheric circulation patterns.

The sources of aerosols include natural (sea salt, biogenic, volcanic and dust) and manmade (combustion of fossil fuel from urban/industrial processes and biomass burning). Because of their short residence times and varied sources optical, physical and chemical characteristics of aerosols and their radiative forcing exhibit strong seasonal and regional variations. On a global scale natural aerosols such as dust and sea salt are found to dominate the northern Africa and oceanic regions above 45^oS respectively [*IPCC*, 2007]. Anthropogenic aerosols (mainly fossil fuel and biomass burning) dominate south Asia, southeast Asia, China and Mexico [*Chung et al.*, 2005]. Aerosols in the northern hemisphere contribute 64% to the global surface forcing [*Chung et al.*, 2005] and Asia is the largest contributor on a global annual mean scale. Aerosols still remain a major source of uncertainty in the prediction of climate change due to inadequate information on the variabilities of aerosol characteristics at regional and temporal scales [e.g. *IPCC*, 2007]. This uncertainty can be reduced by studying the seasonal variations in aerosol radiative forcing over different locations in a region influenced by variety of aerosol sources. The present chapter documents the seasonal variations in clear sky shortwave aerosol radiative forcing over four continental locations spread across India (as discussed in Chapter 3) and adjoining oceanic regions during ICARB cruise campaign (as discussed in Chapter 4). Measured aerosol characteristics (aerosol optical depth, single scattering albedo, total aerosol mass concentrations and mass concentration of different chemical constituents) are utilized in conjunction with aerosol optical properties and radiative transfer models to estimate the aerosol radiative forcing. This study will enable in developing a useful characterization

of the radiative effects of atmospheric aerosols over an aerosol source region, and becomes important in the context of regional and global climate change.

5.1 Aerosol radiative forcing

For the estimation of aerosol radiative forcing (ARF) both over continental locations and marine environments, the radiation code SBDART (Santa Barbara DISORT Atmospheric Radiative Transfer) developed by *Ricchiazzi et al.* [1998] is used. The model is well suited to study the radiation budget of the Earth-atmosphere system. The radiative transfer algorithm used in SBDART is based on a collection of well tested and reliable physical models developed by the atmospheric science community over decades. SBDART computes plane-parallel radiative transfer both in clear and cloudy sky conditions within the Earth's atmosphere and at the surface. However, in the present study, radiative transfer computations are performed only for clear sky conditions. For molecular absorption, SBDART uses the low resolution band models of LOWTRAN-7 atmospheric transmission code. These band models take into account the effects of all radiatively active molecular species found in the Earth's atmosphere and has wavelength resolution of about 0.005 μm in visible and about 0.2 μm in thermal infrared region. Radiative transfer equations are numerically integrated using DISORT (Discrete Ordinate Radiative Transfer) module developed by *Stamnes et al.* [1988].

The discrete ordinate method provides a numerically stable algorithm to solve the equations of plane-parallel radiative transfer in a vertically inhomogeneous atmosphere. The intensity of both scattered and thermally emitted radiations can be computed at different heights and directions. SBDART computes aerosol radiative forcing both in shortwave (SW) (0.2-4.0 μm) and longwave (4.0-40.0 μm) range. However, the longwave aerosol radiative forcing contributes about 10% to the net aerosol radiative forcing, which is much smaller than the contribution of shortwave aerosol radiative forcing to the net forcing [e.g., *Ramanathan et al.*, 2001; *Ganguly et al.*, 2005b; *Ramachandran et al.*, 2006; *Ramachandran and Kedia*, 2010].

Therefore in this thesis work, aerosol radiative forcing estimated only in shortwave range over the study locations/regions is presented and discussed.

5.1.1 Necessary Inputs: Aerosol optical depth, single scattering albedo and asymmetry parameter

The principal input parameters required for calculating aerosol radiative forcing using SBDART are aerosol optical depth (AOD), single scattering albedo (SSA) and asymmetry parameter (g) as a function of wavelength. In the present work, Optical Properties of Aerosols and Clouds (OPAC) model developed by *Hess et al.* [1998] is used to reconstruct the measured aerosol parameters by varying the aerosol components that contributed to the aerosol properties over each measurement location/region and the required aerosol parameters are retrieved in the entire shortwave range. This model consists of ten major aerosol components *viz.,* insoluble, water soluble (including sulfate), black carbon (elemental carbon), mineral dust (coarse, accumulation and nucleation), mineral transported, sea salt (coarse and accumulation) and sulfate droplets as discussed in Chapter 3. Using different combinations of these aerosol components assuming external mixing, different aerosol types are defined, namely, continental clean, continental average, continental polluted, urban, desert, maritime clean, maritime polluted and maritime tropical. Each of these aerosol types correspond to different environments. In addition to this, OPAC model also allows users to define new mixtures from the given aerosol components to best fit the observations and to derive the required optical properties, such as aerosol optical depths, single scattering albedo, asymmetry parameter etc. for the prescribed combination. These parameters are calculated on the basis of the microphysical data (size distribution and spectral refractive index) under the assumption of spherical aerosol particles. As some of the aerosol components are hygroscopic can can uptake water from the atmosphere under favorable conditions, which may in turn change their optical properties, OPAC outputs are available for eight different relative humidity (0%, 50%, 70%, 80%, 90%, 95%,

98% and 99%) conditions [*Hess et al.*, 1998]. Among the ten aerosol components in OPAC, the most important aerosol components based on the aerosol source regions and transport pathways over the study locations/regions can be water soluble, insoluble, black carbon, sea salt and mineral dust. In the present work, the number concentration of these aerosol components are varied to match the measured aerosol properties over the study location/regions.

AOD is the most important parameter affecting radiative forcing and increase in the AOD value will cause an increase in forcing [*Ramachandran et al.*, 2006]. SSA is the second most important parameter required in the estimation of direct radiative forcing [*Russell et al.*, 2002; *Ramachandran et al.*, 2006] after AOD. SSA values can range from 1 (pure scatterer) to 0 (pure absorber). SSA of sulfate and sea salt is 1 at $\lambda = 0.55$ μm while the SSA of black carbon is 0.21 at the same wavelength. *Ramachandran et al.* [2006] showed that shortwave aerosol radiative forcing are linearly related to AODs, while the atmospheric absorption strongly depends on the SSA value and the relation between the two is non linear. Exact knowledge of SSA is crucial and small error in its estimation can flip the sign of aerosol radiative forcing [*Takemura et al.*, 2005]. *Ganguly et al.* [2005b] have shown that for the same AOD and mass loading over the Bay of Bengal region, a decrease in the SSA value by 0.05 can enhance the aerosol induced heat trapping within the atmosphere by nearly 27%. Over land areas, knowledge of SSA is even more critical and any small change in its value can have larger impact resulting from flux changes within and below the aerosol layer such as differential heating rates, changes in atmospheric stability and cloud formation [*Russell et al.*, 2002]. The asymmetry parameter (g) is defined as the intensity-weighted average cosine of the scattering angle and is a measure of the angular distribution of scattered light. The value of g ranges between -1 for entirely backscattered light to +1 for entirely forward scattered light. *d'Almeida et al.* [1991] suggested a range in g for dry aerosol particles at 0.5 μm wavelength between 0.64 and 0.83 depending on the aerosol type and season, with an average value of 0.72 over all aerosol types.

The value of g depends both on the size distribution and chemical composition of aerosols in the atmosphere.

Spectral variation of AOD in the wavelength range of 0.25 to 4.0 μm for different aerosol models defined in OPAC (Chapter 3) varying from continental clean to maritime polluted [*Hess et al.*, 1998] are shown for 0% and 70% RH in Figure 5.1a,b. AOD is found to decrease very sharply for the atmosphere dominated by fine mode aerosols as in seen for urban model in Figure 5.1. In addition, the decrease in AOD with wavelength is more steeper as RH increases for all the aerosol models. Spectral variation of SSA in the wavelength range of 0.25 to 4.0 μm for different aerosol models corresponding to 0% and 70% RH are shown in in Figure 5.1c,d. When aerosols are dry (0% RH) SSA for maritime tropical and clean aerosol models is high (> 0.98) throughout the shortwave spectral range indicating the dominance of scattering aerosols (water soluble and sea salt). SSA for maritime polluted aerosol model decreases because of higher concentration of black carbon aerosols. SSA for urban aerosol is the lowest among the different aerosols (Figure 5.1) due to highest BC concentration. SSA decreases almost linearly from continental clean to continental polluted. In the urban aerosol model black carbon dominates the number mixing ratio (82%) thereby leading to a large reduction in SSA. The sizes of hygroscopic aerosols such as water soluble and sea salt particles can increase as relative humidity increases; as the radius of scattering aerosols increases the scattering coefficient and SSA will increase as seen at 70% RH (Figure 5.1d). Asymmetry parameter is found to be higher for maritime aerosol models when compared to continental models (Figure 5.1e,f). A higher g values represents an aerosol size distribution consisting of bigger particles. The spectral variation of g for continental models differs with respect to the maritime models (Figure 5.1e). g is found to increase when RH increases from 0% to 70% (Figure 5.1f). The measured aerosol properties, however, may have additional components with varying number densities depending on local sources and long range transport which could modify the aerosol properties when compared to those obtained from aerosol models.

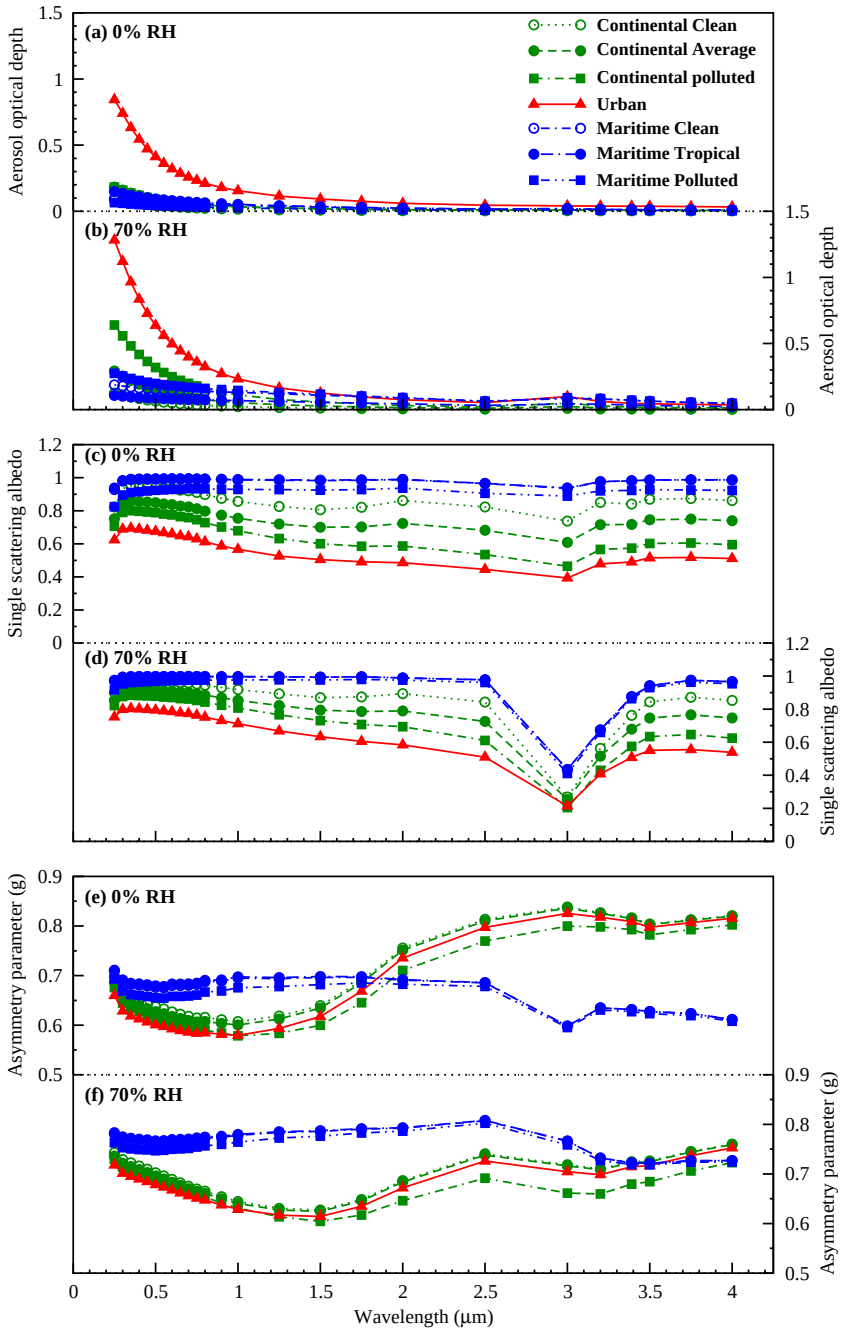

Figure 5.1: *Spectral variation of aerosol optical depth for continental (clean, average and polluted), urban and maritime (clean, tropical and polluted) aerosol models at (a) 0% RH and (b) 70% RH. Spectral variation of single scattering albedo for continental (clean, average and polluted), urban and maritime (clean, tropical and polluted) aerosol models at (c) 0% RH and (d) 70% RH. Asymmetry parameter (g) in the shortwave spectral region of 0.25-4.0 μm for continental (clean, average and polluted), urban and maritime (clean, tropical and polluted) aerosol models at (e) 0% RH and (f) 70% RH.*

The value of g for 0.5 μm at 70% RH are 0.76, 0.77 and 0.75 for maritime clean, tropical and polluted aerosol models, respectively [*Hess et al.*, 1998]; g is <0.7 at 0.5 μm for continental (clean, average and polluted), and urban aerosol models. The g is found to decrease when submicron size particles increase in the aerosol size distribution (Figure 5.1); maritime polluted has more number of fine mode (water soluble particles and black carbon) than maritime clean and tropical aerosol models. Similarly continental clean aerosol model has a higher g than the urban aerosol model (Figure 5.1) [*Kedia et al.*, 2010].

5.1.2 Additional Inputs: Atmosphere, Ozone, Water Vapor and Surface albedo

To perform aerosol radiative forcing calculations atmospheric profiles of temperature, pressure, columnar ozone, water vapor and surface reflectance characteristics are necessary in addition to the above mentioned aerosol properties. Standard tropical atmospheric profiles of temperature and pressure are used in the present study [*McClatchey et al.*, 1972]. Monthly mean columnar ozone and water vapor are obtained from the Total Ozone Mapping Spectrometer (TOMS) [*Reinsel et al.*, 1994] and National Center for Environmental Prediction (NCEP) [*Randel et al.*, 2000] reanalysis respectively. Surface reflectance is an important parameter which can introduce large errors in the estimation of aerosol radiative forcing especially over land [*Wielciki et al.*, 2005]. Though surface reflectance is not an aerosol property, it plays an important role in determining the magnitude and sign of aerosol radiative forcing. It has been observed that partially absorbing aerosols may exert a local negative forcing over a region with low surface reflectance, while it will give a positive value of forcing over a high reflectance surface [e.g., *Haywood and Shine*, 1995]. Surface reflectance is significantly larger for land when compared to ocean. In the present study, surface reflectance measured by MODIS onboard Terra and Aqua satellites (8-Day, Level 3 Global 500m ISIN Grid product, MOD09A1 (Terra) and MYD09A1 (Aqua)) at seven wavelength bands centered at 0.645, 0.859, 0.469,

0.555, 1.24, 1.64 and 2.13 μm are utilized to calculate the Terra-Aqua mean surface reflectance value over all the study locations/regions.

(a) Surface albedo over continental locations

The daily mean surface reflectance (along with $\pm 1\sigma$) obtained from MODIS are used to estimate the seasonal mean surface reflectance over Ahmedabad, Gurushikhar, Kanpur and Gandhi College at seven different wavelength bands during 2006 to 2008 (Table 5.1).

Table 5.1 *Seasonal variation in surface reflectance over Ahmedabad, Gurushikhar, Kanpur and Gandhi College as a function of wavelength obtained from MODIS satellite data.*

Location	**Wavelength** (μm)	**Seasons**			
		Winter (DJF)	**Premonsoon** (MAM)	**Monsoon** (JJAS)	**Postmonsoon** (ON)
Ahmedabad	0.469	0.065 ± 0.007	0.078 ±0.006	0.180 ± 0.075	0.061 ± 0.007
	0.555	0.107 ± 0.011	0.127 ±0.011	0.210 ± 0.068	0.103 ± 0.012
	0.645	0.126 ± 0.013	0.151 ±0.013	0.214 ± 0.067	0.119 ± 0.014
	0.859	0.209 ± 0.019	0.249 ±0.025	0.318 ± 0.054	0.218 ± 0.029
	1.240	0.230 ± 0.018	0.269 ±0.026	0.315 ± 0.045	0.236 ± 0.028
	1.640	0.223 ± 0.017	0.258 ±0.022	0.282 ± 0.050	0.216 ± 0.028
	2.130	0.182 ± 0.017	0.215 ±0.016	0.203 ± 0.039	0.172 ± 0.018
Gurushikhar	0.469	0.039 ± 0.005	0.056 ± 0.008	0.194 ± 0.094	0.031 ± 0.003
	0.555	0.065 ± 0.007	0.091 ± 0.014	0.219 ± 0.088	0.060 ± 0.006
	0.645	0.076 ± 0.010	0.110 ± 0.016	0.212 ± 0.086	0.061 ± 0.007
	0.859	0.211 ± 0.014	0.245 ± 0.031	0.383 ± 0.065	0.243 ± 0.033
	1.240	0.256 ± 0.017	0.299 ± 0.034	0.386 ± 0.048	0.268 ± 0.027
	1.640	0.218 ± 0.019	0.278 ± 0.033	0.314 ± 0.046	0.204 ± 0.019
	2.130	0.143 ± 0.017	0.197 ± 0.027	0.198 ± 0.041	0.120 ± 0.012
Kanpur	0.469	0.056 ± 0.007	0.079 ± 0.016	0.063 ± 0.019	0.065 ± 0.006
	0.555	0.099 ± 0.007	0.132 ± 0.023	0.118 ± 0.024	0.113 ± 0.007
	0.645	0.108 ± 0.009	0.151 ± 0.031	0.118 ± 0.036	0.125 ± 0.011
	0.859	0.247 ± 0.020	0.278 ± 0.025	0.320 ± 0.034	0.268 ± 0.022
	1.240	0.268 ± 0.014	0.311 ± 0.030	0.337 ± 0.036	0.304 ± 0.021
	1.640	0.238 ± 0.022	0.297 ± 0.042	0.272 ± 0.045	0.276 ± 0.018
	2.130	0.174 ± 0.021	0.231 ± 0.045	0.179 ± 0.053	0.202 ± 0.021
Gandhi College	0.469	0.041 ± 0.010	0.065 ± 0.021	0.050 ± 0.045	0.041 ± 0.012
	0.555	0.083 ± 0.012	0.110 ± 0.028	0.095 ± 0.048	0.080 ± 0.013
	0.645	0.080 ± 0.020	0.126 ± 0.040	0.083 ± 0.056	0.077 ± 0.021
	0.859	0.279 ± 0.045	0.263 ± 0.028	0.321 ± 0.035	0.269 ± 0.039
	1.240	0.282 ± 0.027	0.305 ± 0.034	0.319 ± 0.045	0.288 ± 0.035
	1.640	0.222 ± 0.032	0.286 ± 0.060	0.228 ± 0.067	0.218 ± 0.038
	2.130	0.141 ± 0.039	0.212 ± 0.063	0.127 ± 0.075	0.130 ± 0.044

On an average, surface reflectance values are found to be higher during premonsoon and monsoon seasons while the corresponding values are low during winter and postmonsoon seasons over all the four study locations.

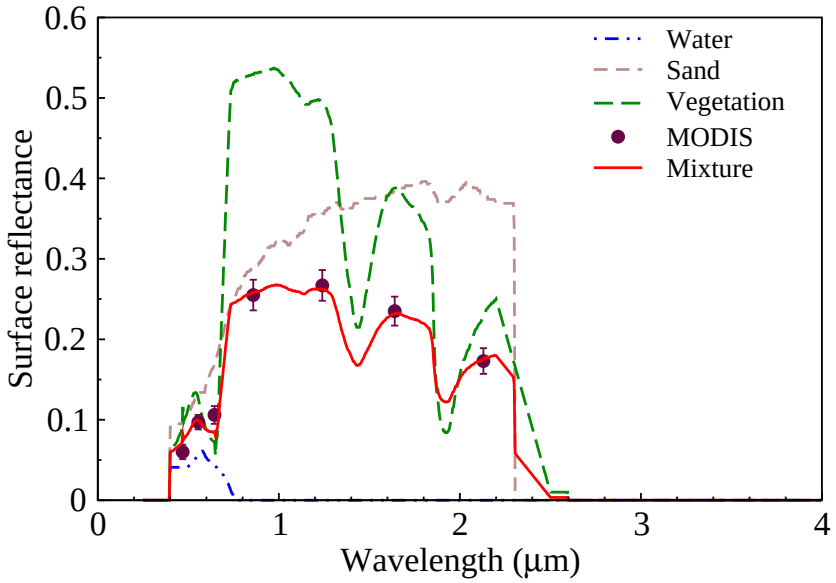

Figure 5.2: *Spectral surface reflectance for different surface types such as sand, vegetation and water. Surface reflectance data from MODIS at 0.47, 0.56, 0.65, 0.86, 1.24, 1.64 and 2.13 μm over Ahmedabad are also shown. Combination of reflectance from different surface type are used to reproduce the spectral dependence of surface albedo obtained from MODIS.*

Surface reflectance for land can be characterized by linear combination of reflectance due to variety of surfaces e.g., sand, vegetation and water. The spectral variation of surface reflectance of water, sand and vegetation is not a smooth function of wavelength as seen in Figure 5.2.

The surface reflectance data from MODIS are available at only seven wavelength bands. However, for the estimation of aerosol radiative forcing using SBDART, surface reflectance values as a function of wavelength for the entire shortwave range are required. Therefore, in the present case spectral surface reflectance are produced by combining sand, vegetation and water in certain proportion such that resultant spectrum of surface reflectance is close to the observed values from

MODIS [e.g., *Ramachandran et al.*, 2006] and used for the estimation of aerosol radiative forcing (Figure 5.2). One sample fitting of this form is shown in Figure 5.2 for Ahmedabad during the month of December 2008 using a combination of 45% sand, 30% vegetation and 25% water reflectance. Similar approach is adopted for surface reflectance calculations over all the study locations during the study period.

(b) Surface albedo over oceanic regions

The MODIS derived surface albedo corresponding to the seven central wavelengths are compared with the surface albedo for sea water [*Viollier*, 1980] as given in SBDART (Table 5.2). The $\pm 1\sigma$ variation from the mean albedo over the Bay of Bengal and the Arabian Sea during March-May 2006 is also given in Table 5.2.

The sea water surface albedo values are higher than the MODIS derived value at 0.555 and 0.645 μm, while it is lower at 0.859 μm (Table 5.2); the surface albedo for sea water is 0 at all other wavelengths. For the estimation of ARF, surface albedo data are utilized from MODIS for the seven wavelength at which the data were available; whereas for rest of the wavelengths where MODIS surface albedo values were not available, sea water surface reflectance characteristics [*Viollier*, 1980] as given in SBDART are used.

Table 5.2: *MODIS Terra/Aqua derived surface reflectance during March-May (2006) in comparison with SBDART albedo values for sea water.*

Wavelength (μm)	**SBDART**	**MODIS surface reflectance**	
		Bay of Bengal	**Arabian Sea**
0.469	0.041	0.029±0.009	0.029±0.005
0.555	0.055	0.013±0.007	0.013±0.004
0.645	0.043	0.008±0.007	0.006±0.004
0.859	0.000	0.007±0.007	0.005±0.004
1.240	0.000	0.008±0.007	0.007±0.004
1.640	0.000	0.014±0.007	0.015±0.005
2.130	0.000	0.011±0.006	0.012±0.003

As the surface reflectance over marine region is lower than land, aerosol radiative forcing is found to differ only by less than 0.5% when sea water albedo is used instead of MODIS measured albedo [*Kedia et al.*, 2010].

5.2 Vertical profiles of aerosol extinction

Vertical profile of aerosols is another important input parameter required to estimate aerosol radiative forcing and subsequently the heating rate. Lack of information on the vertical distribution can introduce uncertainty in the estimation of aerosol radiative forcing as a function of altitude [*IPCC*, 2007]. For example, it was found that the presence of elevated aerosol layers over high reflectance surfaces or a scattering layer can enhance the atmospheric radiative forcing [*IPCC*, 2007].

5.2.1 Continental locations

As ground based measurements of simultaneous collocated lidar data are not available over any of the study locations during the study period, in the present study, the aerosol extinction profiles are obtained from the CALIPSO (Cloud-Aerosol Lidar and Infrared Pathfinder Satellite Observations) lidar measurements and used [*Mamouri et al.*, 2009; *Huang et al.*, 2009]. CALIPSO is a satellite mission designed to measure the vertical structure and optical properties of aerosol. Cloud-Aerosol Lidar with Orthogonal Polarization (CALIOP) onboard CALIPSO has been providing information on the vertical distribution of aerosols and clouds as well as on their optical properties on a global scale since June 2006 [*Winker et al.*, 2007]. In the present work, level 2 aerosol extinction profile data for 0.532 μm at a horizontal resolution of 40 km are obtained over all the four study locations over India and used. The measurement uncertainty in CALIPSO derived aerosol extinction products are reported to be about 40% (*http://wdc.dlr.de/sensors/calipso/*).

The extinction profiles of aerosols from CALIOP have been used successfully to retrieve the composition and concentration of aerosols over the Indo-Gangetic Basin region [*Ganguly et al.*, 2009]. Since an exact CALIOP overpass over a particular

location is possible once in about two months, monthly mean extinction profiles are constructed by averaging all the available profiles corresponding to CALIOP tracks inside a $1^o \times 1^o$ box centered around each study location. The interannual variability for a particular season in aerosol optical properties (AOD, size distribution parameter α and $\alpha^{'}$, SSA and surface reflectance), and the vertical profiles measured over the study locations are much less when compared to the seasonal variability as already discussed in Chapter 3. Therefore, all the aerosol parameters and radiative forcing are calculated as a function of different months for 2006-2008 and are further used for calculating the seasonal mean and presented. The uncertainty, if any, due to the non inclusion of yearly variation in aerosol properties and vertical profiles used in the forcing calculation is found to be small and is not considered in the present study.

Figure 5.3 shows the seasonal variation in clear sky aerosol extinction profiles averaged over all the data available for the period of 2006-2008 over all the study locations.

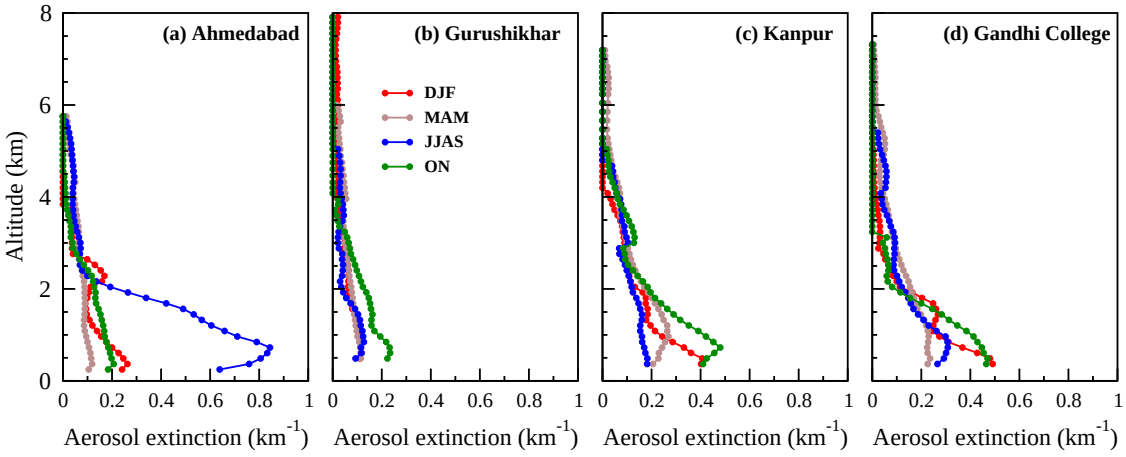

Figure 5.3: *Seasonal variations in aerosol extinction over (a) Ahmedabad, (b) Gurushikhar, (c) Kanpur and (d) Gandhi College) during 2006-2008 as a function of altitude. Each data points represents 5 point running average values.*

The mean extinction profile corresponding to each month over all the study locations are normalized with the measured AODs and used in SBDART to get the

vertical distribution of aerosol radiative forcing and the heating rate [e.g., *Kedia et al.*, 2010; *Ramachandran and Kedia*, 2010]. Throughout the study period, a large seasonal variation in the aerosol extinction profiles are observed over all the study locations as can be seen in Figure 5.3.

Aerosol vertical profiles for different seasons are characterized by higher values of extinction coefficient within the first few kilometers (∼1-2 km) from the surface after which a sharp decrease in the extinction is seen as the altitude increases. Extinction coefficients at the surface are found to be higher during winter and postmonsoon which could be attributed to the presence of inversion layer during these seasons. In addition, extinction values are found to be higher at the surface over the Indo-Gangetic region when compared to the study locations in the west (Figure 5.3). This could be due to higher aerosol concentration over the Indo-Gangetic region as also reflected in the AOD values (Figure 3.7). During winter and postmonsoon seasons, the height of atmospheric boundary layer height remains low which traps the pollutants near surface. Therefore, the extinction values are found to be higher at the surface and decreases at higher altitudes during these seasons over all the locations (Figure 5.3). On the other hand, the boundary layer height is higher during premonsoon and monsoon [e.g., *Ramachandran and Kedia*, 2010]. This provides a larger room for the aerosols to distribute themselves in the atmosphere (Figure 5.3).

5.2.2 Oceanic regions

As CALIPSO data were not available during the cruise period (March-May 2006), aerosol extinction profiles measured during ICARB using a micropulse lidar system from Bhubaneshwar (20.2^{o}N, 85.8^{o}E, 25 March 2006) and Chennai (13.1^{o}N, 80.2^{o}E, 3 April 2006) on the east coast, and Trivandrum (8.5^{o}N, 77^{o}E, 23 April 2006) on the west coast [*Satheesh et al.*, 2009] are used. As simultaneous lidar measured aerosol profiles from the cruise are not available, model aerosol vertical profiles similar to those obtained during the ICARB air segment from micropulse lidar

measurements at 0.523 μm [*Satheesh et al.*, 2009] are constructed and utilized in the sensitivity study reported here. The mean latitude and longitude of the ship positions on 25 March, 3 and 23 April 2006 were 16.9 ^{o}N, 92.7 ^{o}E, 10.0 ^{o}N, 82.8 ^{o}E, and 11.0 ^{o}N, 62.1 ^{o}E, respectively. However, in the present case it is assumed that the vertical structure of aerosols over the marine latitude domain during the above days is similar to those measured on 25 March 2006, 3 April and 23 April 2006 from Bhubaneshwar, Chennai and Trivandrum, respectively. The aerosol extinction profiles are scaled by the respective day's mean AOD and used.

5.3 Calculation

5.3.1 Aerosol radiative forcing

Up to 65 atmospheric layers from the surface to 100 km with varying resolution can be introduced in SBDART. The vertical resolution of the atmosphere in the present study is varied as follows: the resolution is 0.25 km from the surface to 10 km, 1 km from >10 km to 25 km, 5 km between 25 and 50 km, and 10 km between 50 and 100 km. Aerosol radiative forcing (ΔF) at the top of the atmosphere (TOA) and surface (SFC) can be defined as the change between the net (down minus up) flux with and without aerosols as,

$$\begin{aligned} \Delta F_{TOA,SFC} &= Flux(Net)_{with\ aerosol\ TOA,\ SFC} \\ &\quad - Flux(Net)_{without\ aerosol\ TOA,\ SFC}. \end{aligned} \tag{5.1}$$

The difference between radiative forcing at the top of the atmosphere (which is 100 km in this case) and surface is defined as the atmospheric forcing (ATM) and can be written as,

$$\Delta F_{ATM} = \Delta F_{TOA} - \Delta F_{SFC}. \tag{5.2}$$

ΔF_{ATM} represents the amount of energy trapped within the atmosphere due to the presence of aerosols. If ΔF_{ATM} is positive the aerosols contribute to a net gain of radiative flux to the atmosphere leading to a heating (warming), while a negative ΔF_{ATM} indicates a net loss and thereby exhibit a cooling effect. SBDART estimated radiation has been validated against the ground based observations of shortwave radiation. The uncertainty in the SBDART's predicted direct shortwave radiation is found to be about 1%, while the uncertainty in the diffused radiation is about 30% [*Ricchiazzi et al.*, 1998]. The relative standard error in radiative forcing reported in the study, taking into account the uncertainties in the aerosol input parameters and flux estimates is found to be 20% [*Kedia et al.*, 2010; *Ramachandran and Kedia*, 2010].

5.3.2 Atmospheric heating rate

Radiative and subsequently the climate implications of aerosols are assessed in terms of the atmospheric heating rate. The atmospheric forcing in Wm^{-2} (equation 5.2) indicates the amount of radiative flux (energy) absorbed by aerosols. The amount of absorbed energy which is converted into heat is termed as the atmospheric solar heating rate (K/d) and can be calculated as,

$$\frac{\partial T}{\partial t} = \frac{g}{c_p}\left[\frac{\Delta F}{\Delta P}\right] \tag{5.3}$$

where $\partial T/\partial t$ is the heating rate (K/d), g is the acceleration due to gravity, c_p is the specific heat capacity of air at constant pressure and P is the atmospheric pressure [*Liou*, 1980]. Large amount of different kinds of atmospheric aerosols (water soluble, black carbon, sea salt and mineral dust) are concentrated from near surface to up to 3 km [e.g., *Ramanathan et al.*, 2001; *IPCC*, 2007] over urban, continental and marine environments. Therefore, ΔP (in equation 5.3) is considered as 300 hPa which is equal to the pressure difference between the surface and 3 km. For the estimation of heating rate as a function of altitude, the forcing and pressure difference corresponding to two consecutive altitudes are taken.

5.4 Approach

5.4.1 Continental locations

Method 1

In Method 1, ground based measurement of SSA are utilized in addition to the measured AODs over the study locations to constrain the model (OPAC). The SSA values over all the four continental locations are obtained following different approaches as follows:

(a) Ahmedabad

Over Ahmedabad, the SSA values at 0.55 μm are calculated from the in situ measured scattering and absorption coefficients following equation 2.12. Figure 5.4 shows the seasonal mean variation of aerosol scattering coefficient at 0.55 μm over Ahmedabad during 2006-2008. Aerosol types which contribute maximum to the scattering coefficient include water soluble inorganic species such as sulfates and nitrates arising from emissions associated mainly with fossil fuel combustion, industrial emissions and biomass combustion [*Charlson et al.*, 1992; *Penner et al.*, 1994].

Highest β_{sca} value is observed during winter (2.4×10^4 m^{-1}) and postmonsoon (2.3×10^4 m^{-1}) which is followed by the values obtained during premonsoon and monsoon seasons, respectively, in decreasing order of their magnitudes. Higher values of β_{sca} measured during winter and postmonsoon could arise due to shallow boundary layer and an increase in open burning, which contributes significantly to the emission of both scattering and absorbing type species in the atmosphere. During premonsoon and monsoon, decrease in the scattering coefficient is expected because of enhanced coarse mode aerosol concentration (sea salt and dust) in the atmosphere. However, as both dust and sea salt are in coarse mode their effect will be less visible at 0.55 μm.

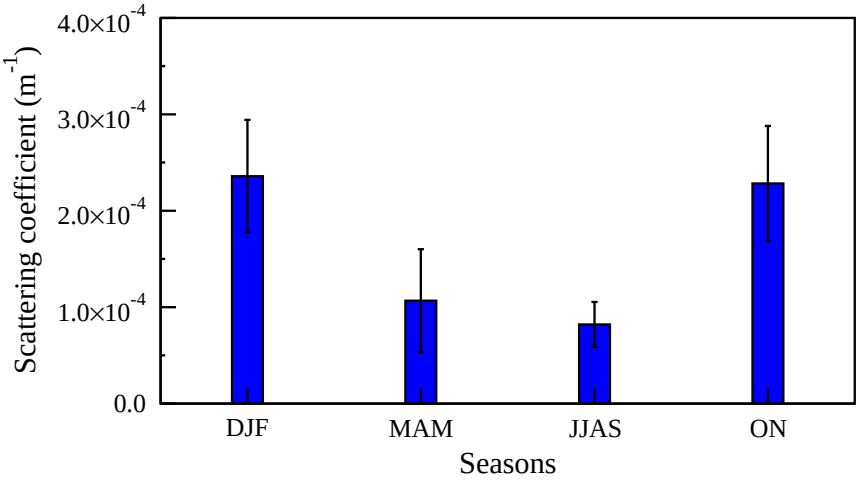

Figure 5.4: *Seasonal variation of scattering coefficient at 0.55 μm over Ahmedabad averaged over all data available from 2006 to 2008. Vertical bars represent ±1σ variation from the mean value.*

In addition, atmospheric boundary layer height increases during premonsoon and monsoon seasons which provides more volume for the aerosols to get distributed. This results in a dilution of their concentration near surface level thereby decreasing the scattering coefficient (Figure 5.4) [e.g., *Ramachandran and Rajesh*, 2008; *Ganguly et al.*, 2006a].

Figure 5.5 shows the seasonal variation of BC mass concentration averaged over 2006 to 2008. BC mass concentrations exhibit a strong seasonal cycle marked by a winter high and a summer low in Ahmedabad (Figure 5.4). The seasonal mean BC mass concentrations are 9.4 ± 2.2 (winter; DJF), 3.9 ± 2.0 (premonsoon; MAM), 2.0 ± 0.5 (monsoon; JJAS), and 9.0 ± 2.0 μg m^{-3} (postmonsoon; ON) respectively.

During winter, fossil fuel emissions and the additional biomass burning combined with the shallow boundary layer result in higher BC mass concentrations over Ahmedabad. BC mass concentration decreases during premonsoon due to increase in the magnitude of wind speeds, and change in the source region and direction of wind (arid/marine) (Figure 3.6). The decrease in BC during monsoon when the rainfall is maximum can be directly related to the wet removal of

aerosols by precipitation. Wind speeds are much weaker during postmonsoon, and aerosols produced in the urban areas do not get properly ventilated or transported to downwind locations. Thus, the local sources over Ahmedabad influence the BC mass concentrations, in addition to atmospheric dynamics (boundary layer, winds, and long range transport) and rainfall [*Ramachandran and Kedia*, 2010].

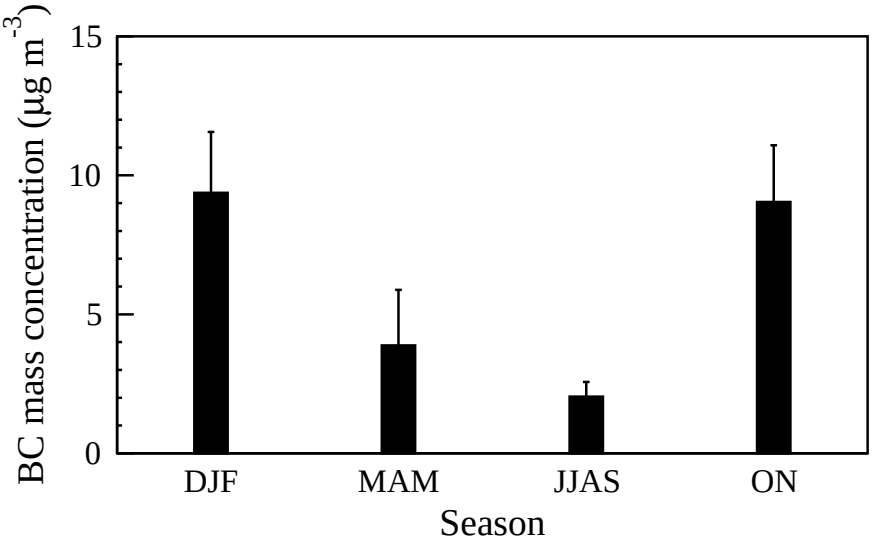

Figure 5.5: *Seasonal variation of black carbon mass concentration averaged over all data available from 2006 to 2008. Vertical bars represent $\pm 1\sigma$ variation from the mean.*

BC mass concentrations during all the seasons in present study are found to be higher than the values obtained during 2003-2005 [*Ganguly et al.*, 2006a] indicating an increasing trend in BC concentration over Ahmedabad. The range of BC mass concentrations measured over Ahmedabad are comparable to those measured in other urban locations in India, such as Hisar (1.5-7.2 μg m^{-3}; *Ramachandran et al*, [2006]), Hyderabad (3.5 μg m^{-3}; *Moorthy et al.*, [2004]), and Mumbai (12.4 $\pm$ 5.1 μg m^{-3}; *Venkataraman et al.*, [2002]). BC over Ahmedabad are higher than the values over coastal stations Trivandrum (1.5 (summer) - 5 (winter) μg m^{-3}; *Babu and Moorthy*, [2002]), Goa (3 μg m^{-3}; *Leon et al.*, [2001]), Visakhapatnam (0.43 (postmonsoon) - 8.01 μg m^{-3} (winter); *Sreekanth et al.*, [2007]); while BC over Ahmedabad are lower than Delhi (29 $\pm$ 14 μg m^{-3}; *Ganguly et al.*, [2006b]), and

Kanpur (6-20 μg m^{-3}; *Tripathi et al.*, [2005]) [*Ramachandran and Kedia*, 2010].

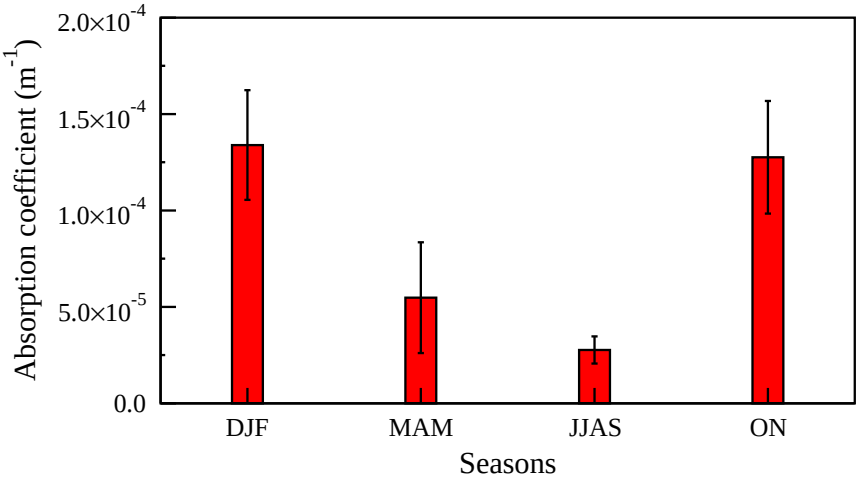

Figure 5.6: *Seasonal variation of absorption coefficient (at 0.55 μm), averaged over all data available from 2006 to 2008. Vertical bars represent $\pm 1\sigma$ variation from the mean value.*

The seasonal variation in the absorption coefficient (β_{abs}) at 0.55 μm averaged over 2006 to 2008 is shown in Figure 5.6. The absorption coefficient derived using a multiwavelength Aethalometer (Chapter 2) are found to exhibit similar seasonal variability as seen in the BC mass concentration as the measurement site is an urban location.

(b) Gurushikhar

Over Gurushikhar, OPAC model is used to reconstruct the measured AOD spectra by varying the concentration of different aerosol species to get the total mass and BC mass concentration value similar to that obtained using high volume sampler over Gurushikhar [*Kumar and Sarin*, 2009; *Ram et al.*, 2008] and the corresponding SSA values are obtained. This approach has been successfully used in many studies e.g., *Ramachandran et al.* [2006]; *Kedia et al.* [2010]. The mass concentration of fine and coarse mode aerosols was found to vary from 1.6-46.1 and 2.3-102 μg m^{-3} respectively during Jan-Dec 2007 [*Kumar and Sarin*, 2009]. In

addition, it was documented that over Gurushikhar dust is the dominant species which contributes uniformly in the range of 60-80% in the coarse mode throughout the year [*Kumar and Sarin*, 2009]. On an annual scale, the black carbon mass concentration was found to vary from 0.06 to 2.3 μg m^{-3} and contributed about 2% of total suspended particulate mass (TSP) over Gurushikhar [*Ram et al.*, 2008].

(c) Kanpur and Gandhi College

SSA calculated from AERONET sun/sky measured aerosol properties are obtained in the wavelength range of 0.4-1.02 μm (at 0.44, 0.675, 0.87 and 1.02) over Kanpur and Gandhi College and utilized. SSA at 0.55 μm is calculated from SSA values at 0.44 and 0.675 μm. The methodology adopted for SSA calculation from ground based measurements are not similar over the study locations in Method 1. As the dependence of aerosol radiative forcing on SSA is not linear, there can be differences in forcing values due to differences in SSA [*IPCC*, 2007; *Ramachandran*, 2007]. Therefore, in Method 2, SSA values are obtained from a single source (global transport model) over all the study locations and utilized.

Method 2

In Method 2, single scattering albedo is calculated over all the four continental locations using GOCART (GeorgiaTech-Goddard Global Ozone Chemistry Aerosol Radiation and Transport) model and used in constraining OPAC. The GOCART model computes AODs of different species (sulfate, sea salt, black carbon and organic carbon) by adopting the published emission inventories and observed meteorological fields as input to chemical transport model [*Chin et al.*, 2002; *Chung et al.*, 2005]. The GOCART model produces a global gridded output at the latitude-longitude resolution of $2.0^o \times 2.5^o$. In this study SSAs are estimated by weighting the individual SSA of black carbon (BC), sulfate, organic carbon (OC), dust and sea salt with their respective AODs following *Chung et al.* [2005]. Sulfate, OC and sea salt aerosols (which are conservative scatterers) were assumed to have an SSA of 1 at 0.55 μm, while SSA of BC was taken as 0.2. SSA of dust was allowed

to vary from 0.98 to 0.90 depending on the amount of BC. The ratio of BC AOD to the sum of dust AOD and BC AOD was chosen as the criteria to determine the dust SSA. When this ratio was less than 0.1, the dust SSA was taken as 0.98 and when this ratio was greater than 0.5 then the SSA for dust was assigned as 0.9. Dust SSA linearly increased from 0.9 to 0.98 when the value of the ratio was between 0.5 and 0.1.

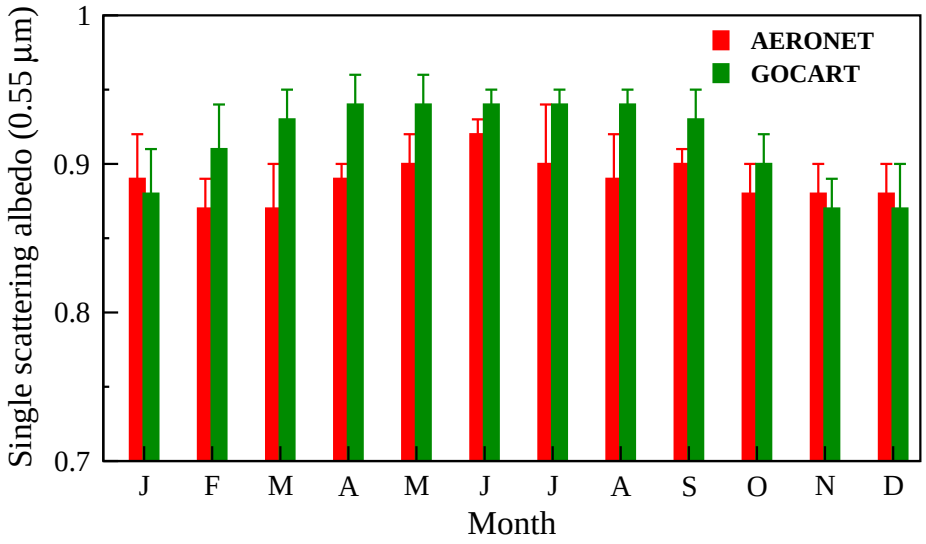

Figure 5.7: *Monthly mean variation in single scattering albedo over Kanpur obtained from AERONET and estimated from GOCART during 2001-2007. The vertical bars represent the variation from the mean for the respective month during 2001-2007.*

The monthly mean AODs corresponding to individual aerosol species are obtained at $2.0^o \times 2.5^o$ resolution centered around the study location and used for the calculation of SSA. The seasonal mean SSA values are calculated for all the four continental locations following this method for the period of Jan 2006 - Dec 2007, as GOCART AOD data for 2008 were not available. Consistency of GOCART model over the Indian region has not been rigorously validated so far. Therefore, the model derived SSA is validated against AERONET SSA before being used for aerosol radiative forcing estimates in this study. The monthly mean SSA values calculated from AERONET are compared with GOCART derived SSA over

Kanpur for the period of 2001-2007.

Figure 5.7 shows the monthly mean variation in SSA estimated from GOCART and that obtained from the AERONET site Kanpur during 2001-2007. The magnitude and the variability in the SSA obtained from GOCART model is found to agree well with the AERONET SSA. Therefore, GOCART derived SSA are obtained for all the four stations and used for the aerosol radiative forcing calculation in Method 2.

Criteria

The basic input parameters required for the estimation of aerosol radiative forcing in the shortwave range are retrieved from OPAC following the same procedure in both the methods (Method 1 and Method 2). The number concentrations of different aerosol species are varied until the following conditions are satisfied: (1) the root mean square (rms) difference between the measured and model AOD spectra is <0.03, thus, constraining the rms difference to within 0.10 AOD, (2) Ångström wavelength exponent α determined for the measured AODs in the 0.4-0.875 μm wavelength region are consistent with model derived α values, and (3) model derived values of single scattering albedo closely matches with the SSA calculated (Method 1/Method 2) over different study locations [*Ramachandran and Kedia*, 2010].

5.4.2 Oceanic regions

Over the marine regions, measurements of total suspended aerosol mass concentration (TSP) and the mass of individual chemical species measured simultaneously using a high volume sampler (HVS) correspond to 50% RH [*Kumar et al.*, 2008] during ICARB are utilized. To obtain the input parameters required for ARF calculation using OPAC, over the Bay of Bengal and the Arabian Sea two additional constraints apart from the above three are used which are as follows. (4) the OPAC estimated total mass concentrations at 50% RH should lie within $\pm 1\sigma$

of the HVS measured TSP mass and (5) OPAC estimated mass concentrations of water soluble, black carbon, sea salt and mineral dust should be within $\pm 1\sigma$ of the respective concentrations analyzed from HVS at 50% RH [*Kedia et al.*, 2010].

5.5 Results and Discussion

5.5.1 Aerosol radiative forcing over continental locations

Seasonal mean AODs calculated at 0.5 μm over all the four locations during 2006-2008 obtained from ground based measurement are shown in Figure 5.8. AOD is found to exhibit a strong seasonal and spatial variation with the highest value over Gandhi College and the lowest AOD over Gurushikhar during all the seasons. AOD is found to be higher during winter over all the locations except for Gurushikhar, where minimum AOD (<0.1) is observed during winter.

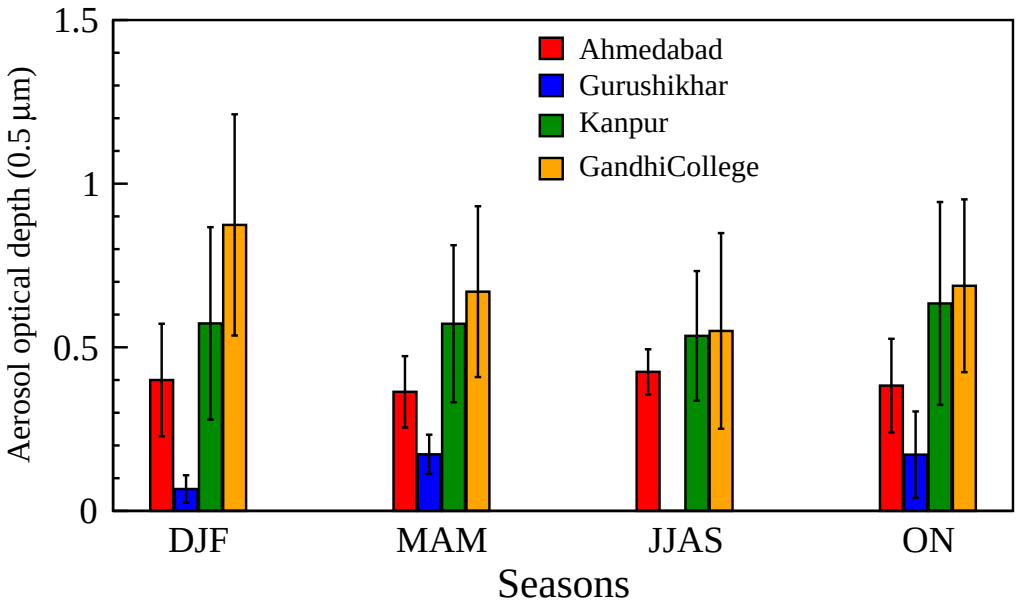

Figure 5.8: *Seasonal variation in aerosol optical depth at 0.5 μm from ground based measurement over Ahmedabad, Gurushikhar, Kanpur and Gandhi College during 2006-2008. The vertical bars represent $\pm 1\sigma$ variation from the mean for the season.*

Both Kanpur and Gandhi College are located in the Indo-Gangetic plain, therefore the AODs over these locations are expected to be similar. However during

winter, AODs are higher over Gandhi College (0.87) than Kanpur (0.57) which could be due to the additional local production of aerosols from biomass burning as Gandhi College is a rural location. In addition, as Gandhi College is situated downwind of major urban centers the transport of pollutants can contribute to the increase in AOD (Figure 3.6).

Average AOD is found to be a factor of four less over Gurushikhar (0.07) than Ahmedabad (0.40) during winter. AODs over Gurushikhar during all the seasons are found to be more than a factor of three less than the value over Kanpur and Gandhi College. AODs over Ahmedabad are found to be about a factor of two less during winter than Gandhi College. Difference in the AODs over Ahmedabad and that over the locations in Ingo-Gangetic plain region is less during the other three seasons. This could be due to the hazy and foggy condition observed in the Indo-Gangetic plain during winter. In addition, pollutants get trapped due to prevailing calm winds and absence of vertical mixing during this time frame [*Ramachandran et al.*, 2006]. It has been shown that the topography, meteorology and aerosol sources in this part of India favor in developing a concentrated pool of airborne particles during winter resulting in higher AODs [*Di Girolamo et al.*, 2004].

Seasonal variation in the SSA values calculated from the ground based measurements (Method 1) are shown in Figure 5.9. Variations in the SSA are found to be similar over both the locations of Indo-Gangetic plain with a value >0.8 throughout the study period (Figure 5.9). In contrast, the SSA is found to be <0.7 over Ahmedabad during all the seasons except for monsoon (0.79). This could be due to differences in the methodology used to obtain the SSA values over these locations. (for example, SSA over Kanpur and Gandhi College are obtained from the inversion of AOD which is a columnar quantity; whereas over Ahmedabad SSA is calculated using the surface measured scattering and absorption coefficients). As most of the BC, which are absorbing species, are concentrated near the surface, the absorption coefficients near the surface will be higher when compared to the

columnar value.

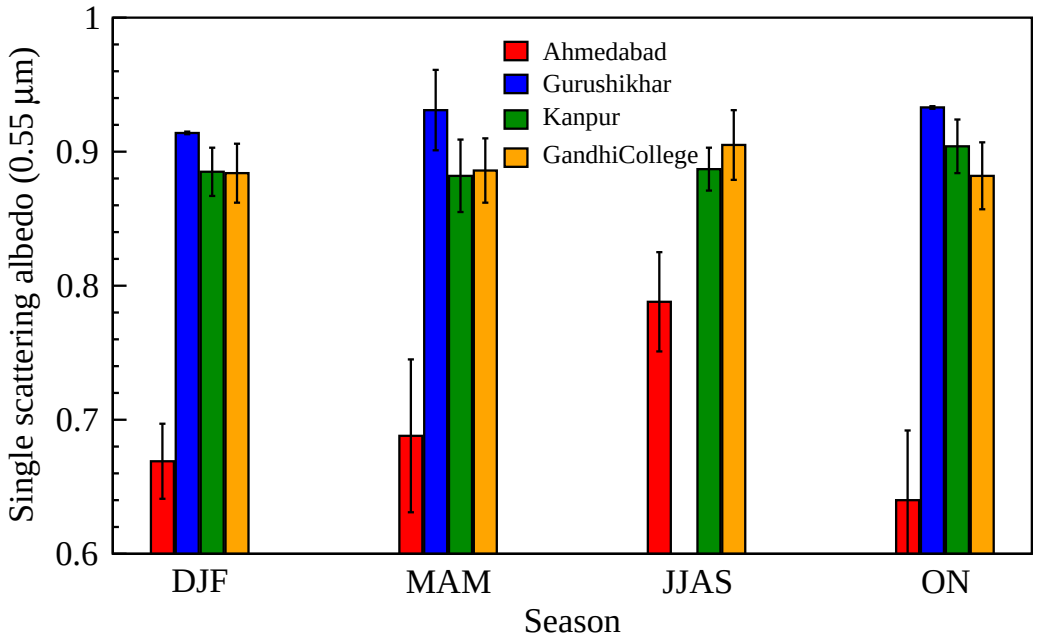

Figure 5.9: *Seasonal variation in single scattering albedo at 0.55 µm over Ahmedabad (measured using Aethalometer and Nephelometer), Gurushikhar (estimated using OPAC), Kanpur (from AERONET) and Gandhi College (from AERONET) during 2006-2008. The vertical bars represent $\pm 1\sigma$ variation from the mean for the respective season.*

Nevertheless, the surface measured SSA has been successfully used in many studies for estimating aerosol radiative forcing over different environments [e.g., *Corrigan et al.*, 2006; *Jayaraman et al.*, 2006; *Ganguly et al.*, 2006b; *Babu et al.*, 2008; *Nair et al.*, 2008; *Pathak et al.*, 2010].

Figure 5.10 presents the seasonal variability in the SSA calculated from the GOCART over all the study locations (Method 2). As GOCART data are available only upto 2007, in the present work SSA obtained from GOCART are the mean of 2006-2007. However, it has been already shown that the interannual variability in SSA from GOCART is not very significant during 2001-2007 (Figure 5.7).

SSA is found to be >0.8 throughout the study period over all the study locations including Ahmedabad. The highest SSA value is observed over Gurushikhar for all

the seasons except in monsoon when SSA corresponding to Ahmedabad is higher. The difference in SSA over Kanpur and Gandhi College are not significant during all the seasons except premonsoon when Gandhi College SSA is lower (Figure 5.10). SSA is found to be higher during premonsoon and monsoon over all the locations. SSA over Ahmedabad during all the seasons is remarkably higher using GOCART data (Figure 5.10) than the values calculated using ground based measurements (Figure 5.9).

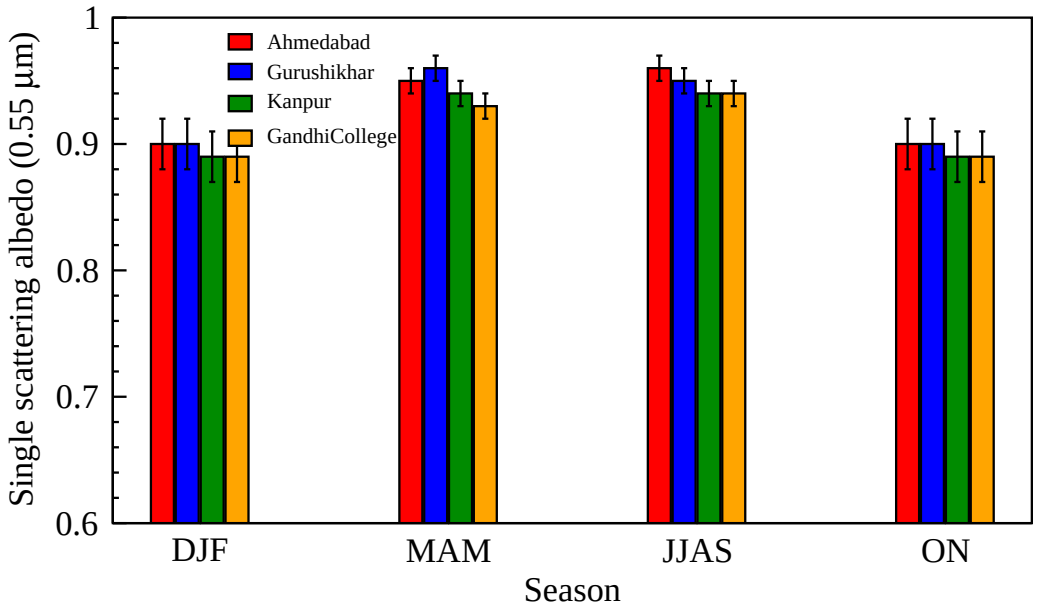

Figure 5.10: *Seasonal variation in single scattering albedo at 0.55 μm from GOCART model over Ahmedabad, Gurushikhar, Kanpur and Gandhi College during 2006-2007. The vertical bars represent $\pm 1\sigma$ variation from the mean for the season.*

For the estimation of aerosol radiative forcing using both the methods OPAC model is used to obtain the required aerosol parameters. In Method 1, SSA obtained from ground based measurements are utilized while the SSA obtained from GOCART are used in Method 2. The spectral variation in AOD, SSA and the asymmetry parameter obtained from OPAC for all the study locations along with the vertical profile of aerosol extinction are used in SBDART to estimate the forcing at different heights for different seasons.

Aerosol radiative forcing and heating rate: Method 1

Figure 5.11 presents the vertical distribution of aerosol radiative forcing and the heating rates during different seasons over all the four study locations estimated using Method 1. At the outset, a large spatial and temporal variability in the aerosol radiative forcing as a function of altitude is observed over all the study locations.

The seasonal variability in the aerosol radiative forcing is found to be stronger over Ahmedabad and weaker over Gurushikhar; while the forcing is found to exhibit similar features over Kanpur and Gandhi College as a function of altitude. Highest forcing is observed at the surface during premonsoon over all the locations when the entire study region is influenced by dust particles. Forcing value is found to decrease by a factor of more than three from ground to that at 4 km over Ahmedabad, Kanpur and Gandhi College; while the change in forcing with altitude is not very significant over Gurushikhar. This could be because of the relatively cleaner atmosphere compared to other three locations as Gurushikhar is a high altitude remote site.

Heating rate is found to be higher where aerosol layers exist, and exhibit spatial and altitudinal differences. The atmospheric heating rate is found to be higher over Ahmedabad ($\geq$0.5 K/d upto about 2 km) during all the seasons. Over Gurushikhar, the heating rate is $<$ 0.3 K/d throughout the study period indicating a lower concentration of absorbing aerosol species as also revealed by higher SSA (Figure 5.9). The seasonal variability in the heating rate is not found to be very significant over Gurushikhar during the study period. The vertical distribution of heating rate is found to be similar over Kanpur and Gandhi College. Heating rate is found to be $\leq$1 K/d over these two locations throughout the study period, which is lower than the values obtained over Ahmedabad. The heating rates are higher during winter and postmonsoon when the BC mass concentrations are also higher and SSA is lower over all the locations. Similar values of heating rates were

observed in the range of (1.1 - 1.8 K/d) over Hanimadhoo island during March 2006 [*Ramanathan et al.*, 2007]. Seasonal mean heating rates were found to be higher than 1.5 K/d in winter and postmonsoon over Ahmedabad [*Ramachandran and Kedia*, 2010]. Heating rates were a factor of 3 higher when BC aerosols were included than the value when BC aerosols were absent [*Ramachandran and Kedia*, 2010]. The higher heating rate is consistent with the lower SSA values observed over Ahmedabad (Figure 5.9).

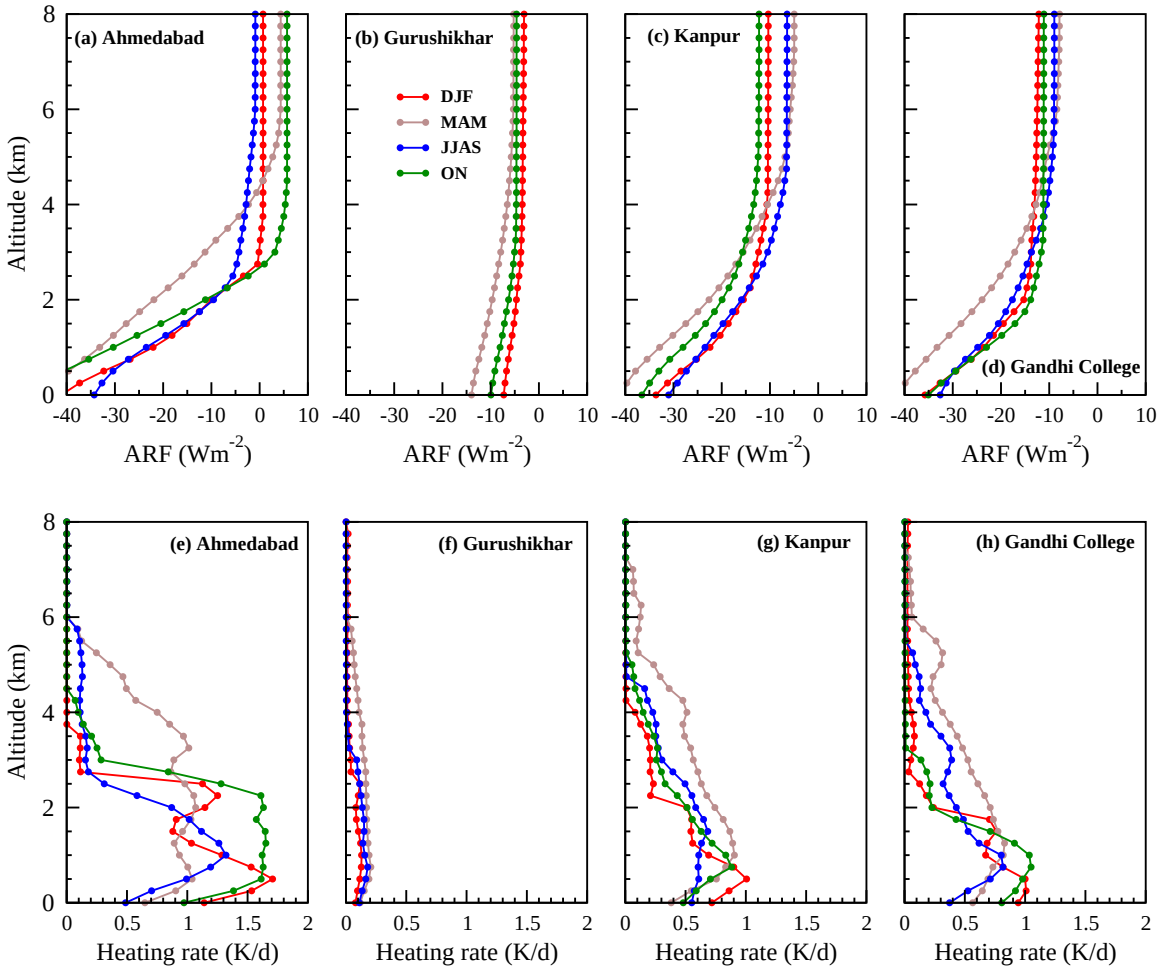

Figure 5.11: *Shortwave aerosol radiative forcing (ARF in Wm^{-2}) and heating rate calculated using Method 1 for different seasons as a function of altitude over Ahmedabad (a, e), Gurushikhar (b, f), Kanpur (c, g) and Gandhi College (d, h) for the period of 2006-2008.*

Seasonal variation in the aerosol radiative forcing calculated at the surface

(SFC), top of the atmosphere (TOA) and in the atmosphere (ATM) estimated using Method 1 are shown in Figure 5.12 for all the study locations. The values in the parenthesis represent the atmospheric heating rates (equation 5.3) for each season. A large seasonal as well as spatial variability in aerosol radiative forcing are observed at all the three atmospheric levels. The forcing is found to be higher over Ahmedabad, while the lowest forcing is observed over Gurushikhar during all the seasons. Lower forcing over Gurushikhar is due to the lower AOD and higher SSA throughout the study period (Figures 5.8, 5.9). It is remarkable that, even if the AOD over Ahmedabad is lower than the AOD value over Kanpur and Gandhi College, the forcing is higher. Higher forcing over Ahmedabad during all the seasons can be attributed to lower SSA as was seen earlier. Over Indo-Gangetic plain, AODs are higher but SSA are also higher (compared to Ahmedabad) which gave rise to lower forcing values. These results highlight the strong influence SSA has on forcing.

The surface cooling over Ahmedabad is found to be minimum during monsoon (-34.3 Wm^{-2}) and maximum during postmonsoon (-48.3 Wm^{-2}). In addition, during postmonsoon the TOA forcing is found to be the highest (5.7 Wm^{-2}). It has been seen that shortwave TOA forcing can become positive when abundant absorbing aerosols are found over higher reflectance regions, thereby resulting in a more positive ATM warming [*Ramachandran and Kedia*, 2010]. It is worth noting that the TOA forcing over Ahmedabad is found to be positive during all the seasons in contrast to the negative value of TOA forcing over other locations. The positive value of TOA forcing is attributed to the higher concentration of absorbing aerosols over Ahmedabad. Over Gurushikhar the maximum value of SFC (-14.0 Wm^{-2}) and ATM (8.9 Wm^{-2}) forcing are observed during premonsoon when the atmosphere is dominated by the long range transported dust particles (Figure 3.6). Forcing is about a factor of four less over Gurushikhar during all the seasons when compared to that over Ahmedabad. The forcing value over both the study locations in Indo-Gangetic plain is not found to exhibit any significant

differences (Figure 5.12). The SFC and TOA forcing are found to be -40.9 Wm^{-2} and 36.2 Wm^{-2} over Kanpur respectively; while the corresponding values are -41.7 Wm^{-2} and 34.2 Wm^{-2}, respectively over Gandhi College during premonsoon which is the highest value of forcing observed over these locations.

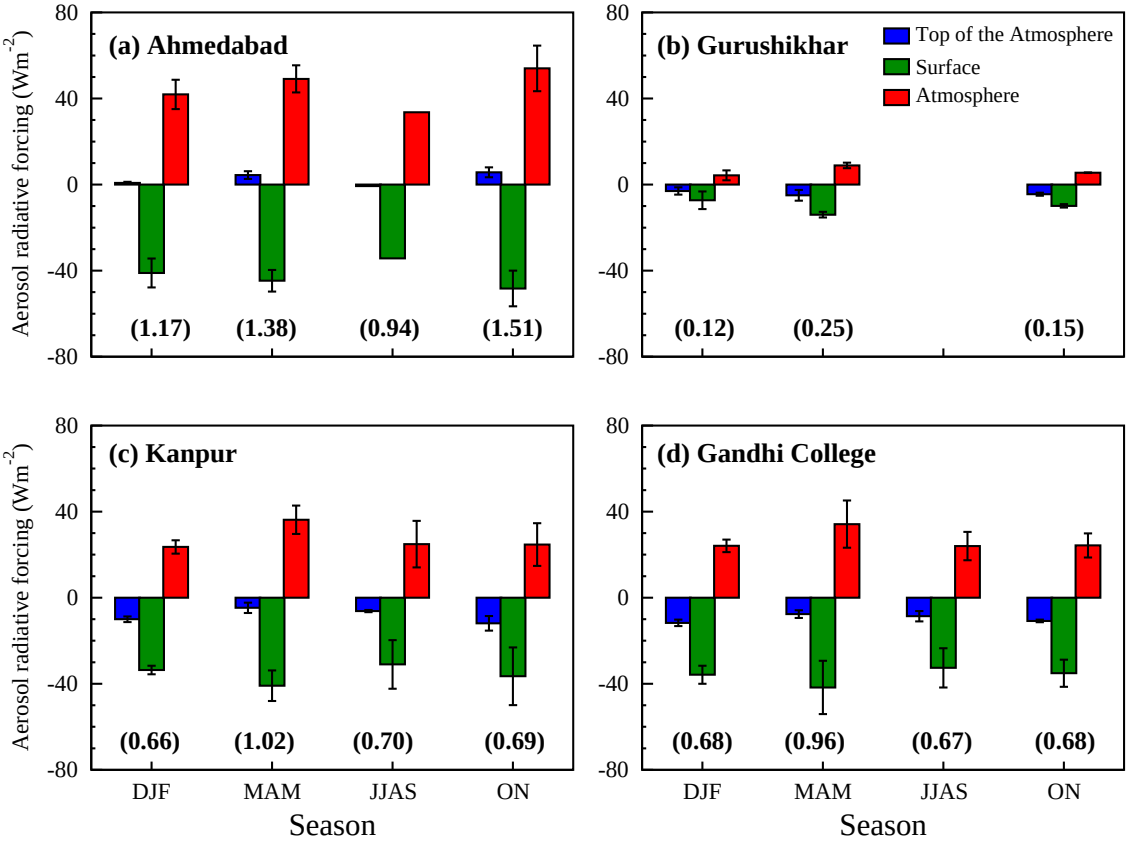

Figure 5.12: *Seasonal variation in aerosol radiative forcing using Method 1 in shortwave range (0.2-4.0 μm) over (a) Ahmedabad, (b) Gurushikhar, (c) Kanpur and (d) Gandhi College during 2006-2008. The vertical bars represent the variation from the mean for the season. The heating rates (Kelvin per day) are given in brackets.*

The atmospheric heating rate is found to exhibit large spatial and temporal variability similar to forcing as seen in Figure 5.12. The maximum heating rate is observed over Ahmedabad during postmonsoon (1.51 K/d) and the minimum value is observed over Gurushikhar during winter (0.12 K/d). Over Ahmedabad, atmospheric heating rate is found to be >0.9 throughout the study period with the

minimum value of 0.94 K/d during monsoon. Heating rate is found to increase by a factor of two from winter to premonsoon (0.25 K/d) over Gurushikhar due to an increase in the abundance of dust aerosols (Figure 3.6). Over the Indo-Gangetic plain, highest value of heating rate is observed during premonsoon with a higher value over Kanpur (1.02 K/d) than Gandhi College (0.96 K/d). The higher heating rate over Kanpur can be attributed to the dust particles as maximum dust loading occurs over Kanpur during premonsoon season [*Singh et al.*, 2004]. During other seasons the heating rate is found to be lower in the range of 0.66-0.70 K/d. The minimum heating rate is observed during winter (0.66 K/d over Kanpur and 0.68 K/d over Gandhi College), which is lower by a factor of two than Ahmedabad (1.17 K/d).

A large difference in the forcing and heating rate is observed over the study locations during different seasons indicating local/regional nature of aerosols and their effect on Earth's atmosphere. In this method (Method 1) SSA values are derived from ground based measurements adopting different approaches, which can give rise to differences in radiative forcing and heating rates. While in Method 2, SSA is obtained from GOCART over all the four study locations following the approach described in section 5.4.1 and used in the estimation of aerosol radiative forcing and heating rates.

Aerosol radiative forcing and heating rate: Method 2

Seasonal variation in aerosol radiative forcing and the heating rate is estimated using GOCART SSA is shown as a function of altitude in Figure 5.13 for all the four study locations. The vertical distribution of forcing is found to be similar to that obtained from Method 1 for all the locations except over Ahmedabad where the values are found to have significantly decreased. Forcing is found to decrease by a factor of two over Ahmedabad in the altitude range of 0 to 4 km using Method 2 when compared to the values obtained from Method 1. Using this method (Method 2), the difference in the forcing values as a function of season is also found to have

decreased. Forcing over Kanpur and Gandhi College exhibit similar values which is a factor of two higher than Ahmedabad forcing during all the four seasons.

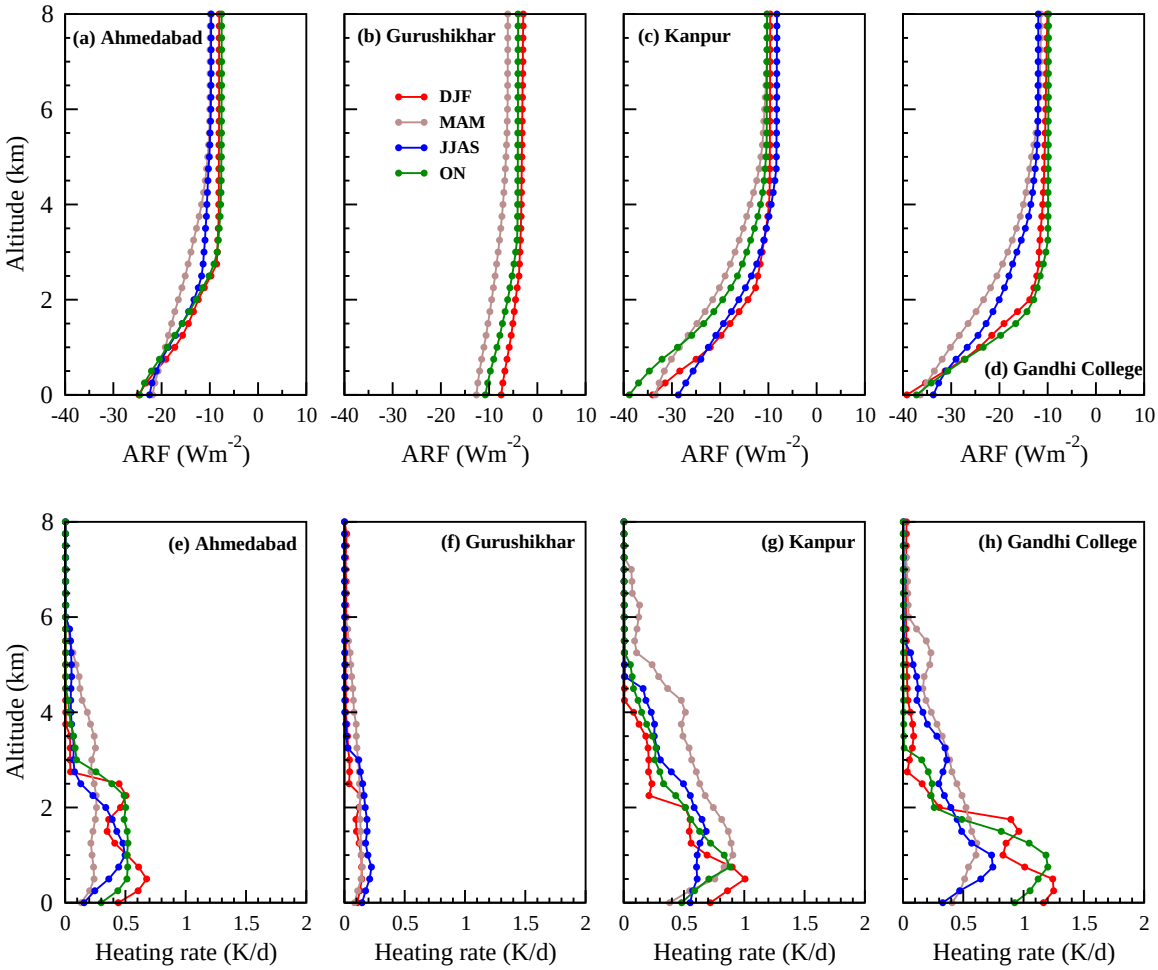

Figure 5.13: *Shortwave aerosol radiative forcing (ARF in Wm^{-2}) and heating rate calculated using Method 2 for different seasons as a function of altitude over Ahmedabad (a, e), Gurushikhar (b, f), Kanpur (c, g) and Gandhi College (d, h) for the period of 2006-2008.*

Out of the two stations in the Indo-Gangetic basin, forcing is higher over Gandhi College during winter and postmonsoon while premonsoon and monsoon forcing is higher over Kanpur. The heating rate is found to decrease by a factor of 3 over Ahmedabad when calculated using Method 2. The reason for the decreased value of heating rate is attributed to a higher value of SSA over Ahmedabad obtained following Method 2 (Figure 5.10). Heating rates are higher in the lower altitude

(<2 km) over all the locations during all the seasons as most of the aerosols are accumulated in the lower altitudes [e.g., *Ramanathan et al.*, 2007; *IPCC*, 2007].

The aerosol radiative forcing at the surface, atmosphere and at the top of the atmosphere estimated using Method 2 are shown in Figure 5.14.

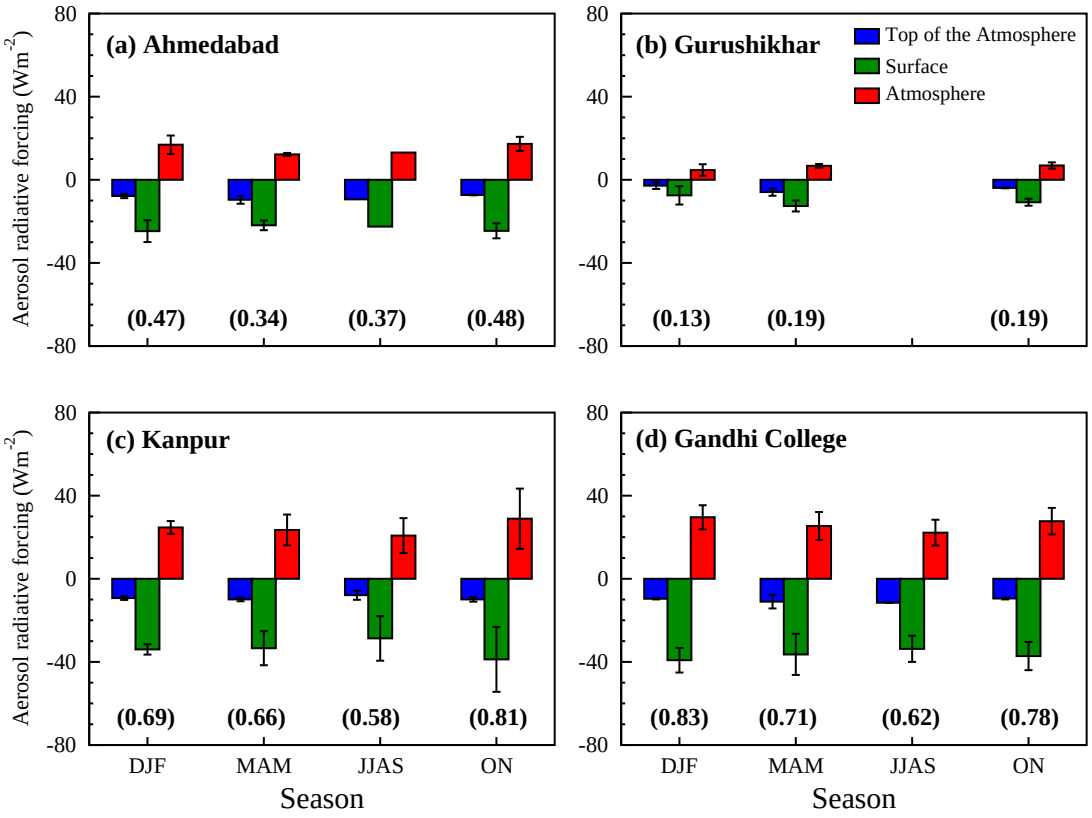

Figure 5.14: *Seasonal variation in aerosol radiative forcing using Method 2 in shortwave range (0.2-4.0 µm) over (a) Ahmedabad, (b)Gurushikhar, (c) Kanpur and (d) Gandhi College during 2006-2008. The vertical bars represent the variation from the mean for the season. The heating rates (Kelvin per day) are given in brackets.*

The atmospheric heating rate over all the locations are given in parenthesis for all the seasons. ARF is found to be highest over Kanpur and Gandhi College followed by Ahmedabad and Gurushikhar. The differences in the forcing is not very significant between Kanpur and Gandhi College; while the forcing is a factor of two less over Ahmedabad and a factor of four less over Gurushikhar consistent

with AOD differences (Figure 5.8). The TOA forcing over Ahmedabad is negative similar to other locations as seen in Figure 5.14 due to higher SSA as compared to those used in Method 1. The ATM forcing is found to be higher during post-monsoon (17.3 Wm^{-2}) and winter (16.9 Wm^{-2}) over Ahmedabad which is more than a factor of two lower than the values estimated using Method 1 (41.9 and 54.0 Wm^{-2} respectively). Heating rates over Ahmedabad during different seasons are in the range of 0.34-0.48 K/d which is at least 0.6 K/d less when compared to the values estimated using Method 1.

Heating rate has increased during winter and premonsoon; while the values decreased during monsoon and postmonsoon over all the locations when estimated using the present method. The reason could be lower values of SSA during monsoon and postmonsoon using GOCART (Figure 5.10). A large difference in the aerosol radiative forcing and the heating rate is observed when different SSA values are used. These results confirm that the forcing and heating rate is sensitive to aerosol single scattering albedo values. The comparison suggests that this issue needs to be re-examined in greater detail because of the spatiotemporal differences in the abundances of different aerosol species, and their optical and radiative properties.

5.5.2 Aerosol radiative forcing over oceanic regions

Aerosol optical depths, total aerosol mass and chemical composition

Measurement of AODs were conducted over the Bay of Bengal and the Arabian Sea during March-May 2006. A large spatial and temporal variability in the AODs were observed over the Bay of Bengal and the Arabian Sea (discussed in Chapter 4). The day to day variation in 0.5 μm AODs measured in situ is plotted in Figure 5.15a. OPAC model estimated aerosol optical depths are found to agree well with the measured AODs (Figure 5.15) following the methodology described in Section 5.4.2.

Bulk-aerosol samples were collected on board *Sagar Kanya* using PALLFLEX^{TM} tissuquartz filters (20×25 cm^2) by operating a high-volume sampler (HVS) over a

time period ranging from 15 to 22 hr [*Kumar et al.*, 2008] during ICARB. Subsequently, aerosol samples were analyzed in the laboratory for their physical and chemical characterization. The TSP mass concentrations were obtained gravimetrically by weighing the full filters before and after sampling. All samples were equilibrated at a relative humidity of 50±5% and at 22±1 °C for 5.6 hr prior to their weighing [*Kumar et al.*, 2008].

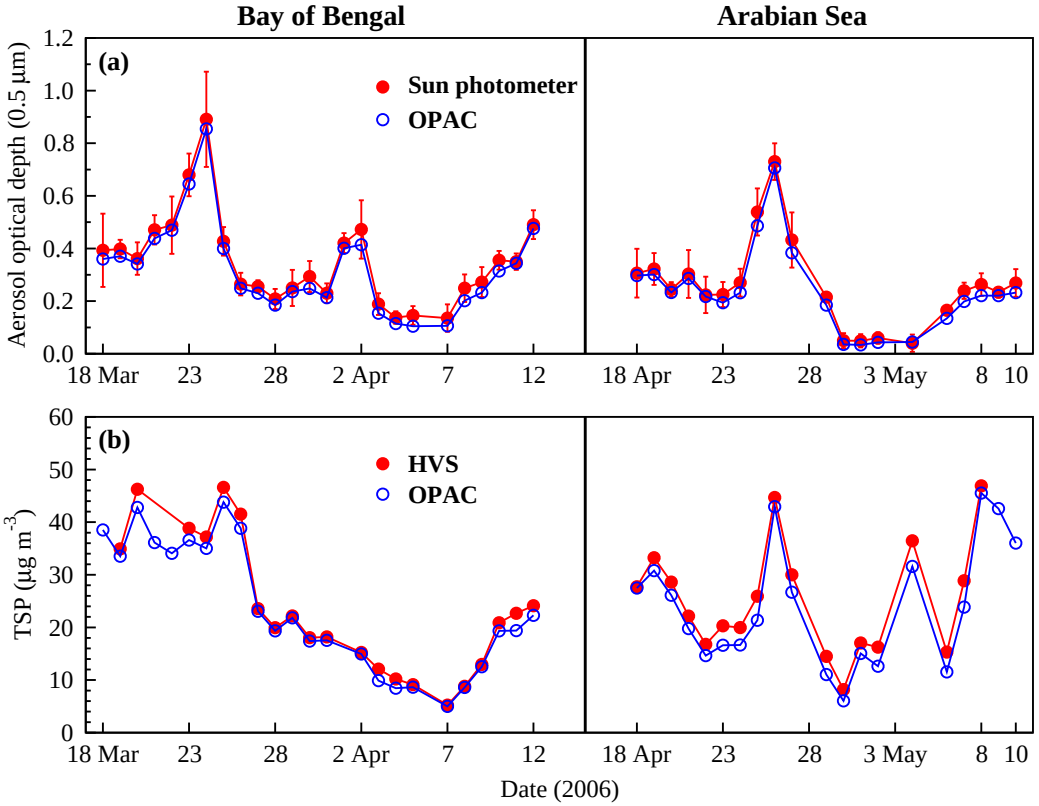

Figure 5.15: *(a) Daily mean AODs at 0.5 µm over the Bay of Bengal and the Arabian Sea. Vertical bars indicate ±1σ variation from the mean. OPAC model estimated aerosol optical depths are also shown. (b) Daily TSP mass measured using high volume sampler (HVS) in comparison with OPAC model estimated aerosol mass concentrations over the Bay of Bengal and the Arabian Sea during March-May 2006.*

Uncertainty in the measured TSP calculated by repeated measurements of filter weight is estimated to be about 15%. The chemical composition of aerosols was obtained by analyzing water soluble (NH_4^+, K^+, Mg^{2+}, Ca^{2+}, Cl^-, NO_3^-, SO_4^{2-}),

crustal element (Al, Fe, Ca) and carbonaceous aerosols [*Kumar et al.*, 2008]. Elemental carbon (EC) and organic carbon (OC) mass concentrations are determined using EC-OC analyzer [*Kumar et al.*, 2008]. The measured concentration of mineral dust was estimated using Al as proxy, based on the assumption that the ratio of Al in minerals to be the same as in the upper continental crust with Al content of 8.04% [*Kumar et al.*, 2008].

Aerosol mass concentration obtained from HVS during the cruise period corresponds to 50±5% RH, while the OPAC estimated mass concentrations are available for different RH values ranging from 0% to 99%. In the present study, a comparison is made between the total mass and species concentrations obtained from OPAC at 50% RH with values obtained from HVS at a mean RH of 50%. The total mass concentrations estimated from OPAC and measured using HVS are found to agree very well (Figure 5.15b). The total suspended particulate mass is found to be in the range of 5-47 μg m^{-3} over the Bay of Bengal and the Arabian Sea, and exhibit spatiotemporal variability similar to AODs (Figure 5.15). OPAC estimated mass concentrations are slightly lower than the HVS mass concentrations. OPAC mass concentrations are lower because in OPAC aerosol particles up to 7.5 μm radius only are considered for calculation of total mass [*Hess et al.*, 1998], whereas, in HVS the upper cutoff radius is about 10 μm [*Ramachandran et al.*, 2006; *Kedia et al.*, 2010]. TSP from HVS and the mass concentrations of different aerosol species are found to compare very well with the OPAC estimates of the same (Figures 5.15b).

In a similar manner, the mass concentrations of water soluble species, sea salt, black carbon and mineral dust from OPAC and HVS over the Bay of Bengal and the Arabian Sea are found to show a good agreement (Figure 5.16). The trends in the variation of water soluble, black carbon and mineral dust are similar to that of TSP over the Bay of Bengal. Sea salt concentrations over the Bay of Bengal did not show much day to day variability and the concentrations are only 2-3 μg m^{-3}. Black carbon mass concentrations are also low (<0.5 μg m^{-3}) over the Bay

of Bengal. Over the Bay of Bengal, water soluble constituents (44%) and mineral dust (48%) while sea salt and black carbon contributed 6 and 2%, respectively, to TSP

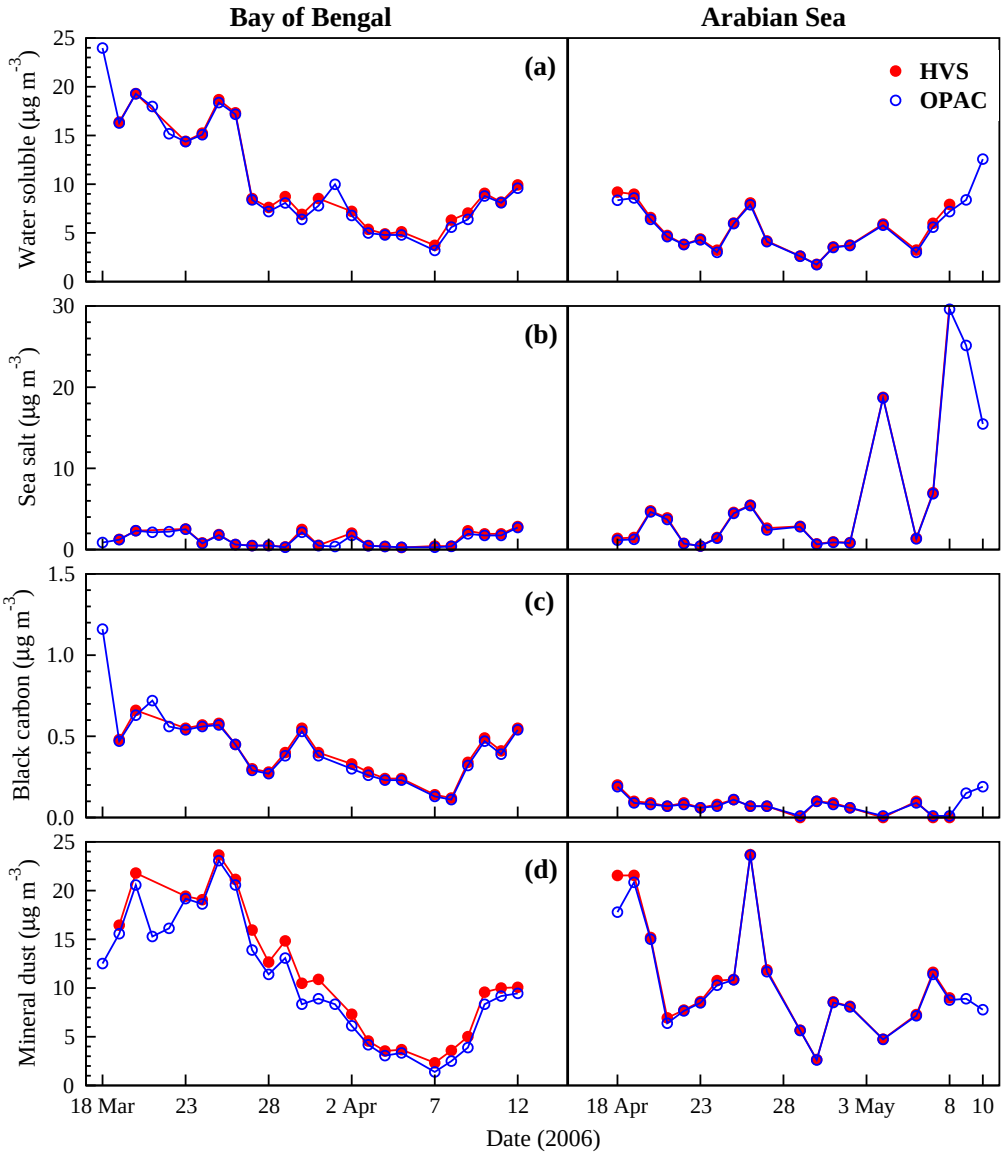

Figure 5.16: *Comparison of (a) water soluble, (b) sea salt, (c) black carbon and (d) mineral dust mass concentrations estimated from OPAC and measured using HVS over the Bay of Bengal and Arabian Sea.*

The variation in the mass fractions of aerosol species over the Arabian Sea during different days exhibit a distinctly different behavior relative to the Bay of Bengal. The water soluble aerosol mass concentration shows similar variation as

that of TSP with a mean value of about 5 μg m^{-3}; while sea salt is found to show a large variability ranging from 5 to 30 μg m^{-3}. BC contribution is nearly insignificant over the Arabian Sea and is lower than that over the Bay of Bengal. Over the Arabian Sea, sea salt contributes about 22% to TSP, whereas, water soluble aerosols and mineral dust contribute 30 and 47%, respectively, and black carbon accounts for 1% of TSP [*Kumar et al.*, 2008; *Kedia et al.*, 2010].

Single scattering albedo and asymmetry parameter

Figure 5.17a presents the day to day variation in SSA at 0.5 μm estimated using OPAC over the Bay of Bengal and the Arabian Sea. OPAC estimated single scattering albedo at 0.5 μm is found to be in the 0.91-0.95 range over the Bay of Bengal region with a mean of 0.93$\pm$0.01 (Figure 5.17a). The highest value of SSA (0.95) is observed on 26 March and the lowest value (0.91) is observed on 30 March. SSA $>$ 0.9 suggests the dominance of scattering aerosols over the Bay of Bengal during March-April 2006. The occurrence of higher SSA is further corroborated by a low (2%) contribution of black carbon to TSP mass. *Nair et al.* [2008] estimated SSA from the scattering and absorption coefficients measured on board using Nephelometer and Aethalometer, respectively. SSA was found to vary from 0.96 to 0.84 over the Bay of Bengal [*Nair et al.*, 2008].

Though the mean SSA values agree well between the present study and *Nair et al.* results, there exist day to day differences. The day to day differences could arise due to the following major reasons: (1) methodology (results in the present study are obtained from the hybrid approach of combining all the chemical composition data and OPAC, while *Nair et al.* [2008] used scattering and absorption coefficients measured by Nephelometer and Aethalometer, respectively), (2) the present approach includes all the absorbing species (black carbon, mineral dust, and organics) while absorption coefficients reported by *Nair et al.* [2008] pertain only to black carbon, (3) sampling (one aerosol sample of 15-22 h in a day is obtained in the present case, while *Nair et al.* [2008] results are obtained from

several data points in a day as the measurements are continuous), and finally, (4) uncertainties (the chemical composition which is used in the determination of SSA can be uncertain by about 15% while the uncertainty in SSA derived by *Nair et al.* [2008] can range from 10 to 40% depending on the absolute value of scattering and absorption coefficients). Also, in a small measure the differences in SSA could have occurred due to different wavelengths used as SSA in the current study is at 0.5 μm while *Nair et al.* [2008] results correspond to 0.55 μm.

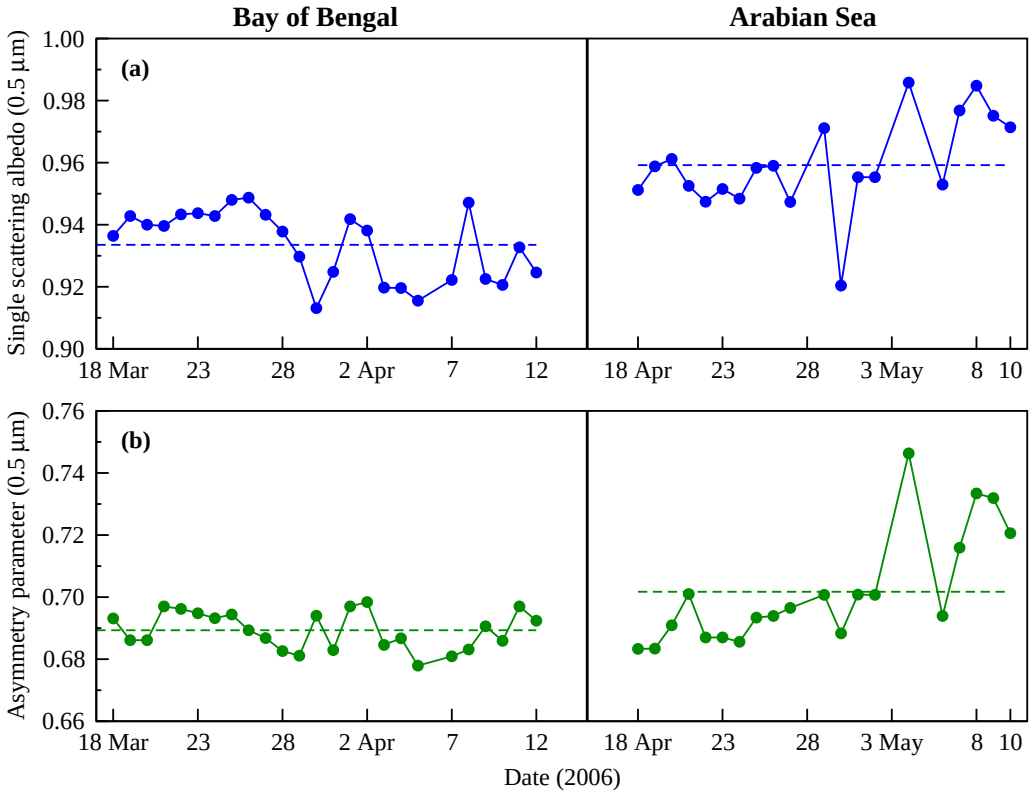

Figure 5.17: *Day to day variation of (a) single scattering albedo (SSA) and (b) asymmetry parameter (g) at 0.5 µm estimated using OPAC over the Bay of Bengal and Arabian Sea during ICARB. The regional averages of SSA and g for the Bay of Bengal and the Arabian Sea are shown as dotted lines.*

The mean SSA over the Arabian Sea is found to be 0.96 which is higher than the Bay of Bengal SSA (0.93). The maximum value of SSA is found to be 0.98 on 4 May when the ship was in the northern Arabian Sea (Figure 5.17a). SSA

value over the Arabian Sea is higher than the Bay of Bengal owing to a lower carbonaceous aerosol mass concentration (Figure 5.16) [*Kedia et al.*, 2010]. SSA values from previous studies conducted prior to ICARB over the Bay of Bengal and the Arabian Sea regions were found to be lower. It should be noted that all the previous studies were conducted over the Bay of Bengal during northeast winter monsoon (December-March) in contrast to the ICARB cruise which was conducted during premonsoon (March-April).

During winter monsoon, the estimated SSAs are lower because of the dominance of absorbing aerosols emanating from fossil fuel and biomass burning mainly from the south Asian region which then get transported across the Bay of Bengal and the Arabian Sea [*Ramachandran*, 2005a, 2005b]. Higher SSA values during the premonsoon season over the Bay of Bengal and the Arabian Sea confirm the dominance of scattering aerosols in the size distribution.

The day to day variation in asymmetry parameter at 0.5 μm over the Bay of Bengal and the Arabian Sea obtained from OPAC model is plotted in Figure 5.17b. The average value of asymmetry parameter is found to be 0.69 $\pm$ 0.01 and 0.70 $\pm$ 0.01 over the Bay of Bengal and the Arabian Sea, respectively. Smaller asymmetry parameters indicate that the aerosol size distribution is dominated by submicron size aerosol particles. Mean SSA at 0.5 μm over the Bay of Bengal and the Arabian Sea are found to be 0.93 $\pm$ 0.01 and 0.96 $\pm$ 0.01, respectively. SSA over the Bay of Bengal is found to be lower than maritime aerosol models (0.97-1.00) indicating the presence of more number of absorbing aerosols than the maritime polluted model. The g is also lower than the maritime models (0.75-0.77) over the Bay of Bengal further supporting the presence of aerosols from long range transport (Figure 4.4). SSA over the Arabian Sea is higher than the Bay of Bengal but still lower than the maritime polluted model. SSA over the Arabian Sea on most of the days are in the range of 0.94-0.96 unlike the SSA over the Bay of Bengal (Figure 5.17). The g over the Arabian Sea is slightly higher than the Bay of Bengal. The differences between the aerosol properties obtained over the Bay of Bengal and the Arabian

Sea, and maritime aerosol models corroborate the long range transport of other types of aerosols in addition to local sources which modified the aerosol optical properties.

Figure 5.18 presents the spectral dependence of aerosol optical depth, SSA and g estimated using OPAC in the wavelength region of 0.25-4.0 μm for selected days with high and low AODs over the Bay of Bengal (Figures 5.18a-c) and the Arabian Sea (Figures 5.178d-f). The measured AOD spectra using sun photometer are also shown along with $\pm 1\sigma$ variation from the mean.

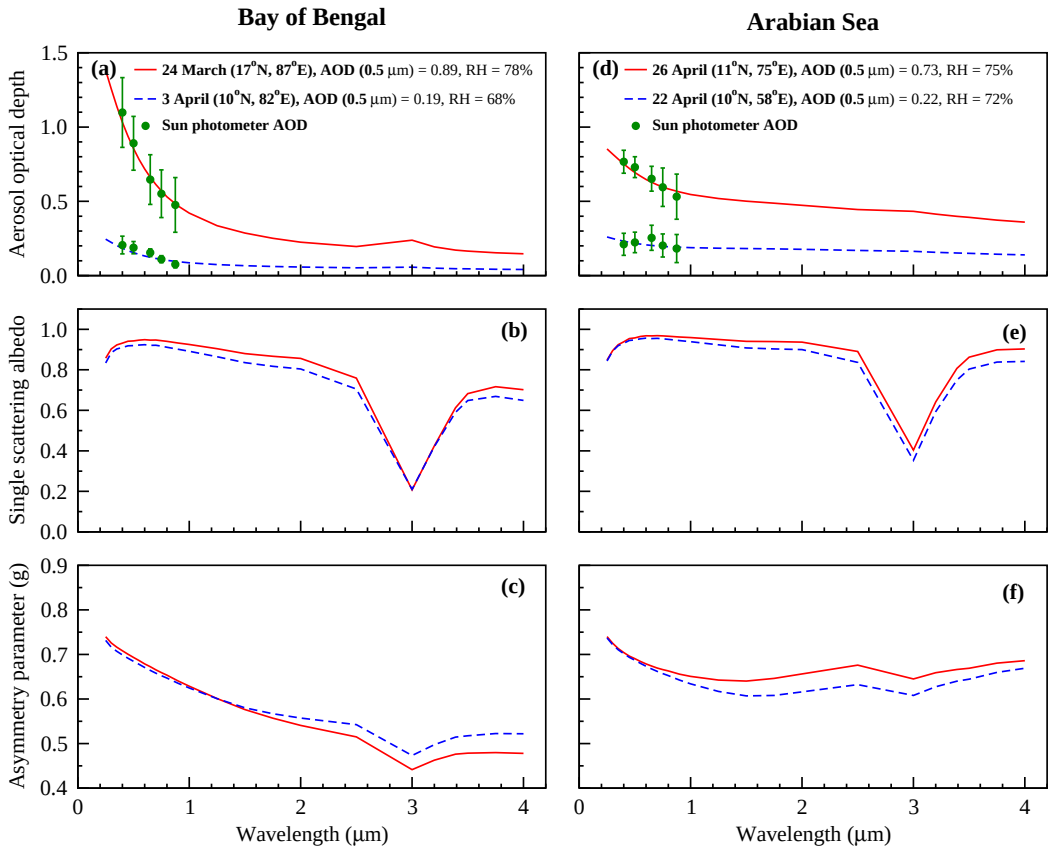

Figure 5.18: *Spectral dependence of (a, d) AOD, (b, e) SSA albedo and (c, f) asymmetry parameter (g) in the 0.25-4.0 µm wavelength range over the Bay of Bengal and the Arabian Sea estimated using OPAC for two selected days of high and low AODs measured over the two oceanic regions. Spectral AODs measured on board using sun photometer are shown as closed circles (a and d). Vertical bars in the measured AODs denote $\pm 1\sigma$ variation from the mean.*

Figure 5.18a shows the AOD spectra for 24 March and 3 April when the mean 0.5 μm AODs were 0.89 and 0.19, respectively. Figure 5.18d shows the AOD spectra obtained over the Arabian Sea on 26 and 22 April when the AODs at 0.5 μm were 0.73 and 0.22, respectively. Spectral dependence is found to be more steeper for the days with higher AODs when compared to the days with lower AODs. This is found to be true for all the days when the AODs are higher over both the oceanic regions. No significant variation in SSA and asymmetry parameter is seen for the days with lower and higher AODs, indicating that the size and the chemical composition are more or less similar during the low and high AOD conditions, and the higher AODs would have resulted due to an increase in the number density. Both SSA and g are found to decrease as wavelength increases.

The enhancement in AOD around 3 μm, and dips in SSA and g (Figures 5.1) are attributed to an increase in the absorption characteristics of water soluble, dust and sea salt aerosols [*d'Almeida et al.*, 1991; *Lacis and Mishchenko*, 1995], while the optical characteristics of carbonaceous aerosols exhibit a gradual decrease with respect to wavelength. All the maritime aerosol models are seen to exhibit similar features [*d'Almeida et al.*, 1991].

Sensitivity analysis

In the present study, sensitivity tests have been conducted to examine (1) the effect of presence of curvatures in AOD spectra (Chapter 3, Chapter 4) on aerosol radiative forcing and heating rate and (2) whether structures in aerosol vertical profiles alter the net atmospheric forcing and heating rate deduced from the top of the atmosphere and surface aerosol radiative forcing and the results are discussed.

(1) Effect of curvature in AOD spectra on radiative forcing

As already discussed in Chapter 3 and Chapter 4, aerosol size distribution is multimodal in the ambient atmosphere. Therefore, the wavelength dependence of AOD does not follow Ångström power law and shows departure from the linear behavior of ln AOD versus ln λ [e.g., *Eck et al.*, 2001] data. A second order

polynomial fit is used under such condition to examine the curvature in the AOD spectra. The coefficient of polynomial fit (α_2) (equation 2.7) contains crucial information about the size distribution, and is the measure of curvature observed in the spectral distribution of AODs.

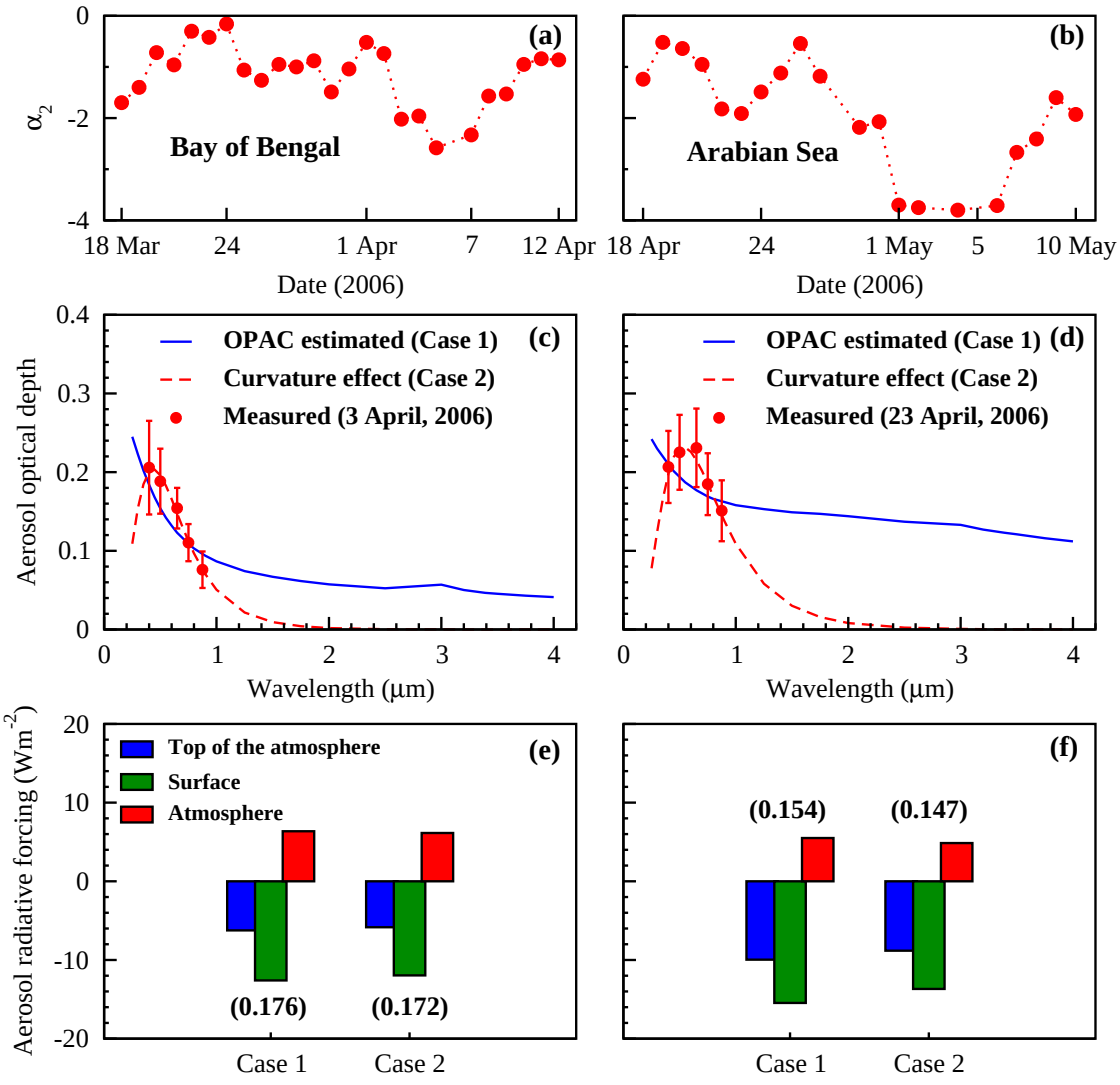

Figure 5.19: *Daily variation in α_2 over the (a) Bay of Bengal and (b) Arabian Sea. Measured AOD spectra in comparison with OPAC estimated AOD spectra over the (c) Bay of Bengal and (d) Arabian Sea. Vertical bars indicate $\pm 1\sigma$ deviation from the mean. AOD spectra determined including curvature effects are also shown. Aerosol radiative forcing determined over the (e) Bay of Bengal and (f) Arabian Sea for both cases: case 1 (OPAC estimated) and case 2 (curvature effect). Atmospheric heating rates (K/d) for both cases are given in brackets.*

Daily mean AOD spectra measured over the Bay of Bengal and the Arabian Sea have been analyzed for curvature effects (Figures 5.19a and 5.19b). The α_2 is found to be <0 for all days over the Bay of Bengal and the Arabian Sea suggesting the dominance of fine mode aerosols, which is in agreement with higher fine mode fraction (>0.60) values obtained [*Kedia and Ramachandran*, 2008] over these oceans. Measured AOD spectra in the 0.4-0.875 μm wavelength range are compared with model (OPAC) estimated AOD spectra and AOD spectra obtained in the 0.25-4.0 μm wavelength region using α_2 values in Figure 5.19 for the Bay of Bengal (3 April) and the Arabian Sea (23 April). α_2 values are found to be -2.02 and -1.91 for 3 and 23 April, respectively.

To ascertain the impact of curvatures in AOD spectra on aerosol radiative forcing and heating rate, AODs in the 0.25-4.0 μm range estimated by combining the measurements and model (OPAC) are replaced with AOD spectra obtained using α_2 (curvature effect) while performing radiative forcing calculations (Figure 5.19). AOD spectra from all the three cases (measured, OPAC estimated and curvature) are found to agree in the 0.4-0.9 μm wavelength range. OPAC estimated AODs are higher at wavelengths less than 0.4 μm, while AODs derived using curvature effect are lower (Figures 5.19c and 5.19d). Model estimated AODs beyond 1 μm are found to decrease following Mie theory and wavelength exponent α, while AODs determined using α_2 show a steep decline beyond 1 μm.

ARFs at TOA, SFC and ATM using aerosol properties from both the cases, namely, model estimated (Case 1) and curvature (Case 2), do not show significant differences (Figures 5.19e and 5.19f). The solar heating rate is found to differ by less than 0.1 K/d, though the heating rates estimated using curvature effect are lower. Major portion ($\sim$72%) of the solar irradiance reaching the Earth's atmosphere lies in the 0.2-1.0 μm wavelength range [*Seinfeld and Pandis*, 1998]. Although the AODs are lower beyond 1 μm due to curvature in AOD spectra, as ARF and heating rate depend on both the AODs and the amount of solar radiation (72% of which lies in the 0.2-1.0 μm wavelength range), they do not differ significantly

when the shape of the AOD spectra varies. Thus, though the curvature effect can modify the shape of the aerosol distribution and can affect the aerosol optical properties depending on the dominance of either fine or coarse mode aerosols or a mixture of both, the sensitivity study reveals that the curvature effect does not significantly influence the radiative effects of aerosols [*Kedia et al.*, 2010].

(2) Influence of aerosol vertical profiles on radiative forcing

Aircraft measurements made during ICARB near the coast and mainland India indicated the presence of elevated aerosol layers [*Moorthy et al.*, 2008; *Satheesh et al.*, 2009]. The aerosol extinction coefficients were found to decrease with an 1/e scaling distance of ∼500 km within the marine boundary layer suggesting the rapidly decreasing impact of continental influence; above the marine boundary layer scaling distances were larger and the gradients were shallower [*Satheesh et al.*, 2009].

Clear sky shortwave aerosol radiative forcing and solar heating rates estimated including aerosol vertical profiles on 25 March, 3 and 23 April are compared with results obtained without including vertical profiles in Figure 5.20. ARF at the surface is about a factor of 2 higher (-25 Wm^{-2}) on 25 March when compared to those obtained on 3 and 23 April similar to the variation in AODs. These results suggest that the AODs and radiative forcing are nearly linearly related. ARF is found to be higher from above the surface to up to ∼4 km when compared to the forcing obtained without including vertical profile (Figures 5.20); above this altitude the aerosol radiative forcing obtained including the aerosol vertical profile is lower. The near surface heating rate is about 0.3 K/d on 25 March and decreases to about 0.2 K/d on 3 and 23 April. In the absence of measured vertical profiles the aerosol extinction is distributed on the basis of scale height which is 1 km for the maritime aerosols [*Hess et al.*, 1998]. Heating rate profiles in both the cases (with and without measured vertical profiles) are found to follow the aerosol extinction profiles (Figures 5.20d, 5.20f). When aerosols are distributed as

a function of scale height the heating rate profile is more smoother, whereas, the heating rates obtained by including aerosol vertical profiles are found to exhibit structures consistent with aerosol extinction at different altitudes.

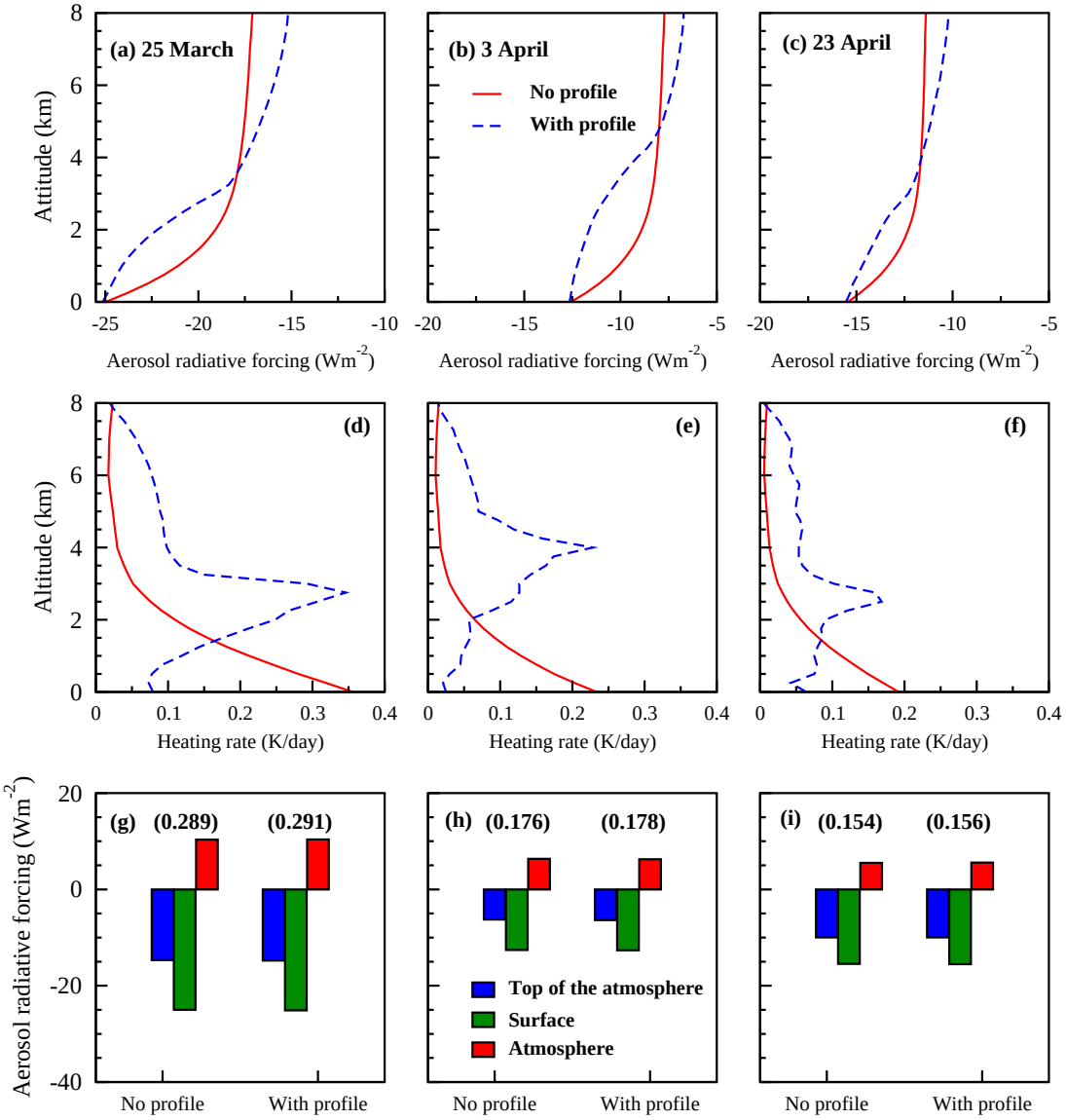

Figure 5.20: *Aerosol radiative forcing as function of altitude on (a) 25 March 2006, (b) 3 April 2006 and (c) 23 April 2006 obtained with and without aerosol vertical profiles. Heating rate (K/d) profiles obtained with and without aerosol vertical profiles in the 0 to 8 km altitude region on (d) 25 March, (e) 3 April and (f) 23 April. Comparison of aerosol radiative forcing at the top of the atmosphere, the surface and in the atmosphere estimated with and without aerosol vertical profiles on (g) 25 March, (h) 3 April and (i) 23 April 2006. Atmospheric heating rates (K/d) for both scenarios on each day are given in brackets.*

Heating rate is found to be higher where aerosol layers exist, and exhibit spatial and altitudinal differences. Heating rate at the aerosol layer peak is found to be >0.3 K/d at 3 km on 25 March, 0.2 K/d on 3 April at 4 km while on 23 April the heating rate is <0.15 K/d peaking below 3 km. However, aerosol radiative forcings at TOA, SFC, ATM, and the heating rates obtained with and without aerosol vertical profiles are found to show negligible differences (Figures 5.20g, 5.20i).

This confirms that the net energy content trapped in the atmosphere remains almost the same with and without vertical profiles, but only its vertical distribution varies [*Kedia et al.*, 2010; *Ramachandran and Kedia*, 2010]. Nevertheless, as simultaneous aerosol vertical profile measurements are not available during the cruise, and as the motivation of the present study is to document the day to day variation in net aerosol radiative forcing between the surface and the top of the atmosphere, aerosol radiative forcing at TOA, SFC and ATM are determined and discussed using the simultaneously measured optical, physical and chemical characteristics of aerosols over the Bay of Bengal and the Arabian Sea.

Daily mean aerosol radiative forcing during ICARB

The daily mean clear sky shortwave aerosol radiative forcings at the top of the atmosphere (TOA), surface (SFC) and atmosphere (ATM) are shown over the Bay of Bengal and the Arabian Sea (Figure 5.21). Aerosol radiative forcings are found to exhibit nearly linearly day to day variability to AODs over the Bay of Bengal and the Arabian Sea. For example, AODs were maximum on 24 March 2006 over the Bay of Bengal region. On 24 March the cruise was in the middle region of the Bay of Bengal. The higher AODs were attributed to the transport of pollutants from the continent [*Kedia and Ramachandran*, 2008]. TOA forcing on 24 March is found to be the highest at -28 Wm^{-2}; SFC forcing is about -52 Wm^{-2} resulting in an atmospheric warming of 24 Wm^{-2}.

As SSA values are higher than 0.90 over the Bay of Bengal, both the top of the atmosphere and surface forcings increase (more negative), thus, resulting in

lesser magnitude of atmospheric warming. In contrast, strongly absorbing aerosols can absorb the radiation reflected upward from the lower layers of the atmosphere and the ocean surface, make the TOA forcing less negative or even positive [e.g., *Podgorny and Ramanathan*, 2001; *Ramachandran*, 2005a, 2005b], increase the SFC forcing, thereby leading to a higher (more positive) atmospheric warming.

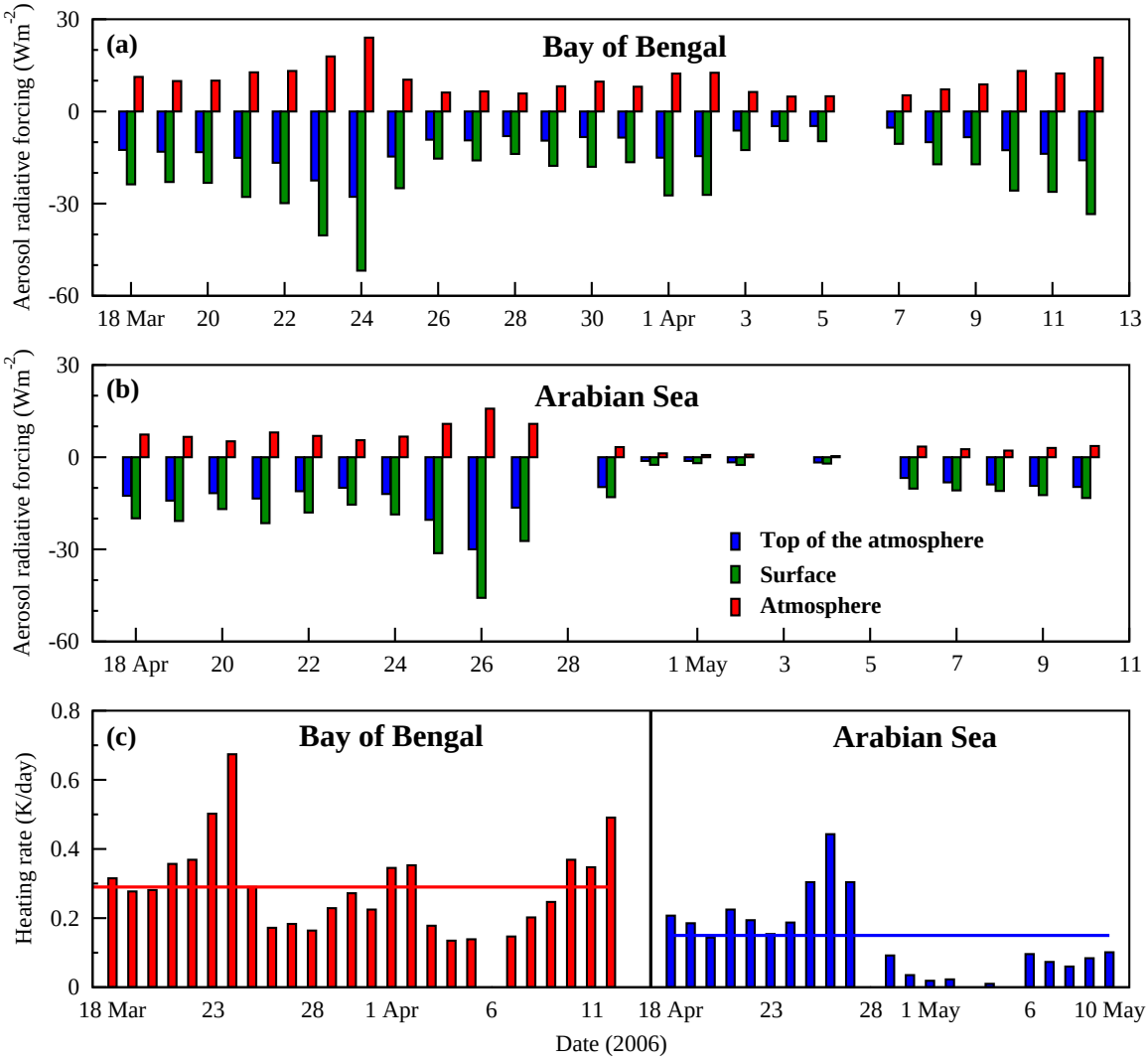

Figure 5.21: *Daily clear sky shortwave aerosol radiative forcing (0.25-4.0 µm wavelength region) at the top of the atmosphere, surface and in the atmosphere over the (a) Bay of Bengal and (b) Arabian Sea during ICARB. (c) Daily solar heating rate (K/d) over the Bay of Bengal and Arabian Sea. The average heating rates in each oceanic region are shown as horizontal lines.*

In the present study, the average aerosol radiative forcing over the Bay of Bengal at the TOA and at the surface are found to be -12.0 ± 5.4 and -22.4 ± 9.8 Wm^{-2}, respectively. The average atmospheric warming is 10.4 ± 4.6 Wm^{-2} over the Bay of Bengal during March-April 2006. Over the Arabian sea the forcing is found to be the highest (-30.0 and -45.8 Wm^{-2} at the TOA and SFC, respectively) on 26 April when the AODs were the highest over the Arabian Sea.

The forcing decreased very sharply as the ship moved into the central part and the minimum value of forcing (-1.2 and -2.0 Wm^{-2} at TOA and SFC, respectively) is observed on 1 May in the central Arabian Sea when the AODs were low. The average radiative forcings over the entire Arabian Sea are found to be -10.5 ± 6.8, -15.8 ± 10.7, and 5.3 ± 3.9 Wm^{-2} at the TOA, SFC and ATM, respectively. The aerosol radiative forcings at all the three altitude levels over the Arabian Sea are found to be lower than that of the Bay of Bengal. The lower radiative forcing is expected because of lower AODs and higher SSAs over the Arabian Sea when compared to the Bay of Bengal.

Atmospheric heating rate

Daily heating rates over the Bay of Bengal and the Arabian Sea during the pre-monsoon season of 2006 are plotted in Figure 5.21c. The heating rate is >0.1 K/d over the Bay of Bengal, while over the Arabian Sea heating rate is lower than 0.1 K/d on a few days concurrent with lower aerosol content (Figure 5.15). Heating rate is maximum (0.67 K/d) on 24 March over the Bay of Bengal when AODs are also the highest, while heating rate is the lowest at 0.14 K/d on 4 April 2006 (Figure 5.21c). The highest heating rate of 0.44 K/d over the Arabian Sea occurred on 26 April. The mean solar heating rate over the Bay of Bengal during ICARB is 0.3 K/d, which is twice larger when compared to that over the Arabian Sea (shown as horizontal lines in Figure 5.21c) [*Kedia et al.*, 2010].

5.5.3 Comparison of aerosol radiative forcing with earlier results

AOD, SSA, aerosol radiative forcing at the SFC, TOA and ATM, and heating rate from the present study are compared with results obtained from earlier studies over different continental locations in India and adjoining marine environments (Table 5.3). Large spatial and temporal differences are observed in the aerosol properties over different locations (Table 5.3). *Ganguly et al.* [2006b] estimated the ARF during 2002-2005 using the measured aerosol properties in radiative transfer model. The results show that the ATM forcing was higher during winter and postmonsoon; while the values were lower during premonsoon and monsoon for 2002-2005 (Table 5.3). ARF and heating rate, and the seasonal variability reported in *Ganguly et al.* [2006b] and in the present study following Method 1 are comparable, however, the differences become larger when compared to the results obtained using Method 2. The TOA forcing was in the range of +8 to -26 Wm^{-2} during 2002-2005; while in the present study the value ranges from +5.7 to -9.6 Wm^{-2} (Table 5.3). The atmospheric heating rate during 2002-2005 were found to be in the range on 0.79-1.57 K/d while the values are in the range of 0.34-1.51 K/d over Ahmedabad in the present study. The forcing and heating rate calculated using Method 2 over Ahmedabad are more than a factor of two lower than the values obtained in Method 1 and also during 2002-2005 [*Ganguly et al.*, 2006b].

Over Kanpur, ARF from present study is found to be similar within $\pm 1\sigma$ variation at the surface using Method 1 and Method 2. The TOA forcing during 2001-2005 was less negative than the present case indicating higher concentration of absorbing aerosols during 2001-2005 [*Dey and Tripathi*, 2008]; while the surface forcing is found to be same within $\pm 1\sigma$ variation during 2001-2005 and the present case (Table 5.3). The TOA forcing is found to be positive in the range of 0.7 to 8.4 Wm^{-2} over Visakhapatnam and 2.7 to 11.7 Wm^{-2} over Delhi during all the seasons indicating higher concentration of absorbing aerosols throughout the year.

Table 5.3: Mean AOD and SSA at 0.5 μm, aerosol radiative forcing (Wm^{-2}) at the top of the atmosphere (TOA), the surface (SFC) and in the atmosphere (ATM) along with the heating rate (K/d) over different environments during the present study in comparison with earlier results.

Location	**Study period**		**AOD**	**SSA**	**Aerosol radiative forcing (Wm^{-2})**			**Heating rate**	**Source**
	Month	Year	0.5 μm	0.55 μm	TOA	SFC	ATM	(K/d)	
Ahmedabad	Dec-Feb	2006-2008	0.40±0.17	0.67±0.03	0.8±0.5	-41.1±6.7	41.9±6.8	1.17	*Present study (Method 1)*
	Mar-May		0.36±0.11	0.69±0.06	4.4 ±1.8	-44.7±5.0	49.1±6.3	1.38	
	Jun-Sep		0.43±0.07	0.79±0.04	-0.7±1.0	-34.3±2.0	33.6±2.0	0.94	
	Oct-Nov		0.38±0.14	0.64±0.05	5.7 ±2.3	-48.3±8.3	54.0±10.6	1.51	
Ahmedabad	Dec-Feb	2006-2008	0.40±0.17	0.90±0.02	-7.8±1.0	-24.7±5.2	16.9±4.4	0.47	*Present study (Method 2)*
	Mar-May		0.36±0.11	0.95±0.01	-9.6±1.9	-21.9±2.4	12.3±0.7	0.34	
	Jun-Sep		0.43±0.07	0.96±0.01	-9.4±0.0	-22.5±0.0	13.1±0.0	0.37	
	Oct-Nov		0.38±0.14	0.90±0.02	-7.3±0.2	-24.6±3.6	17.3±3.4	0.48	
Ahmedabad	Nov-Feb	2002-2005	0.31	0.73	14±4	-41±11	56±15	1.57	*Ganguly et al., (2006a;2006b)*
	Mar-Apr		0.41	0.84	-22±3	-63±10	40±11	1.12	
	May-Sep		0.43	0.81	-26±3	-54±6	28±9	0.79	
	Oct-Nov		0.42	0.73	8±2	-41±5	48±7	1.35	
Gurushikhar	Dec-Feb	2006-2008	0.07±0.04	0.91±0.01	-3.0±1.7	-7.3±4.1	4.3±2.3	0.12	*Present study (Method 1)*
	Mar-May		0.17±0.06	0.93±0.03	-5.0±2.5	-14.0±1.3	8.9±1.3	0.25	
	Jun-Sep		-	-	-	-	-	-	
	Oct-Nov		0.17±0.13	0.93±0.01	-4.5±0.7	-9.9±0.8	5.5±0.1	0.15	
Gurushikhar	Dec-Feb	2006-2008	0.07±0.04	0.90±0.02	-2.8±1.6	-7.5±4.4	4.7±2.8	0.13	*Present study (Method 2)*
	Mar-May		0.17±0.06	0.96±0.01	-5.9±1.8	-12.6±2.6	6.7±0.9	0.19	
	Jun-Sep		-	-	-	-	-	-	
	Oct-Nov		0.17±0.13	0.90±0.02	-3.9±0.2	-10.8±1.7	6.9±1.5	0.19	

Continued

Kanpur	Dec-Feb	2006-2008	0.57±0.29	0.89±0.02	-10.0±1.3	-33.6±2.0	23.6±3.1	0.66	*Present study (Method 1)*
	Mar-May		0.57±0.24	0.88±0.03	-4.7±2.4	-40.9±7.1	36.2±6.6	1.02	
	Jun-Sep		0.53±0.20	0.89±0.07	-6.2±0.5	-31.0±11.3	24.9±10.8	0.70	
	Oct-Nov		0.63±0.31	0.90±0.02	-11.9±3.4	-36.5±13.4	24.7±9.9	0.69	
Kanpur	Dec-Feb	2006-2008	0.57±0.29	0.89±0.02	-9.3±0.9	-34.0±2.5	24.7±3.1	0.69	*Present study (Method 2)*
	Mar-May		0.57±0.24	0.94±0.01	-9.9±0.9	-33.4±8.2	23.5±7.4	0.66	
	Jun-Sep		0.53±0.20	0.94±0.01	-7.9±2.2	-28.7±10.7	20.8±8.4	0.58	
	Oct-Nov		0.63±0.31	0.89±0.02	-9.9±1.1	-38.8±15.6	28.9±14.5	0.81	
Kanpur	Dec-Feb	2001-2005		0.91	-4.8	-34.3	29.5	0.83	*Dey and Tripathi, 2008*
	Mar-May			0.90	-8.3	-34.4	26.1	0.73	
	Jun-Sep			0.89	-0.8	-26.6	25.8	0.72	
	Oct-Nov			0.90	-5.5	-37.0	31.5	0.88	
Gandhi College	Dec-Feb	2006-2008	0.87±0.34	0.88±0.02	-11.7±1.5	-35.8± 4.2	24.1±2.9	0.68	*Present study (Method 1)*
	Mar-May		0.67±0.26	0.89±0.02	-7.6±1.8	-41.7± 12.4	34.2±11.0	0.96	
	Jun-Sep		0.55±0.30	0.91±0.03	-8.6±2.4	-32.6± 9.1	24.0±6.6	0.67	
	Oct-Nov		0.69±0.26	0.88±0.03	-10.8±0.6	-35.1± 6.3	24.3±5.6	0.68	
Gandhi College	Dec-Feb	2006-2008	0.87±0.34	0.89±0.02	-9.6±0.3	-39.2±5.9	29.6±5.8	0.83	*Present study (Method 2)*
	Mar-May		0.67±0.26	0.93±0.01	-11.0±3.3	-36.4±9.9	25.4±6.7	0.71	
	Jun-Sep		0.55±0.30	0.94±0.01	-11.5±0.1	-33.7±6.3	22.2±6.2	0.62	
	Oct-Nov		0.69±0.26	0.89±0.02	-9.5±0.4	-37.2±6.8	27.7±6.4	0.78	
Dibrugarh	Dec-Feb	2008-2009	0.36		-1.0±0.5	-34.2±5.1	33.2±4.7	0.93	*Pathak et al., 2010*
	Mar-May		0.49		-1.4±2.9	-37.1±8.7	35.7±6.4	1.00	
	Jun-Sep		0.41		-1.5±0.1	-33.7±3.2	32.2±3.2	0.90	
	Oct-Nov		0.15		0.1±0.5	-12.5±4.7	12.6±5.2	0.35	

Continued

Trivandrum	Dec-Mar	2000-2003	0.43	0.70 to 0.74	4.1 to 1.8	-48.9 to -44.8	52.9 to 46.6	1.51 to 1.33	*Babu et al., 2008*
	Apr-May		0.40	0.78 to 0.81	0.3 to -1.4	-37.4 to -34.2	37.6 to 32.8	1.08 to 0.93	
	Jun-Sep		0.29	0.81 to 0.84	-1.4 to -2.6	-26.9 to -24.4	25.5 to 21.8	0.73 to 0.62	
	Oct-Nov		0.38	0.82 to 0.85	-1.5 to -2.8	-30.2 to -27.8	28.7 to 25.0	0.82 to 0.71	
Visakhapatnam	Nov-Feb	2005-2006			8.4	-35.78	44.18	1.24	*Sreekanth et al., 2007*
	Mar-May				3.99	-16.8	20.78	0.58	
	Jun-Aug				2.36	-9.9	12.26	0.34	
	Sep-Oct				0.7	-2.81	3.51	0.10	
Delhi	Dec-Feb	2001-2005			5.0	-64.0	69.0	1.94	*Singh et al., 2010*
	Mar-May				2.7	-82.1	84.8	2.38	
	Jun-Sep				11.7	-62.2	74.0	2.08	
	Oct-Nov				5.1	-66.3	71.4	2.00	
Bay of Bengal	Mar-Apr	2006	0.36	0.93	-12.0±5.4	-22.4±9.8	10.4±4.6	0.81	*Kedia et al., 2010*
	Feb	2003	0.43	0.90	-11.6	-29.6	16.01	1.17	*Ganguly et al., 2005b*
	Feb	2003	0.44	0.85	-6.3	-34.2	27.9	2.05	*Vinoj et at., 2004*
	Mar	2001			-6.9	-39.1	32.2		*Vinoj et at., 2004*
	Feb	2001	0.39	0.86	-9	-31	22	1.55	*Ramachandran, 2005a*
Arabian Sea	Apr-May	2006	0.25	0.96	-10.5±6.8	-15.8±10.7	5.3± 3.9	0.59	*Kedia et al., 2010*
	Dec-Apr	1996-2000	0.29	0.93	-9	-22	13	1.23	*Ramachandran, 2005b*
	Mar	2001	0.35	0.90	-7.6	-24.5	16.9	1.35	*Vinoj et at., 2004*
	Mar-Apr	2003	0.44	0.92	-12	-27	15	0.96	*Moorthy et al., 2005*
	Mar-Jun	2003	0.29 to 0.56	0.91 to 0.96	-24.5 to 34.8	-62.1 to 52.1	20.2 to 37.5	0.17 to 0.53	*Babu et al., 2008*

Over Trivandrum, the TOA forcing is found to be negative during monsoon and postmonsoon; while the values are positive during winter and premonsoon [*Babu et al.*, 2008]. Over Dibrugarh, the average ARF are found to be similar during winter, premonsoon and monsoon; while the values are a factor of 3 less at the surface and atmosphere during postmonsoon [*Pathak et al.*, 2010] (Table 5.3). A lower TOA forcing value over Dibrugarh during all the seasons indicates the presence of more scattering aerosols. Among the continental locations the highest ATM forcing value is observed over Delhi (84.8 Wm^{-2}) during premonsoon due to increase in dust loading [*Singh et al.*, 2010], while the lowest value is seen over Gurushikhar during winter ($\sim$4 Wm^{-2}).

The atmospheric heating rate is found to be the highest over Delhi and the lowest over Gurushikhar throughout the entire study period. The difference in the ARF could arise due to many factors such as the difference in the AODs, SSA and surface reflectance as the forcing values intricately depend on these parameters. The average aerosol radiative forcing measured over the Bay of Bengal and the Arabian Sea are compared with the ARF estimated from the few earlier studies over the same region in Table 5.3. The comparison clearly shows that the ATM forcing values obtained over the Bay of Bengal and the Arabian Sea during ICARB are lower than the forcing values obtained in all earlier results (Table 5.3). The mean atmospheric warming over the Bay of Bengal and the Arabian Sea in the present study is the lowest ever obtained in the last decade (1996-2006) (Table 5.3) suggesting the dominance of scattering aerosol species during premonsoon. The earlier studies conducted during winter monsoon season when winds are from the polluted northern hemisphere were marked by the occurrence of higher AODs and lower SSAs, which gave rise to higher ATM (more positive) aerosol radiative forcings. The seasonal and spatial variations in aerosol radiative forcing and heating rate over the Indian subcontinent and the adjoining oceanic regions surrounding India will be useful in the radiative and climate impact assessments.

5.6 Conclusions

Implications of variabilities in aerosol parameters on aerosol radiative forcing are assessed in the study. Measured aerosol parameters are used as inputs in a radiative transfer model and aerosol radiative forcing values are estimated for all study locations both over land and oceans. A discrete ordinate radiative transfer model, SBDART, is used to carry out radiative transfer calculations in the SW region (0.2-4.0 μm). Two different methods are followed to estimate the spectral values of various input aerosol parameters (AOD, SSA and g) required in SBDART for the computation of aerosol radiative forcing over the continental locations. In Method 1, the ground based measurements of SSA and AODs are utilized; while in Method 2 SSA calculated from GOCART model are used in addition to the measured AODs to constrain OPAC model over all the four study locations. Over the oceanic regions, the aerosol radiative forcing is calculated using simultaneously measured aerosol optical, physical and chemical properties.

In Method 1, the SSA value over Ahmedabad is found to be <0.8; while the values are >0.9 during all the seasons at 0.55 μm following Method 2. Over Gurushikhar, Kanpur and Gandhi College the SSA value obtained from both the methods are not found to be significantly different. The highest ARF is seen over Ahmedabad and the lowest values are observed over Gurushikhar following Method 1; while using Method 2, highest ARF is observed over the locations in Indo-Gangetic region.

The ATM forcing is found to be in the range of 33 to 54, 4 to 9, 24 to 36, and 24 to 34 Wm^{-2} in Method 1; while the top of the atmosphere forcing (TOA) are found to be -1 to 6, -3 to -5, -5 to -12, and -8 to -12 Wm^{-2} during winter, premonsoon, monsoon and postmonsoon over Ahmedabad, Gurushikhar, Kanpur and Gandhi College respectively. The atmospheric heating rate is found to be the highest over Ahmedabad and the lowest over Gurushikhar. Heating rate is in the range of 0.9 to 1.5, 0.12 to 0.25, 0.66 to 1.0, and 0.67 to 0.96 K/day over

Ahmedabad, Gurushikhar, Kanpur and Gandhi College respectively during the year. The vertical distribution of aerosol radiative forcing and heating rate showed that aerosols warm the atmosphere from near surface to up to 4 km. On the other hand, ARF and TOA are found to be significantly different when calculated using Method 2 over Ahmedabad and the difference is not very significant over the other three locations. The ATM forcing is found to vary from 12 to 17 Wm^{-2} over Ahmedabad which is more than a factor of two less when compared to the value obtained from Method 1. The atmospheric heating rate is found to decrease by a more than a factor of four (0.34-0.48 K/d) using Method 2 over Ahmedabad. The ATM forcing is found to be in the range of 4.7-6.9 Wm^{-2} over Gurushikhar, while the values are found to be in the range of 22-31 Wm^{-2} over Kanpur and Gandhi College.

Results obtained on the ARF and heating rate over the Bay of Bengal and the Arabian Sea during premonsoon are found to exhibit large day to day variability. Over the Bay of Bengal, the mean ARF is estimated to be -12.0, -22.4, and 10.4 Wm^{-2} at the TOA, SFC, and ATM, respectively. The average ARF is less negative over the Arabian Sea and is -10.5, -15.8, and 5.3 Wm^{-2} at TOA, SFC, and ATM, respectively. The average atmospheric heating rate over the Bay of Bengal is $\sim$0.3 K/d, a factor of 2 higher than that over the Arabian Sea. A sensitivity analysis revealed that (1) the curvature effect in AOD spectra has insignificant impact in modifying the ARF and heating rate, and (2) the net Earth-atmosphere energy content shows minor differences when aerosol vertical profiles are used for the estimation of forcing.

A comparison of ARF obtained in the present study with a few earlier studies over different environments in India showed that the atmospheric forcing and heating rate obtained over Delhi was higher followed by Ahmedabad (Method 1), while the lowest values were observed over Gurushikhar. Forcing and heating rate is found to be in the same range over Kanpur and Gandhi College. A large seeasonal variability in the ARF and heating rates are observed over all the study

locations in India. The mean atmospheric warming and heating rate over the Bay of Bengal and the Arabian Sea in the present study is the lowest ever obtained in the last decade. This is because of the fact that during premonsoon season, scattering aerosols are dominant over these oceanic regions, while during winter winds are from the polluted northern hemisphere which are marked by the occurrence of higher AODs and lower SSAs, which give rise to higher ATM forcings and heating rates. The results on ARF from continental locations in India and adjoining oceanic regions have implications to the assessment of regional and seasonal aerosol climate impacts.

Chapter 6

Summary and scope for future work

This chapter gives a brief summary of the thesis with emphasis on the important results obtained during the work and the scope for the work in future has been discussed.

6.1 Summary of results

6.1.1 Continental region

A detailed study on the spatiotemporal variability of aerosol optical, physical and radiative properties has been carried out over four different locations in India spread over a large region during 2006-2008. Each of the study locations over the Indian subcontinent is chosen as they represent different environments. Ahmedabad and Gurushikhar are situated in the western part of India. Ahmedabad is an urban, industrialized, semi arid, and densely populated location; while Gurushikhar is a high altitude, relatively pristine, remote site. Kanpur and Gandhi College are situated in the most populated and highly polluted Indo-Gangetic plain. Kanpur is an urban, industrialized location; while Gandhi College in Ballia district of Uttar Pradesh is a rural village location situated in the downwind of major urban locations such as Delhi and Kanpur. Aerosol optical properties have been measured over all these continental locations and the influence of observed

aerosol properties on the Earth's radiation budget is examined by estimating the aerosol radiative forcing. The data obtained over all the study locations are classified into four major seasons *viz.,* Winter (Dec-Feb), premonsoon (Mar-May), monsoon (Jun-Sep) and postmonsoon (Oct-Nov) depending on prevailing meteorological conditions. The major findings of the study over continental locations are:

- AODs exhibit prominent seasonal variations in the study locations. Ahmedabad and Gurushikhar show a winter low and a premonsoon or summer high in AODs, while Kanpur and Gandhi College winter AODs are higher than summer AODs. Aerosol sources of different nature coupled with variations in meteorology and dynamics contribute to the observed spatial and seasonal variabilities.

- Spectral variations in AODs also differ among the study locations. AODs at 0.38/0.40 μm over Ahmedabad, Kanpur and Gandhi College are always higher than 0.875 and 1.02 μm AODs. In Gurushikhar AODs at both the above wavelengths are more or less similar throughout the year. AODs in short wavelength (0.38 μm) over Gandhi College are about 20% higher than that over Kanpur; while AODs in near 1.02 μm are nearly the same for all the seasons over both the locations.

- During the entire study period for all the study locations seasonal mean AODs retrieved from ground-based (sun photometers and sun/sky radiometers) and satellite (MODIS and MISR) measurements are found to agree within $\pm 1\sigma$.

- Ångström parameters (α and β) are found to exhibit large spatial and seasonal variations. The α values during postmonsoon and winter are higher than that of premonsoon and monsoon at all the locations. The α values are lower over Gurushikhar throughout the study period (<1.0) indicating the

dominance of coarse mode aerosols. The β values are higher during monsoon in Ahmedabad, Kanpur and Gandhi College due to the abundance of supermicron aerosols.

- AOD ratio, an indicator of whether submicron or supermicron aerosols dominate the aerosol size distribution, is found to show seasonal and spatial variations consistent with AOD variations. Postmonsoon and winter AOD ratios in all the locations are higher ($\geq$2) than those obtained during premonsoon and monsoon.

- Aerosol volume size distributions obtained over Kanpur and Gandhi College showed a bimodal distribution with peaks at fine and coarse mode during all the seasons. The volume concentration in fine mode is ≤ 0.13 μm^3 μm^{-2} throughout the year over both Kanpur and Gandhi College. The coarse mode volume concentration is found to be in the range of (0.11-0.50 μm^3 μm^{-2}). The coarse mode volume concentration during postmonsoon and winter is more than a factor of two less than during premonsoon and monsoon. The increase in coarse mode volume concentration is attributed to the increase in dust loading over these locations.

- Spectral dependence of AOD is examined by deriving the Ångström exponent values in narrow wavelength bands and the results indicated that the size distribution of aerosol was of mixed type with contribution from both fine and coarse mode aerosols over all the study locations. The difference in the α values calculated in the short and long wavelength ranges is found to be negative over all the study locations indicating presence of fine mode with varying concentrations as a function of different seasons.

- The curvature in the AOD spectra is found to be higher over Ahmedabad and Gurushikhar as compared to Kanpur and Gandhi College due to lower turbidity during all the seasons. The value of $\alpha^{'}$ is found to be positive sug-

gesting a bimodal aerosol size distribution throughout the study period over Ahmedabad and Gurushikhar. In contrast, over Kanpur and Gandhi College most of the $\alpha^{'}$ are found to be positive during winter and postmonsoon; while the $\alpha^{'}$ values are mostly negative during premonsoon and monsoon.

- The coefficients of polynomial fit (α_1 and α_2) are found to exhibit strong spatial and seasonal variability. More than 80 % of AOD spectra are found to have the value of $\alpha_2 - \alpha_1$ between 1 and 2 during winter indicating dominant fine mode aerosols; while during premonsoon and monsoon the value became 50 % due to increase in the coarse mode aerosols over all the study locations. During postmonsoon, the percentage of spectra with $\alpha_2 - \alpha_1$ between 1 and 2 is less than 65 % over Ahmedabad and Gurushikhar; while it is $>$ 90% over the locations in Indo-Gangetic plain region.

- The seasonal mean BC mass concentrations measured over Ahmedabad during 2006-2008 are found to be 9.4±2.2, 3.9±2.0, 2.0±0.5, and 9.0±2.0 μg m^{-3} during winter, premonsoon, monsoon and postmonsoon respectively. The seasonal average absorption coefficients are 1.3×10^{-4}, 0.6×10^{-4}, 0.3×10^{-4} and 1.3×10^{-4} m^{-1} during winter, premonsoon, monsoon and postmonsoon respectively. The seasonal mean scattering coefficients are found to be 2.4×10^{-4}, 1.1×10^{-4}, 0.8×10^{-4} and 2.3×10^{-4} m^{-1} during winter, premonsoon, monsoon and postmonsoon respectively. The SSA calculated using scattering and absorption coefficients at 0.55 μm are found to be 0.67, 0.69, 0.79, and 0.64 during winter, premonsoon, monsoon and postmonsoon respectively.

- Aerosol radiative forcing estimated from Method 1 (using ground based measured SSA from different techniques) are found to be the highest over Ahmedabad and the lowest over Gurushikhar during all the seasons due to lower SSA over Ahmedabad. The top of the atmosphere (TOA) and surface (SFC) forcing over Ahmedabad is found to be about 0.8, 4.4, -0.7, 5.7 and -41.1,

-44.7, -34.3, -48.3 Wm^{-2} during winter, premonsoon, monsoon, and post-monsoon respectively. The TOA forcing over Gurushikhar is found to be in the range of -3 to -5 Wm^{-2}. The SFC forcing over Gurushikhar is found to be a factor of four less than Ahmedabad and is in the range of -7.3 to -14.0 Wm^{-2}. Over Kanpur and Gandhi College, the TOA and SFC forcing is similar and is in the range of -4.7 to -11.9 Wm^{-2} and -31.0 to 41.7 Wm^{-2} respectively, using Method 1.

- The forcing values estimated using the SSA obtained from GOCART model (Method 2) are found to exhibit distinct behavior in contrast to Method 1. The highest forcing is seen over the locations in the Indo-Gangetic region and the lowest values are observed over Gurushikhar during all the seasons. The SFC forcing over Ahmedabad is about a factor of two less using Method 2. The TOA forcing is found to be in the range of -7 to -10 Wm^{-2} during different seasons. Over the other three locations the difference in the forcing values obtained from Method 1 and Method 2 are found to be same within $\pm 1\sigma$ variation.

- A comparison between the forcing and heating rate obtained in present study and the values obtained over different environments showed the forcing and heating rate is highest over Delhi followed by Ahmedabad while the lowest values are observed over Gurushikhar. Forcing and heating rate is found to be in the same range over Kanpur and Gandhi College. A large spatial and temporal variability in the ARF and heating rate is observed over all the study locations in India.

6.1.2 Oceanic regions

Measurement and analysis of aerosol characteristics are conducted over the oceanic regions adjoining Indian subcontinent during premonsoon season of March-May, 2006. The major objective of this work was to study the effect of transport of pol-

lutants from highly populated and industrialized areas of Indo-Gangetic plain to the otherwise clean oceanic region of the Bay of Bengal and the Arabian Sea during premonsoon season. Measurements of AODs were conducted during the entire cruise period at five different wavelength bands using a sun photometer. The spectral dependence of aerosol optical depth (curvature effect) has been investigated to get some crucial information about the size distribution of aerosols and their spatial variability. The implications of the presence of these aerosols over the Bay of Bengal and the Arabian Sea are quantified in terms of aerosol radiative forcing. Important results obtained from the present study over the oceanic regions are summarized below:

- Aerosol optical depths over the Bay of Bengal are higher than that over the Arabian Sea for all the wavelengths during the entire period of observation. This indicates higher columnar concentration of aerosols over the Bay of Bengal than the Arabian Sea. AODs from MODIS (Terra and Aqua) satellites showed a good agreement with the measured AODs with a higher correlation greater than 90% at 0.5 and 0.875 μm, indicating a good consistency between the ground based and satellite derived AODs.

- The mean value of Ångström exponent α is found to be higher over the Bay of Bengal region (1.12) compared to the Arabian Sea (0.73), which indicates a higher concentration of smaller size aerosols over the Bay of Bengal than over the Arabian Sea.

- The anthropogenic influence in the measured AODs over the Bay of Bengal and the Arabian Sea is calculated by three independent methods and they are found to agree well within $\pm 1\sigma$. The results showed that the contribution of anthropogenic sources to the aerosols over the Bay of Bengal (68-75%) is higher than that of the Arabian Sea (51-65%).

- Spatial variations in aerosol optical properties as function of latitude and

longitude are analyzed over the Bay of Bengal and the Arabian Sea during the cruise period. AODs are found to increase with latitude from 4^oN to 20^oN over the Bay of Bengal while over the Arabian Sea these variations are not significant.

- Seven days air back trajectory analysis performed over both the oceanic regions during the study period showed that at 500 m and above the air masses originate from different arid/semiarid, continental regions surrounding the Bay of Bengal and the Arabian Sea, and of marine origin (the Bay of Bengal and the Arabian Sea) suggesting different source regions and aerosol types. A comparative analysis of AODs and air back trajectories confirmed that the AODs are higher over both the oceanic regimes when the ship was cruising near the coast and when the winds originate and pass through arid and densely populated urban regions before reaching the measurement locations.

- More than 90% of the AOD spectra measured over the Bay of Bengal and the Arabian Sea are found to have positive $\alpha^{'}$, thus suggesting a bimodal aerosol size distribution with the dominance of fine mode aerosols. The coefficient of determination (R^2) for polynomial fit of ln τ versus ln λ is found be greater than 0.9 for 92% of the AOD spectra measured over the Bay of Bengal, while 80% of the Arabian Sea AOD spectra have R^2 values >0.9. In contrast, when least squares fits are applied only 69% (Bay of Bengal) and 15% (Arabian Sea) of AOD spectra are found to have $R^2 > 0.9$.

- Over the Bay of Bengal, for 76% of AOD spectra the α_2 - α_1 value is >1 and <2, suggesting the dominance of fine mode aerosols from a wide variety of fine mode fractions. In contrast, over the Arabian Sea the difference between α_2 and α_1 is <1 for 84% of the AOD spectra, clearly indicating the dominance of coarse mode aerosols. The scatter plots between α_2 - α_1 and 0.5 μm AODs confirm that the Bay of Bengal AOD spectra are predominantly made up of particles from a wide variety of fine mode fractions or mixture of modes while

the Arabian Sea was dominated by coarse mode aerosols.

- Spatial and temporal heterogeneity in aerosol radiative forcing and heating rate are investigated over the Bay of Bengal and the Arabian Sea for the premonsoon season of 2006. The measured AOD, total aerosol mass and chemical composition in combination with a radiative transfer model are used to estimate the radiative forcing over the Bay of Bengal and the Arabian Sea for individual days. A large day to day variability in the aerosol radiative forcing is observed over both the oceanic regions similar to the variation in AODs.

- The average aerosol radiative forcings over the Bay of Bengal are estimated to be -12.0, -22.4 and 10.4 W m^{-2} at TOA, SFC and ATM, respectively. Over the Arabian Sea the average forcings are found to be -10.5, -15.8, and 5.3 W m^{-2} at TOA, SFC and ATM respectively.

- A sensitivity test revealed that the aerosol radiative forcing and heating rate do not differ significantly when curvatures in aerosol optical depth spectra exist, because the radiative effects of aerosols depend both on the AODs and the incoming solar radiation, 72% of which lies in the 0.2-1.0 μm wavelength range. Another sensitivity study showed that the presence or the absence of aerosol vertical profiles does not significantly modify the net energy content of the Earth-atmosphere system at the top of the atmosphere, at the surface and in the atmosphere.

- The solar heating rates are found to be higher than 0.1 K/d over the Bay of Bengal with an average value of 0.3 K/d which is twice higher than the value over the Arabian Sea. A comparison of aerosol radiative forcing and heating rate with previous results obtained over the Bay of Bengal and the Arabian Sea revealed that the atmospheric warming and the associated heating rate are lower during the present study. This is because of the fact that during

premonsoon season scattering aerosols are dominant over these oceanic regions, while during winter higher AODs and lower SSAs gives rise to higher ATM forcings and heating rates.

6.2 Scope for future work

The present study investigated the spatial and temporal variability in aerosol properties over the Indian subcontinent and the adjoining oceanic regions. For a better estimation of radiative effect of aerosols and to reduce the uncertainty in aerosol effect on climate, a detailed study of this kind should be conducted over different parts of India on a longer time scale. This type of analysis on characterization of aerosol size distribution over different locations both over land and ocean can be used in modeling the regional and seasonal aerosol radiative effects of aerosols. The results obtained will be helpful in remote sensing for refinement, evaluation and validation of the retrieval algorithms, and in estimating the impact of seasonal and spatial variations due to aerosols on regional and global climate.

As seen in the present study, there exist large spatial and temporal variability in the aerosol characteristics indicating contribution of different sources over the study locations/region. The identification of source regions of aerosols present over the study locations will enhance the understanding on the observed variability in the aerosol properties.

In situ measurements can be used to improve the satellite retrieval algorithm on a regional scale and also in global scenario. Continuous comparison of ground based and satellite measurements coupled with modeling studies are required for better understanding of the direct and indirect effects of aerosols on regional and global scales and their temporal variability.

Aerosol radiative forcing was estimated in the present study by treating aerosols of different types as external mixtures. However, in the ambient atmosphere, aerosols are present in different mixing states and this can cause large differences in the estimation of forcing [e.g., *IPCC*, 2007; *Jacobson*, 2001; *Lesins et al.*, 2002].

Therefore, computation of different microphysical properties such as refractive index and size distribution is very important for a more accurate determination of aerosol radiative forcing. A detailed knowledge about the aerosol mixing state will be useful in reducing the uncertainty in the estimation of aerosol radiative forcing [*Jacobson*, 2001; *Lesins et al.*, 2002]. In addition, simultaneously measured aerosol vertical profile can help to reduce the uncertainty and quantify aerosol radiative forcing as a function of altitude.

Another important parameter that can affect aerosol forcing is the shape of aerosol. For estimation of radiative forcing, aerosols are generally considered as spherical particles. However, it has been shown that the scattering properties of nonspherical particles can be significantly different than the equivalent spherical particles [*Mishchenko et al.*, 1997]. It was shown that assumption of spherical particles can introduce significant errors in retrieval of AODs from reflectance data as in the case of satellite measurements. Measurements of shape of the aerosol particles and aerosol phase function are therefore necessary to determine more accurately the direct and indirect radiative effects of aerosols.

As discussed in Chapter 1, *Menon et al.* [2002] showed that due to increasing BC concentration from various industrial emissions and fossil fuel combustion, the amount of solar radiation reaching the Earth's surface reduces. As a result, atmospheric stability decreases and it significantly contributes to the change in rainfall pattern. *Ramanathan et al.* [2005] showed that the solar dimming effect causes a reduction in evaporation from the ocean surface, thereby decreases the latitudinal gradient in the sea surface temperature. This whole process increases the atmospheric stability and causes causes weakening of the monsoon rainfall in South Asia [*Ramanathan et al.*, 2005]. On the other hand, *Lau et al.* [2006] suggested an Elevated Heat Pump Hypothesis. According to them, increased dust or black carbon aerosols are responsible for producing anomalous rainfall. This discussion highlights the complexity of the problem in estimating the effect of aerosols on rainfall pattern. Other studies indicate that urban and industrial air pollution can

have significant effect on hydrological cycle and therefore on the rainfall pattern [*Rosenfeld et al.*, 2000; *Lau et al.*, 2006]. Since aerosols play an important role in the formation of cloud by acting as cloud condensation nuclei, measurements of seasonal and interannual variabilities of different aerosol parameters along with cloud characteristics will be useful and necessary to study the aerosol-cloud interaction and thereby the indirect effect of aerosols, as well as their effect on monsoonal rainfall.

References

Abdou, W. A., et al. (2005), Comparison of coincident Multiangle Imaging Spectroradiometer and Moderate Resolution Imaging Spectroradiometer aerosol optical depths over land and ocean scenes containing Aerosol Robotic Network sites, *J. Geophys. Res., 110*, doi:10.1029/2004JD004693.

Acharya, Y. B., and A. Jayaraman (1995), Sun-photometry using photodiode open circuit voltage measurements, *Rev. Sci. Instrum., 66*, 4087-4090.

Adeyewa, Z. D., and E. E. Balogun (2003), Wavelength dependence of aerosol optical depth and the fit of the Ångström law, *Theor. Appl. Climatol., 74*, 105-122.

Albrecht, B. A. (1989), Aerosols, cloud microphysics, and fractional cloudiness, *Science, 245*, 1227-1230.

Anderson, T. L., et al. (1996), Performance characteristics of a high-sensitivity, three-wavelength total scatter/backscatter nephelometer, *J. Atmos. Oceanic Technol., 13*, 967-986.

Anderson, T. L., and J. A. Ogren (1998), Determining aerosol radiative properties using the TSI 3563 integrating nephelometer, *Aerosol Sci. Technol., 29*, 57-69.

Anderson, T. L.,Y. Wu, D. A. Chu, B. Schmid, J. Redemann, and O. Dubovik (2005), Testing the MODIS satellite retrieval of aerosol fine-mode fraction, *J. Geophys. Res., 110*, doi:10.1029/2005JD005978.

Andreae, M. O. (1995), Climatic effects of changing atmospheric aerosol levels. In: Henderson Sellers, A. (Ed.),*World Survey of Climatology, vol. 16, Future Climates of the World, Elsevier*, NewYork, pp. 341-392.

Ångström, A. (1961), Techniques of determining the turbidity of the atmosphere, *Tellus, 13*, 214-223.

Babu, S. S., and K. K. Moorthy (2002), Aerosol black carbon over a tropical coastal station in India, *Geophys. Res. Lett., 29*, doi:10.1029/2002GL015662.

Babu, S. S., V. S. Nair, and K. K. Moorthy (2008), Seasonal changes in aerosol characteristics over Arabian Sea and their consequence on aerosol short-wave radiative forcing: Results from ARMEX field campaign, *J. Atmos. Sol. Terr. Phys., 70*, doi:10.1016/j.jastp, 820-834.

Bhat, G. S., et al. (2001), BOBMEX: The Bay of Bengal Monsoon Experiment, *Bull. Amer. Meteor. Soc., 82*, 2217-2243.

Bodhaine, B. A. (1995), Aerosol absorption measurements at Barrow, Mauna Loa and the south pole, *J. Geophys. Res., 100*, 8967-8975.

Bond, T., and R. W. Bergstrom (2006), Light absorption by carbonaceous particles: An investigative review, *Aerosol Sci. Tech., 40*, 27-67.

Cachorro, V. E., R. Vergaz, and A. M. de Frutos (2001), A quantitative comparison of a Ångström turbidity parameter retrieved in different spectral ranges based on spectroradiometer solar radiation measurements, *Atmos. Environ., 35*, 5117-5124.

Charlson, R. J., S. E. Schwartz, J. M. Hales, R. D. Cess, J. A. Coakley, J. E. Hansen, and D. J. Hofmann (1992), Climate forcing by anthropogenic aerosols, *Science, 255*, 423-430.

Chin, M., et al. (2002), Tropospheric aerosol optical thickness from the GOCART model and comparison with satellite and sunphotometer measurements, *J. Atmos. Sci., 59*, 748-757.

Christopher, S. A., and J. Zhang (2004), Cloud-free shortwave aerosol radiative effect over oceans: Strategies for identifying anthropogenic forcing from Terra satellite measurements, *Geophys. Res. Lett., 31*, doi:10.1029/2004GL020510.

Chung, C. E., V. Ramanathan, D. Kim, and I. A. Podgorny (2005), Global anthropogenic aerosol direct forcing derived from satellite and ground-based observations, *J. Geophys. Res., 110*, doi:10.1029/2005JD006356.

Corrigan, C. E., V. Ramanathan, and J. J. Schauer (2006), Impact of monsoon transitions on the physical and optical properties of aerosols, *J. Geophys. Res., 111*, doi:10.1029/2005JD006370.

d'Almeida, G. A., P. Koepke, and E. P. Shettle (1991), *Atmospheric Aerosols: Global Climatology and Radiative Characteristics*, 561 pp., A. Deepak, Hampton, Va.

Dani, K. K., R. S. Maheskumar, and P. C. S. Devara (2003), Study of total column atmospheric aerosol optical depth, ozone and precipitable water content over Bay of Bengal during BOBMEX-99, *Proc. Indian Acad. Sci., 112*, 205-221.

Devara, P. C. S., R. S. Maheskumar, P. E. Raj, K. K. Dani, and S. M. Sonbawne (2001), Some features of columnar aerosol optical depth, ozone and precipitable water content observed over land during the INDOEX-IFP99, *Meteorol. Z., 10*, doi: 10.1127/0941-2948/2001/0010-0123.

Dey, S., S. N. Tripathi, R. P. Singh, and B. N. Holben (2004), Influence of dust storms on the aerosol optical properties over the Indo-Gangetic basin, *J. Geophys. Res., 109*, doi:10.1029/2004JD004924.

Dey, S., and S. N. Tripathi (2008), Aerosol direct radiative effects over Kanpur in the Indo-Gangetic basin, northern India: Long-term (2001-2005) observations and implications to regional climate, *J. Geophys. Res., 113*, doi:10.1029/2007JD009029.

Diner, D. J., et al. (2001), MISR aerosol optical depth retrievals over southern Africa during the SAFARI-2000 winter season campaign, *Geophys. Res. Lett., 28*, doi:2001GL013188.

Di Girolamo, L., et al. (2004), Analysis of Multi-angle Imaging SpectroRadiometer (MISR) aerosol optical depths over greater India during winter 2001-2004, *Geophys. Res. Lett., 31*, doi:10.1029/2004GL021273.

Draxler, R. R., and G. D. Hess (1998), An overview of the HYSPLIT-4 modeling system for trajectories, dispersion and deposition, *Aust. Meteorol. Mag., 47*, 295-308.

Dubovik, O., and M. D. King (2000), A flexible inversion algorithm for retrieval of aerosol optical properties from Sun and sky radiance measurements, *J. Geophys. Res., 105*, 20673-20696.

Dubovik, O., A. Smirnov, B. N. Holben, M. D. King, Y. J. Kaufman, T. F. Eck, and I. Slutsker (2000), Accuracy assessments of aerosol optical properties retrieved from Aerosol Robotic Network (AERONET) Sun and sky radiance measurements, *J. Geophys. Res., 105*, 9791-9806.

Dubovik, O., et al. (2002), Variability of absorption and optical properties of key aerosol types observed in worldwide locations, *J. Atmos. Sci., 59*, 590-608.

Dutkiewicz, V. A., S. Alvi, B. M. Ghauri, M. I. Choudhary, L. Husain (2009), Black carbon aerosols in urban air in South Asia, *Atmos. Environ., 43*, 1737-1744.

Eck, T. F., et al. (1999), Wavelength dependence of the optical depth of biomass burning, urban, and desert dust aerosols, *J. Geophys. Res., 104*, 31333-31349.

Eck, T. F., B. N. Holben, O. Dubovik, A. Smirnov, I. Slutsker, J. M. Lobert, and V. Ramanathan (2001), Column-integrated aerosol optical properties over the Maldives during the northeast monsoon for 1998-2000, *J. Geophys. Res., 106*, 28555-28566.

Eck, T. F., et al. (2005), Columnar aerosol optical properties at AERONET sites in central eastern Asia and aerosol transport to the tropical mid-Pacific, *J. Geophys. Res., 110*, doi:10.1029/2004JD005274.

Eldering, A., J. A. Ogren, Z. Chowdhury, L. S. Hughes, and G. R. Cass (2002), Aerosol optical properties during INDOEX based on measured aerosol particle size and composition, *J. Geophys. Res., 107*, doi:10.1029/2001JD001572.

Gadhavi, H., and A. Jayaraman (2010), Absorbing aerosols: contribution of biomass burning and implications for radiative forcing, *Ann. Geophys., 28*, 103-111.

Ganguly, D., H. Gadhavi, A. Jayaraman, T. A. Rajesh, and A. Misra (2005a), Single scattering albedo of aerosols over the central India: Implications for the regional aerosol radiative forcing, *Geophys. Res. Lett., 32*, doi:10.1029/2005GL023903.

Ganguly, D., A. Jayaraman, and H. Gadhavi (2005b), In situ ship cruise measurements of mass concentration and size distribution of aerosols over Bay of Bengal and their radiative impacts, *J. Geophys. Res., 110*, D06205, doi:10.1029/2004JD005325.

Ganguly, D., A. Jayaraman, and H. Gadhavi (2006a), Physical and optical properties of aerosols over an urban location in western India: Seasonal variabilities, *J. Geophys. Res., 111*, doi:10.1029/2006JD007392.

Ganguly, D., A. Jayaraman, T. A. Rajesh, and H. Gadhavi (2006b), Wintertime aerosol properties during foggy and nonfoggy days over urban center Delhi and their implications for shortwave radiative forcing, *J. Geophys. Res., 111*, doi:10.1029/2005JD007029.

Ganguly, D., P. Ginoux, V. Ramaswamy, D. M. Winker, B. N. Holben, and S. N. Tripathi (2009), Retrieving the composition and concentration of aerosols over the Indo-Gangetic basin using CALIOP and AERONET data, *Geophys. Res. Lett., 36*, doi:10.1029/2009GL038315.

Gassó, S., and N. T. O'Neill (2006), Comparisons of remote sensing retrievals and in situ aerosol fine mode fraction during ACE-Asia, *Geophys. Res. Lett., 33*, doi:10.1029/2005GL024926.

Gundel, L. A., R. L. Dod, H. Rosen and T. Novakov (1984), The relationship between optical attenuation and black carbon concentrations for ambient and source particles, *Sci. Total Environ., 36*, 197-202.

Hansen, A. D. A., H. Rosen, and T. Novakov (1984), The Aethalometer - an instrument for the real-time measurement of optical absorption by aerosol particles, *Sci. Total Environ., 36*, 191-196.

Haywood, J. M., and K. P. Shine (1995), The effect of anthropogenic sulfate and soot on the clear-sky planetary radiation budget, *Geophys. Res. Lett., 22*, 603-606.

Haywood, J. M., and V. Ramaswamy (1998), Global sensitivity studies of the direct radiative forcing due to anthropogenic sulfate and black carbon aerosols, *J. Geophys. Res., 103*, 6043-6058.

Haywood, J., O. Boucher (2000), Estimates of the direct and indirect radiative forcing due to tropospheric aerosols: A review, *Rev. Geophys., 38*, 10.1029/1999RG000078, 513-543.

Hess, M., P. Koepke, and I. Schult (1998), Optical properties of aerosols and clouds: The software package OPAC, *Bull. Am. Meteorol. Soc., 79*, 831-844.

Holben, B. N., et al. (1998), AERONET - A federated instrument network and data archive for aerosol characterization, *Remote Sens. Environ., 66*, 1-16.

Holben, B. N., et al. (2001), An emerging ground-based aerosol climatology: Aerosol optical depth from AERONET, *J. Geophys. Res., 106*, 12067-12097.

Huang, J., Q. Fu, J. Su, Q. Tang, P. Minnis, Y. Hu, Y. Yi, and Q. Zhao (2009), Taklimakan dust aerosol radiative heating derived from CALIPSO observations using the Fu-Liou radiation model with CERES constraints, *Atmos. Chem. Phys., 9*, 4011-4021.

Intergovernmental Panel on Climate Change (2007), Summary for policymakers, in Climate Change 2007: The Physical Science Basis. *Contribution of Working Group I to the Fourth Assessment Report of the Intergovernmental Panel on Climate Change*, edited by S. Solomon et al., pp. 129-234, Cambridge Univ. Press, New York.

Isaksen, I. S. A., et al. (2009), Atmospheric composition change: Climate Chemistry interactions, *Atmos. Environ., 43*, 5138-5192.

Jacobson, M. Z. (2001), Strong radiative heating due to the mixing state of black carbon, *Nature, 409*, 695-697.

Jacobson, M. Z. (2002), Atmospheric pollution: history, science, and regulation, *Cambridge university press*, Cambridge, pp. 1-412, New York.

Jaenicke, R. (1993), Tropospheric aerosols in aerosol-cloud-climate interactions, edited by P. V. Hobbs, *Academic, San Diego, Calif.*, pp. 1-31.

Jayaraman, A., D. Lubin, S. Ramachandran, V. Ramanathan, E. Woodbridge, W. D. Collins, and K. S. Zalpuri (1998), Direct observations of aerosol radiative forcing over the tropical Indian Ocean during the January-February 1996 pre-INDOEX cruise, *J. Geophys. Res., 103*, 13827-13836.

Jayaraman, A., et al. (2006), Spatial variations in aerosol characteristics and regional radiative forcing over India: Measurements and modeling of 2004 road campaign experiment, *Atmos. Environ., 40*, 6504-6515.

Jethva, H., S. K. Satheesh, and J. Srinivasan (2005), Seasonal variability of aerosols over the Indo-Gangetic basin, *J. Geophys. Res., 110*, doi:10.1029/2005JD005938.

Junge, C. E. (1955), The size distribution and aging of natural aerosols as determined from electrical and optical measurements in the atmosphere, *J. Meteorol., 12*, 13-25.

Kahn, R. A., B. J. Gaitley, J. V. Martonchik, D. J. Diner, K. A. Crean, and B. Holben (2005), Multiangle Imaging Spectroradiometer (MISR) global aerosol optical depth validation based on 2 years of coincident Aerosol Robotic Network (AERONET) observations, *J. Geophys. Res., 110*, doi:10.1029/2004JD004706.

Kahn, R. A., et al. (2007), Satellite-derived aerosol optical depth over dark water from MISR and MODIS: Comparisons with AERONET and implications for climatological studies, *J. Geophys. Res., 112*, doi:10.1029/2006JD008175.

Kaufman, Y. J., D. Tanré, L. Remer, E. Vermote, A. Chu, and B. N. Holben (1997), Operational remote sensing of tropospheric aerosol over land from EOS Moderate Resolution Imaging Spectroradiometer, *J. Geophys. Res., 102*, 17051-17067, doi:10.1029/96JD03988.

Kaufman, Y. J., D. Tanre, and O. Boucher (2002), A satellite view of aerosols in the climate system, *Nature, 419*, 215-223.

Kaufman, Y. J., O. Boucher, D. Tanré, M. Chin, L. A. Remer, and T. Takemura (2005), Aerosol anthropogenic component estimated from satellite data, *Geophys. Res. Lett., 32*, doi:10.1029/2005GL023125.

Kaskaoutis, D. G., and H. D. Kambezidis (2006), Investigation into the wavelength dependence of the aerosol optical depth in the Athens area, *Quart. J. R. Meteorol. Soc.*, 132, 2217-2234.

Kaskaoutis, D. G., H. D. Kambezidis, N. Hatzianastassiou, P. G. Kosmopoulos, and K. V. S. Badarinath (2007), Aerosol climatology: Dependence of the Angstrom exponent on wavelength over four AERONET sites, *Atmos. Chem. Phys. Discuss., 7*, 7347-7397.

Kedia, S., and S. Ramachandran (2008a), Features of aerosol optical depths over the Bay of Bengal and the Arabian Sea during premonsoon season: Variabilities and anthropogenic influence, *J. Geophys. Res., 113*, doi:10.1029/2007JD009070.

Kedia, S., and S. Ramachandran (2008b), Latitudinal and longitudinal variation in aerosol characteristics from Sun photometer and MODIS over the Bay of Bengal and Arabian Sea during ICARB, *J. Earth Syst. Sci., 117*, 375-387.

Kedia, S., and S. Ramachandran (2009), Variability in aerosol optical and physical characteristics over the Bay of Bengal and the Arabian Sea deduced from Ångström exponents, *J. Geophys. Res., 114*, doi:10.1029/2009JD011950.

Kedia, S., S. Ramachandran, A. Kumar, and M. M. Sarin (2010), Spatiotemporal gradients in aerosol radiative forcing and heating rate over Bay of Bengal and Arabian Sea derived on the basis of optical, physical, and chemical properties, *J. Geophys. Res., 115*, doi:10.1029/2009JD013136.

Kumar, A., A. K. Sudheer, and M. M. Sarin (2008), Chemical characteristics of aerosols in MABL of Bay of Bengal and Arabian Sea during spring intermonsoon: A comparative study, *J. Earth Syst. Sci., 117*, 325-332.

Kumar, A., and M. M. Sarin (2009), Mineral aerosols from western India: Temporal variability of coarse and fine atmospheric dust and elemental characteristics, *Atmos. Environ., 43*, 4005-4013.

Kleidman, R. G., et al. (2005), Comparison of moderate resolution imaging spectroradiometer (MODIS) and aerosol robotic network (AERONET) remote-sensing retrievals of aerosol fine mode fraction over ocean, *J. Geophys. Res., 110*, doi:10.1029/2005JD005760.

Lacis, A. A., and M. I. Mishchenko (1995), Climate forcing, climate sensitivity, and climate response: A radiative and modeling perspective on atmospheric aerosols, in *Aerosol Forcing of Climate*, edited by R. J. Charlson and J. Heintzenberg, pp. 11-42, John Wiley, Hoboken, N. J.

Lau, K.-M., M.-K. Kim, and K.-M. Kim (2006), Asian summer monsoon anomalies induced by aerosol direct forcing: The role of the Tibetan Plateau. *Climate Dyn., 26*, 855-864.

Lesins, G., P. Chylek, and U. Lohmann (2002), A study of internal and external mixing scenarios and its effect on aerosol optical properties and direct radiative forcing, *J. Geophys. Res., 107*, 10.1029/2001JD000973.

Levy, R. C., L. A. Remer, S. Mattoo, E. F. Vermote, and Y. J. Kaufman (2007), Second-generation operational algorithm: Retrieval of aerosol properties over land from inversion of moderate resolution imaging spectroradiometer spectral reflectance, *J. Geophys. Res., 112*, doi:10.1029/2006JD007811.

Leon, J.-F., et al. (2001), Large-scale advection of continental aerosols during INDOEX, *J. Geophys. Res., 106*, 28427-28439.

Liou, K. N. (1980), *An Introduction to Atmospheric Radiation*, 392 pp., Academic Press, San Diego, Calif.

Mamouri, R. E., V. Amiridis, A. Papayannis, E. Giannakaki, G. Tsaknakis, and D. S. Balis (2009), Validation of CALIPSO space-borne-derived attenuated backscatter coefficient profiles using a ground-based lidar in Athens, Greece, *Atmos. Meas. Tech., 2*, 513-522.

McClatchey, R. A., R. W. Fenn, J. E. A. Salby, F. E. Volz, and J. S. Garing (1972), *Optical Properties of the Atmosphere, 3rd ed., Environ. Res. Pap., 411*, 108 pp., Air Force Cambridge Res. Lab., Cambridge, Mass.

Meehl, G. A., and J. M. Arblaster (2002), Indian monsoon GCM sensitivity experiments testing tropospheric biennial oscillation transition conditions, *J. Climate, 15*, 923-944.

Menon, H. B. (2004), Calibration of an optical equation to analyse the atmospheric turbidity and water quality of an estuarine environment, *J. Ind. Soc. Rem. Sens., 32*, 287-300.

Menon, S., J. Hansen, L. Nazarenko, and Y. Lou (2002), Climate Effects of Black Carbon Aerosols in China and India, *Science, 297*, 2250-2253.

Mishchenko, M. I., et al. (1997), Modeling phase functions for dustlike tropospheric aerosols using a shape mixture of randomly oriented polydisperse spheroids, *J. Geophys. Res., 102*, 16831-16847.

Morys, M., F. M. Mims III, S. Hagerup, S. E. Anderson, A. Baker, J. Kia and T. Walkup (2001), Design calibration, and performance of MICROTOPS II handheld ozone monitor and sun photometer, *J. Geophys. Res., 106*, 14573-14582.

Moorthy, K. K., S. S. Babu, S. V. Sunilkumar, P. K. Gupta, and B. S. Gera (2004), Altitude profiles of aerosol BC, derived from aircraft measurements over an inland urban location in India, *Geophys. Res. Lett., 31*, doi:10.1029/2004GL021336.

Moorthy, K. K., S. S. Babu, S. K. Satheesh (2005), Aerosol characteristics and radiative impacts over the Arabian Sea during inter-monsoon season: results from ARMEX field campaign, *J. Geophys. Res., 62*, 192-206.

Moorthy, K. K., S. K. Satheesh, S. S. Babu, and C. B. S. Dutt (2008), Integrated Campaign for Aerosols, Gases and Radiation Budget (ICARB): An overview, *J. Earth Syst. Sci., 117*, 243-262.

Murphy, D. M., S. Solomon, R. W. Portmann, K. H. Rosenlof, P. M. Forster, and T. Wong (2009), An observationally based energy balance for the Earth since 1950, *J. Geophys. Res., 114*, doi:10.1029/2009JD012105.

Nair, S. K., K. Parameswaran, and K. Rajeev (2005), Seven year satellite observations of the mean structures and variabilities in the regional aerosol distribution over the oceanic areas around the Indian subcontinent, *Ann. Geophys., 23*, 2011-2030.

Nair, V. S., S. S. Babu, and K. K. Moorthy (2008), Spatial distribution and spectral characteristics of aerosol single scattering albedo over the Bay of Bengal inferred from shipborne measurements, *Geophys. Res. Lett., 35*, doi:10.1029/2008GL033687.

Niranjan, K., B. L. Madhavan, and V. Sreekanth (2007), Micro pulse lidar observation of high altitude aerosol layers at Visakhapatnam located on the east coast of India, *Geophys. Res. Lett., 34*, doi:10.1029/2006GL028199.

Novakov, T., V. Ramanathan, J. E. Hansen, T. W. Kirchstetter, M. Sato, J. E. Sinton, and J. A. Sathaye (2003), Large historical changes of fossil-fuel black carbon aerosols, *Geophys. Res. Lett., 30*, 13-24, doi:10.1029/2002GL016345.

O'Neill, N. T., T. F. Eck, B. N. Holben, A. Smirnov, and O. Dubovik (2001), Bimodal size distribution influences on the variation of Ångström derivatives in spectral and optical depth space, *J. Geophys. Res., 106*, 9787-9806, doi:10.1029/2000JD900245.

Patadia, F., P. Gupta, and S. A. Christopher (2008), First observational estimates of global clear sky shortwave aerosol direct radiative effect over land, *Geophys. Res. Lett., 35*, doi:10.1029/2007GL032314.

Pathak, B., G. Kalita, K. Bhuyan, P. K. Bhuyan, K. K. Moorthy (2010), Aerosol temporal characteristics and its impact on shortwave radiative

forcing at a location in the North East of India, *J. Geophys. Res.*, doi:10.1029/2009JD013462.

Penner, J.E., et al. (1994), Quantifying and minimizing uncertainty of climate forcing by anthropogenic aerosols, *Bull. Amer. Meteor. Soc., 75*, 375-400.

Podgorny, I., and V. Ramanathan (2001), A modeling study of the direct effect of aerosols over the tropical Indian Ocean, *J. Geophys. Res., 106*, 24097-24105.

Quinn, P. K., D. J. Coffman, T. S. Bates, T. L. Miller, J. E. Johnson, E. J. Welton, C. Neususs, M. Miller, and P. J. Sheridan (2000), Aerosol optical properties during INDOEX 1999: Means, variability, and controlling factors, *J. Geophys. Res., 107*, doi:10.1029/2000JD000037.

Rajeev, K., V. Ramanathan, and J. Meywerk (2000), Regional aerosol distribution and its long-range transport over the Indian Ocean, *J. Geophys. Res., 105*, 2029-2043.

Rajeev, K., and V. Ramanathan (2001), Direct observations of clear-sky aerosol radiative forcing from space during the Indian Ocean experiment, *J. Geophys. Res., 106*, 17221-17235.

Ram, K., M. M. Sarin, and P. Hegde (2008), Atmospheric abundances of primary and secondary carbonaceous species at two high-altitude sites in India: Sources and temporal variability, *Atmos. Environ., 42*, 6785-6796.

Ramanathan, V., et al. (2001), Indian Ocean Experiment: An integrated analysis of the climate and the great Indo-Asian haze, *J. Geophys. Res., 106*, 28371-28398.

Ramanathan, V., et al. (2005), Atmospheric brown clouds: impacts on South Asian climate and hydrologic cycle, *Proc. Natl Acad. Sci. USA, 102*, 5326-5333.

Ramanathan, V., et al. (2007), Warming trends in Asia amplified by brown cloud solar absorption, *Nature, 448*, 575-578.

Ramanathan, V., and G. Carmichael (2008), Global and regional climate changes due to black carbon, *Nature Geoscience, 1*, 221-227.

Ramachandran, S. (1995), Aerosols in the tropical middle atmosphere, *Ph.D. Thesis, Maharaja Sayajirao University of Baroda*, Vadodara, 177 pp.

Ramachandran, S., and A. Jayaraman (2003a), Spectral aerosol optical depths over Bay of Bengal and Chennai: I-Measurements, *Atmos. Environ., 37*, 1941-1949.

Ramachandran, S., and A. Jayaraman (2003b), Spectral aerosol optical depths over Bay of Bengal and Chennai. part II: Sources, anthropogenic influence and model estimates, *Atmos. Environ., 37*, 1951-1962.

Ramachandran, S. (2004), Spectral aerosol optical characteristics during northeast monsoon over the Arabian Sea and the Indian Ocean: 2. Ångström parameters and anthropogenic influence, *J. Geophys. Res., 109*, doi:10.1029/2003JD004483.

Ramachandran, S. (2005a), Aerosol radiative forcing over Bay of Bengal and Chennai: Comparison with maritime, continental, and urban aerosol models, *J. Geophys. Res., 110*, D21206, doi:10.1029/2005JD005861.

Ramachandran, S. (2005b), Premonsoon shortwave aerosol radiative forcings over the Arabian Sea and tropical Indian Ocean: Yearly and monthly mean variabilities, *J. Geophys. Res., 110*, doi:10.1029/2004JD005563.

Ramachandran, S., R. Rengarajan, A. Jayaraman, M. M. Sarin, and S. K. Das (2006), Aerosol radiative forcing during clear, hazy, and foggy conditions over a continental polluted location in north India, *J. Geophys. Res., 111*, doi:10.1029/2006JD007142.

Ramachandran, S. (2007), Aerosol optical depth and fine mode fraction variations deduced from Moderate Resolution Imaging Spectroradiometer (MODIS) over four urban areas in India, *J. Geophys. Res., 112*, doi: 10.1029/2007JD008500.

Ramachandran, S., and T. A. Rajesh (2007), Black carbon aerosol mass concentrations over Ahmedabad, an urban location in western India: Comparison with urban sites in Asia, Europe, Canada, and the United States, *J. Geophys. Res., 112*, doi:10.1029/2006JD007488.

Ramachandran, S., and T. A. Rajesh (2008), Asymmetry parameters in the lower troposphere derived from aircraft measurements of aerosol scattering coefficients over tropical India, *J. Geophys. Res., 113*, doi:10.1029/2008JD009795.

Ramachandran, S., and R. Cherian (2008), Regional and seasonal variations in aerosol optical characteristics and their frequency distributions over India during 2001-2005, *J. Geophys. Res., 113*, doi:10.1029/2007JD008560.

Ramachandran, S., and S. Kedia (2010), Black carbon aerosols over an urban region: Radiative forcing and climate impact, *J. Geophys. Res., 115*, doi:10.1029/2009JD013560.

Randel, W. J., F. Wu, and D. J. Gaffen (2000), Interannual variability of the tropical tropopause derived from radiosonde data and NCEP reanalyses, *J. Geophys. Res., 105*, 15509-15523.

Reid, J. S., T. F. Eck, S. A. Christopher, P. V. Hobbs, and B. N. Holben (1999), Use of the Ångström exponent to estimate the variability of optical and physical properties of aging smoke particles in Brazil, *J. Geophys. Res., 104*, 27473-27489.

Reinsel, G. C., et al (1994), Seasonal trend analysis of published ground-based and TOMS total ozone data through 1991, *J. Geophys. Res., 99*, 5449-5464.

Remer, L. A., et al. (2005), The MODIS aerosol algorithm, products, and validation, *J. Atmos. Sci., 62*, 947-973.

Remer, L. A., et al. (2008), Global aerosol climatology from the MODIS satellite sensors, *J. Geophys. Res., 113*, doi:10.1029/2007JD009661.

Ricchiazzi, P., S. Yang, C. Gautier and D. Sowle (1998), SBDART, A research and teaching tool for plane-parallel radiative transfer in the Earths atmosphere, *Bull. Am. Meteorol. Soc., 79*, 2101-2114.

Rosenfeld, D., et al. (2000), Suppression of rain and snow by urban and industrial air pollution, *Science, 287*, 1793-1796.

Russell, P. B., et al. (2002), Comparison of aerosol single scattering albedos derived by diverse techniques in two North Atlantic experiments, *J. Atmos. Sci., 59*, 609-619.

Satheesh, S. K., et al. (2009), Vertical structure and horizontal gradients of aerosol extinction coefficients over coastal India inferred from airborne lidar measurements during the Integrated Campaign for Aerosol, Gases and Radiation Budget (ICARB) field campaign, *J. Geophys. Res., 114*, doi:10.1029/2008JD011033.

Schuster, G. L., O. Dubovik, and B. N. Holben (2006), Angstrom exponent and bimodal aerosol size distributions, *J. Geophys. Res., 111*, doi:10.1029/2005JD006328.

Seinfeld, J., and S. Pandis (1998), Atmospheric Chemistry and Physics: From Air Pollution to Climate Change, 1362 pp., *John Wiley, Hoboken*, N. J.

Singh, R. P., S. Dey, S. N. Tripathi, V. Tare, and B. Holben (2004), Variability of aerosol parameters over Kanpur, northern India, *J. Geophys. Res., 109*, doi:10.1029/2004JD004966.

Singh, S., K. Soni, T. Bano, R. S. Tanwar, S. Nath, and B. C. Arya (2010), Clear-sky direct aerosol radiative forcing variations over mega-city Delhi, *Ann. Geophys., 28*, 1157-1166.

Smirnov, A., et al. (2000), Cloud-Screening and Quality Control Algorithms for the AERONET Database, *Remote Sens. Environ., 73*, 337-349.

Smirnov, A., B. N. Holben, Y. J. Kaufman, O. Dubovik, T. F. Eck, I. Slutsker, C. Pietras, and R. N. Halthore (2002), Optical properties of atmospheric aerosol in maritime environments, *J. Atmos. Sci., 59*, 501-523.

Spencer, M. T., J. C. Holecek, C. E. Corrigan, V. Ramanathan, and K. A. Prather (2008), Size-resolved chemical composition of aerosol particles during a monsoonal transition period over the Indian Ocean, *J. Geophys. Res., 113*, doi:10.1029/2007JD008657.

Sreekanth, V., K. Niranjan, and B. L. Madhavan (2007), Radiative forcing of black carbon over eastern India, *Geophys. Res. Lett., 34*, doi:10.1029/2007GL030377.

Stamnes, K., S. C. Tsay, W. Wiscombe, and K. Jayaweera (1988), Numerically stable algorithm for discrete-ordinate-method radiative transfer in multiple scattering and emitting layered media, *Appl. Opt., 27*, 2502-2509.

Tahnk, W. R., and J. A. Coakley Jr. (2002), Aerosol optical depth and direct radiative forcing for INDOEX derived from AVHRR: Observations, January March 1996-2000, *J. Geophys. Res., 107*, doi: 10.1029/2000JD000183.

Takemura, T., T. Nozawa, S. Emori, T.Y. Nakajima, and T. Nakajima (2005), Simulation of climate response to aerosol direct and indirect effects with aerosol transport-radiation model, *J. Geophys. Res., 110*, doi:10.1029/2004JD005029.

Tripathi, S. N., S. Dey, V. Tare, S. K. Satheesh, S. Lal, and S. Venkataramani (2005), Enhanced layer of black carbon in a north Indian industrial city, *Geophys. Res. Lett., 32*, L12802, doi:10.1029/2005GL022564.

Twomey, S. (1977), Atmospheric Aerosols, *Elsevier Scientific Publishing Co.*, New York, pp. 302, NY.

Venkataraman, C., C. K. Reddy, S. Josson, and M. S. Reddy (2002), Aerosol size and chemical characteristics at Mumbai, India during the INDOEX-IFP (1999), *Atmos. Environ., 36*, 1979-1991.

Venkataraman, C., G. Habib, A. Eiguren-Fernandez, A. H. Miguel, and S. K. Friedlander (2005), Residential Biofuels in South Asia: Carbonaceous Aerosol Emissions and Climate Impacts, *Science, 307*, 1454-1456.

Vinoj, V., S. S. Babu, S. K. Satheesh, K. K. Moorthy, and Y. J. Kaufman (2004), Radiative forcing by aerosols over the Bay of Bengal region derived from ship-borne, island-based, and satellite (Moderate-Resolution Imaging Spectroradiometer) observations, *J. Geophys. Res., 109*, doi:10.1029/2003JD004329.

Viollier, M. (1980), Teledetection des concentrations de seston et pigments cholorophylliens contenus dans lOcean, These de Doctorat dEtat, 217 pp., Univ. des Sci. et Technol. de Lille, Lille, France.

Wielicki, B. A., T. Wong, N. Loeb, P. Minnis, K. Priestley and R. Kandel (2005), Changes in Earths Albedo Measured by Satellite, *Science, 308*, 825.

Winker D. M., W. H. Hunt, and M. J. McGill (2007), Initial performance assessment of CALIOP, *Geophys. Res. Lett., 34*, doi:10.1029/2007GL030135.

Weingartner, E., H. Saathoff, M. Schnaiter, N. Streit, B. Bitnar, and U. Baltensperger (2003), Absorption of light by soot particles: Determination of the absorption coefficient by means of aethalometers, *J. Aerosol Sci., 34*, 1445-1463.

Young, A. T. (1994), Air mass and refraction, *Appl. Opt., 33*, 1108-1110.

Yu, H., R. E. Dickinson, M. Chin, Y. J. Kaufman, M. Zhou, L. Zhou, Y. Tian, O. Dubovik, and B. N. Holben (2004), Direct radiative effect of aerosols as determined from a combination of MODIS retrievals and GOCART simulations, *J. Geophys. Res., 109*, doi:10.1029/2003JD003914.

List of Publications

1. *Features of aerosol optical depths over Bay of Bengal and the Arabian Sea during premonsoon season: Variabilities and anthropogenic influence*
   Sumita Kedia, and S. Ramachandran
   Journal of Geophysical Research, 113, doi:10.1029/2007JD009070, 2008.

2. *Variations in aerosol characteristics derived from MODIS over Bay of Bengal and the Arabian Sea during ICARB*
   Sumita Kedia, and S. Ramachandran
   Journal of Earth System Sciences, 117, 375-387, 2008.

3. *Variability in aerosol optical and physical characteristics over the Bay of Bengal and the Arabian Sea deducted from Ångström exponents*
   Sumita Kedia, and S. Ramachandran
   Journal of Geophysical Research, 114, doi:10.1029/2009JD011950, 2009.

4. *Spatiotemporal gradients in aerosol radiative forcing and heating rate over Bay of Bengal and Arabian Sea derived on the basis of optical, physical, and chemical properties*
   Sumita Kedia, S. Ramachandran, Ashwini Kumar, and M. M. Sarin
   Journal of Geophysical Research, 115, doi:10.1029/2009JD013136, 2010.

5. *Black carbon aerosols over an urban region: Radiative forcing and climate impact*
   S. Ramachandran, and **Sumita Kedia**

Journal of Geophysical Research, 115, doi:10.1029/2009JD013560, 2010.

6. *Variability in spectral distribution of aerosol optical depths over continental locations in south Asia*
   S. Ramachandran, and **Sumita Kedia**
   Journal of Geophysical Research, Under review, 2010.

7. *Seasonal variations in aerosol optical characteristics and size distribution over different environments in south Asia*
   Sumita Kedia, and S. Ramachandran
   to be submitted to Atmospheric Environment, 2010.

8. *Aerosol radiative forcing and heating rate over different continental regions in south Asia: Shortwave, longwave and seasonal variations*
   Sumita Kedia, S. Ramachandran, and Rohit Srivastava
   to be submitted to Journal of Geophysical Research, 2010.